v.2

# LATERAL CREEP BEHAVIOUR OF DISCRETE "WINKLER" PILE ELEMENTS IN ICE

by

**Robert M. Kenyon**

A Thesis
Presented to the University of Manitoba
in Partial Fulfilment of the Requirements
for the Degree of **Doctor of Philosophy**
in the Department of Civil and Geological Engineering

Winnipeg, Manitoba

**January, 1994**

# LATERAL CREEP BEHAVIOUR OF DISCRETE "WINKLER" PILE ELEMENTS IN ICE

BY

ROBERT M. KENYON

A Thesis submitted to the Faculty of Graduate Studies of the University of Manitoba in partial fulfillment of the requirements of the degree of

DOCTOR OF PHILOSOPHY

# CHAPTER 5

# ANALYSIS OF THE BAR CREEP TESTS

## 5.1 INTRODUCTION

The experimental bar test results, presented in Chapter 4, consisted of seven single stage tests plus 1 multi-stage test of 5 load increments. The first load increment of the multi-stage test was analyzed as a single stage test, so that an equivalent of eight single stage test results were analyzed, plus the multi-stage test which is now reduced to four increments.

The analysis of the bar tests was performed in two ways. First, the data were analyzed in terms of the power law creep theory, outlined in Chapter 2. As discussed in Chapter 2, this theory is in general use in permafrost engineering, but it has not been tested extensively for laterally loaded piles. The first analysis was performed, therefore, to determine how well power law creep theory described the creep behaviour of the bar, and, by extension, to determine how applicable power law theory is to the creep of laterally loaded piles in permafrost.

The second analysis consisted of comparing the bar creep test data with the results of single stage pressuremeter data in similar ice (Kjartanson, 1986; Kjartanson et al., 1988; Shields et al., 1989). The pressuremeter is routinely used to predict the behaviour of laterally loaded piles in unfrozen soils since the test is thought to simulate well the behaviour of a laterally loaded pile (Baguelin et al., 1978). The comparison presented in this chapter is of particular interest, because both the pressuremeter and the bar were of similar dimensions, and because both tests were performed in similar ice,

at the same temperature, and over the same range of stresses. Because of the similarity in bar and pressuremeter diameters, there was no scale effect to be accounted for (Smith, 1983). Preliminary analysis of the bar versus the pressuremeter tests has been presented and discussed previously (Kenyon et al., 1990), but the analysis is presented here in a more complete fashion.

## 5.2 ANALYSIS OF THE BAR TESTS IN TERMS OF POWER LAW CREEP THEORY

Analysis of the power law creep model consisted of the following steps:

**Step 1.** Determining the pseudo-instantaneous horizontal subgrade reaction modulus, K, from

$$K = pB/y$$

where:

p = equivalent frontal pressure

B = bar diameter or width

y = pseudo-instantaneous displacement at t = 1 minute

and K has units of pressure.

**Step 2.** Determining the constitutive primary creep parameters $\sigma_{c_p}$, $n_p$, and $b_p$ for the ice, assuming Rowley et al.'s (1973) proposed transformation from cylindrical cavity expansion to a translating rigid strip footing. The transformation was presented in subsection 2.3.4.2. This thesis uses the subscripts p and s, respectively, to distinguish between the Winkler Bar

determined primary and secondary creep parameters.

**Step 3.** Determining the constitutive secondary creep parameters $\sigma_{c_s}$ and $n_s$ for the ice, also as outlined in subsection 2.3.4.2 and according to the formulation by Nixon (1984).

The pseudo-instantaneous modulus, K, (Step 1) is a variation of the subgrade reaction modulus proposed by Terzaghi (1955) as a deformation characteristic of soils. K is commonly used in modelling the reaction of laterally loaded piles (Baguelin et al., 1978) in unfrozen soil, and is used in laterally-loaded-pile analysis programs, such as PILATE (Bankratz et al., 1981).

In Steps 2 and 3, primary and secondary power law creep analyses were completed for both the single stage tests and for the multi-stage test. The creep parameters analyzed from each type of test are compared. The comparison is of interest because one of the reasons for conducting a multi-stage test is to be able to use the multi-stage test results to predict single stage behaviour over a wide variety of applied loads (Rowley et al., 1973). Multi-stage tests are less expensive and easier to perform than a series of single stage tests.

The following sub-section details the procedures followed in processing the bar test results.

### 5.2.1 Processing the Bar Test Results

This subsection summarizes the data processing procedures which were followed. Subsequent subsections present the results of the analyses.

Processing the bar test results included the following steps, for both the single and multi-stage tests:

1. Determine the pseudo-instantaneous (elastic plus plastic) response, K = pB/y at the beginning of each test, or beginning of each stage of the multi-stage test. The pseudo-instantaneous displacement was determined at an arbitrarily assigned elapsed time of 1 minute, to be consistent with the data processing of the pressuremeter test results (Shields et al., 1989).
2. Subtract the pseudo-instantaneous displacement from the total displacement to obtain the creep displacement.
3. Determine the end of primary creep, and separate the primary creep phase from the secondary creep phase.
4. Analyze the primary creep data to determine $\sigma_{c_p}$, $n_p$, and $b_p$.
5. Analyze the secondary creep data to determine $\sigma_{c_s}$ and $n_s$.

#### 5.2.1.1 Determining the Pseudo-Instantaneous Displacement

In this thesis, the pseudo-instantaneous response is taken to be the one minute displacement, to be consistent with previously reported pressuremeter test results in similar ice (Kjartanson, 1986; Shields et al., 1989). Neither Kjartanson nor Shields reported on the instantaneous response, but they did reference their calculations of primary creep strains to an initial cavity radius at the one minute interval. This approach has also been taken by other researchers for pile load tests (Rowley et al., 1973), and for

pressuremeter tests (Ladanyi and Eckhart, 1983).

#### 5.2.1.2 Determining the End of Primary Creep

The approach followed to determine the end of primary creep is similar to that outlined by Mellor and Cole (1982), by Azizi (1989), and by Shields et al. (1989).

Mellor and Cole's (1982) approach consisted of examining rates of change of displacement (or displacement rate) versus time, usually in log-log space. Figure 5.1 illustrates axial strain rates versus elapsed time from Mellor and Cole's (1982) constant uniaxial stress tests and constant uniaxial strain rate tests on polycrystalline ice. Figure 5.2 presents a similar plot from Shields et al.'s (1989) pressuremeter tests. Both plots are in log-log space and in both cases the strain rates decrease to a minimum before accelerating into tertiary creep. The inflection point representing the minimum strain rate was taken to be the end of primary creep.

This thesis examines three different graphical approaches to determine the end of primary creep:

1. Creep displacement rates versus elapsed time in log-log space.
2. Creep displacement versus time in log-log space.
3. Creep displacement rate versus time in arithmetic space.

It has been suggested by Rowley et al. (1973, 1975), by Nixon (1984), and by Neukirchner and Nixon (1987), that a pile or bar begins to behave in a "perfectly rigid" manner at the end of primary creep. Tests 9 to 12 actually measured the bending of the bar, and so it was thought of interest to determine whether in fact the bar did stop changing shape (bending strain became constant) at the end of primary creep. Hence,

the plot of rate of change of bending strain versus time was analyzed and the results compared with the traditional primary creep determinations.

Finally, not only is it of interest to a potential designer to be able to predict when primary creep might end, but also to predict at what displacement it might end. Mellor and Cole (1982) had determined that under uniaxial compression testing, the primary creep of polycrystalline ice ends at approximately 0.9 to 1.0% axial strain. On the other hand, Shields et al. (1989) reported that primary creep of ice under pressuremeter testing ended at circumferential creep strains ranging from 1.15% to 7.15%. The question remained: Did such a relationship exist for the bar tests, and, if so, what was the comparison to the compression and pressuremeter tests?

#### 5.2.1.3 Determining the Constitutive Creep Parameters $\sigma_{c_p}$, $n_p$, and $b_p$ from Primary Creep

The constitutive equations describing the primary creep of a cylindrical Winkler element were given in Chapter 2. Rowley et al. (1973, 1975) proposed that the primary creep displacement of a cylindrical Winkler beam element be given by Equation (2.24), repeated here as:

$$\frac{y}{B} = \frac{\pi}{8}\left[\left[1 + \frac{\sqrt{3}}{2}^{n_p+1}\left(\frac{2}{n_p}\right)^{n_p}\left[\frac{p-p_o}{\sigma_{c_p}}\right]^{n_p}\left(\frac{\dot{\epsilon}_c}{b_p}\right)^{b_p} t^{b_p}\right]^2 - 1\right] \quad (5.1)$$

Rearranging (5.1) results in:

$$\sqrt{\frac{8y}{\pi B} + 1} - 1 = \left(\frac{\sqrt{3}}{2}\right)^{n_p+1}\left(\frac{2}{n_p}\right)^{n_p}\left[\frac{p-p_o}{\sigma_{c_p}}\right]^{n_p}\left(\frac{\dot{\epsilon}_c}{b_p}\right)^{b_p} t^{b_p} \quad (5.2)$$

which can be expressed as:

$$\sqrt{\frac{8y}{\pi B} + 1} - 1 = F\, t^{b_p} \quad (5.3)$$

where:

$$F = M\left[\frac{p-p_o}{\sigma_c}\right]^{n_p} \quad (5.4)$$

and

$$M = \left(\frac{\sqrt{3}}{2}\right)^{n_p+1}\left(\frac{\dot{\epsilon}_c}{b_p}\right)^{b_p}\left(\frac{2}{n_p}\right)^{n_p} \quad (5.5)$$

Each of the variables is as defined in Chapter 2.

For the bar tests, $p_o$, the insitu horizontal pressure in the ice at $r = \infty$ has been set equal to zero. As discussed in Chapter 3, elastic stress analysis of the test bar in the tank, following the approach introduced by Baguelin et al. (1977), had shown that the stresses at the ice-tank boundary are negligible. More recently this has been confirmed experimentally for the pressuremeter case by Goodman (1992).

Solution of the creep parameters $\sigma_{c_p}$, $n_p$, and $b_p$ may be found from two log-log plots, after Andersland et al. (1978), which are illustrated in Figure 5.3. First, taking the logarithm of both sides of Equation (5.3) yields:

$$\log \left[ \sqrt{\frac{8y}{\pi B}+1} - 1 \right] = \log F + b_p \log t \ , \tag{5.6}$$

which is an equation for a straight line in log-log coordinates.

When $\left[ \sqrt{\frac{8y}{\pi B}+1} - 1 \right]$ is plotted versus time in a log-log plot, the creep curves linearize with a slope equal to $b_p$, as illustrated in the upper plot of Figure 5.3. F is the intercept at log t = 0, that is to say when t = 1 (in this thesis, when t = 1 hour).

Next, writing Equation (5.4) in log form gives:

$$\log F = \log M + n_p \log p - n_p \log \sigma_{c_p} \ . \tag{5.7}$$

which is also an equation for a straight line.

A plot of p versus F (lower part of Figure 5.3) allows $n_p$, the arithmetic slope of the line, to be measured. The intercept at log p = 0, that is when p = 1 (in this thesis, when p = 1 MPa) is called F1, where:

$$\log F1 = \log M - n_p \log \sigma_{c_p} \tag{5.8}$$

M is given by Equation (5.5) into which $b_p$ and $n_p$ are substituted. This thesis arbitrarily assigns $\dot{\epsilon}_c$ a value of 0.0006 $hr^{-1}$, for consistency with Ladanyi (1972). Equation (5.8)

can be written in the form:

$$\sigma_{c_p} = \left[\frac{M}{F1}\right]^{\frac{1}{n_p}} \tag{5.9}$$

and the value of $\sigma_{c_p}$ determined from M, F1 and $n_p$.

### 5.2.1.4 Determining the Creep Parameters $\sigma_{c_s}$, $n_s$ from Secondary Creep

Two constitutive equations were outlined in Chapter 2 to describe the secondary creep displacement of a cylindrical Winkler element.

Nixon (1978) proposed Equation (2.25), repeated here as:

$$\dot{u} = I\, a\, \dot{\epsilon}_c \left[\frac{p}{\sigma_{c_s}}\right]^{n_s} \tag{5.10}$$

Here, a is the bar radius, and I is given by (2.26), rewritten here as:

$$I = \left[\frac{2}{n_s}\right]^{n_s} \left[\frac{\sqrt{3}}{2}\right]^{n_s+1} \tag{5.11}$$

Foriero and Ladanyi (1989) proposed that I be taken from the solution by Vivatrat

(1984) as given by (2.27):

$$I = \left[ \frac{2(n_s+1)\ (n_s+3)}{\pi n_s^2 \left[ \frac{4}{\sqrt{3}} \right]^{\frac{(n_s+1)}{n_s}}} \right]^3 \qquad (5.12)$$

As discussed in Chapter 2, the variations on I, the shape or influence factor, occur due to differing assumptions regarding the flow of the bar through the creeping medium. Foriero and Ladanyi (1989) had compared (5.11) and (5.12) using $n_s = 3$, and concluded that each gave similar results.

To solve for $n_s$, Equation (5.10) is plotted in log-log space as $\dot{u}$ versus p, and the arithmetic slope of the best fit line gives the value of $n_s$, the stress creep exponent. Once the magnitude of $n_s$ has been determined, then the shape factor, I, is calculated, according to Equations (5.11) or (5.12).

Finally, the value of the creep proof stress, $\sigma_{c_s}$, is determined by substituting $n_s$ and I in (5.10), assuming that $p = 1$ and taking the creep proof strain $\dot{\epsilon}_c = 0.0006\ hr^{-1}$ .

### 5.2.2 Analysis of Single Stage Tests (Creep Displacement at Ends of the Bar)

This subsection presents the analysis of the single stage tests, following the data processing methodology outlined in the previous subsection. In this subsection, and in subsection 5.2.3, the creep displacements measured at the ends of the bar just above the ice surface, as reported in Chapter 4, are analyzed. Subsection 5.2.4 repeats the analysis

of subsections 5.2.2 and 5.2.3, but using the calculated creep displacements of the midpoint of the embedded length of the bar. Displacements of the midpoint of the bar were calculated following the Conjugate Beam method using measured displacements and bending strains of the bar.

#### 5.2.2.1 Pseudo-Instantaneous Displacements

Analysis of the pseudo-instantaneous response determines the pseudo-instantaneous horizontal subgrade reaction modulus K = pB/y. Test data summarizing pB versus y, at an elapsed time of 1 minute, are given in Table 5.1. Because the initial loading was applied slowly, the loads were always less than the full target loads at 1 minute. Table 5.1 shows that, for example, the actual applied loads at t = 1 minute ranged from 29.9% to 96.6% of the full target load. The measured values of pB and y at 1 minute were used to determine K, nevertheless.

The line shown on Figure 5.4 represents regression analysis performed on the slopes through the origin and through each data point. This approach forces the line through the origin. The result is K = 215 MPa.

Although the pB-y relationship is linear, it does, at least theoretically, represent elastic plus plastic behaviour (Hult, 1966). This thesis makes no attempt, however, to separate the two. Instead, it follows the approach of Andersland, Sayles, and Ladanyi (1978), who suggested the term pseudo-instantaneous be used to describe this initial response, without attempting to separate the elastic behaviour from the plastic response.

#### 5.2.2.2 Determine End of Primary Creep

As discussed in 5.2.1.2, the end of primary creep is determined by examining plots of:

1. Creep displacement rates versus time in log-log space.
2. Creep displacements versus time in log-log space.
3. Creep displacement rates versus time in arithmetic space.

**Plots of Creep Displacement Rates Versus Time (log-log)**

Figure 5.5 presents a summary plot of creep displacement rates versus time in log-log space for the single stage bar tests. Repeat test results have been omitted to improve clarity. The creep displacement rates during the first portion of the bar tests decrease steadily to some minimum creep rate which then becomes constant with time. In other words, the bar undergoes primary creep behaviour initially, and then moves into a secondary creep (constant creep displacement rate) phase which continues through until the end of the test. Tertiary, or accelerating creep was not observed for the bar tests.

The creep behaviour of the bar differs, therefore, from the pressuremeter tests shown on Figure 5.2, in that secondary creep in the pressuremeter tests was an inflection point separating primary creep from tertiary creep (Shields et al., 1989).

The solid line running through the test data represents a best fit power law line through the points where primary creep is interpreted to have ended for each test, i.e. where displacement rates first became constant. This line is similar in concept to the line drawn through Mellor and Cole's (1982) data on Figure 5.1.

Figure 5.6 presents a typical plot of creep displacement rate versus time in log-log

space for Test 10 (p = 1.75 MPa). Here one can readily determine that primary creep ended after approximately 12 hours of elapsed time. Similar plots for all single stage tests were prepared and analyzed to determine the end of primary creep. Individual plots for these tests are placed in Appendix C, which contains all 3 types of plots used to determine the end of primary creep.

**Plots of Creep Displacement Versus Time (log-log)**

One can also examine plots of creep displacement versus time in log-log space to determine the end of primary creep. Figure 5.7 presents a summary plot of all single stage tests. Again repeat tests have been removed for clarity.

Overall individual curves typically have an elongated mirror image "S" shape which can be divided into three phases. The first phase consists of the very early stages of the tests where the shapes of the curves are curvilinear downwards. The duration of this first phase ranged from 0.5 hrs at the highest pressure of 2.25 MPa, to 3.0 hrs at the lowest pressure of 1.0 MPa. The second phase consists of the linear portion of the curve in log-log space (representing a power law relationship with respect to time). The linear portion was followed by the third phase, where the curves began to bend upwards.

The first phase of behaviour has been observed by others, particularly in pressuremeter testing (Ladanyi and Eckhart, 1983; Fensury, 1985; Kjartanson, 1986), and has been attributed to stress redistribution around the pressuremeter borehole as the test is starting (Murat et al., 1986). The second phase, or straight line portion of the log-log plot, represents the primary creep portion of the test where, as shown by Equation (5.1), creep displacement is a power law function of time. The end of primary

creep is taken as the end of the straight line portion of this plot, and is marked on Figure 5.7 by a line drawn through the interpreted ends of primary creep.

Figure 5.8 presents a typical plot of creep displacement versus time in log-log space for Test 10. As in Figure 5.5, primary creep appears to end at approximately 12 hours. Similar individual plots for all tests are found in Appendix C.

**Creep Displacement Rates Versus Time (arithmetic space)**

Arithmetic plots of creep rate versus time were also analyzed to determine the end of primary creep. A single plot summarizing all tests is not practical in arithmetic space because the secondary creep displacement rates vary so widely. Figure 5.9, for Test 10 p = 1.75 MPa, is a typical plot. On this figure, only the first 20 hours of the 450 hour long test are shown, in order to increase the horizontal scale. Again it is evident that primary creep ended at 12 hours. Plots for the other tests are found in Appendix C.

**Summary of Analysis To Determine The End Of Primary Creep**

The interpretation of when primary creep ended, according to each of the three different graphs examined, is summarized on Table 5.2, for each of the single stage tests.

Each of the three types of graphs, which were analyzed to determine the time when primary creep ended, gave essentially the same result for each of the single stage tests. This observation is reinforced by Figure 5.11 which illustrates the time to end of primary creep as a function of applied frontal pressure. Figure 5.11 also suggests that the time when primary creep ends is a power law function of the applied frontal pressure for the bar. For the single stage tests, the time to the end of primary creep is given by

the equation:

$$t = 38.9\ p^{-2.58} \qquad (5.13)$$

where t has units of hrs and p is in MPa. This equation is represented by the solid line on Figure 5.11. This line is the best fit through the combination of all three methods used to interpret the end of primary creep, i.e., through all data points shown on Figure 5.11.

Table 5.2 compares the time to end of primary creep for the bar tests to the time to end of primary creep of the equivalent pressuremeter tests. (The end of primary creep for the pressuremeter tests represents the inflection point on Figure 5.2.) Note that at all pressures from 1.0 to 2.25 MPa, the primary creep phase for the pressuremeter lasted much longer than it did during the bar tests. The reason for this is not understood at this time.

Not only can the time to the end of primary creep be predicted, but so can the displacement at which primary creep ends. Figure 5.12 shows the relationship between the displacement at the end of primary creep and the applied frontal stress. Here the displacements are normalized with respect to the bar radius (in percent) to allow comparison with the pressuremeter creep test results. Shields et al. (1989) reported that the primary creep phase during pressuremeter testing in similar ice ended at circumferential strains ($\Delta r/r_o$) ranging from 1.15% to 7.15%. For the bar tests, primary creep ended at normalized displacements (y/r) of between 2 and 5%.

Note on Figure 5.12 that the end of primary creep, (y/r), for the single stage bar tests increased with applied pressure. Neither Mellor and Cole (1982) nor Shields et al.

(1989) observed this phenomenon in the ice.

**Does the Bar Begin to Behave in a Rigid Fashion at the End of Primary Creep?**

As discussed in Chapter 2, Rowley et al. (1973, 1975), Nixon (1984), and Neukirchner and Nixon (1987) had suggested that a pile will begin to behave in a rigid fashion at the beginning of secondary creep. If so, then the bending strains in the bar should stabilize and become constant at the end of primary creep. This hypothesis had not been previously tested experimentally.

A series of seven strain gauges were mounted along the backside of the bar prior to the last four tests so that the bending strain of the bar could be measured. Figure 5.10 shows the rate of change of bending strain of the bar versus time for Test 10. For clarity, only the first 20 hours of the test are shown. It evident that the bending strain stopped changing at 12 hours, which is the time that has been interpreted as the end of primary creep according to Figures 5.6, 5.8 and 5.9. Similar graphs of bending strain rate versus time for the remaining tests are found in Appendix C.

The time when the bar stopped bending was coincident with the end of primary creep, as is illustrated on Figure 5.11. The dashed line represents the time when the bar stopped bending for the four tests where this behaviour was recorded. It is difficult to discern the dashed line because it is virtually coincident with the solid line representing the interpreted end of primary creep.

### 5.2.2.3 Determine Primary Power Law Creep Parameters $\sigma_{c_p}$, $n_p$ and $b_p$ (End of the Bar)

The previous subsection 5.2.3 detailed the analysis to define the duration of the primary creep phase for each of the single stage tests. This subsection presents the analysis to determine the constitutive primary creep parameters $\sigma_{c_p}$, $n_p$, and $b_p$, following the method of processing the primary creep data outlined in subsection 5.2.1.3. This subsection uses creep displacements of the ends of the bar (point of load application at ice surface).

**Determine $b_p$**

The first step is to define the power law relationship between creep displacement and time in order to determine the creep parameter $b_p$. To do this one follows Equation (5.3) and plots Rowley et al.'s (1973, 1975) transformed displacement, $\sqrt{8y/\pi B+1}\ -1$ versus time in log-log space. On such a plot, the results of the single stage tests are a series of straight lines, whose average arithmetic slope is the value of $b_p$. Figure 5.13 illustrates the results for the single stage tests. The very early creep stages of each test have been included in Figure 5.13 and the solid lines represent the regression line through all primary creep data, including the initial curved section. The results plot as a series of more or less parallel lines, with the exceptions of the 1.0 MPa test whose slope is noticeably flatter than the others, and the 1.25 MPa test whose slope is noticeably steeper. Table 5.3 summarizes values of $b_p$, for the individual single stage tests, which ranged from 0.231 to 0.337, with an average value of 0.271.

The slopes of the regression lines through the individual tests are influenced by the very early portions of the test. The problem is illustrated by Figure 5.14 which isolates the results for Test 10 (1.75 MPa). Here it can be seen that the results have a curvilinear downwards shape for the first 0.2 hours (12 minutes) of the test. The remainder of the data, from 0.2 hrs to the end of primary creep at 12 hours, plots as a straight line.

If the early curvilinear portions of the individual tests are ignored or deleted, as was the practice with pressuremeter test data prior to 1986 (Ladanyi and Eckardt, 1983; Fensury, 1985; Kjartanson, 1986), then Figure 5.15 results. The best fit power law relationship can now be calculated for points that truly lie in a straight line. The lines are more or less parallel, except for the 1.0 MPa test. Figure 5.16 illustrates a typical individual test result, using Test 10.

Table 5.3 summarizes the values of $b_p$ calculated as the best fit through the straight line portions of the primary creep data of Figure 5.15. The average value of $b_p$ is 0.206, as compared to the previous 0.271.

While theoretically $b_p$ is not stress-dependent, nevertheless, the possibility is examined in Figures 5.17 and 5.18. Other researchers, such as Eckardt, (1981) and Fensury (1985) had observed that $b_p$ values from pressuremeter testing in frozen sand increased as a function of applied stress. Figure 5.17 presents $b_p$ as a function of frontal pressure, p, based on the regression lines of Figure 5.13. Figure 5.18 summarizes the same relationship for $b_p$ calculated using only the straight line portion of primary creep (Figure 5.15). The solid horizontal line, on both graphs, represents the average value of $b_p$. It appears, from Figures 5.17 and 5.18, that $b_p$ is not stress dependent for the bar

tests in ice.

The notes of Table 5.3 list the $b_p$ values determined from Kjartanson's (1986) pressuremeter tests, as reported by Shields et al. (1989). It was found that $b_p = 0.64$ when the pressuremeter data was corrected for stress redistribution following Murat et al. (1986), whereas $b_p = 0.50$ when the pressuremeter data was not corrected. These values compare to $b_p = 0.27$ and $b_p = 0.21$, respectively, when the primary creep of the ends of the bar is considered.

**Determine $n_p$**

Values of $n_p$ and $\sigma_{c_p}$ were determined by preparing plots similar to the lower graph on Figure 5.3, and solving Equations (5.7) through (5.9), with the help of Equation (5.5).

Figures 5.14 and 5.16 illustrate typical interpretations of the unit time intercept, F. Similar plots were prepared for each of the single stage tests, and are included as Appendix D. Values of F are summarized on Table 5.3.

Figures 5.19 and 5.20 illustrate the determination of $n_p$. It was found that:

$n_p$ = 1.23 for the best fit line through all the points, using all the primary creep data (Figure 5.19).

$n_p$ = 1.03 for the best fit line through all the points, using only the straight line portion of primary creep curves (Figure 5.20).

A value of $n_p = 1.03$ suggests that the primary creep is almost a linear function of stress.

However, if the one bar test result from the 1.0 MPa test is ignored, the value of $n_p$ for the remaining points is much higher, namely 1.88 instead of 1.23, and 1.62 instead of 1.03. Pressuremeter tests in the same ice gave $n_p = 2.47$.

**Determine $\sigma_{c_p}$**

Once values of $b_p$ and $n_p$ have been determined, then the value of $\sigma_{c_p}$ can be calculated using Equations (5.8) and (5.9):

$\sigma_{c_p}$ = 19.7 MPa for the best fit through all primary creep data.

$\sigma_{c_p}$ = 51.9 MPa for the best fit through the straight line portion of primary creep.

Ignoring the results of the 1.0 MPa test leads to $\sigma_{c_p}$ values of 6.5 and 12.0 MPa. This compares to $\sigma_{c_p} = 1.97$ MPa for the pressuremeter tests as calculated by this author from Shields et al. (1989) test data.

A summary of the constitutive primary creep parameters, as determined for the single stage tests is presented on Table 5.4.

### 5.2.2.4 Determine Secondary Creep Parameters $\sigma_{c_s}$, and $n_s$ from Single Stage Tests

Once the primary creep parameters were determined, then the constitutive secondary creep parameters were determined as outlined in subsection 5.2.1.4.

The secondary displacement rates were calculated as the least squares best fit through the linear secondary displacement portions of the test results, which were shown in the previous chapter on Figure 4.4.

Table 5.5 lists the individual secondary displacement rates for the single stage and multi-stage bar tests, and compares them to the minimum strain rates from the pressuremeter tests.

When the bar secondary displacement rates, from Table 5.5, are plotted versus equivalent frontal pressure, p, in log-log space, the arithmetic slope of the best fit line through the data represents the secondary creep exponent $n_s$. This relationship and resulting calculation of $n_s$ is summarized on Figure 5.21. The slope of the best fit line gives $n_s = 3.84$. This value of $n_s$ is in contrast to the value of $n_p$ from the primary creep phase, where $n_p$ was determined to be either $n_p = 1.23$ (all primary creep data), or $n_p = 1.03$ (straight line portion of all primary creep phase), or 1.88 and 1.62, respectively, when the 1.0 MPa test is ignored.

Next the values of I, the shape factor in Equations (5.11) and (5.12), according to Nixon (1984), and according to Foriero and Ladanyi (1989), were calculated to be $I = 0.041$ and $I = 0.123$, respectively.

Finally, the values of $\sigma_{c_s}$, were calculated from Equation (5.10), assuming

$\dot{\epsilon}_c$ = 0.0006 hr$^{-1}$, as previously, and I as determined in the previous paragraph. The values of $\sigma_{c_s}$ are 1.46 with Nixon's I, and 1.10 with Foriero and Ladanyi's I.

The above calculations complete the determination of the constitutive power law creep parameters from the single stage tests. The following subsection analyzes the multi-stage test.

### 5.2.3 Analysis of the Multi-Stage Test (End of the Bar Movements)

This subsection presents the analysis of the multi-stage test, following the same form of analysis as for the single stage tests. The multi-stage test was actually comprised of five stages. However, the first stage results were analyzed as a single stage tests (p = 1.25 MPa). The remaining four stages at p = 1.5 MPa, p = 1.75 MPa, p = 2.00 MPa, and p = 2.25 MPa are analyzed here.

#### 5.2.3.1 Pseudo-Instantaneous Displacements

Figure 5.22 illustrates the pB versus y relationship for the multi-stage test, and compares it to the same relationship from the single stage data. On this figure, pB represents the applied value at the end of one minute for each particular stage. The lateral displacement at any stage is the accumulated pseudo-instantaneous response from all previous stages, plus the measured response of this stage of the test. The magnitude of K for the multi-stage test is 290 MPa, versus K = 215 MPa for the single stage tests.

### 5.2.3.2 Determine End of Primary Creep

When analyzing the creep phase of each stage of the multi-stage test, each stage was treated as if it was an equivalent single stage test. In other words, all previous accumulated time and displacements were deleted, and the displacement and time at the beginning of each stage was set to zero for analysis purposes.

The end of primary creep is again determined by examining plots of:

1. Creep displacement rates versus time, in log-log space.
2. Creep displacement versus time, in log-log space.
3. Creep displacement rates versus time, in arithmetic space.

**Plots of Creep Displacement Rates Versus Time (log-log)**

Figure 5.23 summarizes creep displacement rates versus time in log-log space for the second through fifth stages of the multi-stage test. As in the single stage tests, each stage is characterized by decreasing creep displacement rates versus time, followed by a constant displacement rate until the end of each stage. The solid horizontal lines represent the best fit interpretation of the secondary creep displacement rates, which are summarized on Table 5.5. Here, as was the case in Figure 5.6 for the single stage Test 10, the horizontal lines are also used as a visual aid to interpret when creep rates first become constant. No tertiary creep (accelerating rates) is observed.

The solid diagonal line on Figure 5.23 is drawn through the interpreted end of primary creep. These end-of-primary-creep times are summarized on Table 5.6.

**Plots of Creep Displacement Versus Time (Log-log)**

Figure 5.24 summarizes creep displacement versus time in log-log space for each of the stages. As in the single stage tests, the curves have the form of an elongated mirror image of the letter "s", although the shape is not as pronounced in the multi-stage test. The solid horizontal line represents the displacement at the end of the straight line, middle portion of the curves, which marks the end of primary creep. The times are summarized on Table 5.6. The end of primary creep was not as clear and distinct on Figure 5.24 as it had been for the single stage tests on Figure 5.7.

**Plots of Displacement Rates Versus Time**

Figures 5.25 and 5.26 are graphs of displacement rates versus time in arithmetic space. Each graph represents one of the four stages of the multi-stage tests.

An arrow has been placed on each graph to indicate the interpreted end of primary creep, when the displacement rate becomes constant.

**Summary of Analysis to Interpret the End of Primary Creep (Multi-Stage Test)**

Figure 5.27 summarizes the interpretations from the three types of plots used to determined the end of primary creep. This summary is also detailed on Table 5.6. As was observed from the single stage test results on Figure 5.7, there is good agreement between conclusions drawn from each of the three types of plots used to interpret the end of primary creep.

Figure 5.27 also compares the interpreted time to end of primary creep from the multi-stage tests with the time to end of primary creep as interpreted from the single

stage test results. There appears to be reasonable agreement. The primary creep phase did, however, last longer for a given pressure for each single stage test than for the corresponding multi-stage test.

On Figure 5.27 the solid diagonal line represents the least squares power law best fit interpretation, through the combination of the three approaches, of the time to end of primary creep. The equation of this line is:

$$T\ (\text{hrs}) = 50.8 \times p^{-4.00} \tag{5.15}$$

where p is the equivalent frontal pressure in MPa.

As was the case for the single stage tests, the creep displacement, (y/r), at the end of primary creep increased with the applied frontal pressure, p. Figure 5.30 summarizes this relationship. Figure 5.30 also compares the results of the multi-stage test to those of the single stage tests of Figure 5.12. Primary creep ended during the multi-stage test at much lower normalized displacements than during the single stage tests. Primary creep ends at (y/r) values ranging from 0.75 to 1.25% for the multi-stage test, compared to 2 to 5% for the single stage tests.

The time when the bar stopped bending was again coincident with the end of primary creep, as is illustrated on Figure 5.27. Figures 5.28 and 5.29 illustrate the change in bending rate versus time for each of the four multi-stages. Again the bar stops bending when primary creep ends.

### 5.2.3.3 Determine Primary Creep Parameters $b_p$, $n_p$ and $\sigma_{c_p}$

The determination of primary creep parameters, $b_p$, $n_p$, and $\sigma_{c_p}$, followed the same procedure for the multi-stage test as outlined for the single stage tests.

**Determine $b_p$**

Figure 5.31 summarizes Rowley et al.'s (1973) transformed primary creep displacement versus elapsed time, plotted in log-log space. All primary creep data is shown on this plot, including the early stages where the trace of the data is "s" shaped. Three of the four stages plot as parallel lines, with the slope of the 2.25 MPa stage being flatter than the three lower pressures.

Values of $b_p$, as summarized on Table 5.7, averaged 0.541 and ranged from 0.363 for the 2.25 MPa stage to 0.651 for the 1.50 MPa stage.

Figure 5.32 summarizes a second interpretation where the early "s" shaped portion of each curve was deleted, and only the straight line portion of the primary creep data remains. Now the average value of $b_p$, also summarized on Table 5.7, equals 0.532 and $b_p$ ranges from 0.467 to 0.574.

Table 5.8 compares the primary creep parameters from the multi-stage tests to the single stage test results of Table 5.4. The average values of $b_p$ for the multi-stage tests differ from those interpreted from the single stage tests. They are similar, however, with those reported for the single stage pressuremeter tests (Shields et al., 1989).

Figure 5.33 shows the multi-stage $b_p$ values as a function of pressure for the two

different ways the results were interpreted. The average $b_p$ from the pressuremeter test results, is shown for comparison purposes.

**Determine $n_p$ and $\sigma_{c_p}$**

When the unit time (1 hr) intercepts for each stage (F values) are taken from Figures 5.31 and 5.32, and plotted versus applied pressure, the primary creep exponent $n_p$ is determined, as shown on Figure 5.34. The values were $n_p = 2.70$ for the best fit line through all primary creep data, and $n_p = 2.37$ through the straight line portion of the primary creep data.

As was the case with $b_p$, the values of $n_p$ determined from the multi-stage test differ from the values of $n_p$ determined from the single stage bar tests (see Table 5.8). They do, however, compare well with the results from the single stage pressuremeter tests.

The value of the creep proof stress parameter, $\sigma_{c_p}$, was determined to be $\sigma_{c_p} =$ 2.77 MPa for all of the primary creep data, and $\sigma_{c_p} = 3.57$ MPa for only the straight line portion of the primary creep data, for the multi-stage test. Comparisons are made with the single stage bar tests, the pressuremeter tests, and compression tests in Table 5.8.

#### 5.2.3.4 Determine Secondary Creep Parameters $\sigma_{c_s}$ and $n_s$

Secondary displacement rates for both the single stage and multi-stage bar tests were summarized on Table 5.5. It is apparent from an examination of Table 5.5 that at equivalent frontal pressures, the secondary displacement rates were similar. In fact there was more discrepancy between one set of two single stage tests at 2.25 MPa, than there was between the single stage loaded tests and corresponding stages of the multi-stage test.

Figure 5.35 plots secondary displacement rates versus equivalent frontal pressures for both single stage and multi-stage bar tests, and compares them to the pressuremeter test results of Kjartanson (1986). The secondary displacement rates for the pressuremeter are the minimum radial displacement rates determined from Kjartanson's (1986) data shown on Figure 5.2. The results all plot close to a single line. Nevertheless, the pressuremeter creep rates are everywhere faster than the bar rates. The actual rates are compared in Table 5.5. On average the pressuremeter expanded at a rate 1.30 times the rate that the bar displaced.

### 5.2.4 Determine Primary Creep Parameters from Creep Displacements of Midpoints of the Bar

The previous two subsections 5.2.2 and 5.2.3 analyzed the bar test data in both primary and secondary creep by using the creep displacements measured at the point of lateral load application, which was approximately 50 mm off the ice surface. In these subsections, no account was taken of the fact that the bar did not remain straight, but in fact bent slightly when load was applied.

When it became apparent that the midpoint of the bar lagged behind the ends, it was decided to calculate the displacements of the bar at this point. It would then be possible to determine $\sigma_{c_p}$, $n_p$, and $b_p$ at the midpoint and compare these to the values determined for the movement of the ends of the bar.

Following discussions with Dr. G.A. Morris (pers. comm., 1992), the bending displacements of the bar were calculated using the Conjugate Beam Method. The calculations required that the distribution of bending strains along the bar be known. The technique could be applied only to the last four single stage tests (Tests 9 to 12 Stage 1) and to the multi-stage test (Test 12 Stages 2 to 5), where the bending strains had been measured. Calculated bending displacements were added to the measured end displacements to define the shape and displacement of the bar in the ice at any particular time and at selected points along the bar's embedded length.

Figures 5.36 through 5.39 show the shape and displacement of the bar in the ice at arbitrarily selected times during the primary creep phase of the single stage tests.

On these figures the top and bottom y-axes represent the points where the load was applied to the bar; points which were 50 mm removed from the ice. The bar was physically embedded in the ice between -50 mm and -660 mm.

It is apparent from Figures 5.36 through 5.39 that the bar did bend and change shape in the primary creep phase of the single stage loaded tests. For example, on Figure 5.36, the midpoint of the embedded depth of the bar translated approximately 0.65 mm during the first 4.5 hr, while at the point of load application, the bar translated 2.3 mm.

Figures 5.40 through 5.43 show the shape and displacement of the bar in the ice at select times during the primary creep phase of the multi-stage tests. The zero minute pile displacements represent the shape at the beginning of that particular stage of loading due to the load which had been applied during the previous stage. The bar does not change shape appreciably during the primary creep phase; both the middle and the ends of the bar displace more or less the same distance. In other words, once the first stage loading deformed the bar, subsequent stage loadings caused the bar to translate in a rigid fashion.

Figure 5.44 through 5.46 illustrate the determination of the primary creep parameters $b_p$ and $n_p$, from the single stage tests, using the creep displacement of the bar at the midpoint of its embedded depth. Note that some of the early readings (1 minute, typically) have been deleted to examine the straight line portion of the creep data. The $b_p$ values are listed on Table 5.8, where they can be compared to $b_p$ values deduced from the creep displacement of the ends of the bar. The new average $b_p$ value is 0.512, versus $b_p = 0.271$ and $b_p = 0.206$ for the ends of the bar. The $b_p$ value of 0.512 gives better agreement with Shields et al. (1989) who reported $b_p = 0.64$ for pressuremeter tests in the same ice. Figure 5.45 shows this comparison.

According to Figure 5.46, the new $n_p = 1.32$ versus previously calculated $n_p$ values of 1.23 and 1.03, using all tests, or $n_p = 1.88$ and 1.62 when the 1.0 MPa test is ignored.

Figures 5.47 through 5.49 repeat this analysis for the multi-stage test. The magnitude of the $b_p$ values are taken from Figure 5.47, and compared on Figure 5.48 to the $b_p$ values from the single stage tests, and to those determined from the

pressuremeter.

The $n_p$ value determined from the multi-stage test was $n_p = 3.45$ which is better agreement with the pressuremeter test results ($n_p = 2.45$) and is also closer to the value of $n_p = 3$ generally recommended for routine foundation design in ice or ice-rich soils (Morgenstern et al., 1980; Foriero and Ladanyi, 1989).

The various values of $\sigma_{c_p}$, $n_p$, and $b_p$ are summarized and compared on Table 5.8.

### 5.2.5 Compare the Fit of the Power Law Creep Model Versus the Test Data (Displacements Measured at the Ends of the Bar)

This subsection examines how well the power law creep model fits the test data. All displacements are calculated or measured at the ends of the bar, 50 mm off the ice surface at the point of load application.

**Fit of Single Stage Power Law Creep Model Versus Single Stage Tests**

Figures 5.50 through 5.53 compare the pseudo-instantaneous plus primary power law creep model, determined in subsection 5.2.2, versus the actual primary creep test data of the single stage tests. The solid curve on these figures represents the power law creep model determined by taking the best fit through all of the primary creep displacement versus time (log-log plot) data of all tests, while the dashed curve represents the power law creep model determined when analyzing only the straight line portion of the creep displacement versus time (log-log plot) relationship. Both models predict

displacements which are within 20% of the measured displacement. There appears to be little accuracy to be gained by ignoring the very early portions of the creep data in the analysis.

Figures 5.54 through 5.57 present a comparison similar to that in Figures 5.50 through 5.53, but now secondary creep displacement has been added. The comparison is calculated pseudo-instantaneous plus primary plus secondary creep versus the test data. In four of the eight tests, the power law creep curves run through the test data, and in the remaining four tests the agreement is within 20%.

**Fit of Multi-Stage Power Law Creep Model Versus Multi-Stage Test (Displacements Measured at the Ends of the Bar)**

Figures 5.58 through 5.62 compare the power law creep model determined from the multi-stage test results in subsection 5.2.3 with the test data. The effects of averaging are apparent.

In Figure 5.58, the power law creep model is shown versus the entire five stages of the multi-stage test, including the instantaneous plus primary and secondary phases of each stage. In this case the power law creep model from the single stage tests (subsection 5.2.2) was applied to the first stage of the multi-stage test; the power law creep model from the multi-stage test itself was used to describe the succeeding four stages. During three of the five stages, the curve described by the power law creep model runs through the test data, and the agreement is very close in the other two stages.

Figures 5.59 and 5.60 examine the primary creep phase of each multi-stage test in closer detail. Here the model for pseudo-instantaneous plus primary creep is

compared with the measured displacements. The curves described by the model run through the test data, and the agreement is excellent.

Figures 5.60 and 5.61 present a similar comparison to Figures 5.59 and 5.60, but now the combined pseudo-instantaneous plus primary plus secondary creep calculations are used. The curves described by the creep model run through the test data, and the agreement is excellent.

**Fit of Multi-Stage Power Law Creep Model Versus Single Stage Tests (Displacement Measured at Ends of the Bar)**

In foundation engineering, the purpose of performing a multi-stage pile test in the field is to be able to predict how single stage loaded piles will behave over a range of applied loads. Figures 5.63 through 5.70 compare the power law creep model determined from the multi-stage loaded test with the single stage test results.

In Figures 5.63 through 5.66 the comparisons are made for the pseudo-instantaneous plus primary creep phases of the single stage tests. The power law creep model derived from the multi-stage test does not predict well the single stage test data. For each of the eight single stage tests, the model under-predicts bar displacements by at least 50%.

Figures 5.67 through 5.70 repeat the comparison with secondary creep added in. Because both the multi-stage creep test and the single stage creep tests yielded similar secondary creep displacement rates, the agreement now appears more accurate than when just pseudo-instantaneous plus primary creep were compared. The total displacements shown on these figures are predominantly secondary creep displacements.

The agreement of the power law creep model versus the data is discussed in greater detail in Chapter 6.

## 5.3 COMPARISON OF BAR TEST RESULTS VERSUS PRESSUREMETER TEST RESULTS

A preferred method of designing laterally loaded piles is to use the results of pressuremeter tests (Baguelin et al., 1978; Meyerhof, 1985). While this approach is considered routine practice in unfrozen soils, Chapter 2 demonstrated that the practice had not been tested in ice-rich frozen soils and ice.

The comparison between pressuremeter and pile is carried out in 2 parts. First, the creep strains $[(r-r_o)/r_o]$ from the pressuremeter tests of Kjartanson (1986) are compared to the normalized creep displacements (y/a) of the bar where:

- $r$ = the pressuremeter cavity radius at time t
- $r_o$ = the initial cavity radius of the pressuremeter tests (here at time t = 1 minute)
- $y$ = the creep displacement of the bar
- $a$ = the radius of the bar.

Recall that the bar radius and the initial cavity radius of the pressuremeter test were approximately the same, so there are no scale effects to consider.

Second, the pressuremeter primary and secondary power law constitutive creep parameters for the ice, as deduced from Kjartanson's (1986) data by Shields et al. (1989), are inserted into (a) the primary creep power law model of Rowley et al. (1973, 1975) for laterally loaded bars, and (b) Nixon's (1984) secondary creep model for

laterally loaded piles. The combined primary and secondary creep model predictions are then compared to the bar test data.

### 5.3.1 Direct Comparison of Pressuremeter Versus Bar Data

A direct visual comparison of Kjartanson's (1986) single stage loaded pressuremeter creep data with the single stage bar creep data is presented on Figures 5.71 through 5.76. Figures 5.71 through 5.73 compare the early creep portions of the tests, while Figures 5.74 through 5.76 examine the entire creep curves. The pressuremeter data is Kjartanson's (1986), as published by Shields et al. (1989). Only creep is considered for both the pressuremeter and the bar, because the pseudo-instantaneous response for Kjartanson's (1986) tests is not known. The main findings of the direct visual comparison are discussed below.

The comparison of the early portions of the single stage loaded tests is made on Figures 5.71 through 5.73 for pressures of 1.00, 1.25, 1.50, 1.75, 2.00 and 2.25 MPa. (The term "early" is used because primary creep did not end at the same elapsed time for pressuremeter and bar tests.) The figures show data to the end of primary creep for the pressuremeter tests, for which the primary creep phase lasted longer than for the bar tests.

During the early portions of the tests, the ends of the bar experienced substantially larger normalized displacements, y/a, than the corresponding pressuremeter tests. This was true for all pressures from 1.00 MPa to 2.25 MPa.

At the same time, however, the midpoint of the bar (available for p = 1.00, 1.25, 1.75 and 2.25 MPa) tracked only slightly below the pressuremeter test.

Figures 5.74 through 5.76 compare primary plus secondary plus tertiary creep of the pressuremeter test with primary plus secondary creep of the bar. Because the pressuremeter test moves directly from primary creep into tertiary (accelerating) creep, pressuremeter creep strains soon overtake the bar. During the latter stages of the pressuremeter's tertiary creep phase, neither the normalized creep displacements of the end of the bar, nor the normalized creep displacements of the midpoint of the bar track the pressuremeter test.

### 5.3.2 Comparison of Bar Data Versus Power Law Creep Model Using Creep Parameters from the Pressuremeter Test

In this subsection, the creep parameters $\sigma_c$, n, and b as determined from the pressuremeter tests by Shields et al. (1989) are inserted into the power law creep models for primary and secondary creep for the bar, and these models are then used to predict the behaviour for the bar. The pressuremeter creep parameters are listed on Table 5.4 for primary creep and on Figure 5.35 for secondary creep. This is the approach which might be taken in geotechnical engineering practice when, for example, designing laterally loaded piles. The primary creep model is Rowley et al.'s (1973, 1975) model for laterally loaded piles as represented by Equation (2.24), while the secondary creep model is Nixon's (1984) represented by Equation (2.25).

In applying the model the following assumptions were followed:

1. The duration of the primary creep phases were taken from the pressuremeter tests, as listed on Table 5.2 (where they are also compared to the end of primary creep for the bar tests). Primary creep always lasted longer during pressuremeter

testing than during the bar tests, but the correspondence between the two has not been established. A designer would probably have only the pressuremeter tests.

2. Two assumptions (trials) were considered in modelling secondary creep. In Trial 1 the minimum creep strain rates $[(r-r_o)/r_o]$ $hr^{-1}$ from the pressuremeter tests were assumed to directly represent the secondary normalized creep displacement rate (y/a) $hr^{-1}$ for the bar tests. This correspondence has previously been proposed in the literature (Kenyon et al., 1990). In Trial 2, the minimum pressuremeter strain rates are reduced by (1/1.3), because this thesis has determined that the minimum strain rate of the pressuremeter test was 1.3 times faster (subsection 5.2.3.4) than the normalized secondary displacement rate of the corresponding bar test.

The prediction of the model is compared to the test data on Figures 5.77 to 5.82. The main findings of the comparison are:

1. During the early portions of the tests (Figures 5.77 through 5.79), the model under-predicts the creep displacements of the ends of the bar, and slightly over-predicts the creep displacements of the midpoint of the bar.

2. When primary creep and secondary creep are both considered (Figures 5.80 through 5.82), and when the pressuremeter determined minimum strain rates are reduced by (1/1.3) i.e. Trial 2, then there is close agreement between the creep model and the bar data.

**TABLE 5.1 Summary of Pseudo-Instantaneous Displacements from the Single Stage Tests**

| Test No. | Target Q (kN) | Target p (MPa) | Q @ 1 min. (kN) | % of Target Q @ 1 min. (%) | pB @ 1 min. (MPa-mm) | Lateral Displacement, y, @ 1 min. (mm) |
|---|---|---|---|---|---|---|
| 5 | 46.5 | 2.00 | 13.9 | 29.9 | 45.6 | 0.16 |
| 6 | 40.7 | 1.75 | 25.0 | 61.4 | 82.0 | 0.31 |
| 7 | 34.8 | 1.50 | 13.1 | 37.6 | 43.0 | 0.18 |
| 8 | 52.3 | 2.25 | 49.3 | 94.3 | 161.7 | 0.82 |
| 9 | 52.3 | 2.25 | 30.3 | 57.9 | 99.3 | 0.38 |
| 10 | 40.7 | 1.75 | 39.3 | 96.6 | 129.0 | 0.61 |
| 11 | 23.3 | 1.00 | 17.9 | 76.8 | 58.8 | 0.43 |
| 12 Stage 1 | 29.0 | 1.25 | 23.5 | 81.0 | 77.0 | 0.31 |

Notes:

1. Q is the lateral load applied at the top and bottom end of the bar, i.e. total load forcing the bar sideways = 2Q.

2. p is the equivalent lateral pressure, assuming a uniform pressure distribution.

$$p = 2Q / (\text{projected frontal area of bar}) = 2Q / (B \times L)$$

where B = bar diameter
and L = embedded length

**TABLE 5.2**

**Summary of Analysis to Determine the Time to the End of Primary Creep for Single Stage Bar Tests Versus Equivalent Single Stage Pressuremeter Tests (Shields et al., 1989)**

| Test No. | Target Pressure p (MPa) | Time to End of Primary Creep BAR TESTS | | | | PMT | |
|---|---|---|---|---|---|---|---|
| | | (1) Creep vs Time (Log-Log Plot) (hrs) | (2) Creep Rate vs. Time (Log-Log Plot) (hrs) | (3) Creep Rate vs. Time (Arithmetic Plot) (hrs) | Best Fit Through (1), (2), (3) (hrs) | Creep Strain Rate vs. Time (log-log) (hrs) | Bending Strain Becomes Constant (hrs) |
| 5 | 2.00 | 5 | 5 | 5 | 6 | 13 | N/A |
| 6 | 1.75 | 12 | 6 | 9 | 9 | 17 | N/A |
| 7 | 1.50 | ≈ 12 | ≈ 20 | 21 | 14 | 25 | N/A |
| 8 | 2.25 | 4 | 5 | 5 | 5 | 8 | N/A |
| 9 | 2.25 | 4.5 | 5 | 5 | 5 | 8 | 4.5 |
| 10 | 1.75 | 12 | 12 | 12 | 9 | 17 | 12 |
| 11 | 1.00 | 40 | 30 | 36 | 39 | 270 | - |
| 12 Stage 1 | 1.25 | 20 | 20 | - | 22 | 100 | 20 |

Note:

1. Time to end of primary creep (hrs) = $38.9 \times p^{-2.58}$, where p is expressed in MPa (see Figure 5.11).
2. Time to end of primary creep for single stage pressuremeter tests taken from Figure 5.2 (after Shields et al., 1989).

## TABLE 5.3

**Summary of $b_p$ and F Values Determined from Single Stage Test Results Using Creep Displacements of the Ends of the Bar**

| Test No. | Equiv. Frontal Pressure p (MPa) | Best Fit Through All Primary Creep | | Best Fit Through Straight Line Portion of Primary Creep | | Using Creep Displacement of Mid-point of Bar | |
|---|---|---|---|---|---|---|---|
| | | $b_p$ | F @ 1 hr | $b_p$ | F @ 1 hr | $b_p$ | F @ 1 hr |
| 5 | 2.00 | 0.265 | 0.0150 | 0.221 | 0.0155 | N/A | N/A |
| 6 | 1.75 | 0.246 | 0.0138 | 0.167 | 0.0144 | N/A | N/A |
| 7 | 1.50 | 0.258 | 0.0093 | 0.245 | 0.0094 | N/A | N/A |
| 8 | 2.25 | 0.284 | 0.0208 | 0.220 | 0.0214 | N/A | N/A |
| 9 | 2.25 | 0.266 | 0.0167 | 0.229 | 0.0170 | 0.611 | 0.209 |
| 10 | 1.75 | 0.283 | 0.0126 | 0.210 | 0.0135 | 0.567 | 0.122 |
| 11 | 1.00 | 0.231 | 0.0088 | 0.144 | 0.0102 | 0.410 | 0.046 |
| 12 Stage 1 | 1.25 | 0.337 | 0.0059 | 0.212 | 0.0074 | 0.459 | 0.085 |
| Average $b_p$ | | 0.271 | - | 0.206 | - | 0.512 | - |

Note:

1. $b_p$ from pressuremeter testing = 0.64 (Shields et al., 1989), when results are corrected for stress redistribution after Murat et al. (1986).

2. $b_p$ from pressuremeter testing = 0.50 using test data with no corrections (Shields et al., 1989).

## TABLE 5.4

**Summary of Primary Creep Parameters $\sigma_{c_p}$ , $n_p$, $b_p$ Determined from the Single Stage Test Results (Creep Displacements of Ends of Bar)**

| Type of Test | Method of Interpreting Data | $\sigma_{c_p}$ [1] (MPa) | $n_p$ | $b_p$ |
|---|---|---|---|---|
| Bar Single Stage | Best fit through all primary creep data. | 19.7 | 1.23 | 0.271 |
| | Best fit through straight line portion of primary creep data. | 51.9 | 1.03 | 0.206 |
| | Best fit through all primary creep data, ignoring 1.0 MPa test. | 6.5 | 1.88 | 0.271 |
| | Best fit through straight line portion of primary creep data, ignoring 1.0 MPa test. | 12.0 | 1.62 | 0.206 |
| | Best fit using creep displacement of midpoint of bar. | 14.3 | 1.32 | 0.512 |
| Pressuremeter Single Stage | Pressuremeter testing (Shields et al., 1989). See Note 2. | 1.97 | 2.47 | 0.64 |
| Compression Testing | Compression creep tests (Azizi, 1989). | $\approx 4$ | 2.43 | 0.64 |

Notes:

1. $\dot{\epsilon}_c = 0.0006 hr^{-1}$

## TABLE 5.5

**Summary of Secondary Creep Rates for All Bar Tests and Minimum Strain Rates for Kjartanson's (1986) Single Stage Pressuremeter Tests**

| Bar Tests | | Secondary Creep Displacement Rates (Bar Tests) | | | |
|---|---|---|---|---|---|
| | | Single Stage Tests | | Multi-Stage Test | |
| # | (MPa) | (mm/hr) | y/a/hr | (mm/hr) | y/a/hr |
| 5 | 2.00 | 0.054 | 0.00143 | - | |
| 6 | 1.75 | 0.033 | 0.000874 | - | |
| 7 | 1.50 | 0.018 | 0.000477 | - | |
| 8 | 2.25 | 0.100 | 0.002649 | - | |
| 9 | 2.25 | 0.081 | 0.00215 | - | |
| 10 | 1.75 | 0.032 | 0.000848 | - | |
| 11 | 1.00 | 0.004 | 0.000106 | - | |
| 12 Stage 1 | 1.25 | 0.009 | 0.000238 | - | |
| 12 Stage 2 | 1.50 | - | - | 0.016 | 0.000424 |
| 12 Stage 3 | 1.75 | - | - | 0.031 | 0.000821 |
| 12 Stage 4 | 2.00 | - | - | 0.061 | 0.001616 |
| 12 Stage 5 | 2.25 | - | - | 0.101 | 0.00268 |
| Pressuremeter Tests Minimum Creep Strain Rates $(\frac{r-r_o}{r_o})$ /hr | | | | | |
| | 1.0 | - | 0.000139 | (+1.31) | |
| | 1.25 | - | 0.000322 | (+1.35) | |
| | 1.50 | - | 0.000634 | (+1.33) | |
| | 1.75 | - | 0.00114 | (+1.30,) (1.34) | compared to bar tests |
| | 2.00 | - | 0.00189 | (+1.32) | |
| | 2.25 | - | 0.00293 | (+1.07,) (1.36) | |

Notes: y = bar creep displacement; a = bar radius; r = pressuremeter cavity radius; $r_o$ = pressuremeter cavity radius at t = 1 minute.

## TABLE 5.6

**Summary of Analysis to Determine the End of Primary Creep During Each Stage of Multi-Stage Test**

| Test # 12, Stage # | Target Pressure p (MPa) | Time to End of Primary Creep | | | | |
|---|---|---|---|---|---|---|
| | | Creep vs Time (Log-Log Plot) (hrs) | Creep Rate vs. Time (Log-Log Plot) (hrs) | Creep Rate vs. Time (Arithmetic Plot) (hrs) | Best Fit Through All Data (hrs) | Bending Strain Becomes Constant (hrs) |
| 2 | 1.50 | 12 | 14.0 | 14.0 | 10.0 | 8.0 |
| 3 | 1.75 | 4 | 4.0 | 4 | 5.4 | 4.0 |
| 4 | 2.00 | 3.5 | 6.5 | 6.4 | 3.2 | 3.6 |
| 5 | 2.25 | 1.7 | 1.7 | 1.6 | 2.0 | 2.6 |

Note:

1. BEST FIT TIME (hrs) = $p^{-4.00}$ x 50.8 where p is expressed in MPa.

## TABLE 5.7

**Summary of Creep Displacements at End of Primary Creep (Multi-Stage Test)**

| Test # 12, Stage # | Target Pressure p (MPa) | Time to End of Primary Creep | | | | |
|---|---|---|---|---|---|---|
| | | (1) Creep vs Time (Log-Log Plot) (%) | (2) Creep Rate vs. Time (Log-Log Plot) (%) | (3) Creep Rate vs. Time (Arithmetic Plot) (%) | Best Fit Through (1), (2), (3) (%) | Bending Strain Becomes Constant (%) |
| 2 | 1.50 | 0.85 | 1.00 | 1.00 | 0.73 | 0.73 |
| 3 | 1.75 | 0.64 | 0.64 | 0.64 | 0.64 | 0.64 |
| 4 | 2.00 | 0.93 | 1.49 | 1.48 | 0.94 | 0.94 |
| 5 | 2.25 | 0.84 | 0.84 | 0.82 | 1.11 | 1.11 |

## TABLE 5.8

**Summary of $b_p$ and F Values Determined from Multi-Stage Test Results**

| Test 12 Stage No. | Equiv. Frontal Pressure p (MPa) | Best Fit Through All Primary Creep | | Best Fit Through Straight Line Portion of Primary Creep | | Using Creep Displacement of Mid-point of Bar | |
|---|---|---|---|---|---|---|---|
| | | $b_p$ | F @ 1 hr | $b_p$ | F @ 1 hr | $b_p$ | F @ 1 hr |
| 2 | 1.50 | 0.651 | 0.0013 | 0.504 | 0.0016 | 0.710 | 0.0005 |
| 3 | 1.75 | 0.574 | 0.0019 | 0.574 | 0.0019 | 0.542 | 0.0010 |
| 4 | 2.00 | 0.583 | 0.0028 | 0.583 | 0.0028 | 0.824 | 0.0014 |
| 5 | 2.25 | 0.363 | 0.0038 | 0.467 | 0.0040 | 0.627 | 0.0022 |
| Average $b_p$ | | 0.54 | | 0.53 | | | |

## TABLE 5.9

**Summary of Primary Creep Parameters $\sigma_{c_p}$ , $n_p$, $b_p$ Determined from the Multi-Stage Test Results (As Compared to the Results of Other Tests)**

| Type of Test | Method of Interpreting Data | $\sigma_{c_p}$ (MPa) [1] | $n_p$ | $b_p$ |
|---|---|---|---|---|
| Bar Multi-Stage Test | Best fit through all primary creep. | 2.77 | 2.70 | 0.54 |
| | Best fit through straight line portion of primary creep. | 3.56 | 2.37 | 0.53 |
| | Best fit using creep displacement of midpoint of bar. | 1.65 | 3.45 | 0.67 |
| Bar Single Stage | Best fit through all primary creep data. | 19.7 | 1.23 | 0.271 |
| | Best fit through straight line portion of primary creep data. | 51.9 | 1.03 | 0.206 |
| | Best fit through all primary creep data, ignoring 1.0 MPa test. | 6.5 | 1.88 | 0.271 |
| | Best fit through straight line portion of primary creep data, ignoring 1.0 MPa test. | 12.0 | 1.62 | 0.206 |
| | Best fit using creep displacement of midpoint of bar. | 14.3 | 1.32 | 0.512 |
| Pressuremeter Single Stage | Pressuremeter testing (Shields et al., 1989). | 1.97 | 2.47 | 0.64 |
| Compression Testing | Compression creep tests (Azizi, 1989). Single stage tests. | $\approx$ 4 | 2.43 | 0.64 |

Notes:

1. $\dot{\epsilon}_c = 0.0006 hr^{-1}$

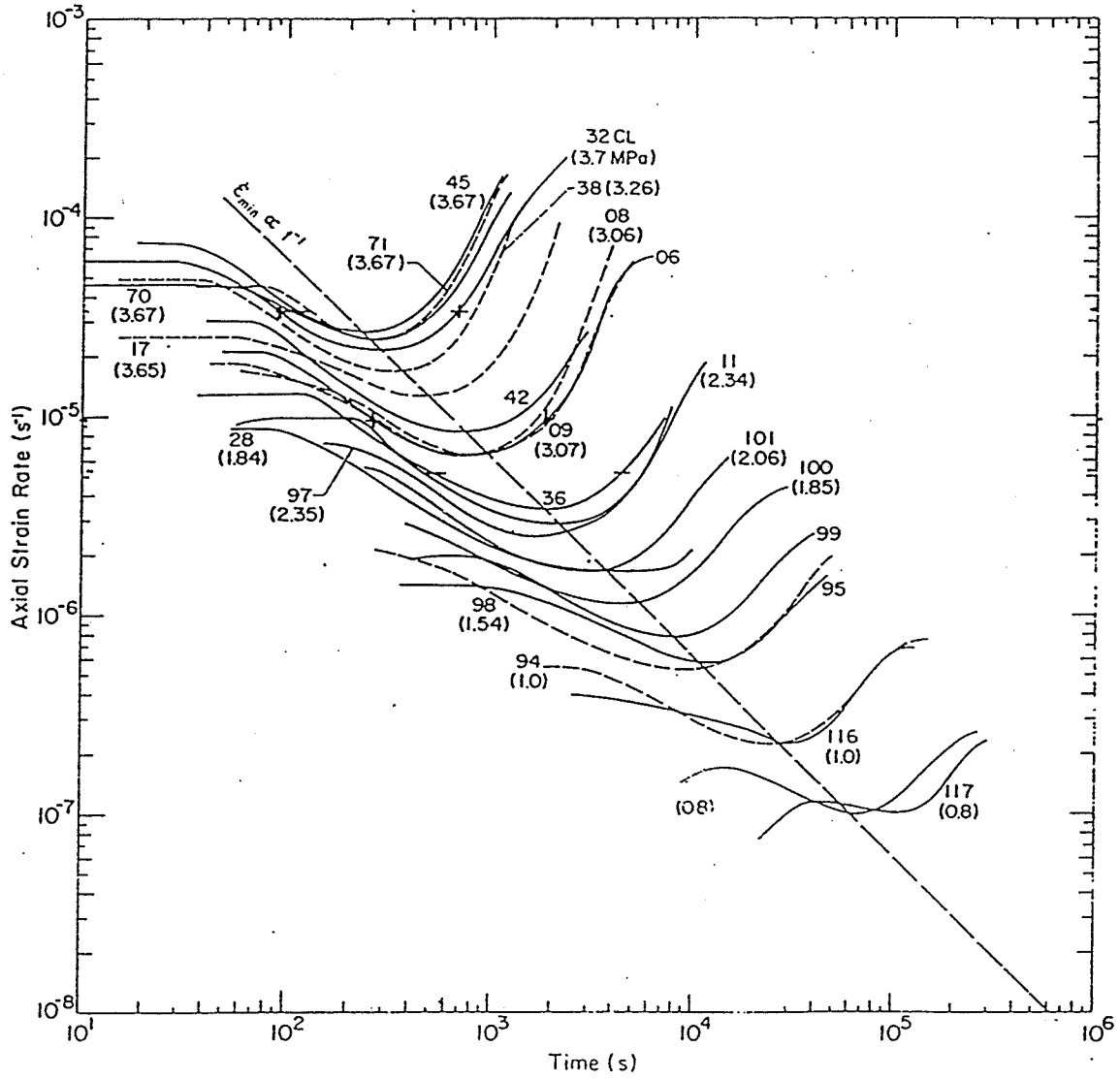


Figure 5.1 Determination of the end of primary creep of ice in uniaxial creep (after Mellor and Cole, 1982).

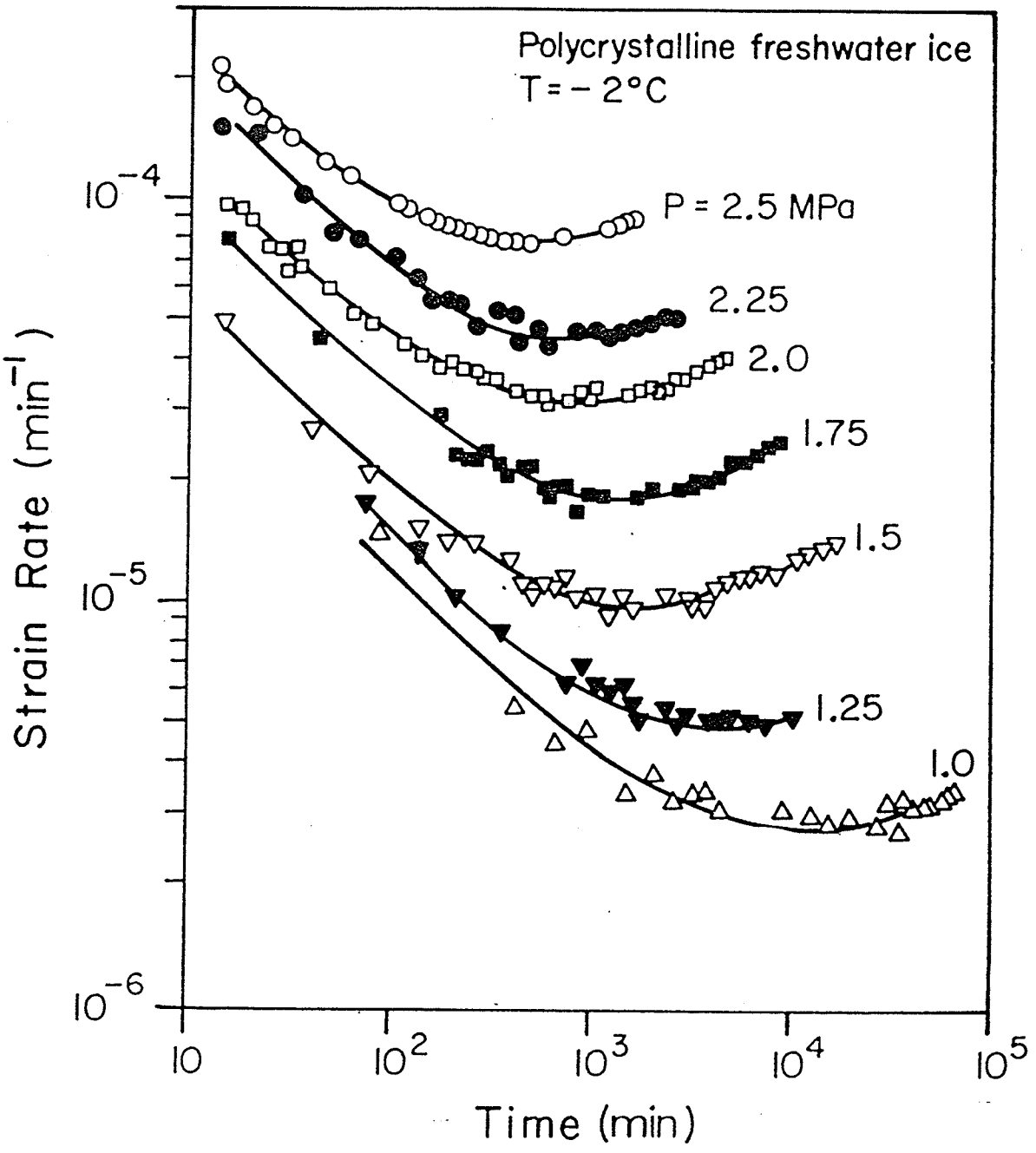


Figure 5.2 Determination of the end of primary creep of ice from pressuremeter testing (after Shields et al., 1989).

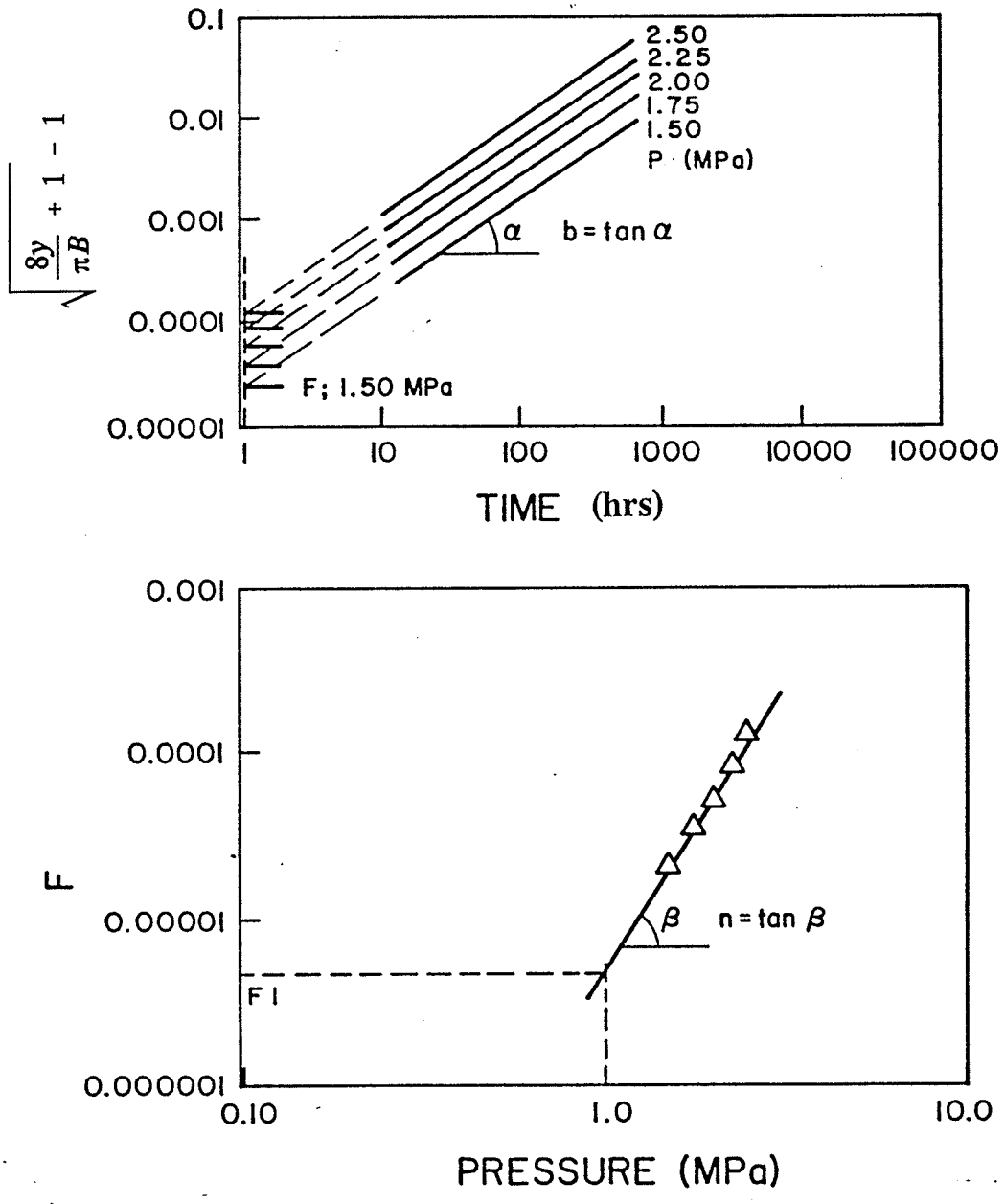


Figure 5.3 Typical graphical procedure to determine the primary creep parameters n, b for the bar tests (after Andersland et al., 1978).

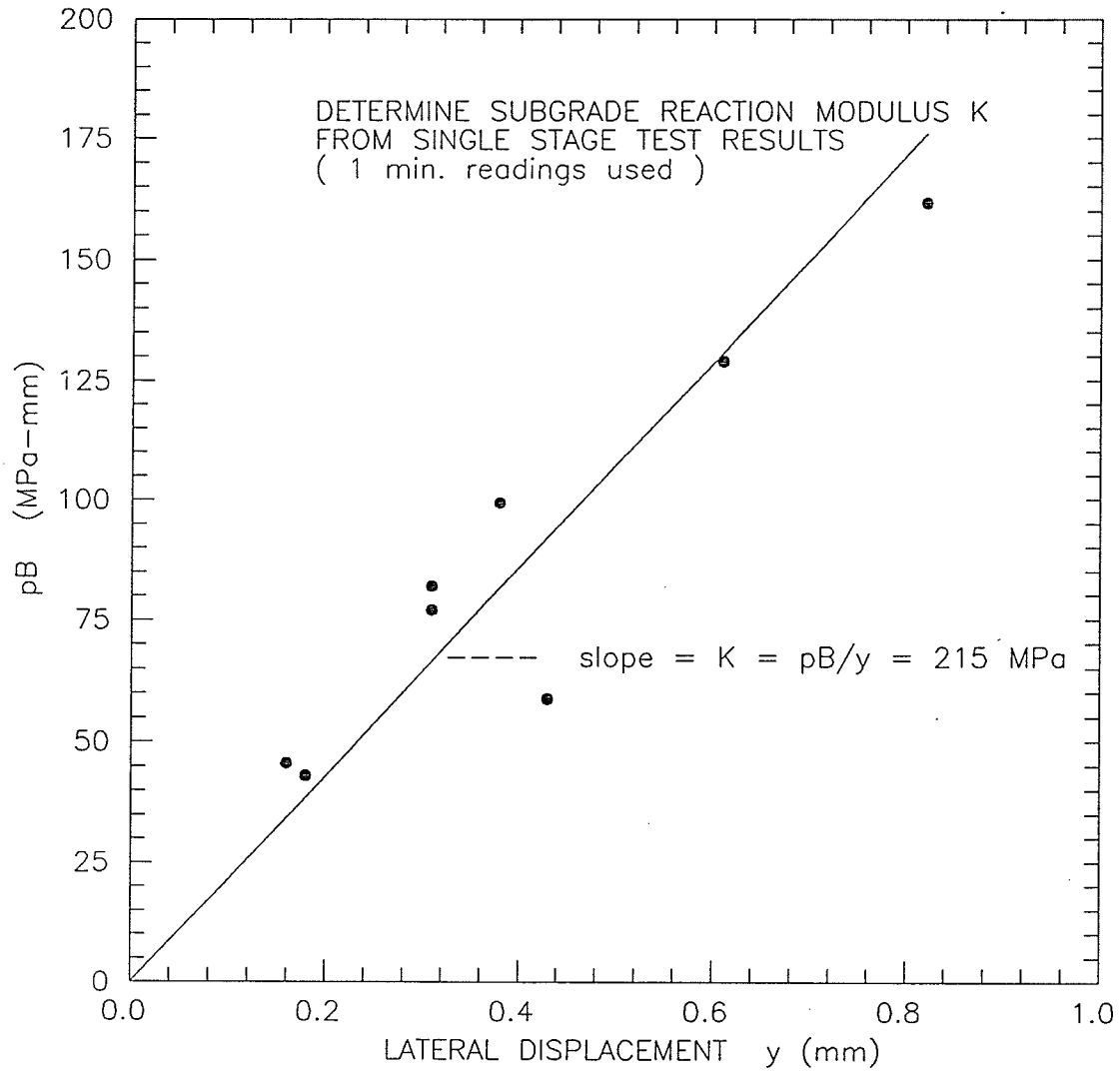


Figure 5.4 pB-y relationship for single stage tests.

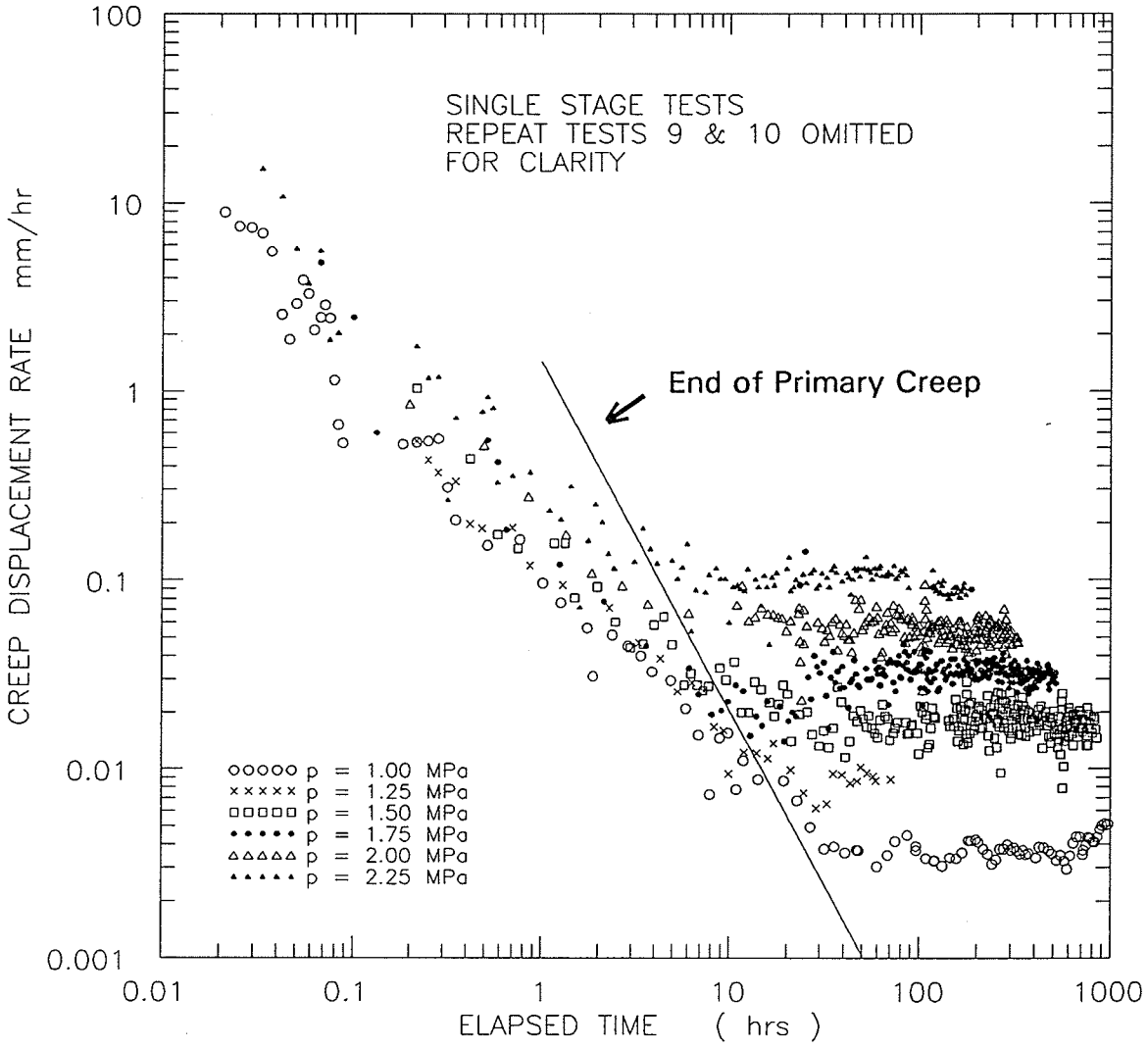


Figure 5.5 Summary of creep displacement rates versus elapsed time (log-log) for single stage bar tests.

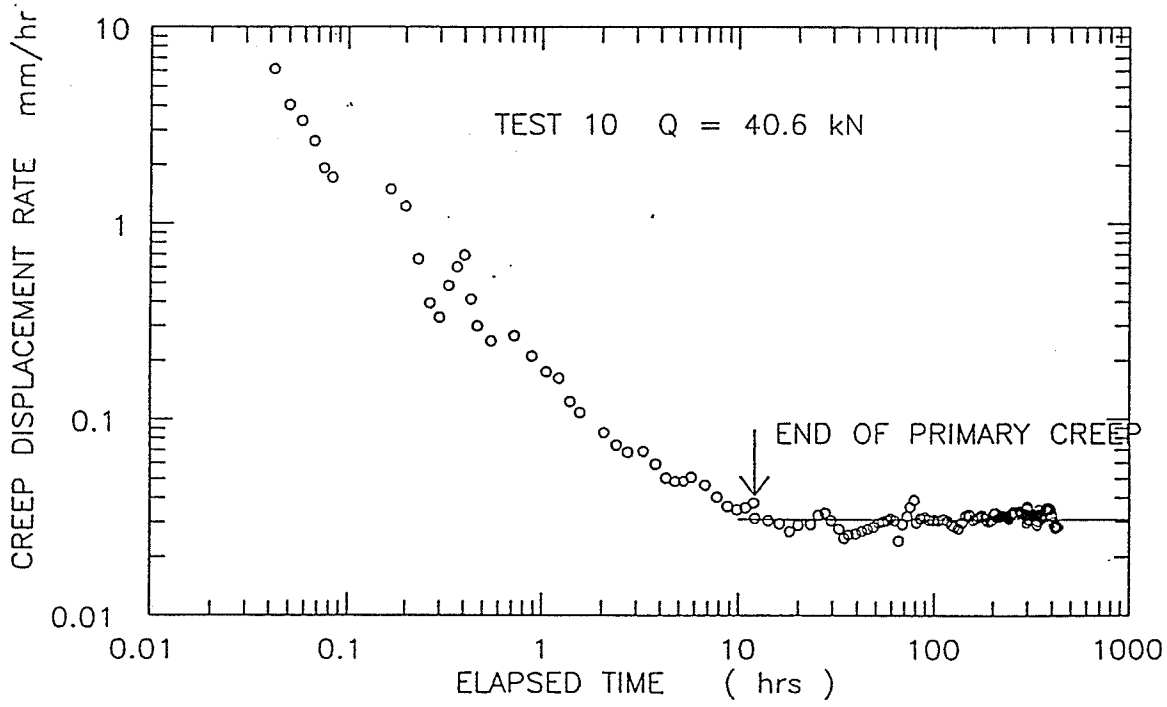


Figure 5.6 Creep displacement rates versus time (log-log) for Test 10.

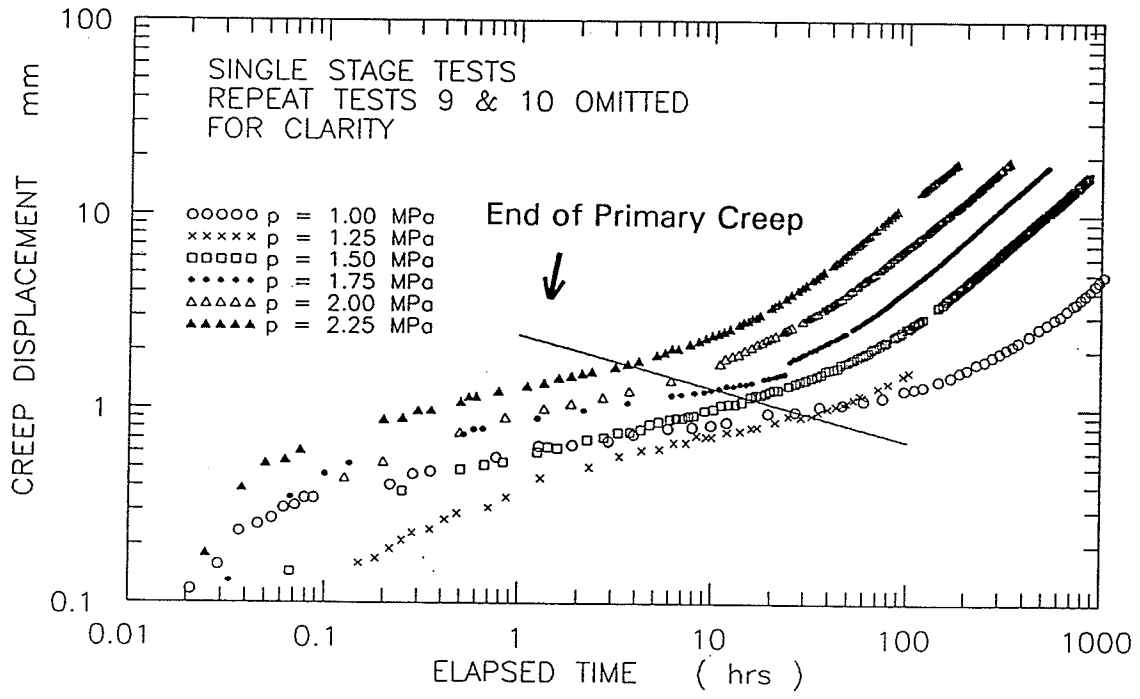


Figure 5.7 Summary of creep displacement versus time for single stage bar tests.

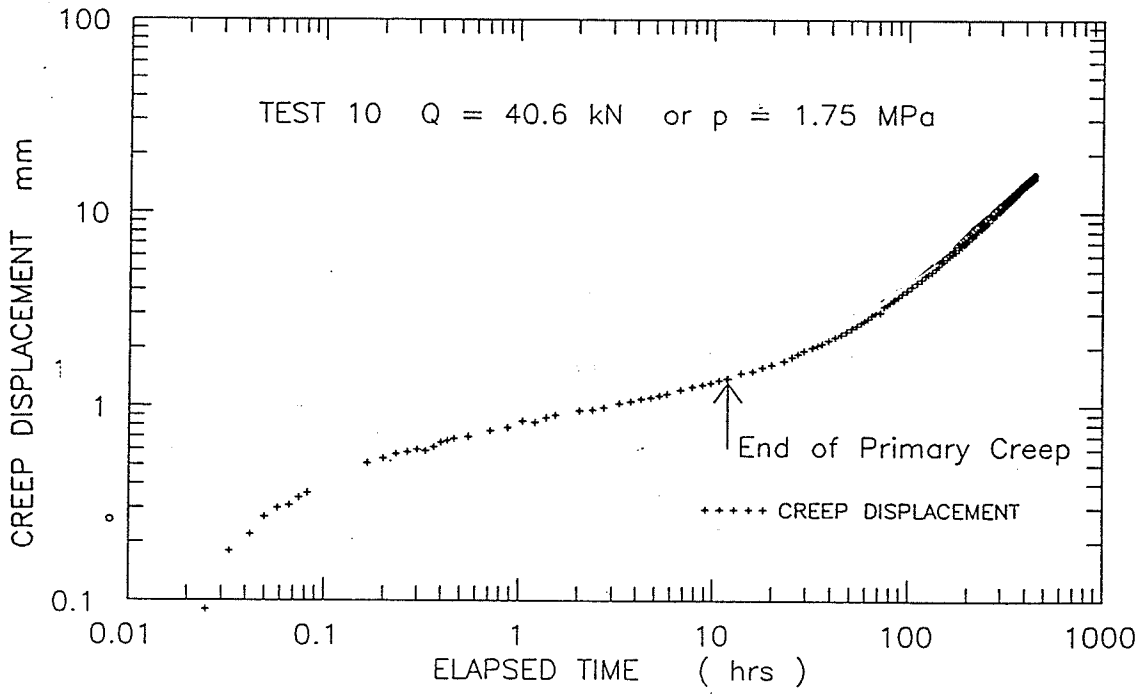


Figure 5.8 Creep displacement versus time (log-log) for Test 10.

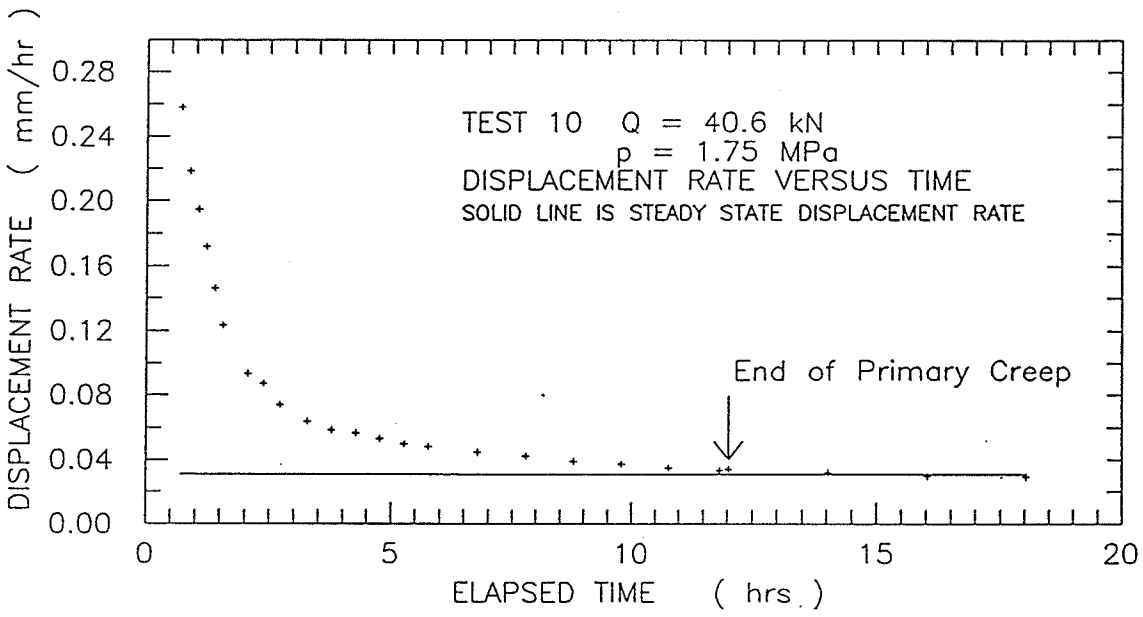


Figure 5.9 Creep displacement versus time (arithmetic space) for Test 10.

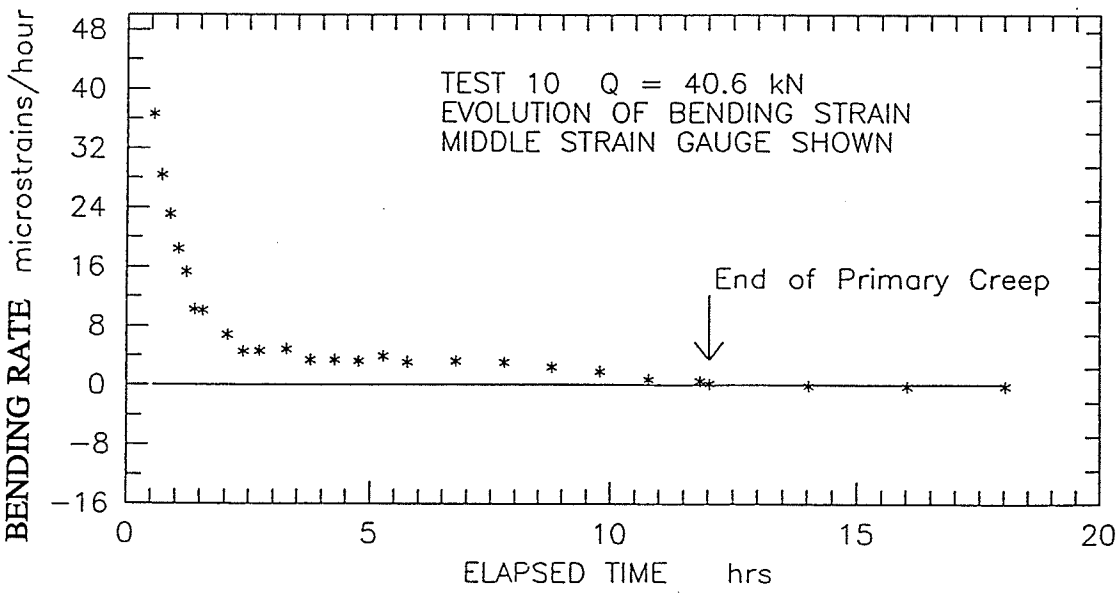


Figure 5.10 Rate of change of bending strain versus time for Test 10.

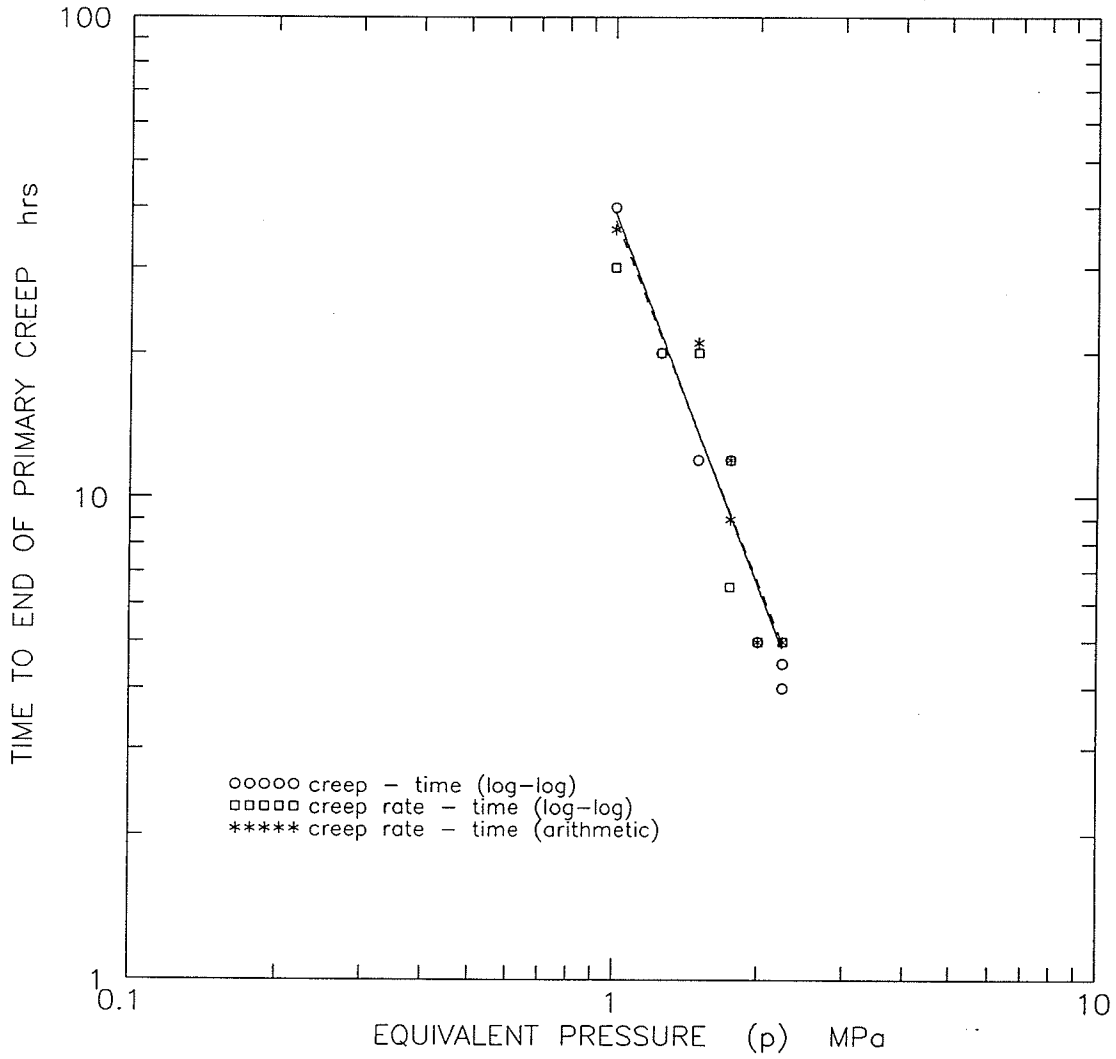


Figure 5.11 Summary of time to end of primary creep versus applied frontal pressure, single stage tests.

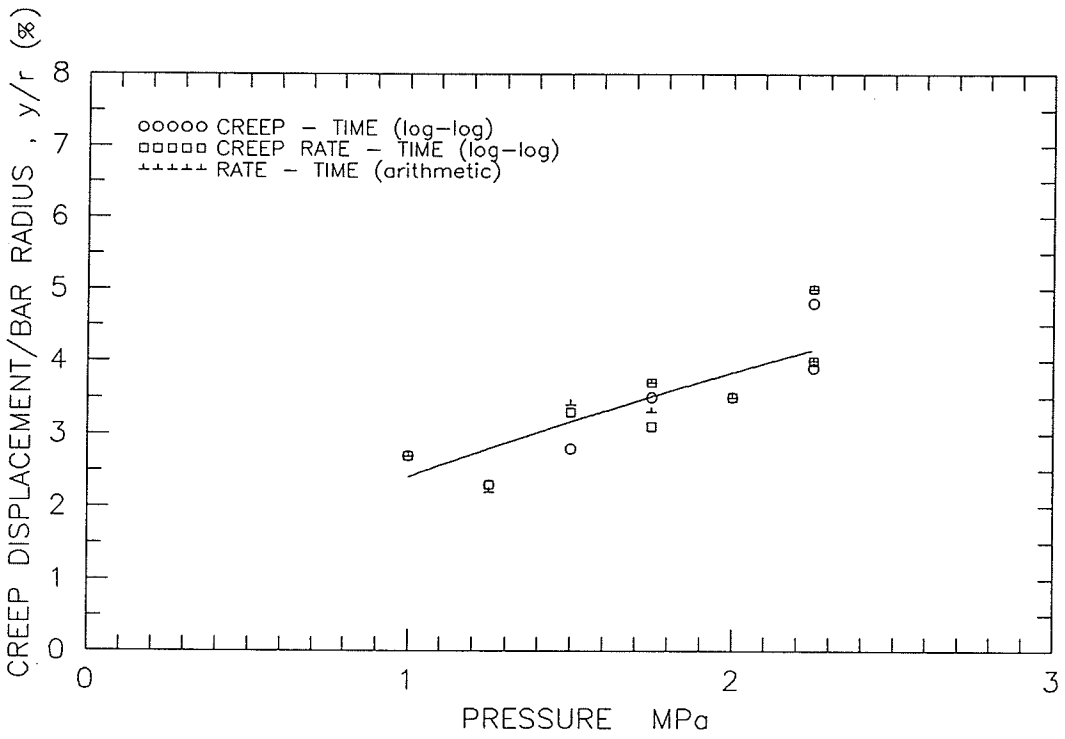


Figure 5.12 Summary of creep displacement at end of primary creep versus applied frontal pressure, single stage tests. Note that creep displacement is normalized with respect to bar radius.

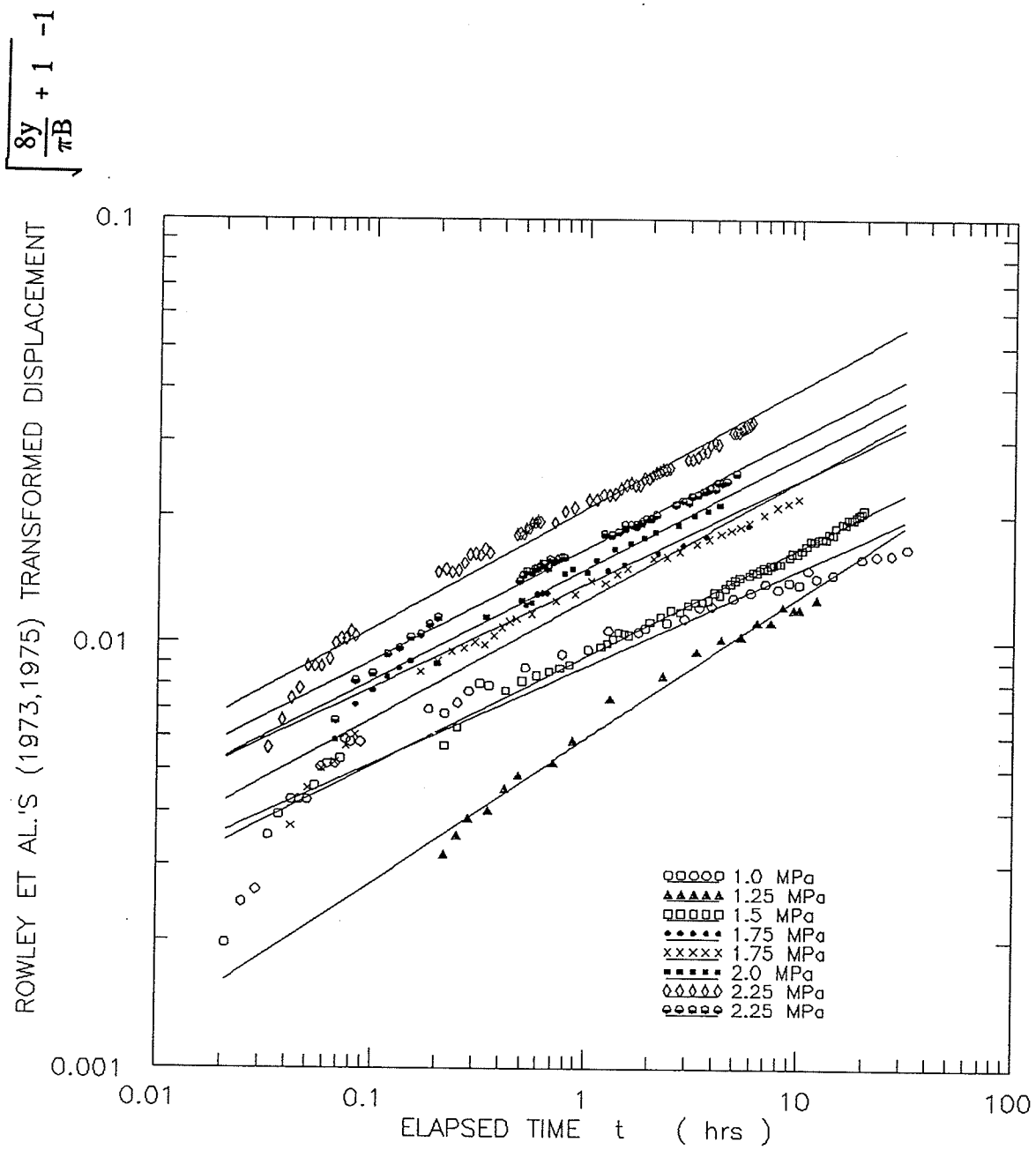


Figure 5.13 Summary of determination of '$b_p$', taking best fit through all primary creep data (single stage tests).

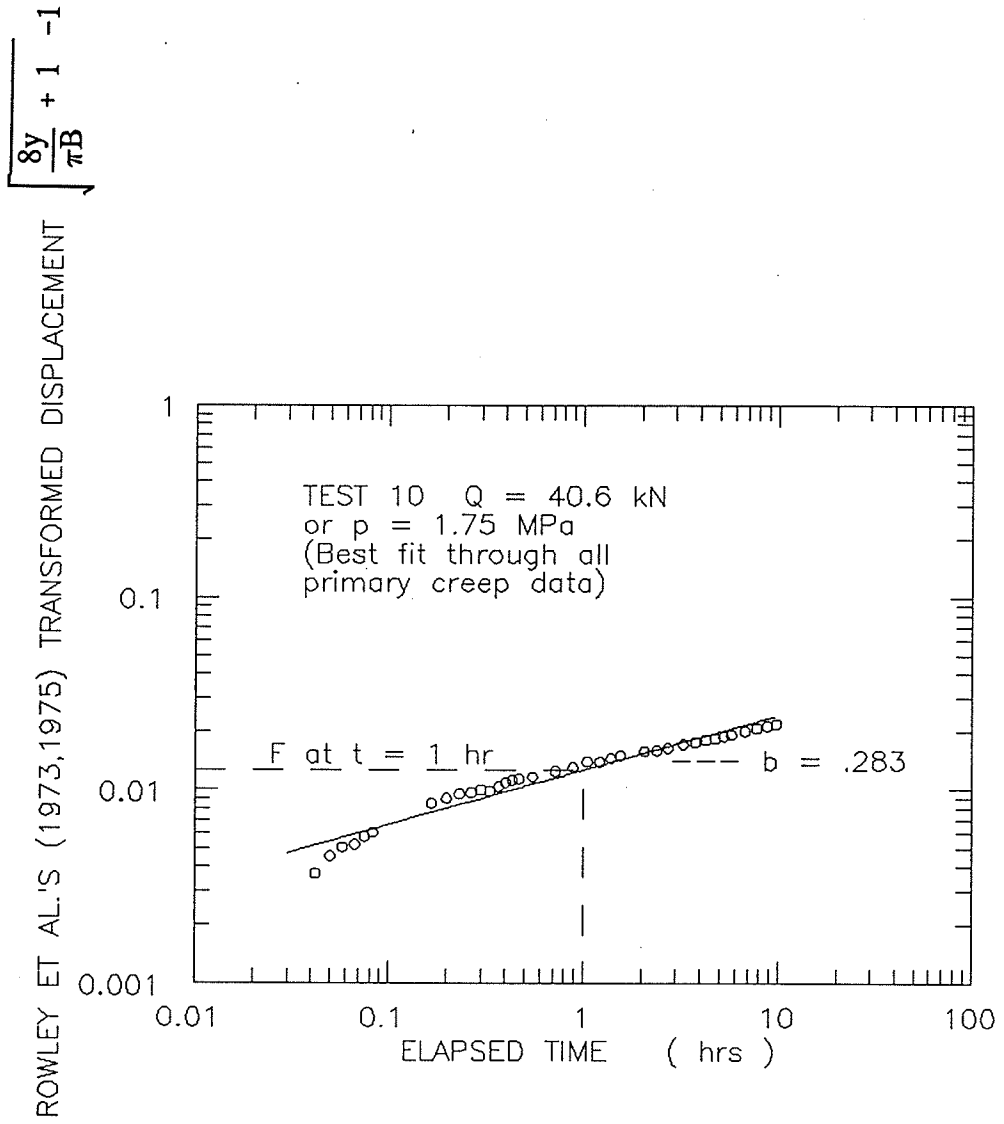


Figure 5.14 Typical determination of '$b_p$', taking best fit through all primary creep data (single stage tests).

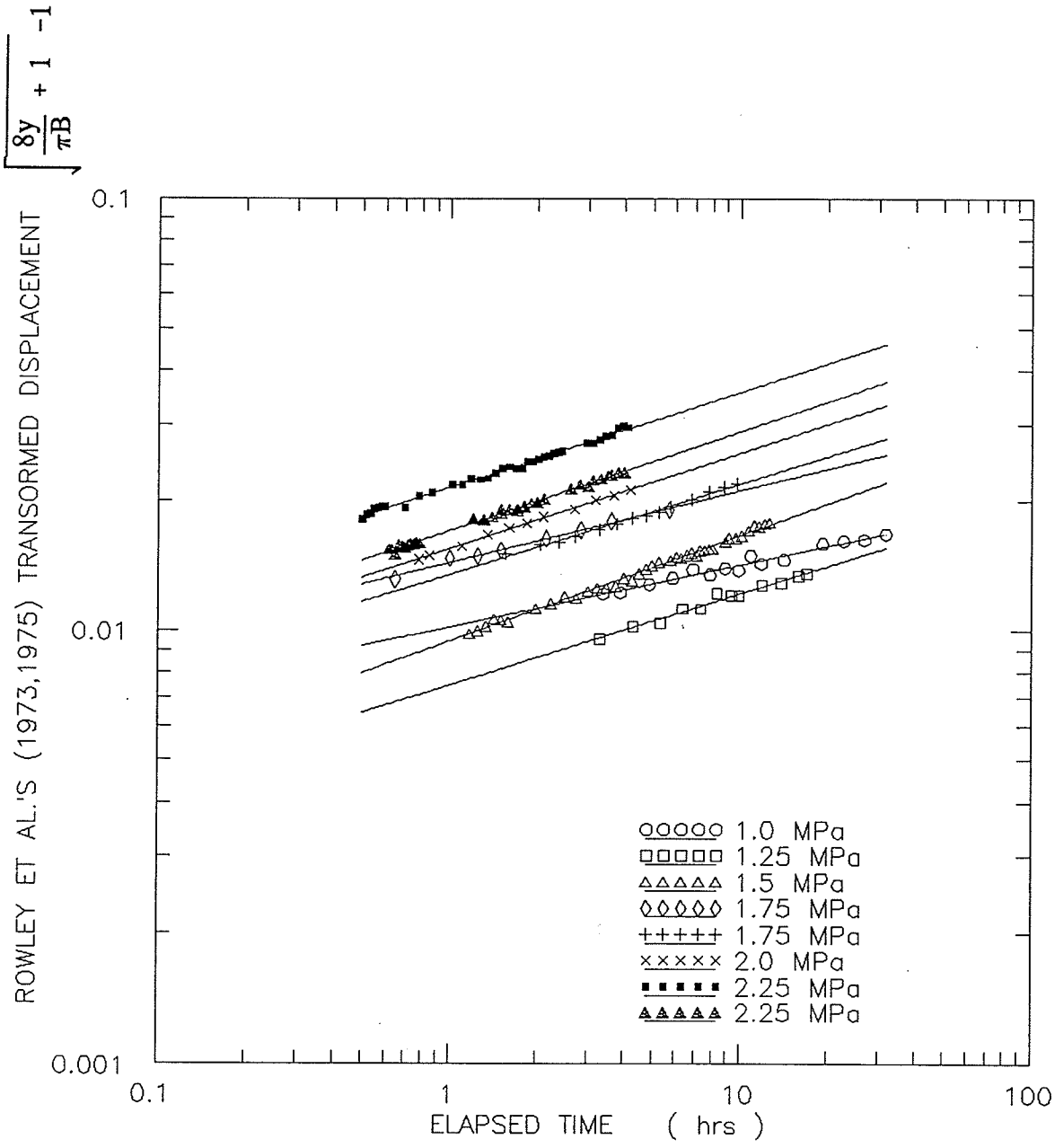


Figure 5.15 Summary of determination of '$b_p$', taking best fit through straight line portion of primary creep data (single stage tests).

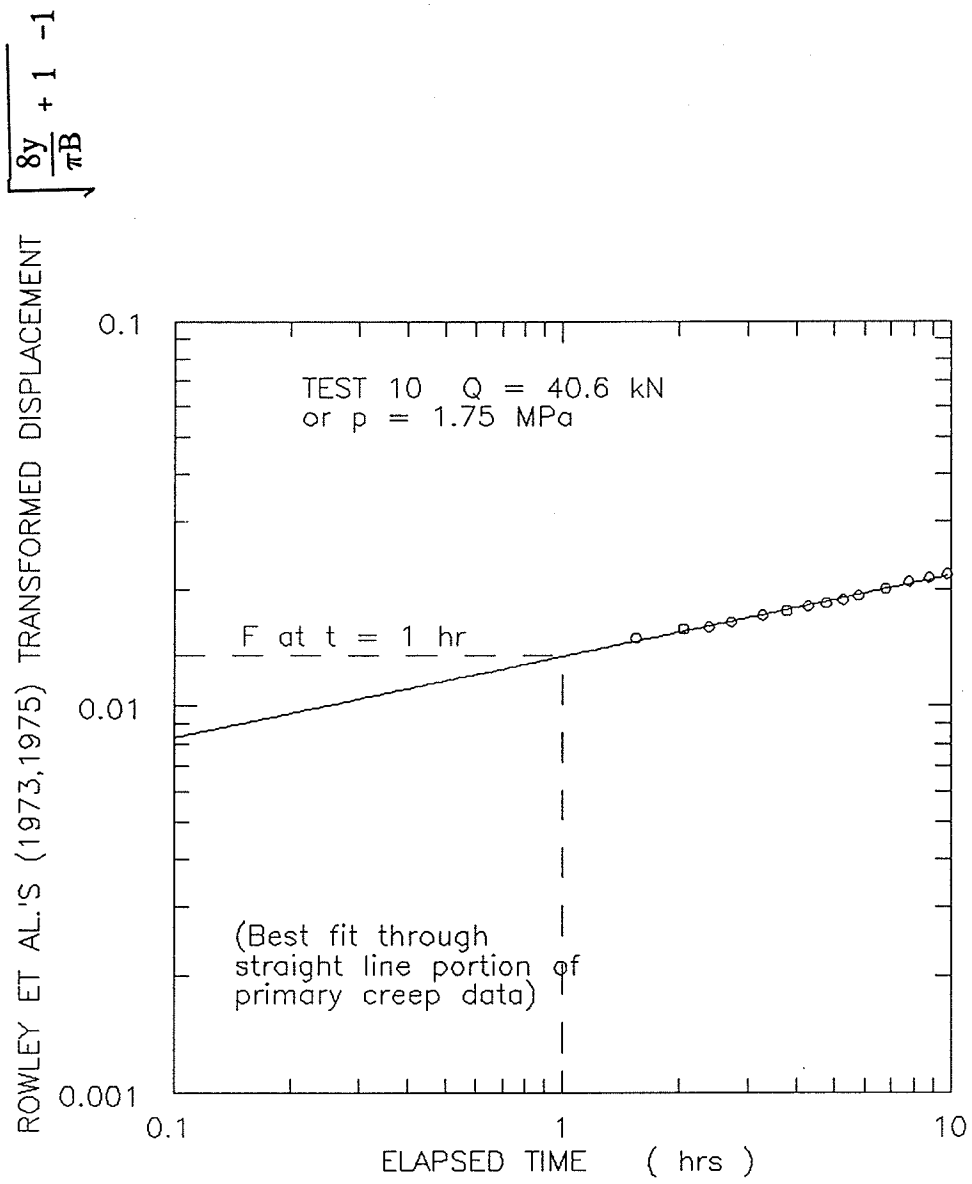


Figure 5.16 Typical determination of '$b_p$', taking best fit through straight line portion of primary creep data (single stage tests).

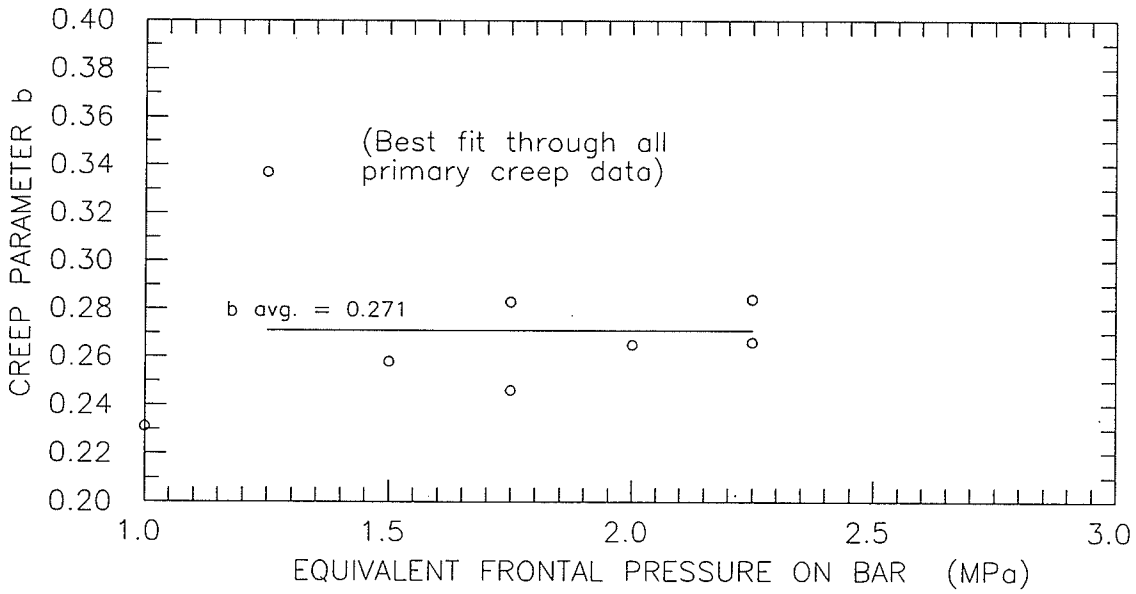


Figure 5.17 Sensitivity of '$b_p$' versus pressure.
Best fit through all primary creep data.

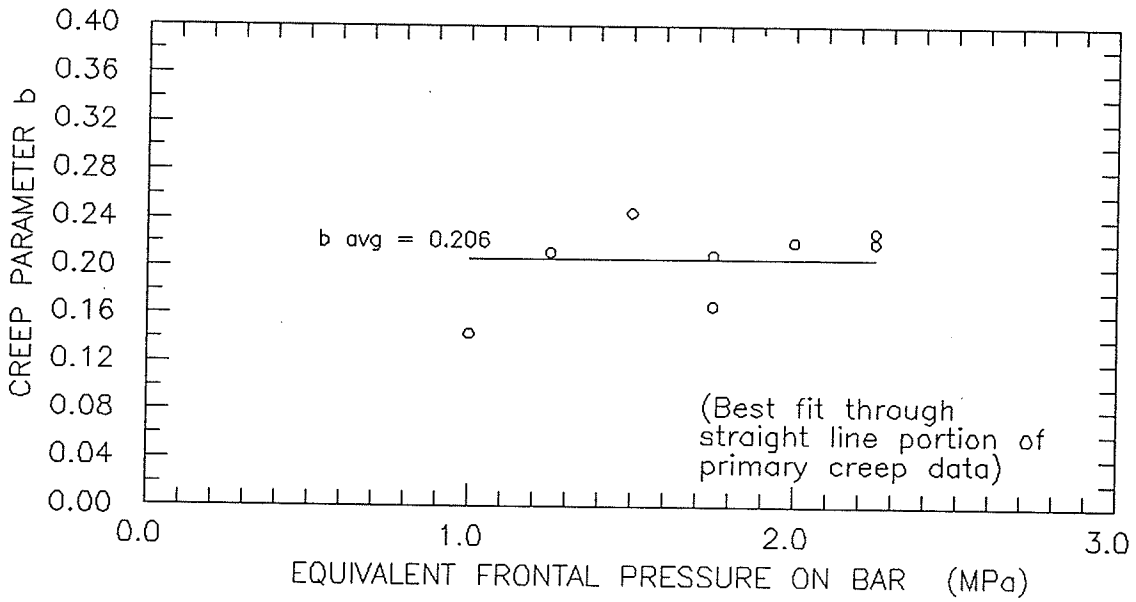


Figure 5.18 Sensitivity of '$b_p$' versus applied pressure.
Best fit through straight line portion of primary creep data.

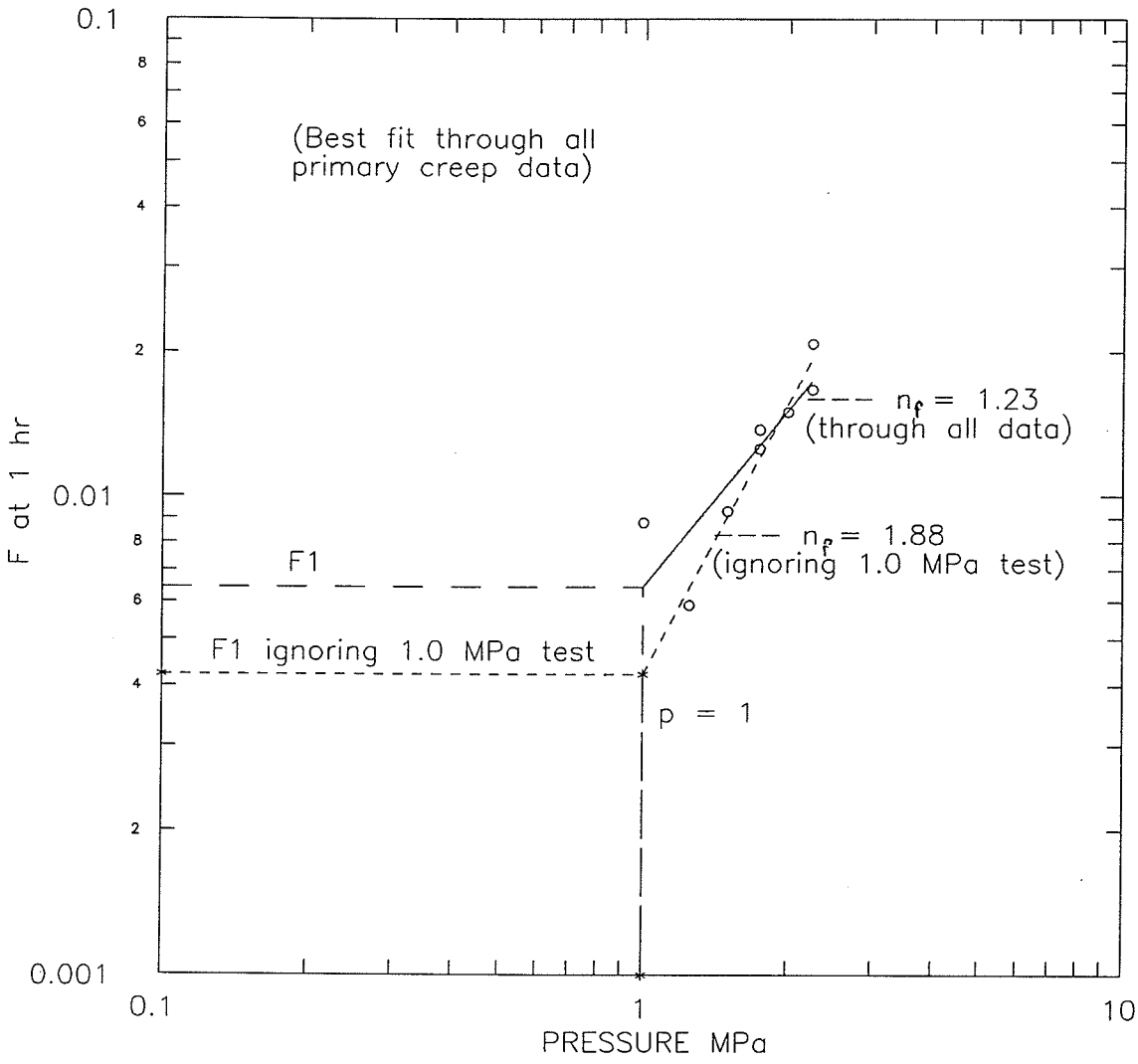


Figure 5.19 Determination of '$n_p$', using best fit through all primary creep data of single stage tests.

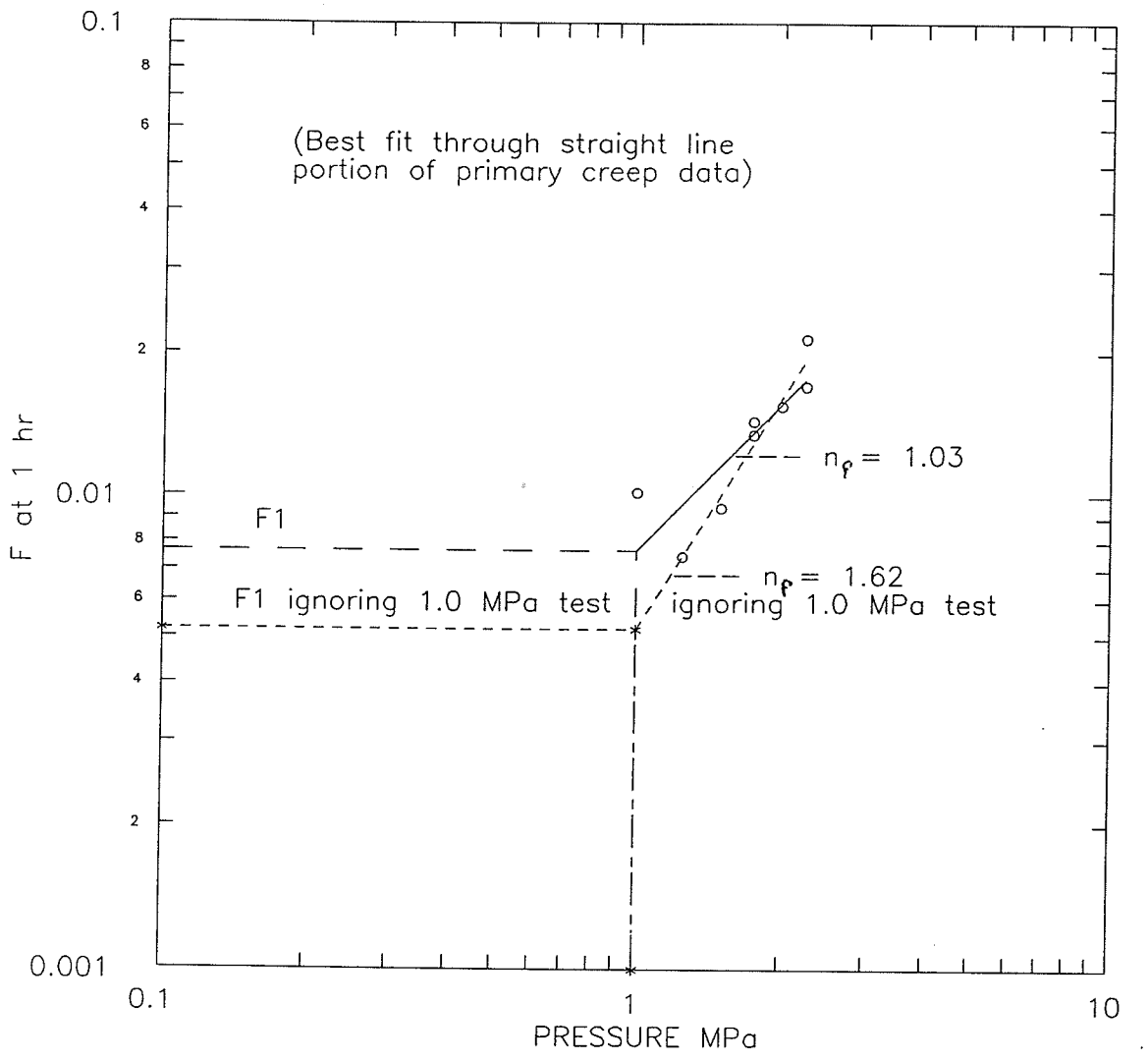


Figure 5.20 Determination of '$n_p$', using best fit through straight line portion of primary creep of single stage tests.

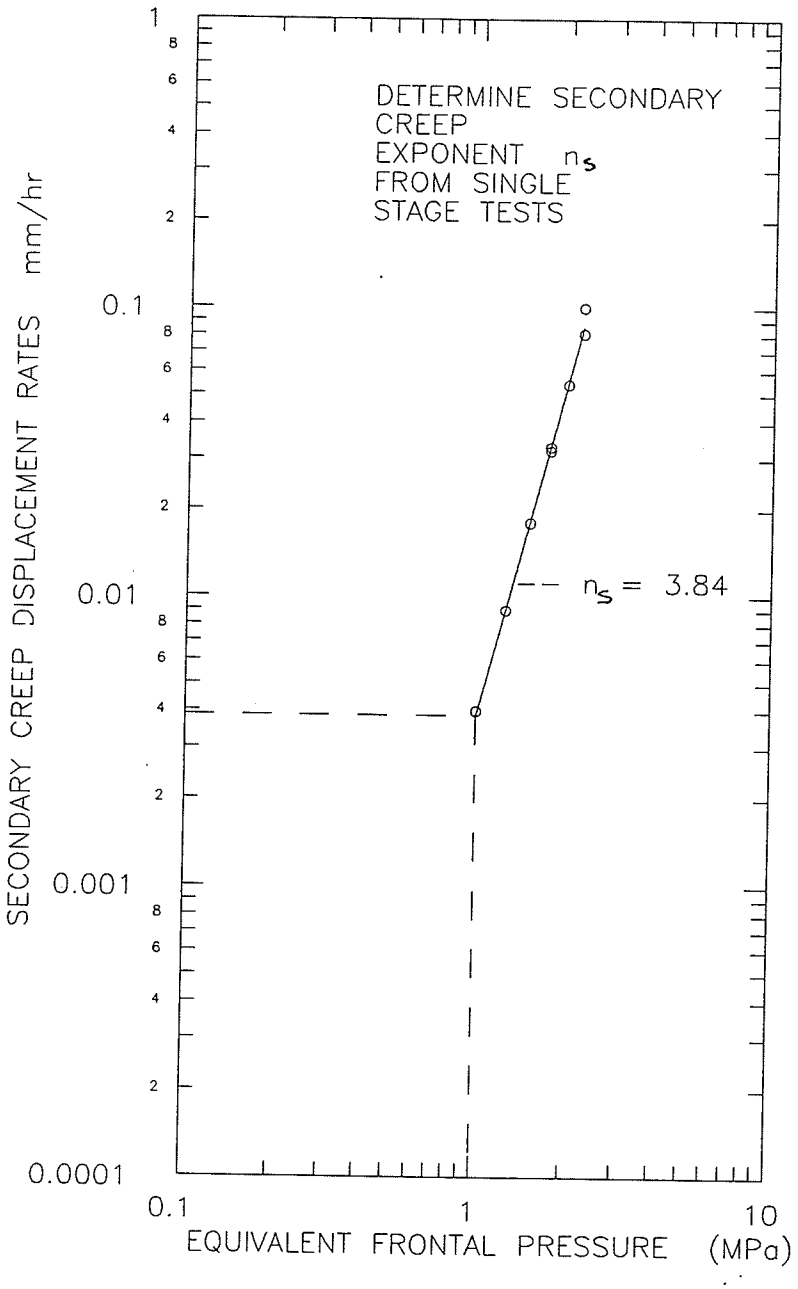


Figure 5.21 Determination of $n_s$ for secondary creep for single stage tests.

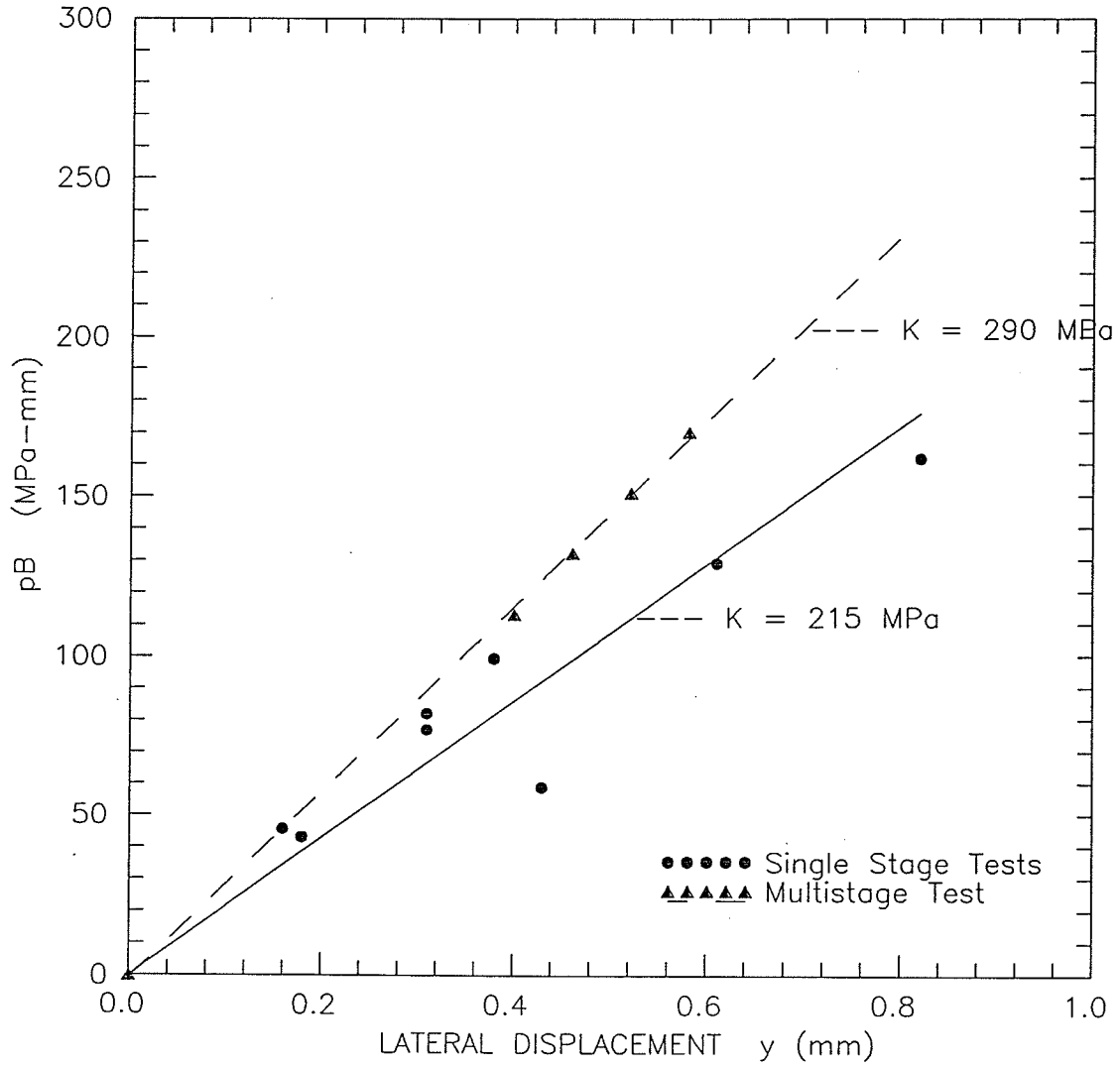


Figure 5.22 pB-y relationship for multi-stage test.

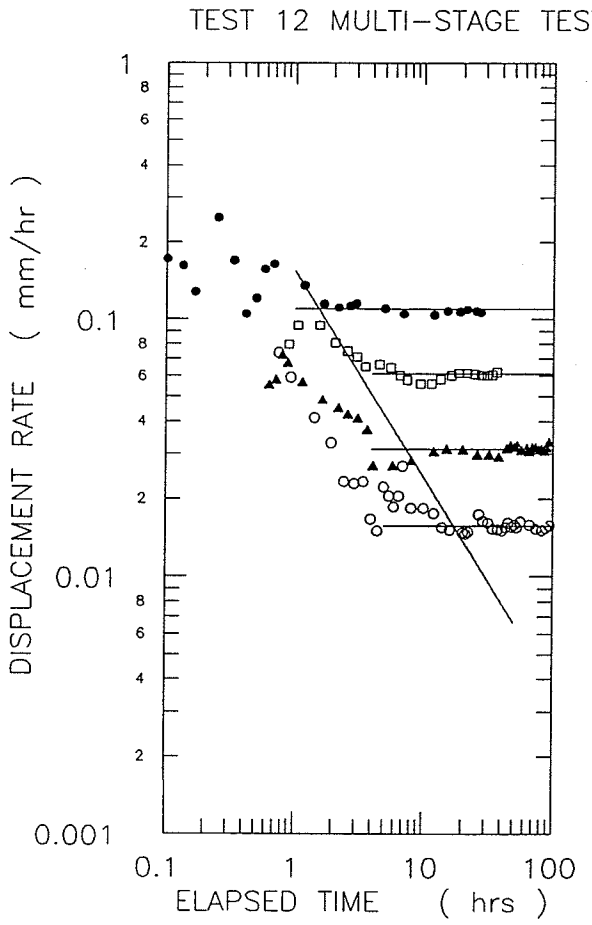


Figure 5.23 Summary of creep displacement rates versus time (log-log) for multi-stage test.

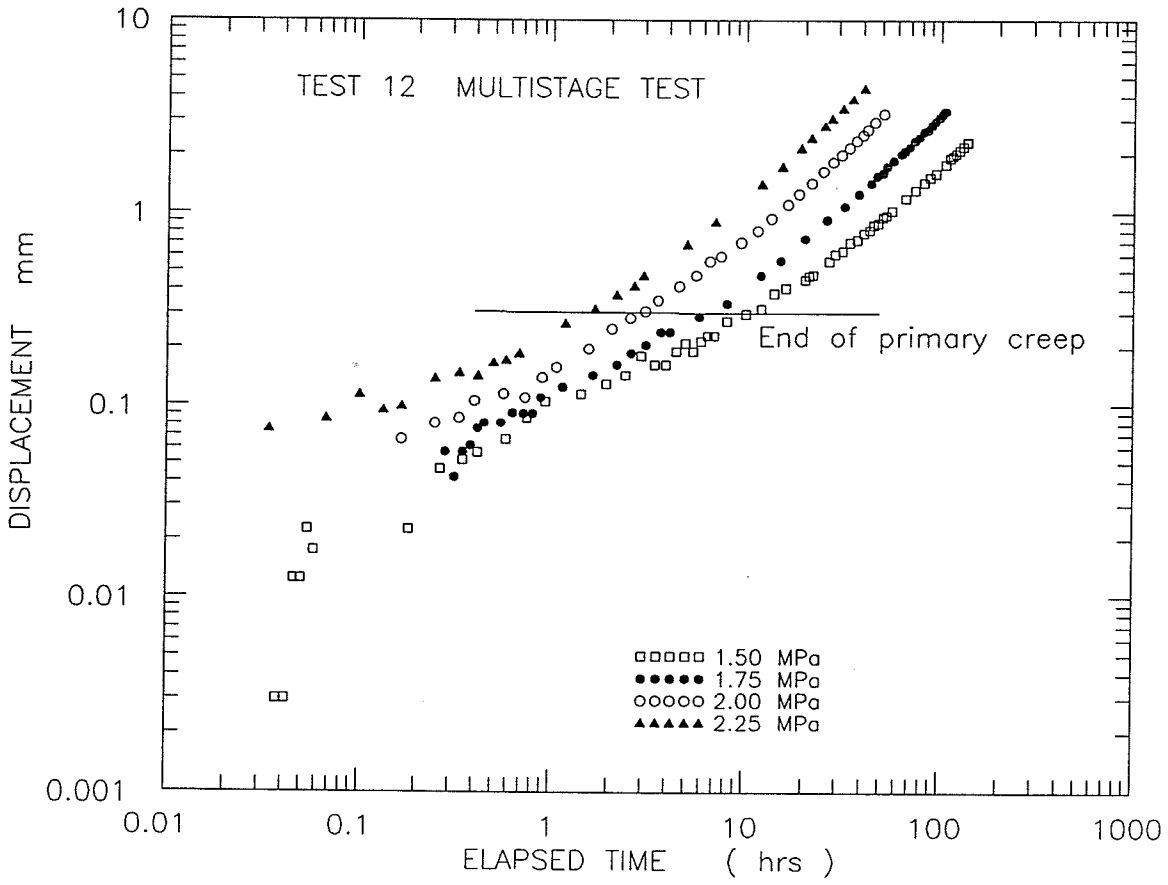


Figure 5.24 Summary of creep displacement versus time (log-log) for multi-stage test.

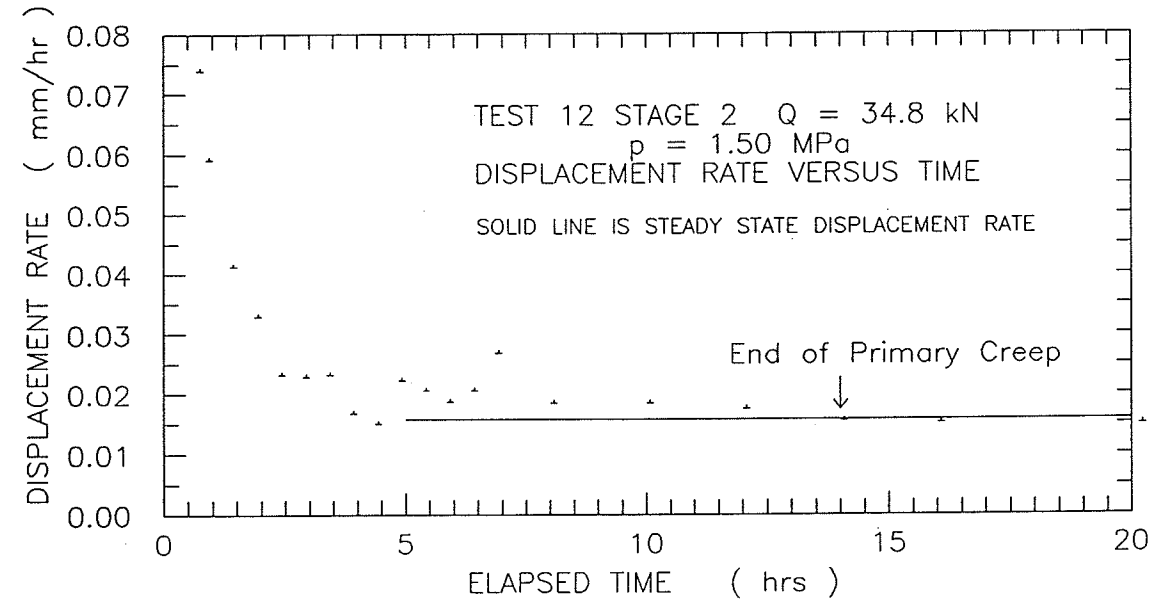


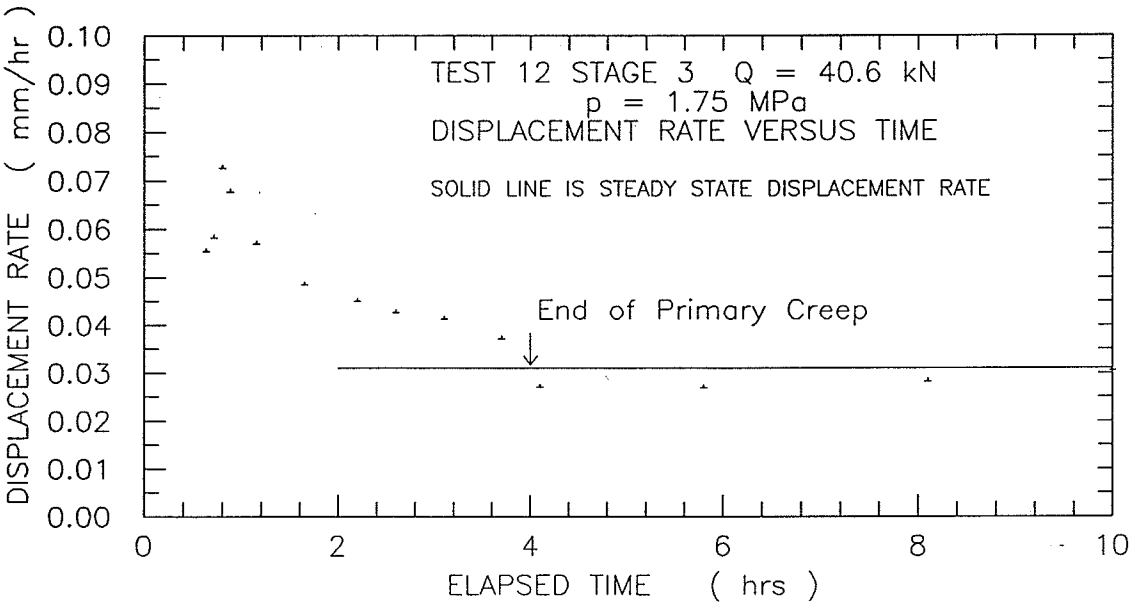


Figure 5.25 Displacement rate versus time
(Stage 2 and Stage 3 of multi-stage test).

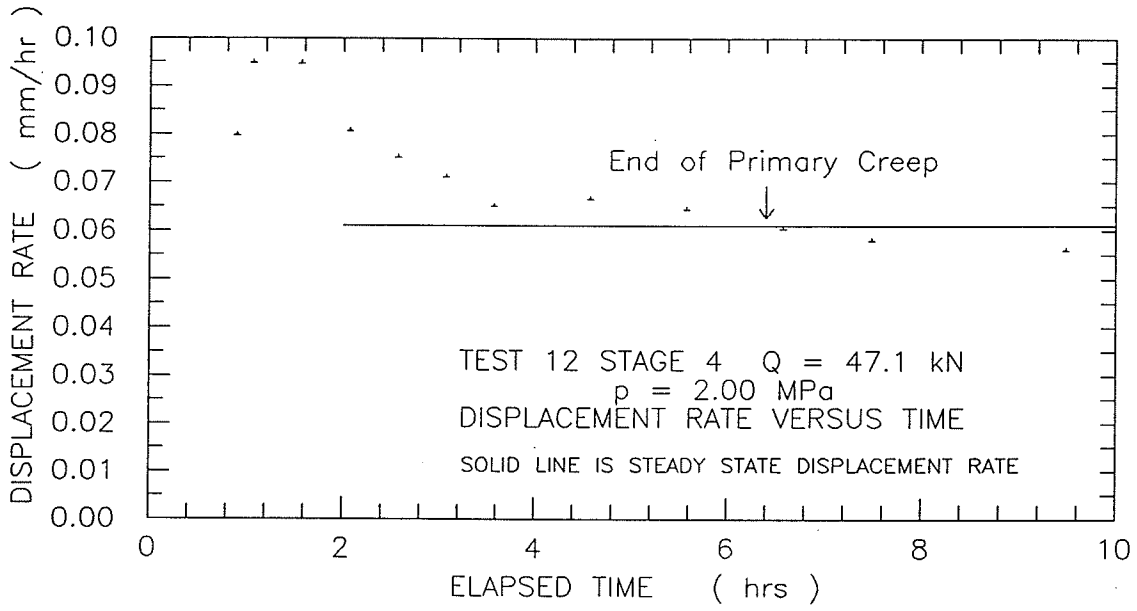


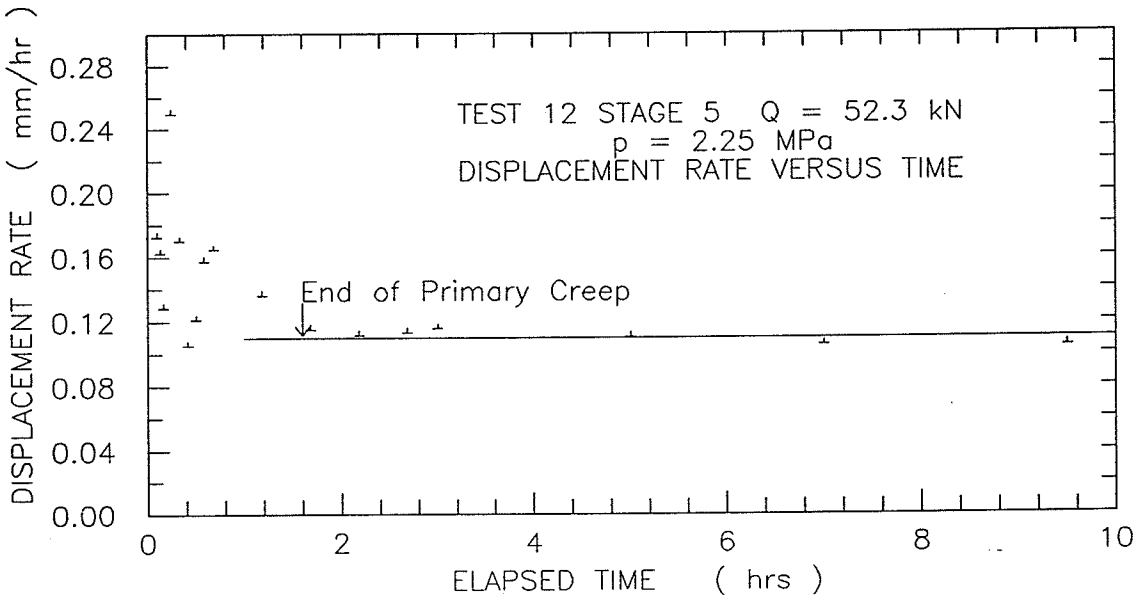


Figure 5.26 Displacement rate versus time
(Stage 4 and Stage 5 of multi-stage test).

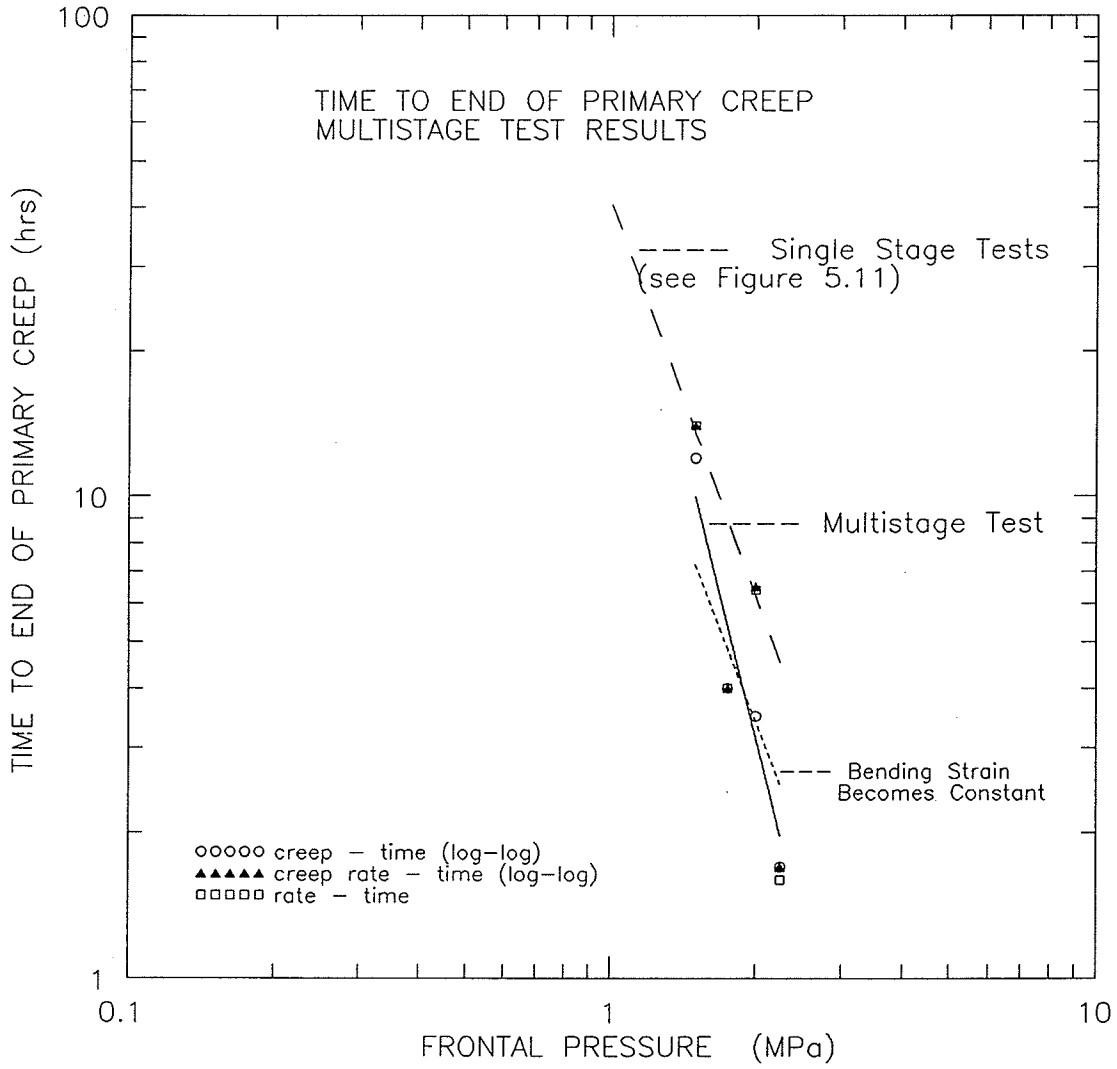


Figure 5.27 Time to end of primary creep: multi-stage tests versus single stage tests.

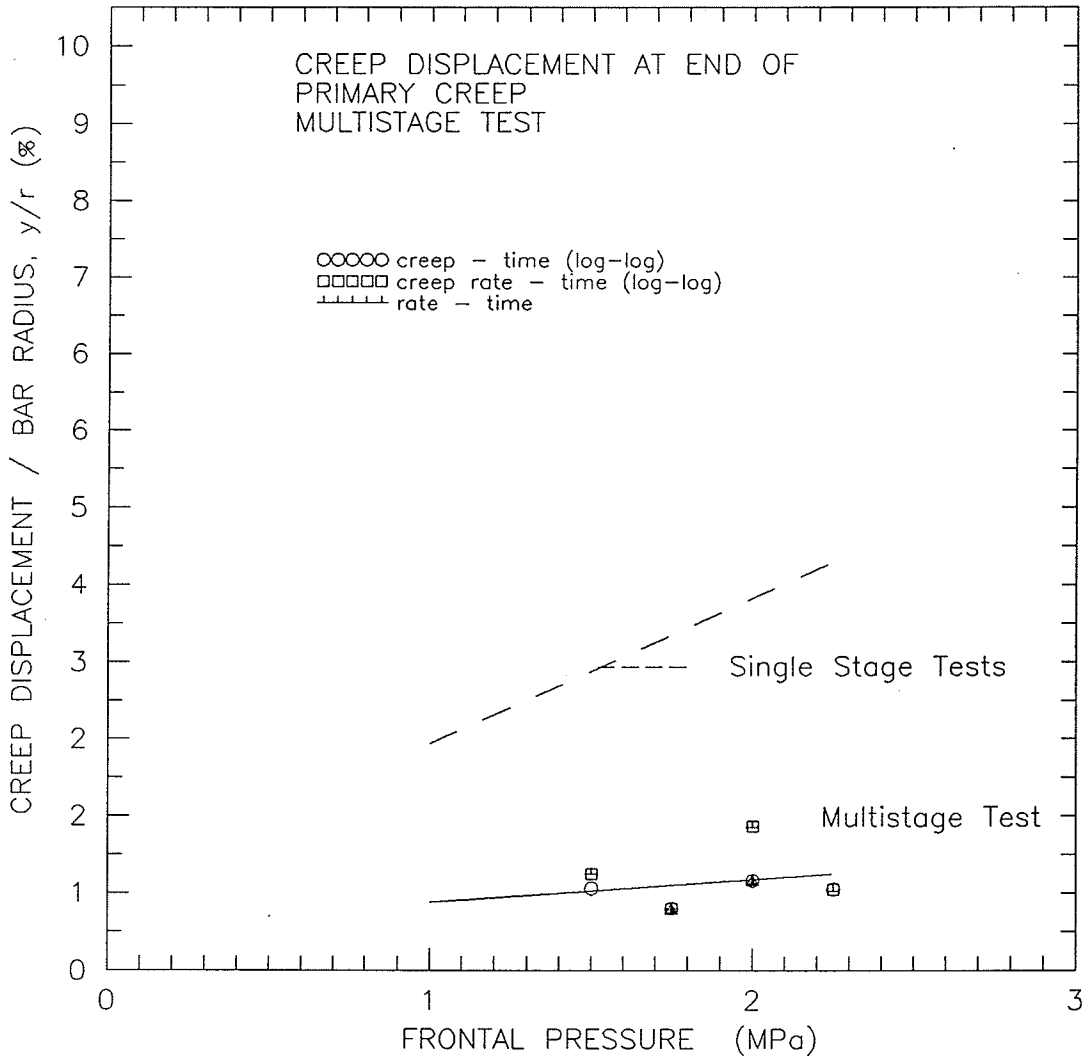


Figure 5.28 Normalized creep displacement at end of primary creep: multi-stage tests versus single stage tests.

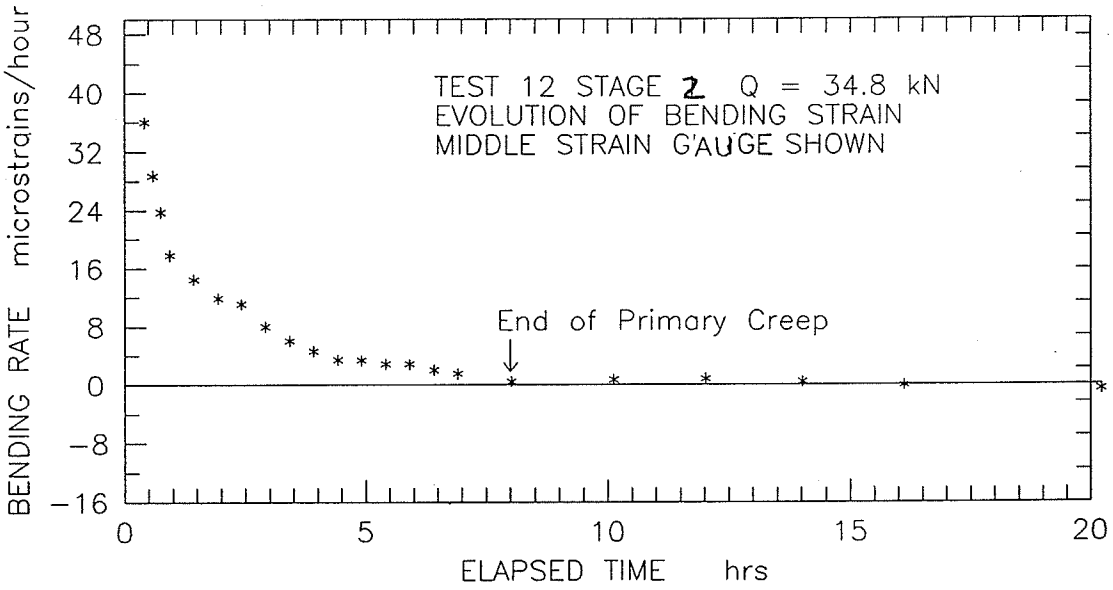


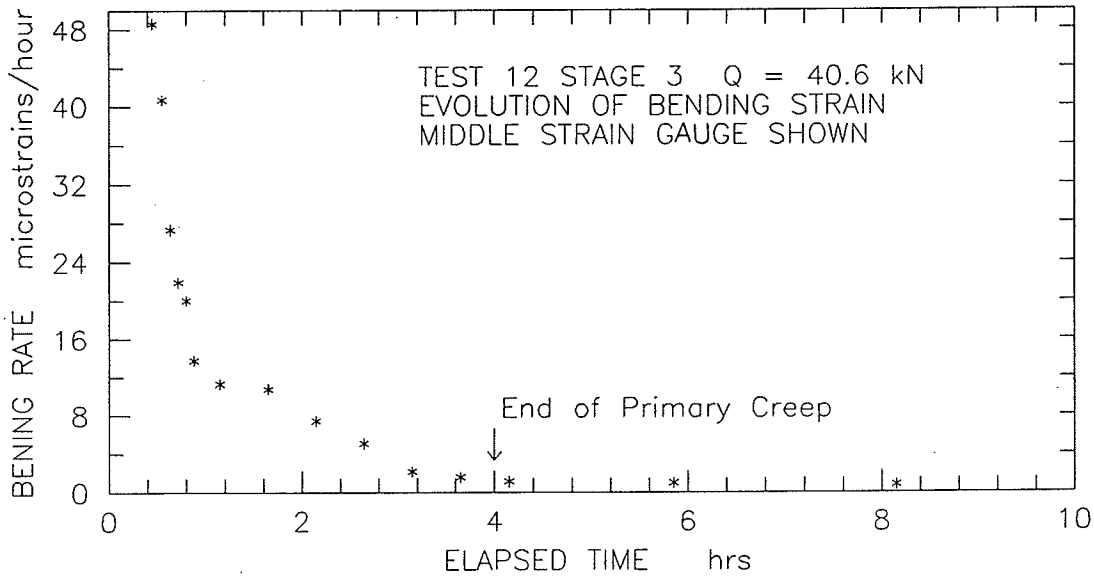


Figure 5.29 Bending strain rate versus time
(Stage 2 and Stage 3 of multi-stage test).

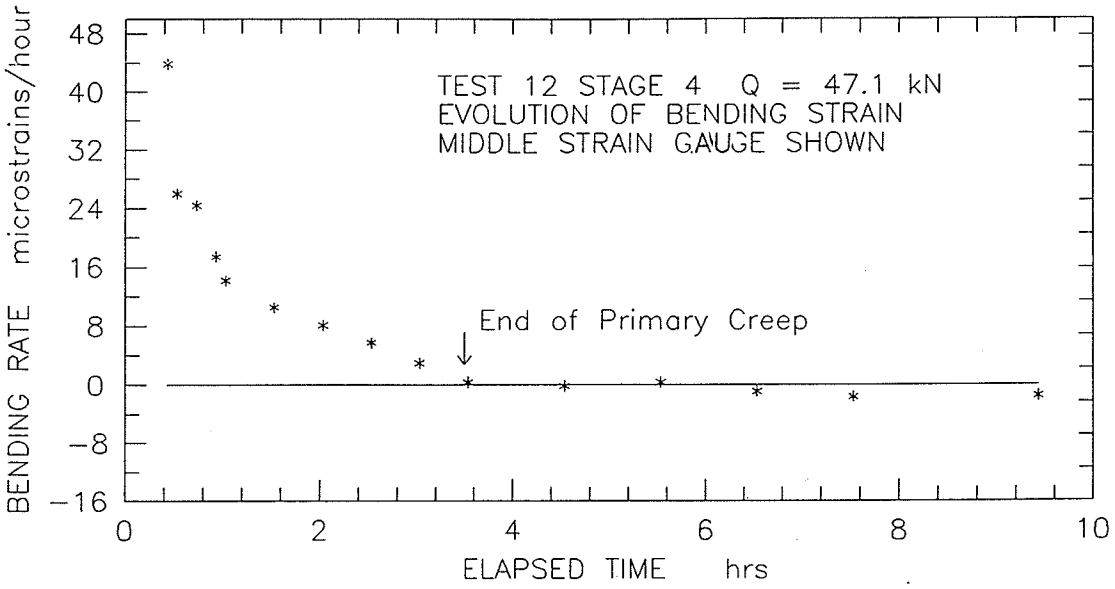


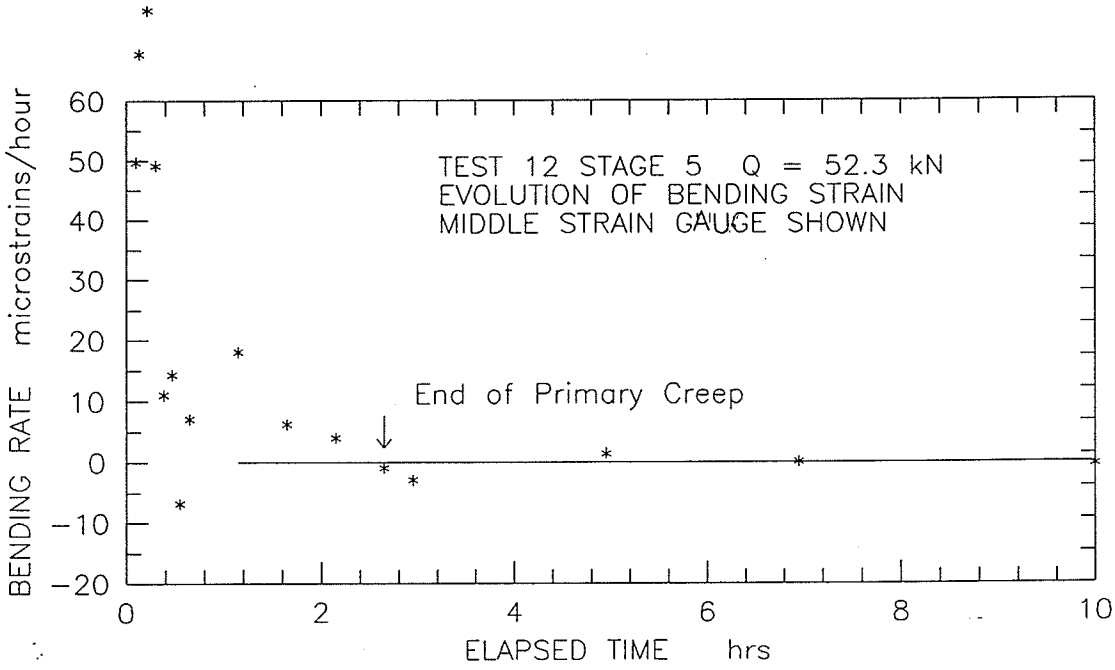


Figure 5.30 Bending strain rate versus time
(Stage 4 and Stage 5 of multi-stage test).

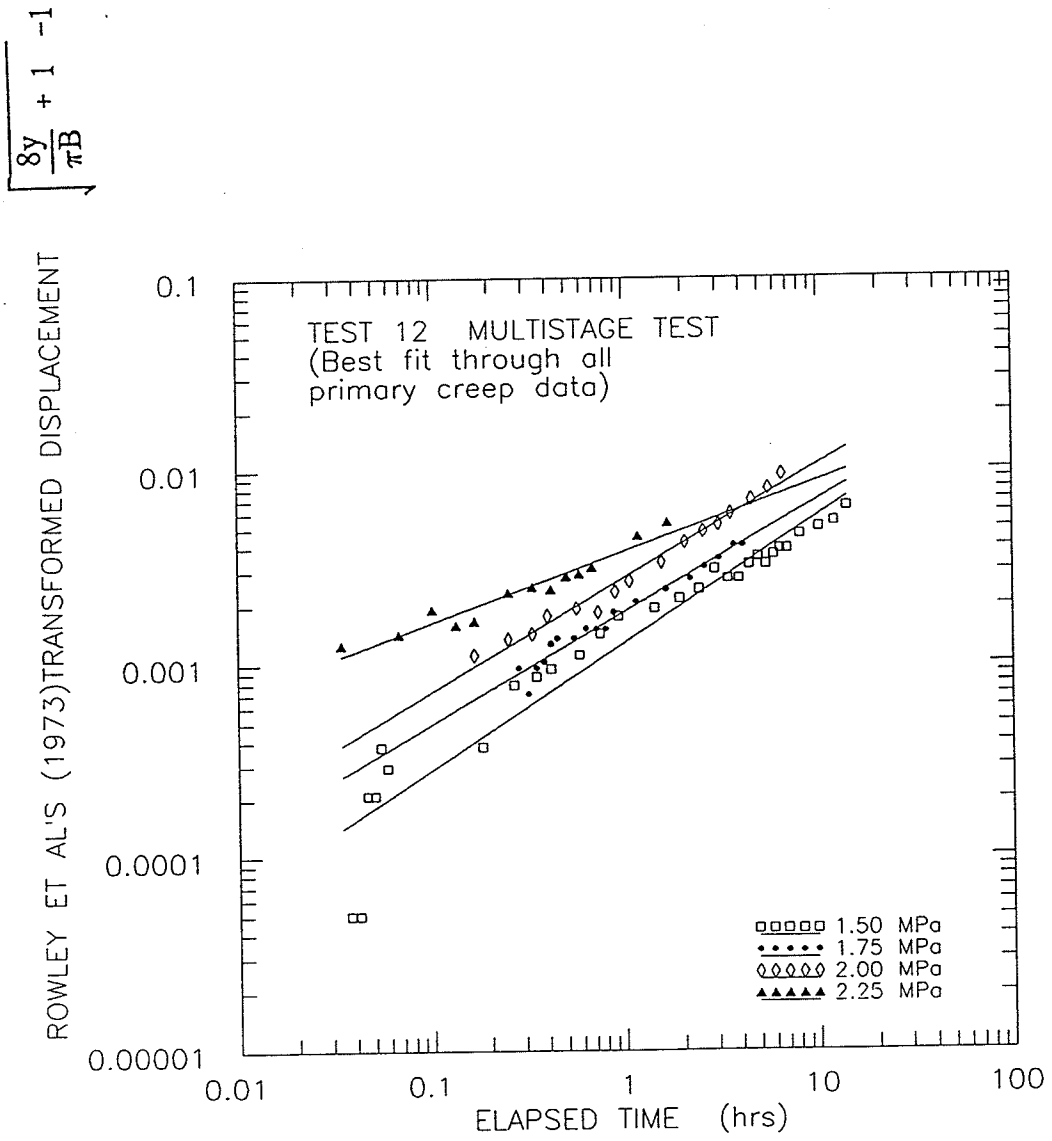


Figure 5.31 Summary of determination of $b_p$ taking best fit through all primary creep data (multi-stage test).

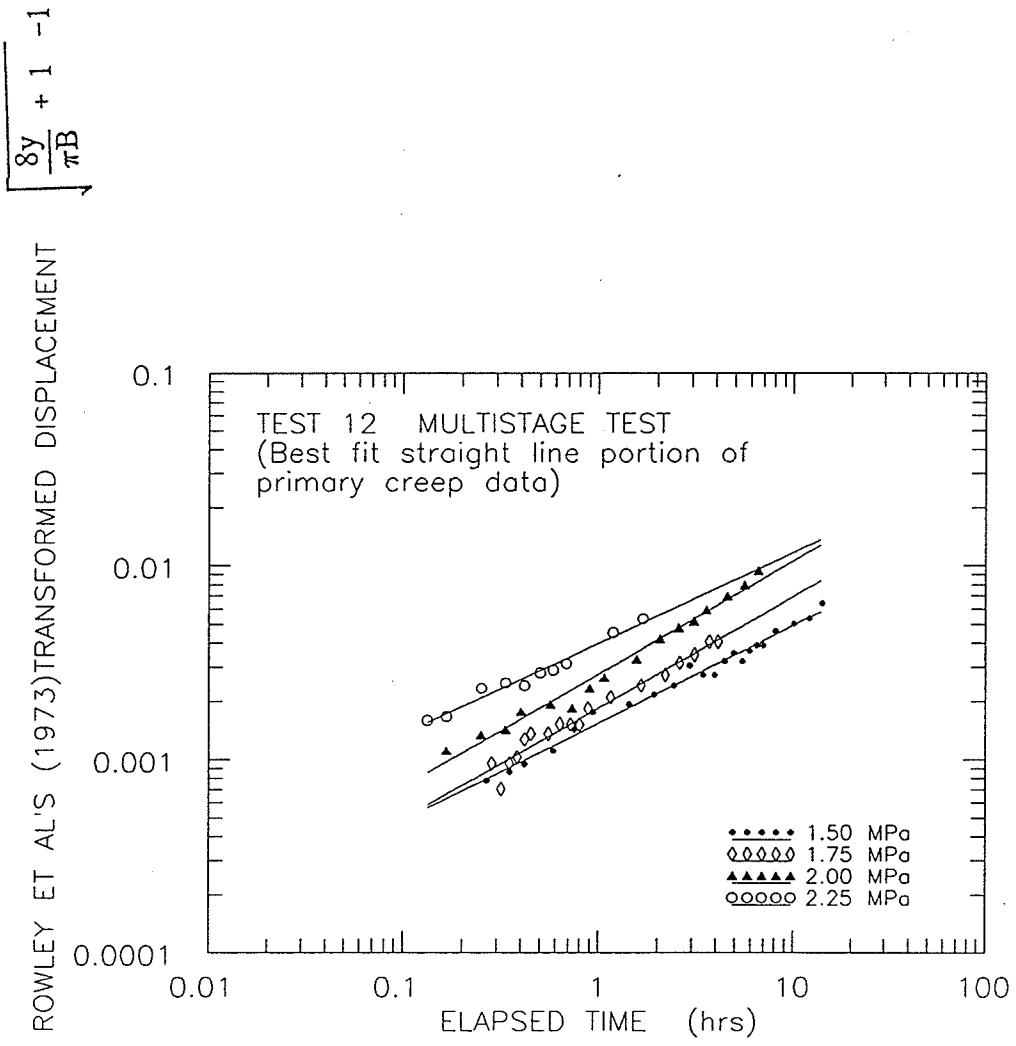


Figure 5.32 Summary of determination of $b_p$ taking best fit through straight line portion of primary creep data (multi-stage test).

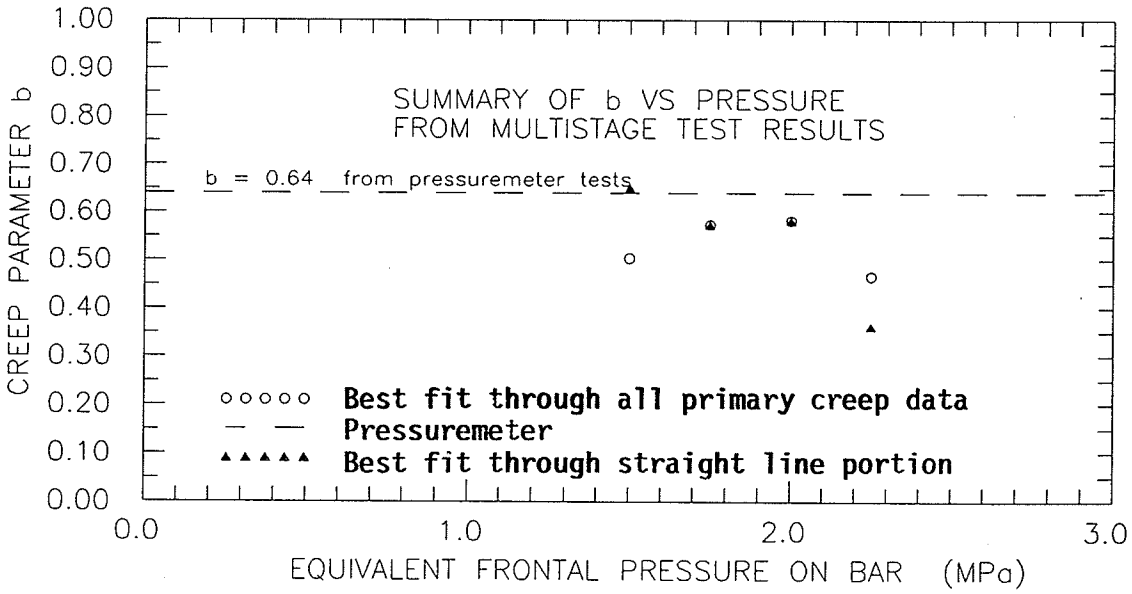


Figure 5.33 Sensitivity of primary creep parameter $b_p$ versus applied frontal pressure, p (multi-stage test).

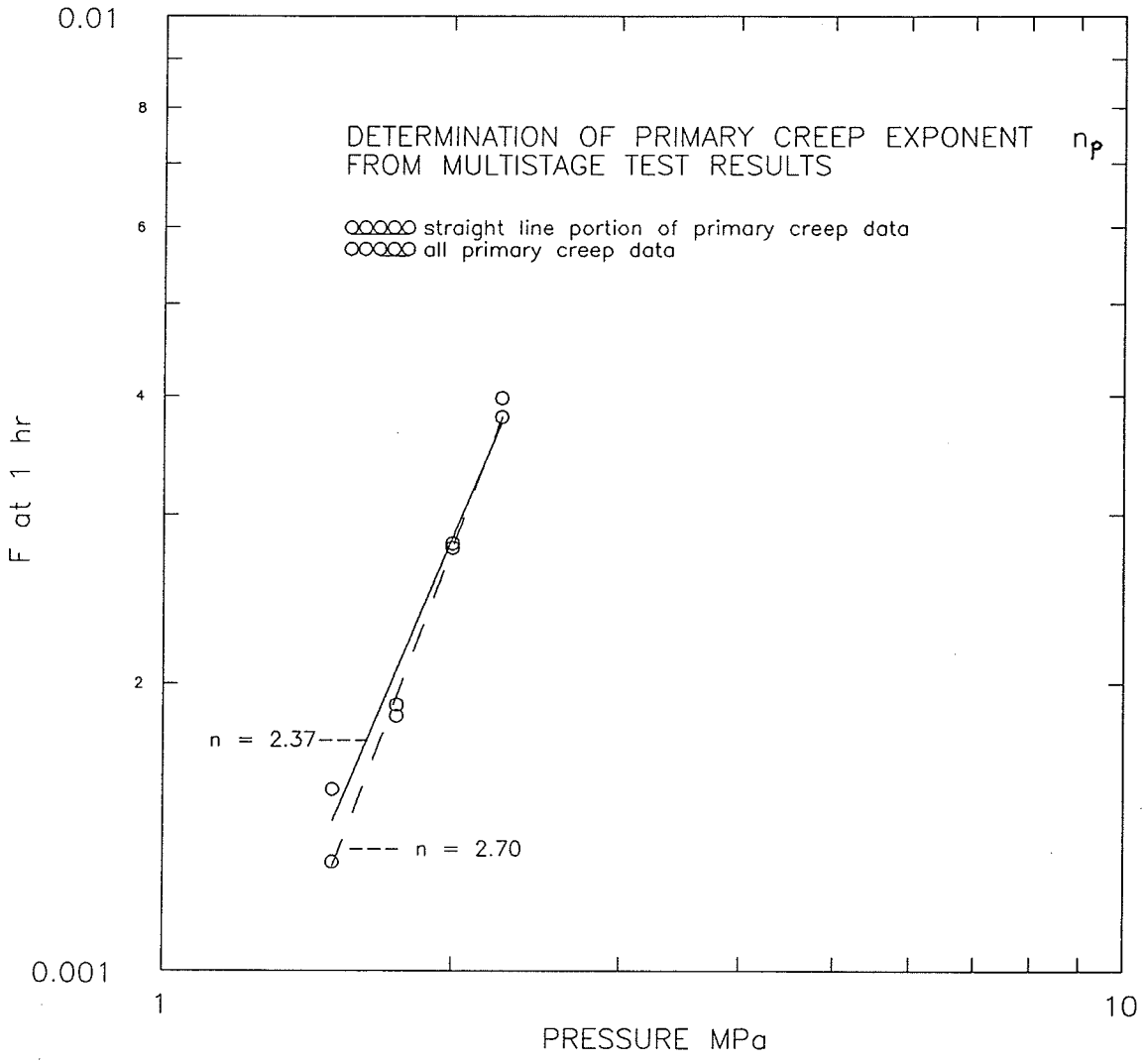


Figure 5.34 Summary of determination of $n_p$ from primary creep phase of multi-stage test.

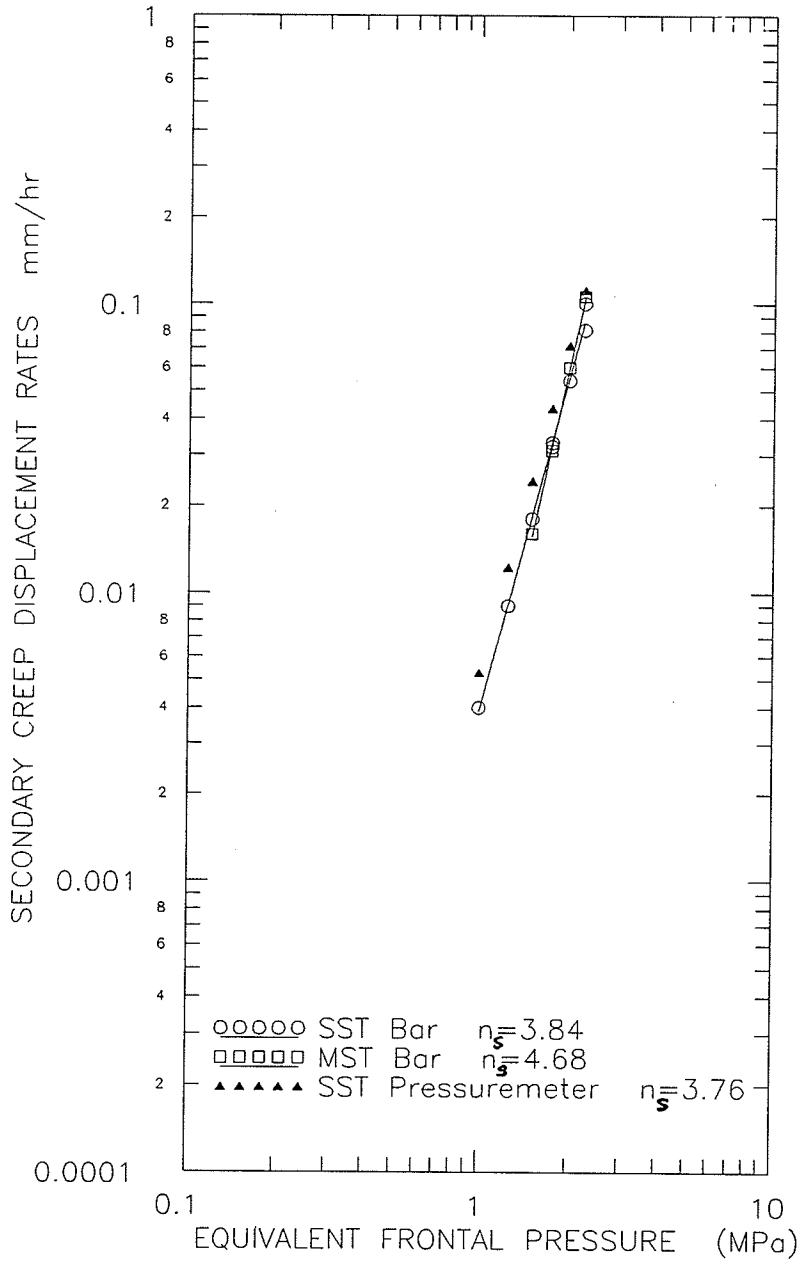


Figure 5.35 Summary of determination of $n_s$ from secondary creep phase of multi-stage test.

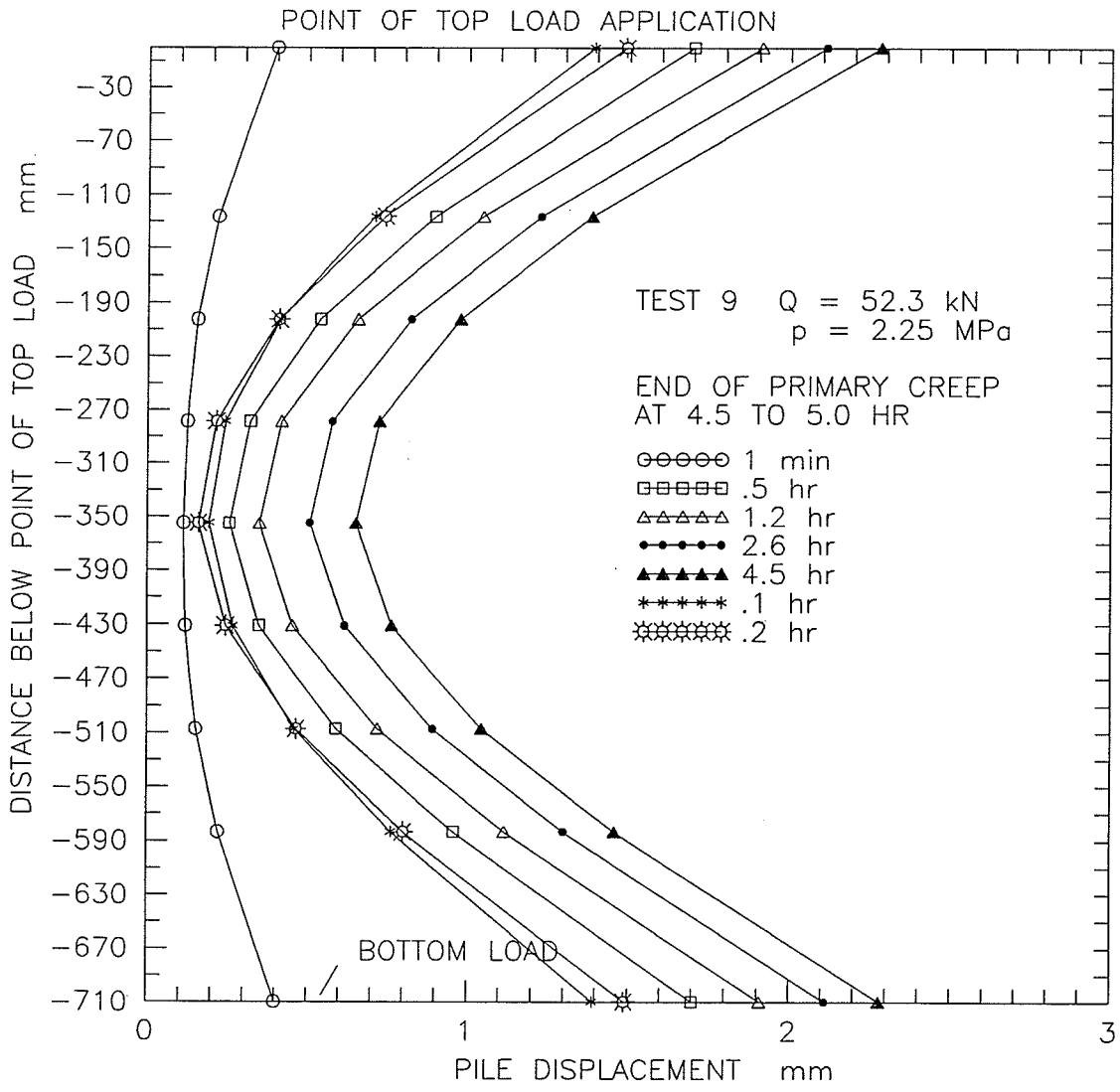


Figure 5.36 Deformed shape of bar during primary creep phase of Test 9 (single stage test).

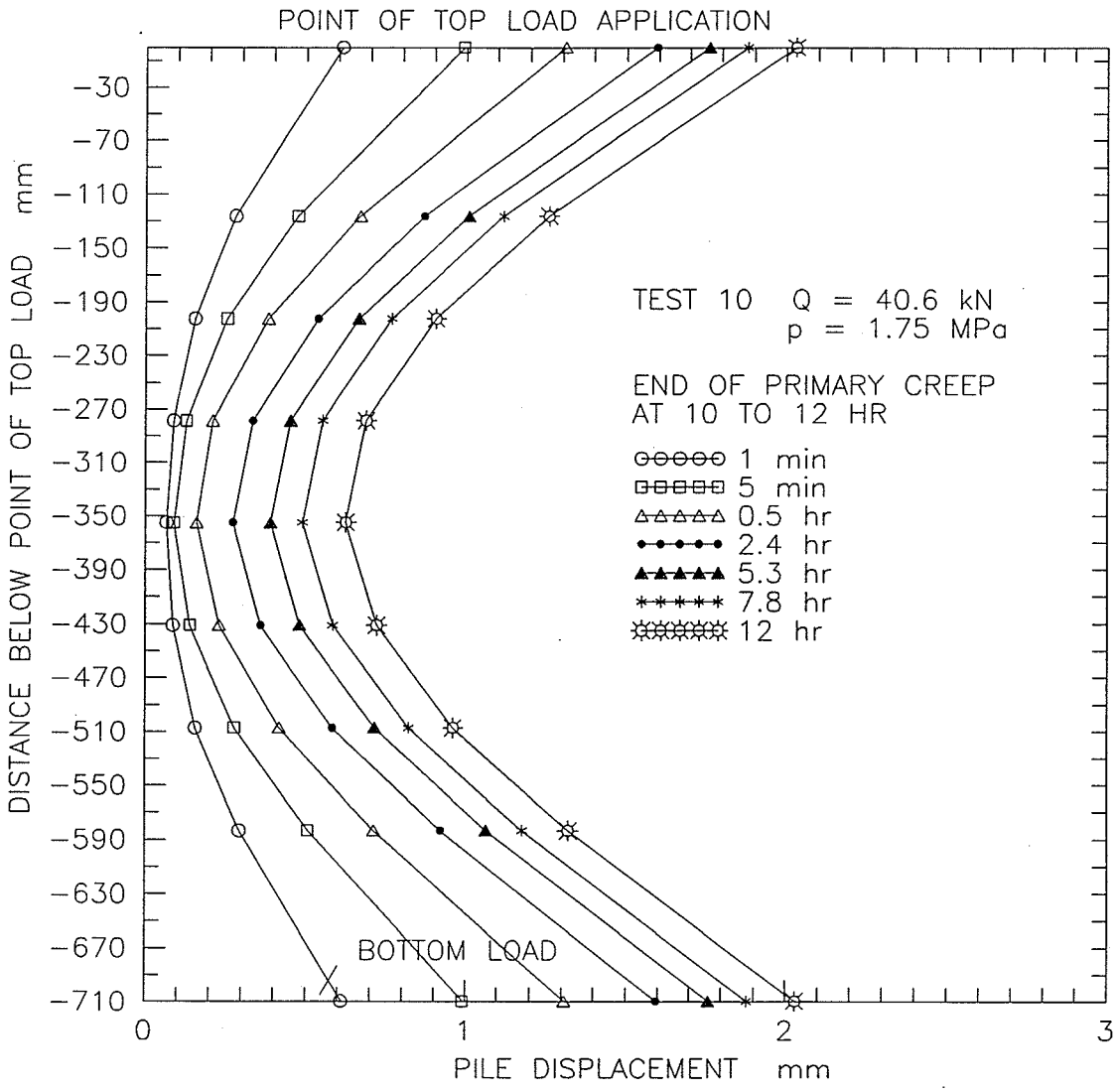


Figure 5.37 Deformed shape of bar during primary creep phase of Test 10 (single stage test).

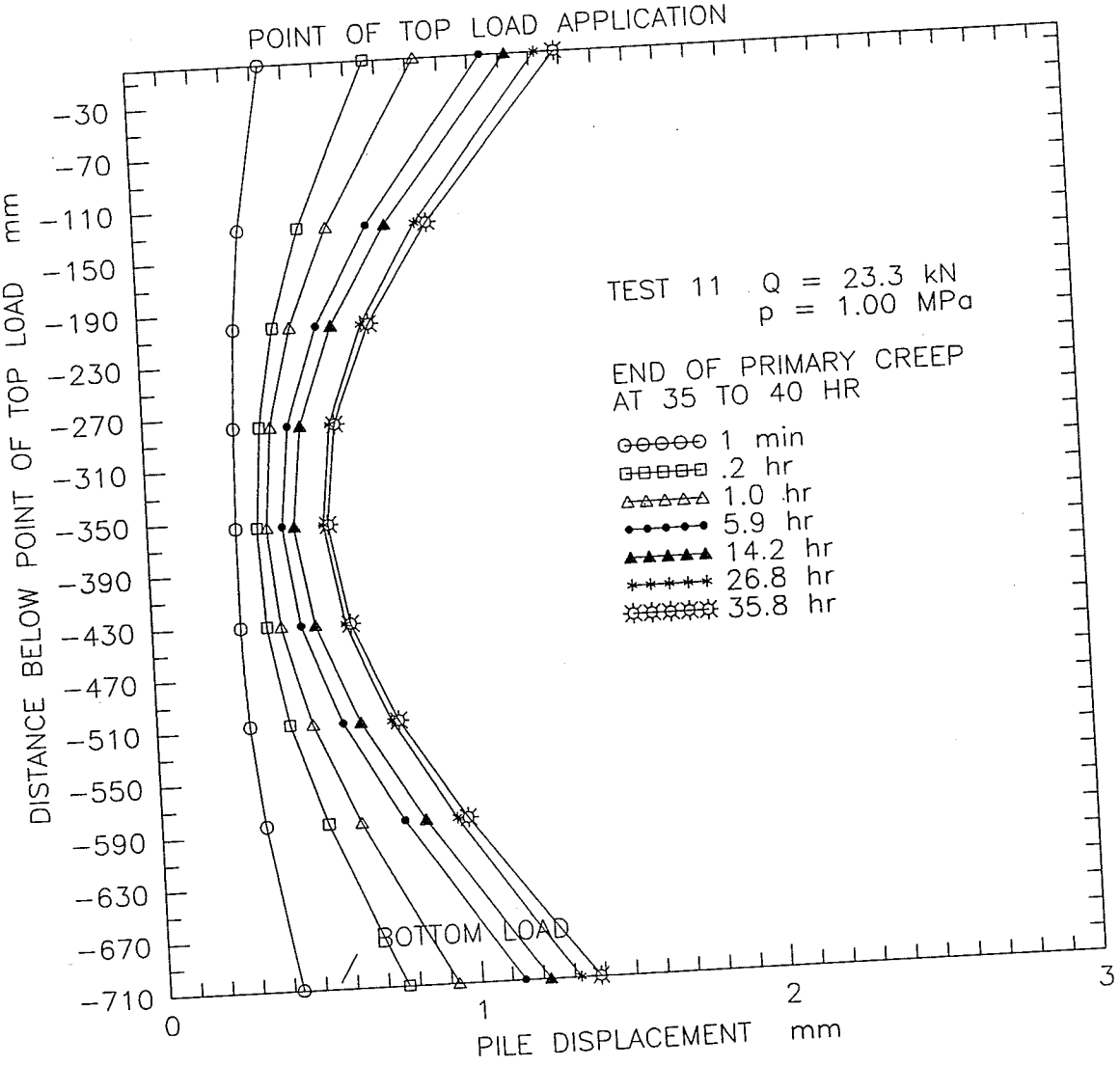


Figure 5.38 Deformed shape of bar during primary creep phase of Test 11 (single stage test).

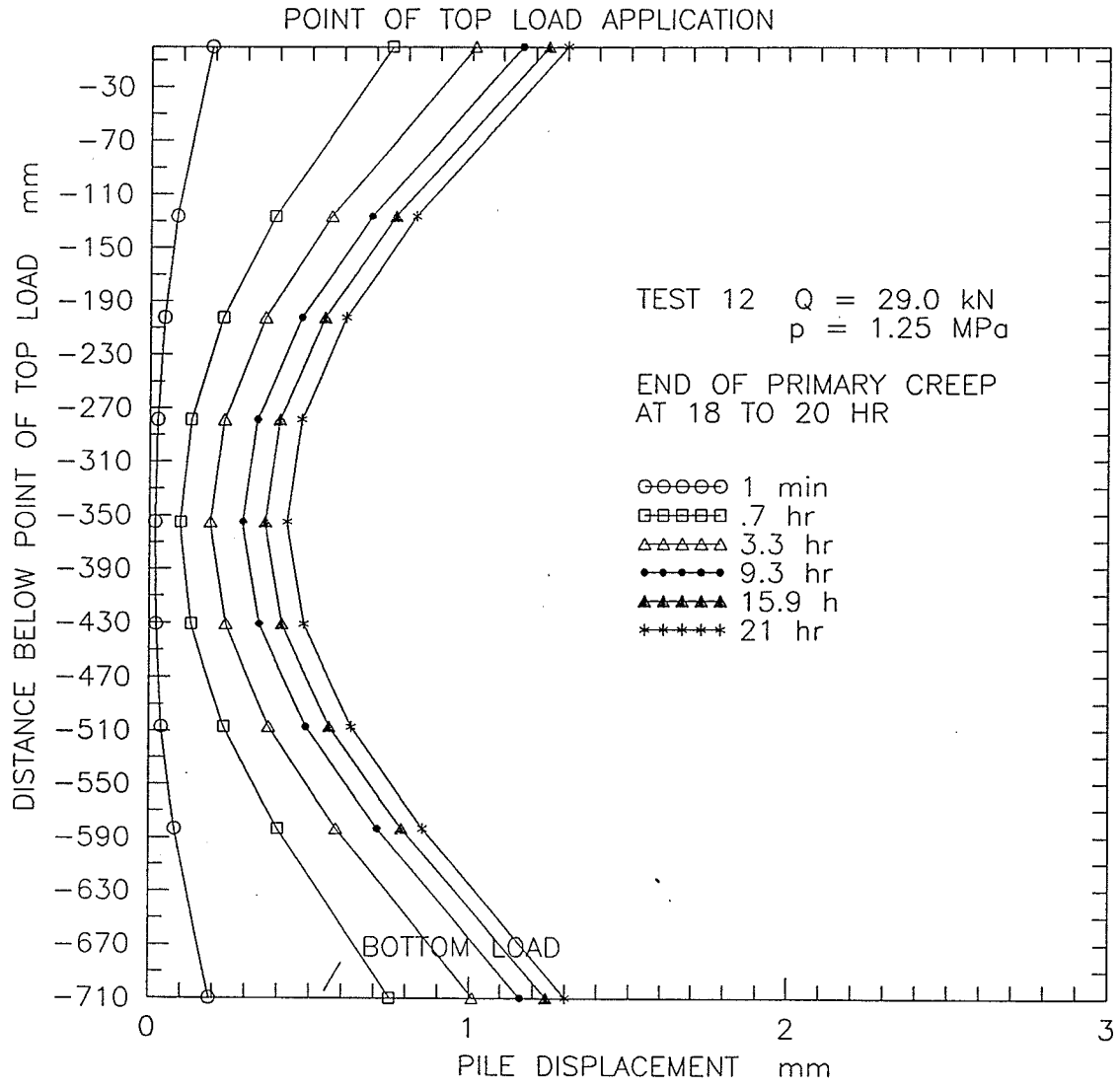


Figure 5.39 Deformed shape of bar during primary creep phase of Test 12, Stage 1.

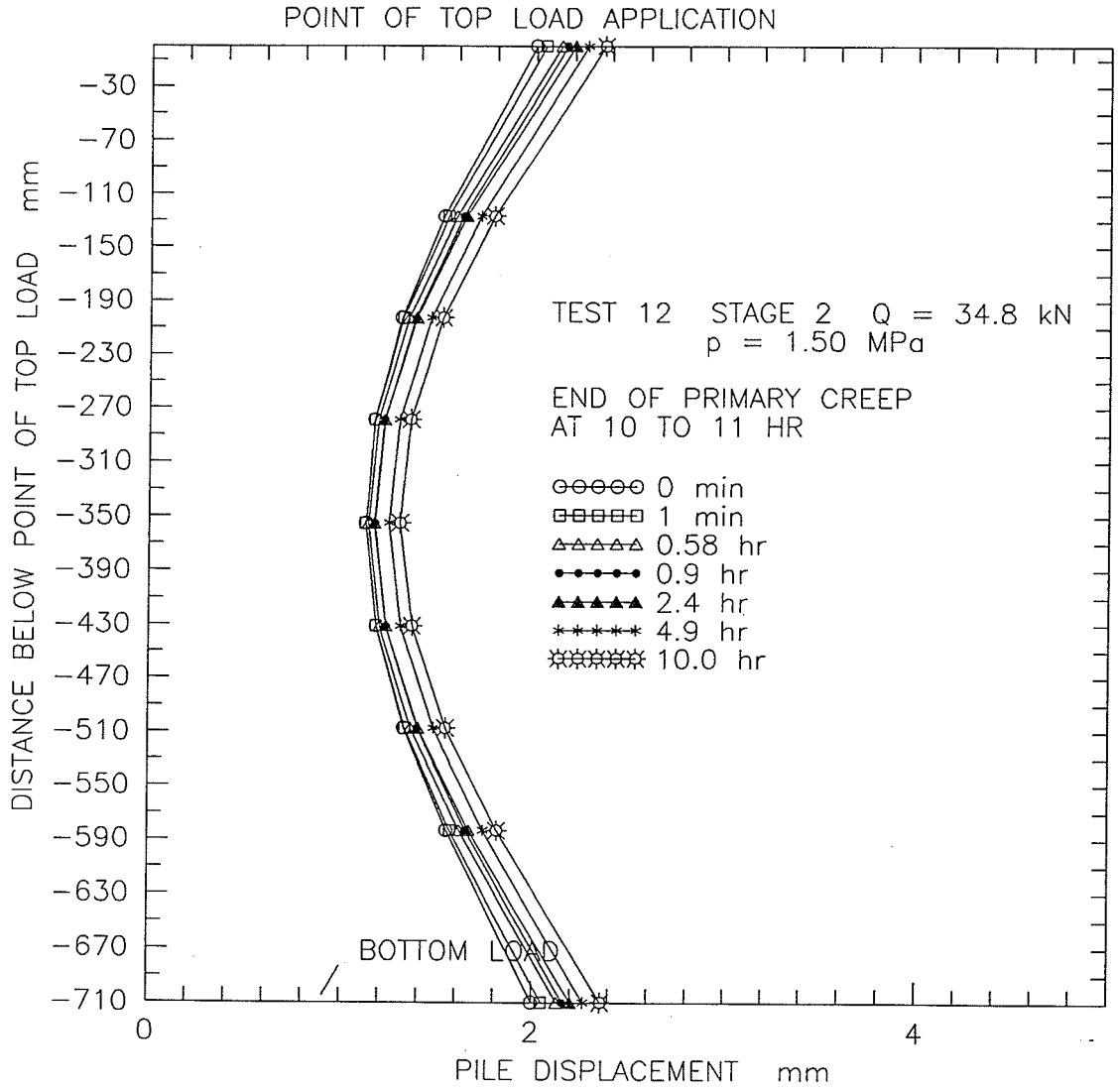


Figure 5.40 Deformed shape of bar during primary creep phase of Test 12, Stage 2 (multi-stage test).

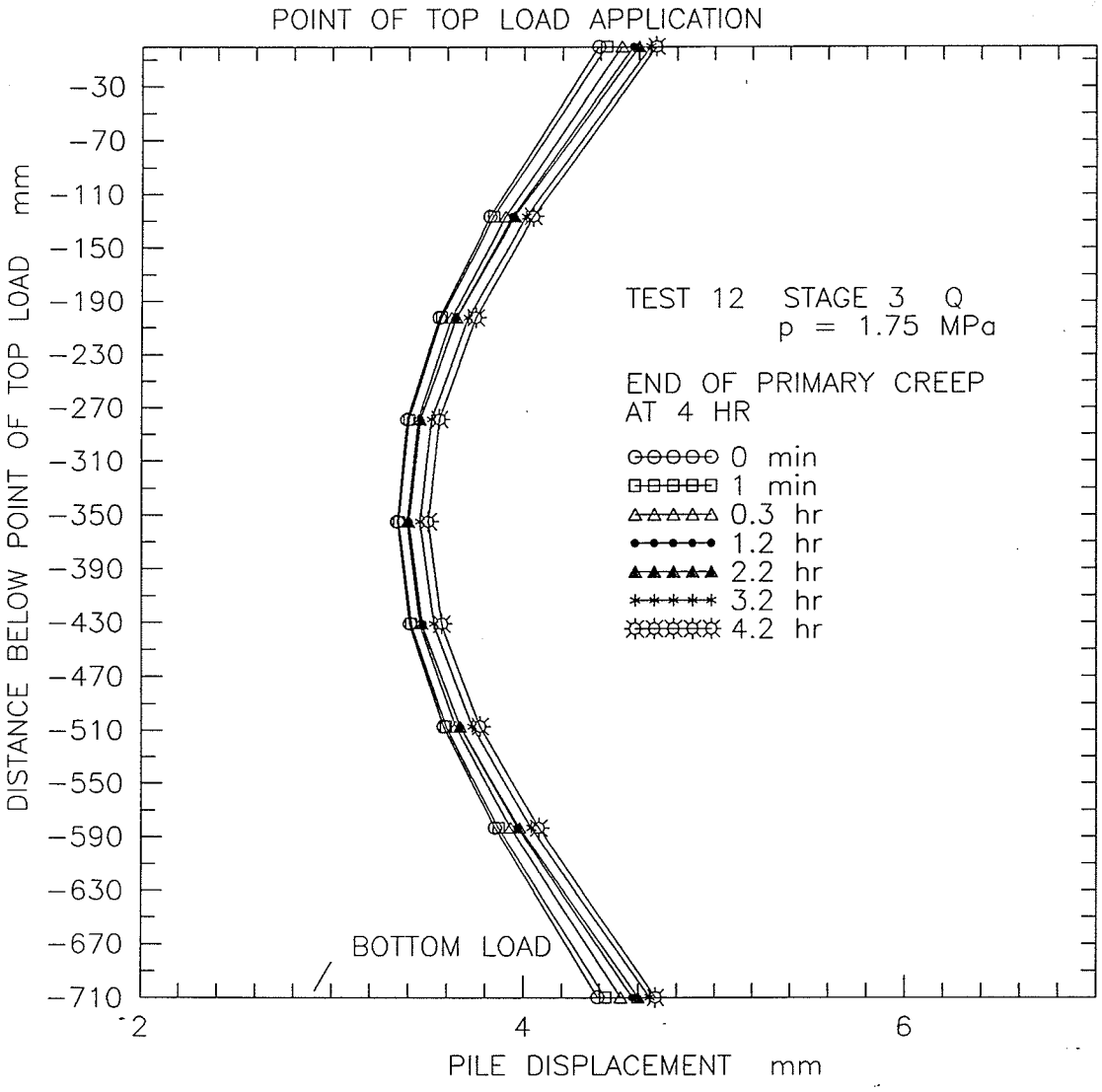


Figure 5.41 Deformed shape of bar during primary creep phase of Test 12, Stage 3 (multi-stage test).

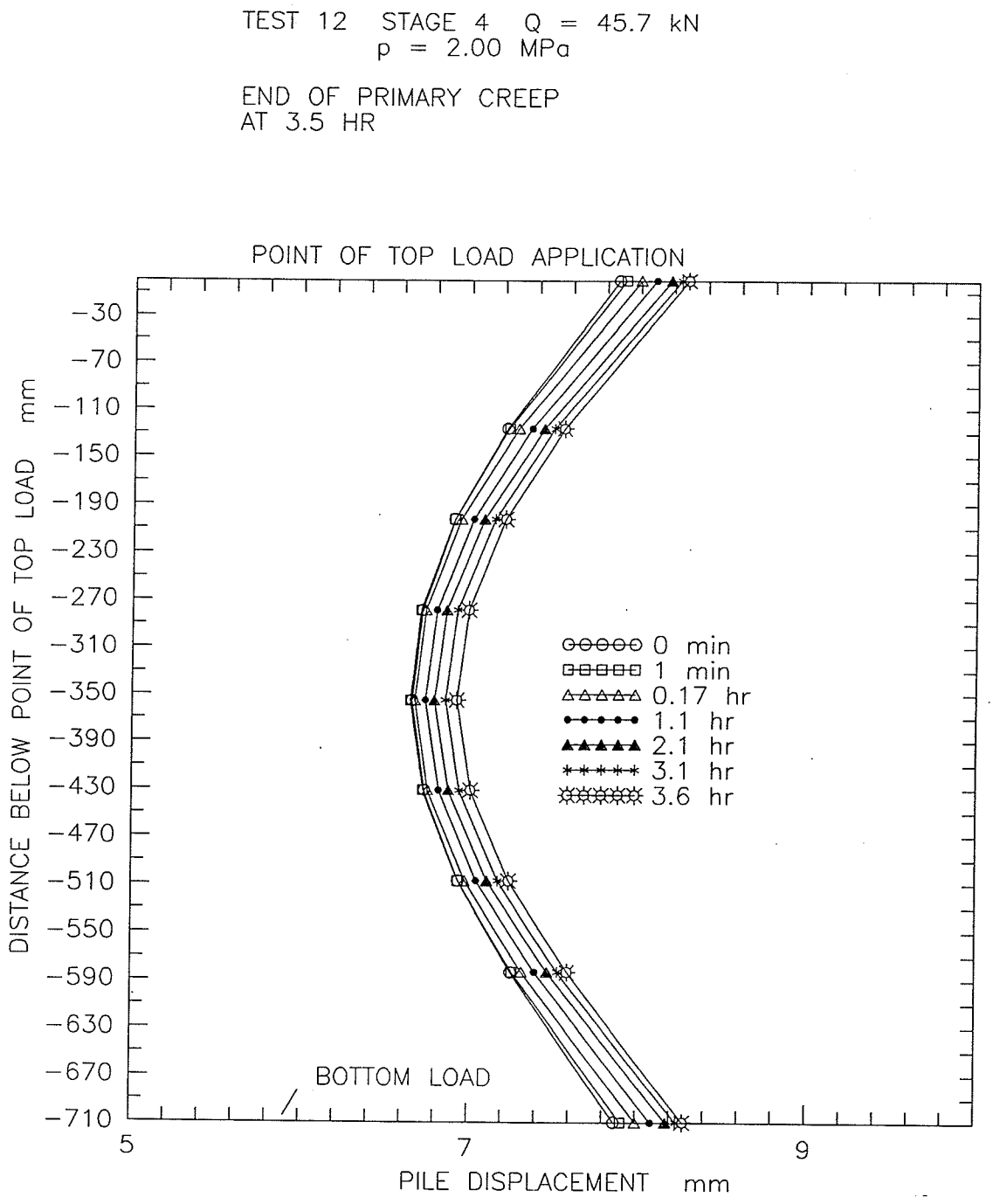


Figure 5.42 Deformed shape of bar during primary creep phase of Test 12, Stage 4 (multi-stage test).

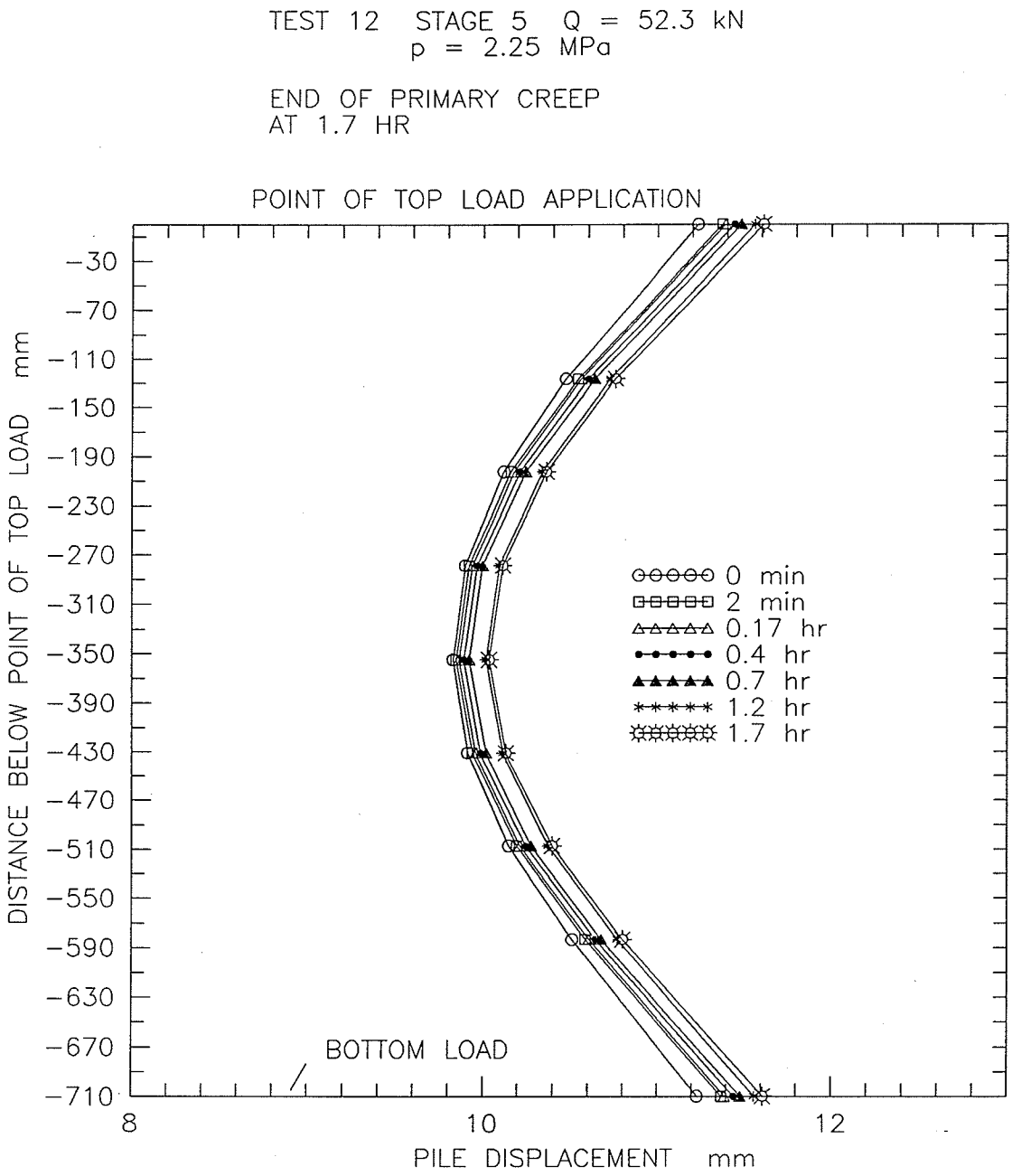


Figure 5.43 Deformed shape of bar during primary creep phase of Test 12, Stage 5 (multi-stage test).

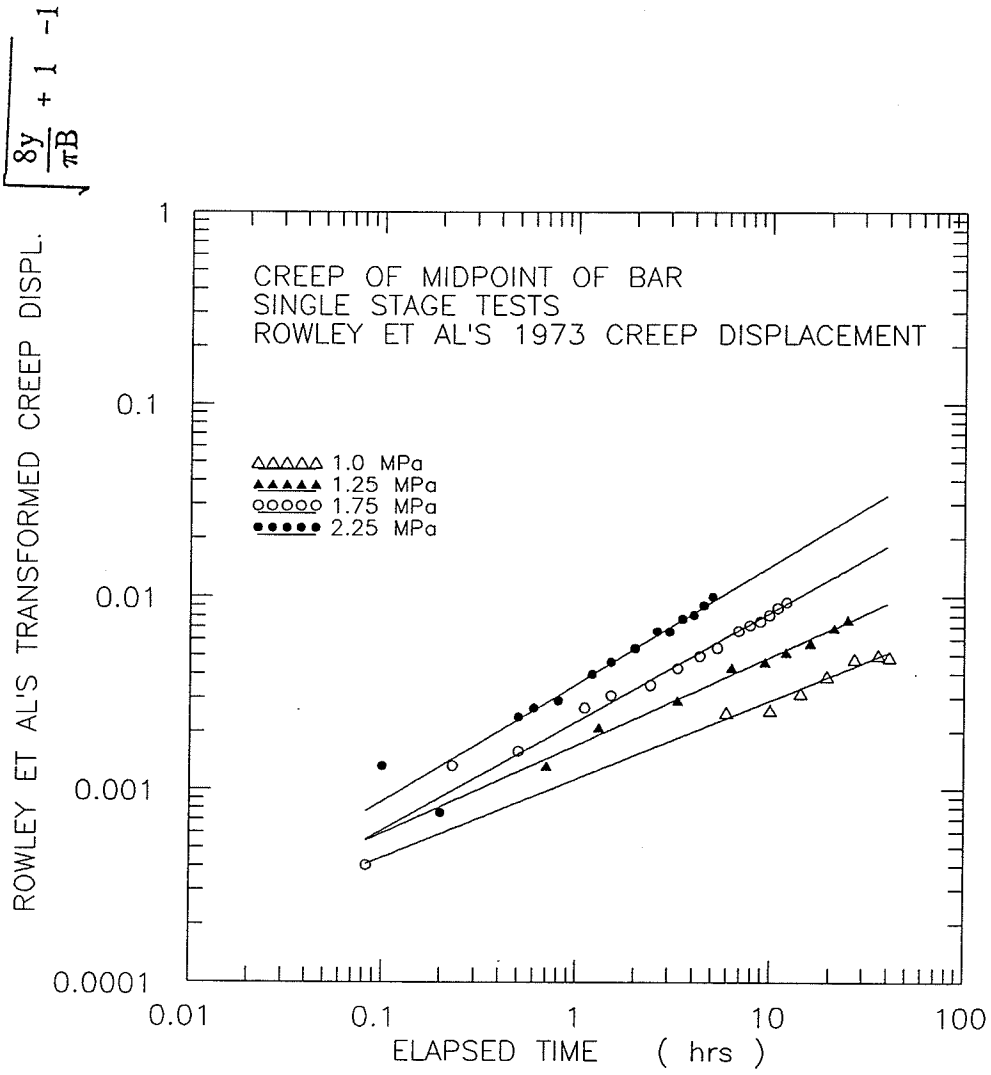


Figure 5.44 Summary of determination of $b_p$ taking best fit through primary creep displacements of the midpoint of the embedded length of the bar (single stage tests).

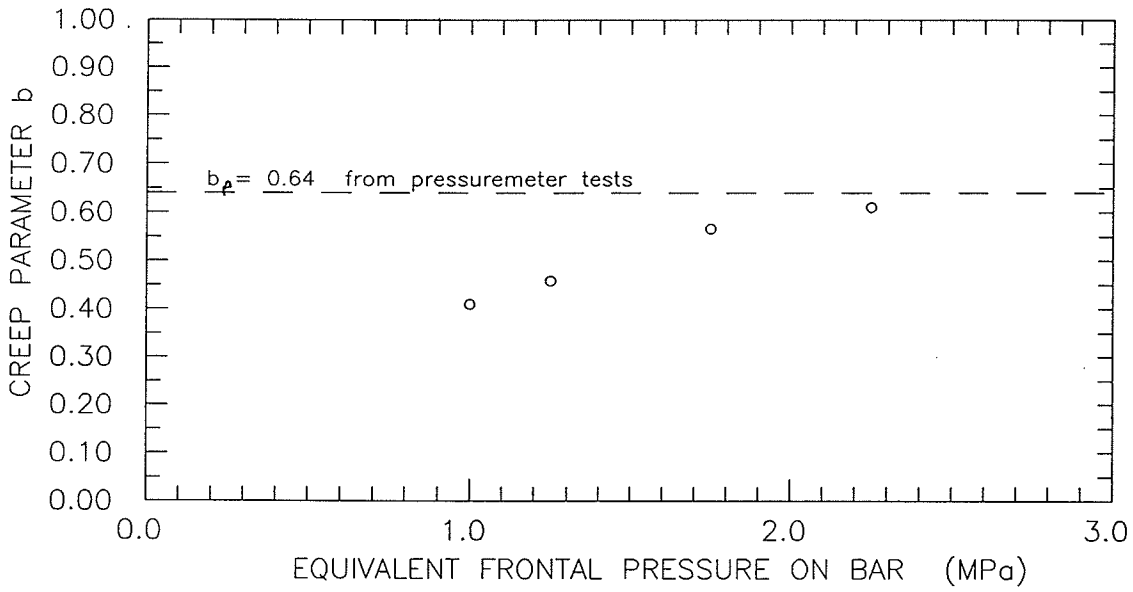


Figure 5.45 Sensitivity of $b_p$ versus pressure. Best fit through primary creep displacements of the midpoint of the embedded length of the bar (single stage tests).

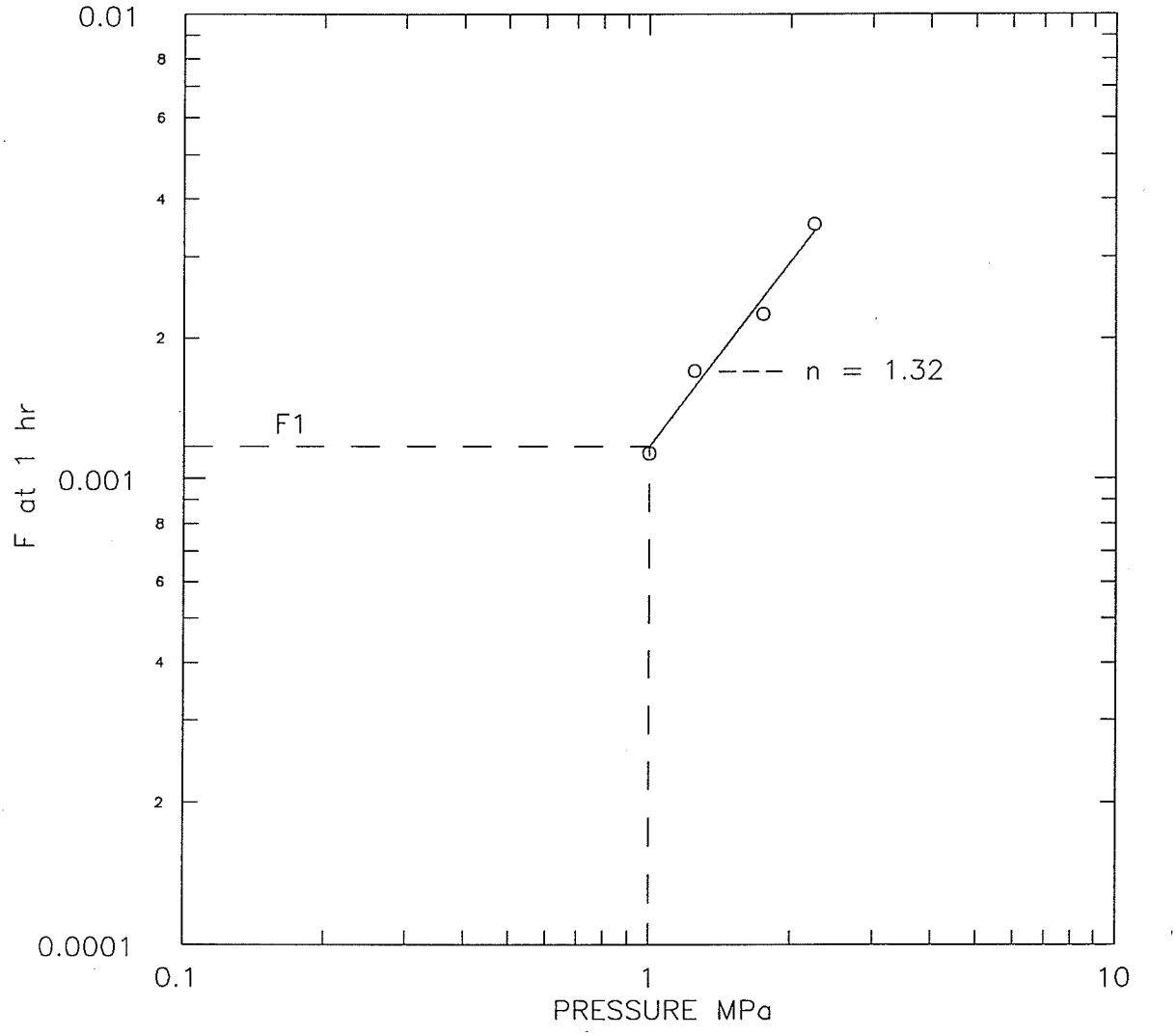


Figure 5.46 Determination of $n_p$ using primary creep displacements of the midpoint of the embedded length of the bar (single stage tests).

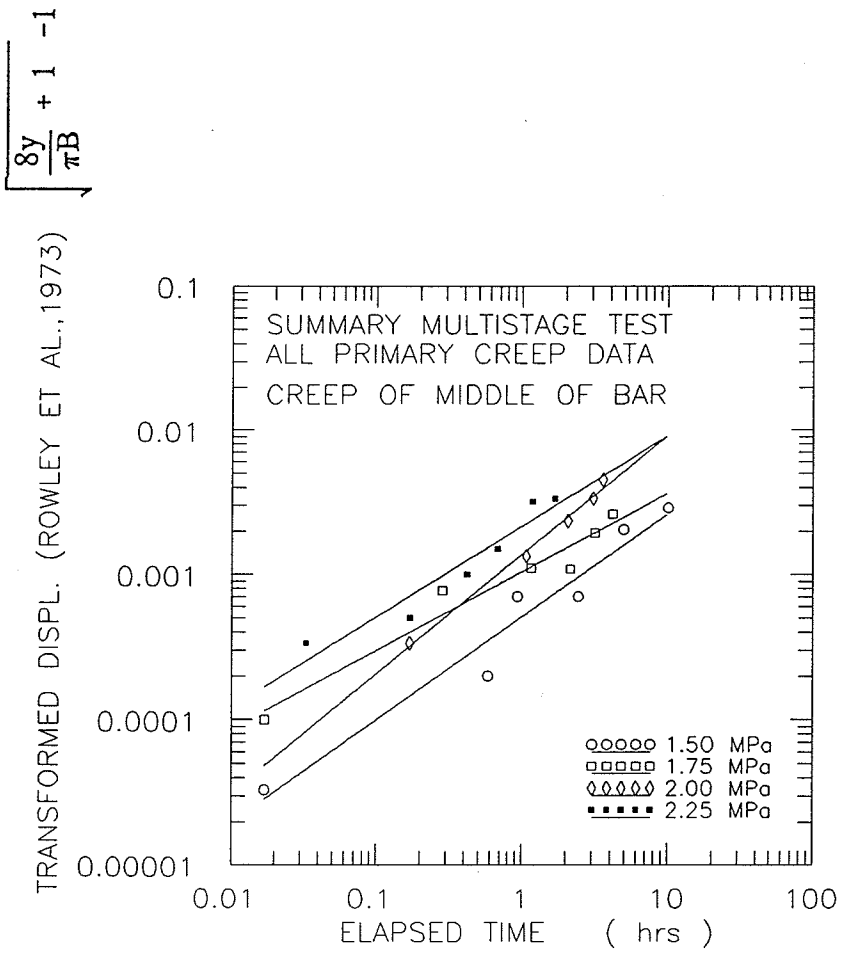


Figure 5.47 Summary of determination of $b_p$ taking best fit through primary creep displacements of the midpoint of the embedded length of the bar (multi-stage test).

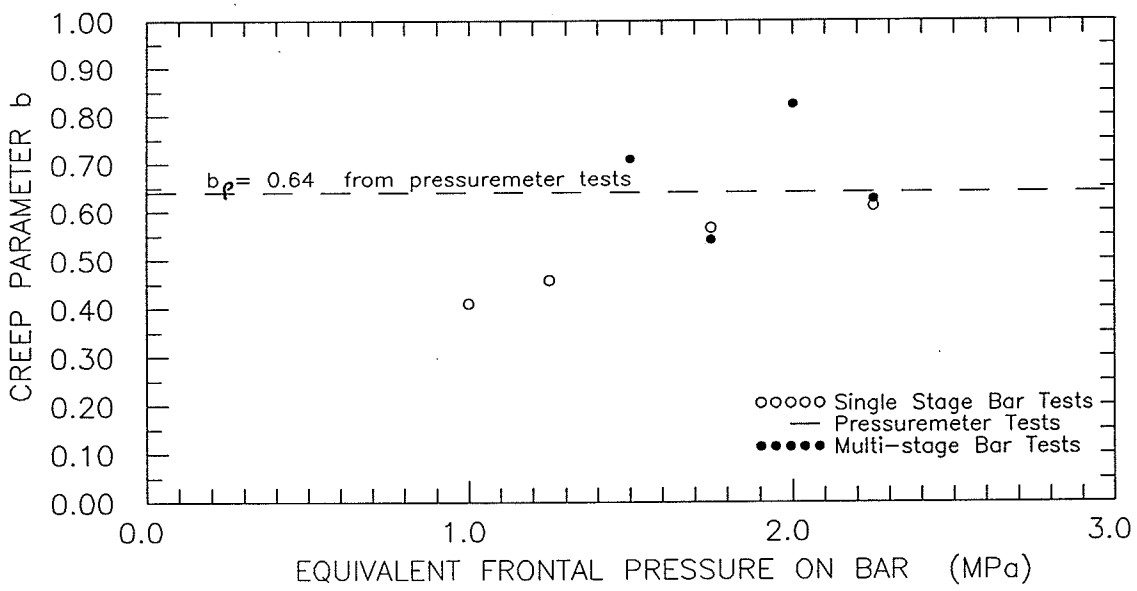


Figure 5.48 Sensitivity of $b_p$ versus pressure. Best fit through primary creep displacements of the midpoint of the embedded length of the bar (single stage and multi-stage tests).

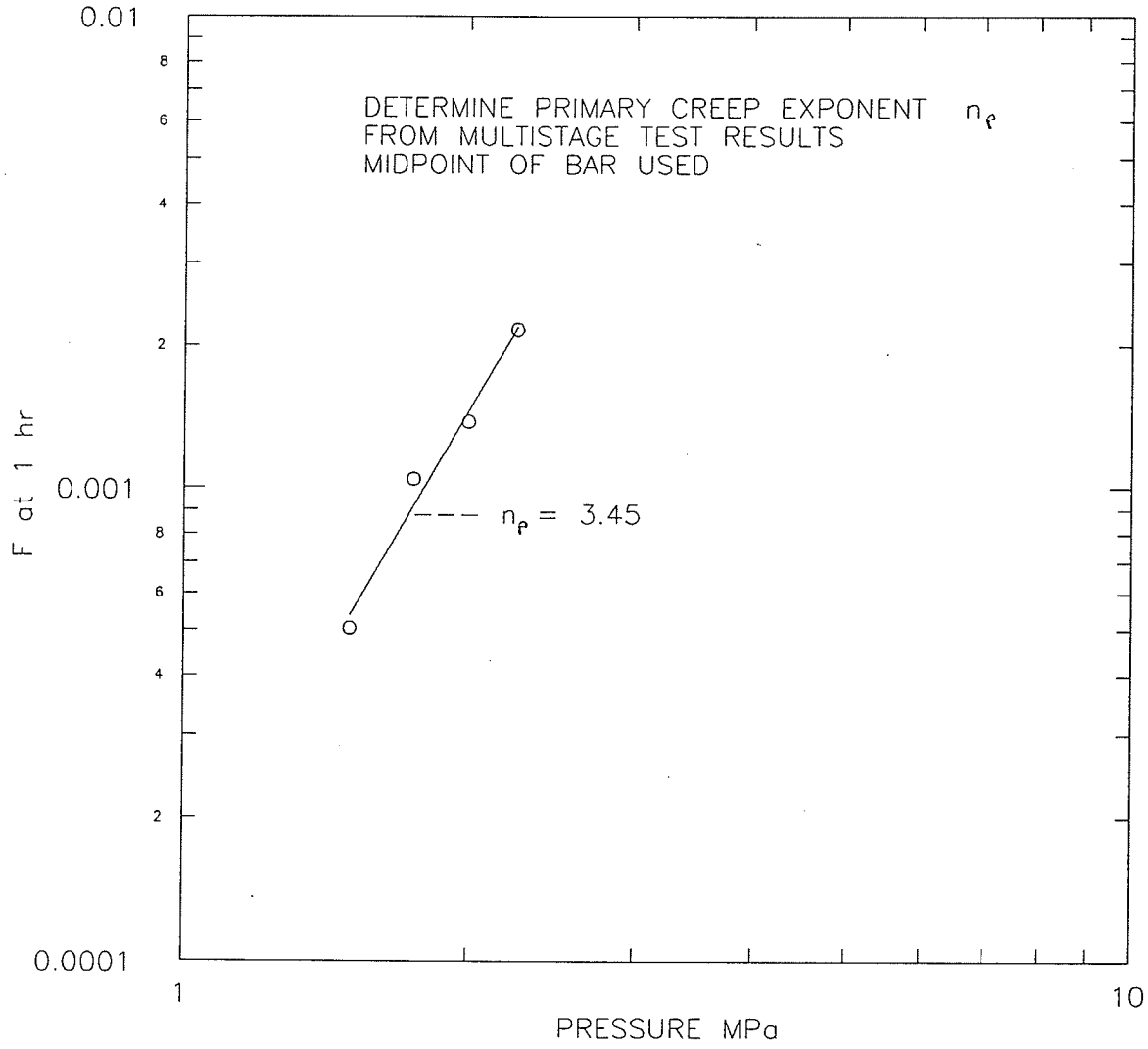


Figure 5.49 Determination of $n_p$ using primary creep displacements of the midpoint of the embedded length of the bar (multi-stage tests).

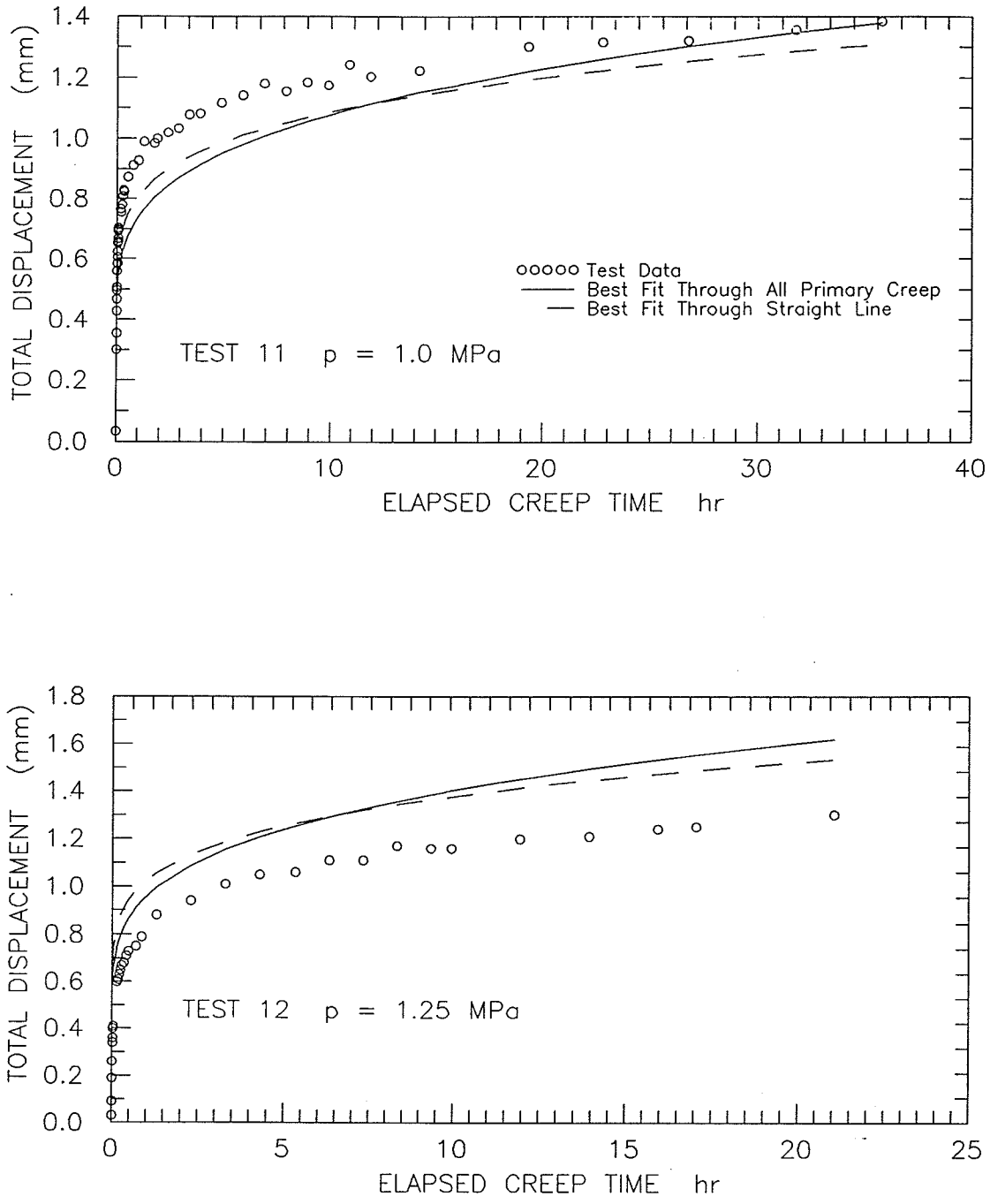


Figure 5.50 Compare pseudo-instantaneous plus primary power law creep model versus test data (p = 1.00 MPa, p = 1.25 MPa) for single stage loaded tests.

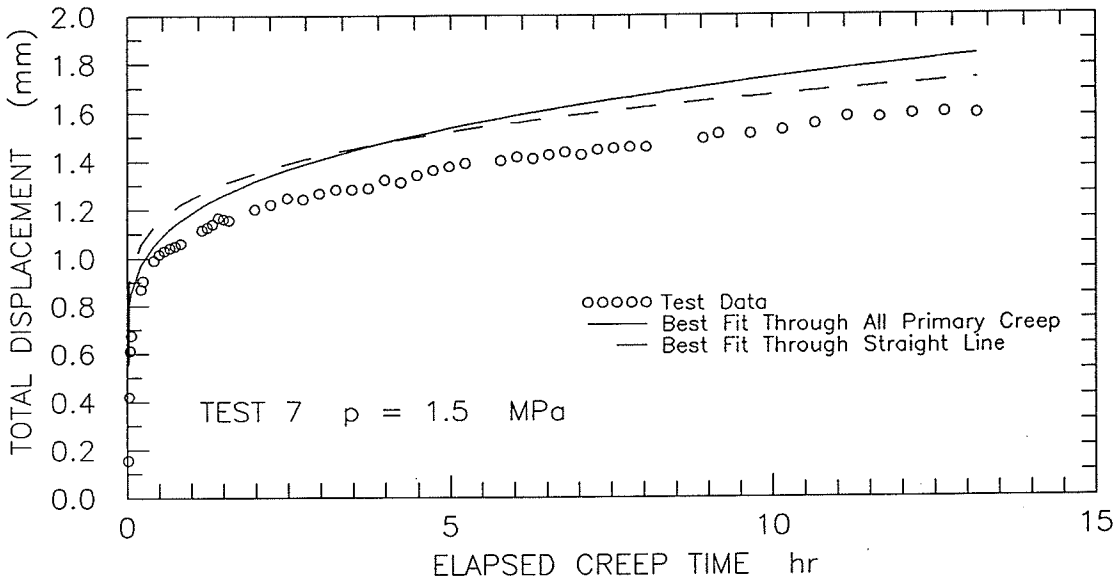


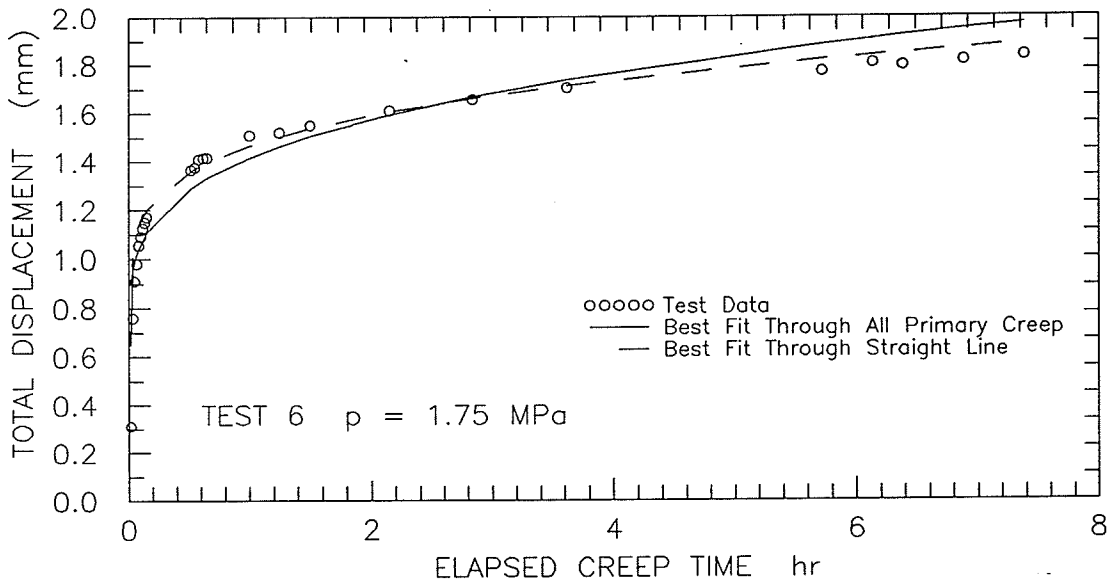


Figure 5.51 Compare pseudo-instantaneous plus primary power law creep model versus test data (p = 1.50 MPa, p = 1.75 MPa) for single stage loaded tests.

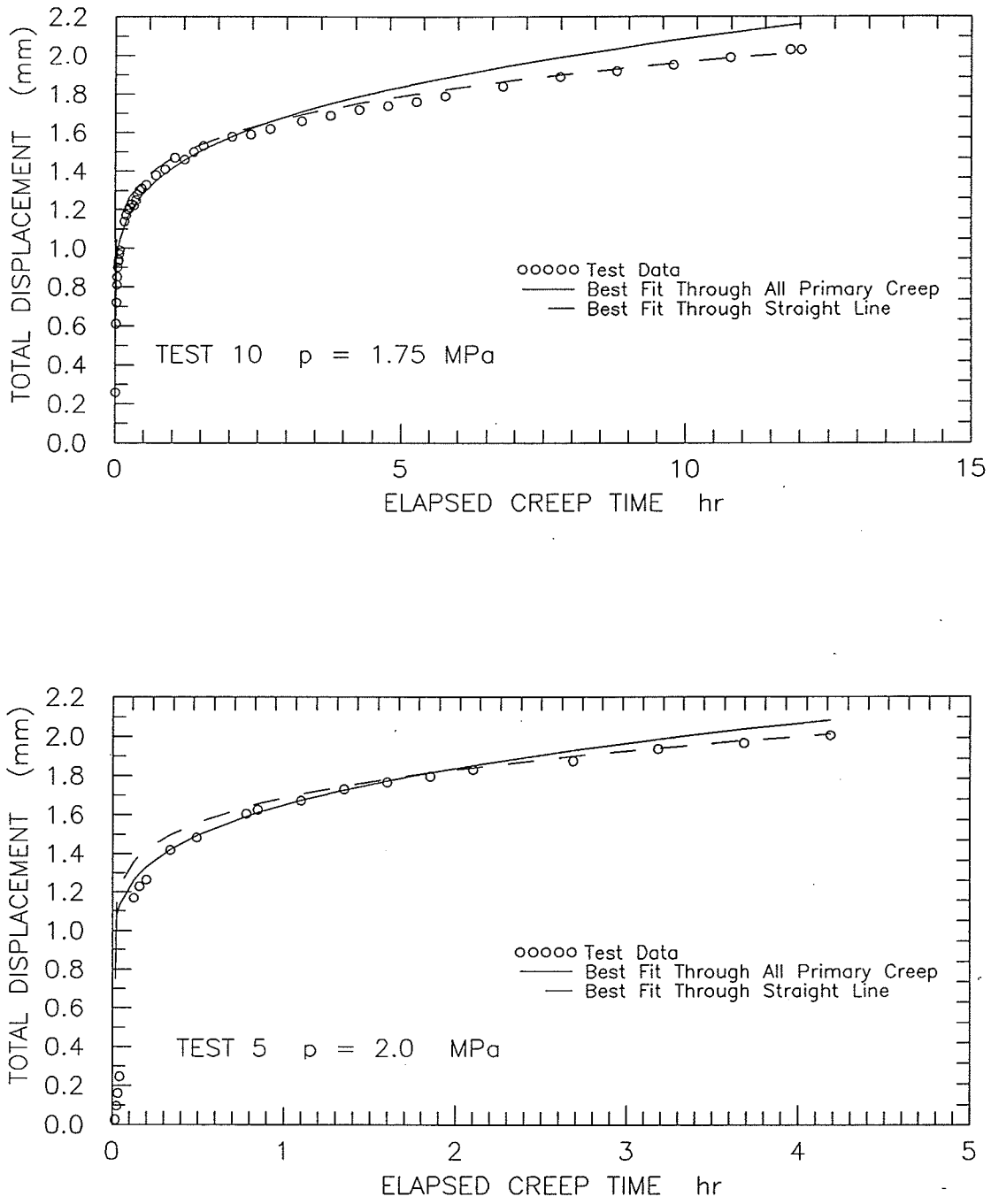


Figure 5.52 Compare pseudo-instantaneous plus primary power law creep model versus test data (p = 1.75 MPa, p = 2.00 MPa) for single stage loaded tests.

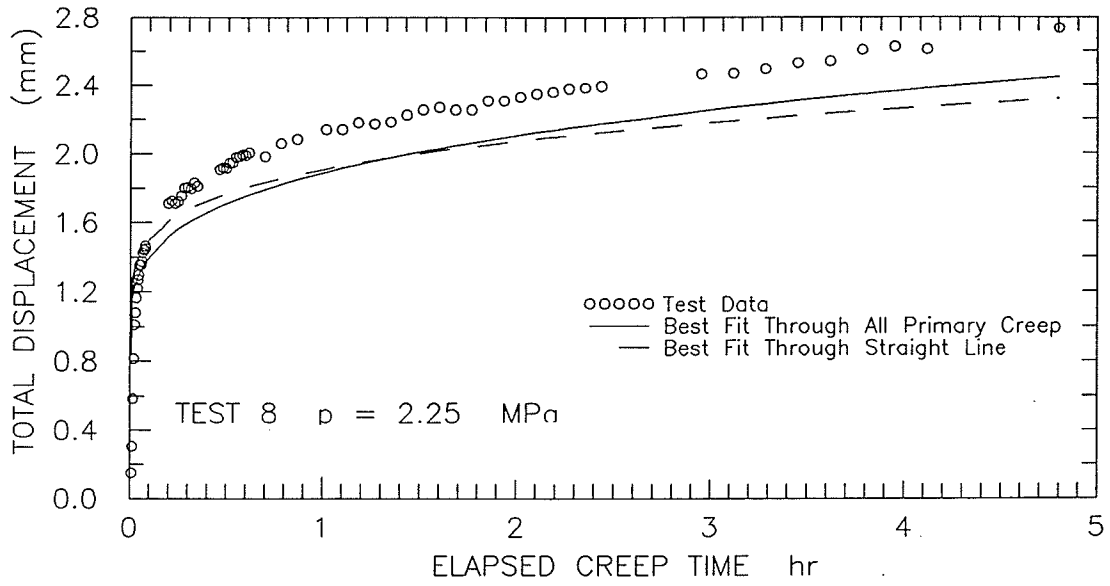


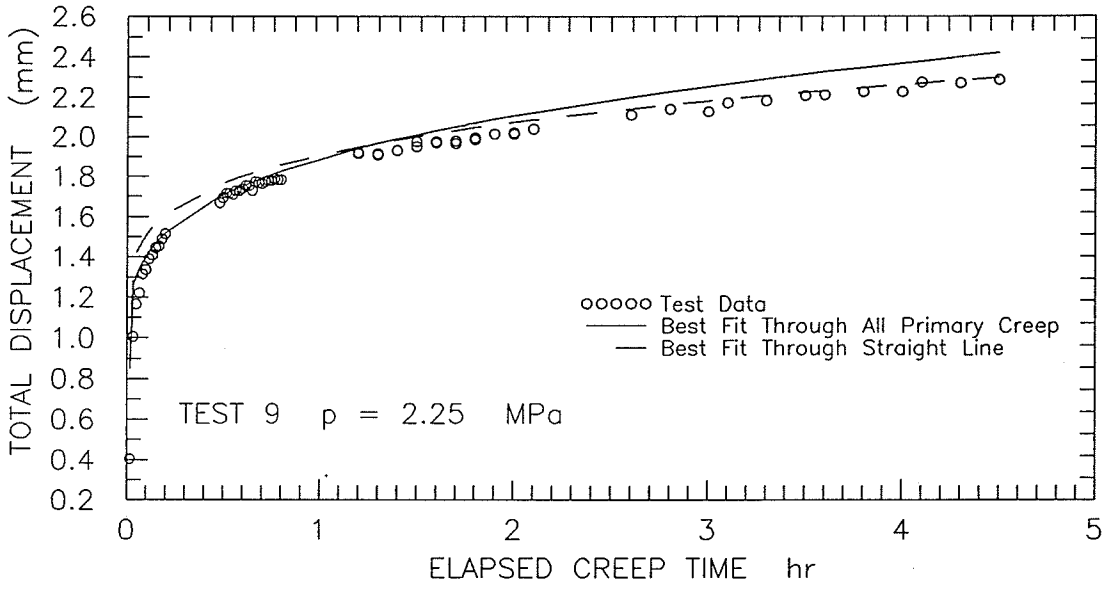


Figure 5.53 Compare pseudo-instantaneous plus primary power law creep model versus test data (p = 2.25 MPa) for single stage loaded tests.

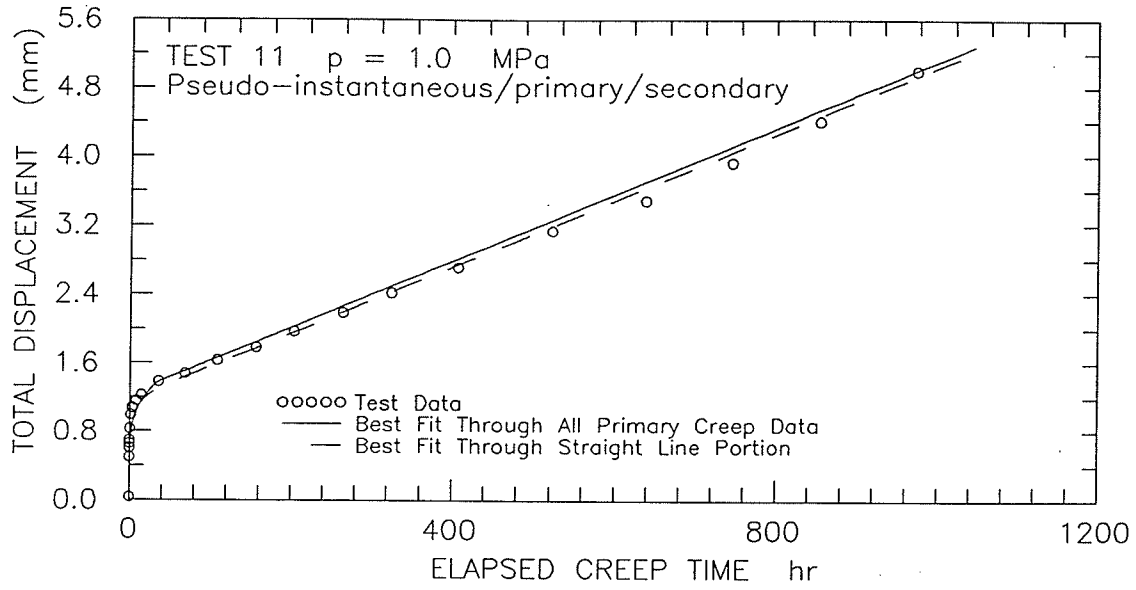


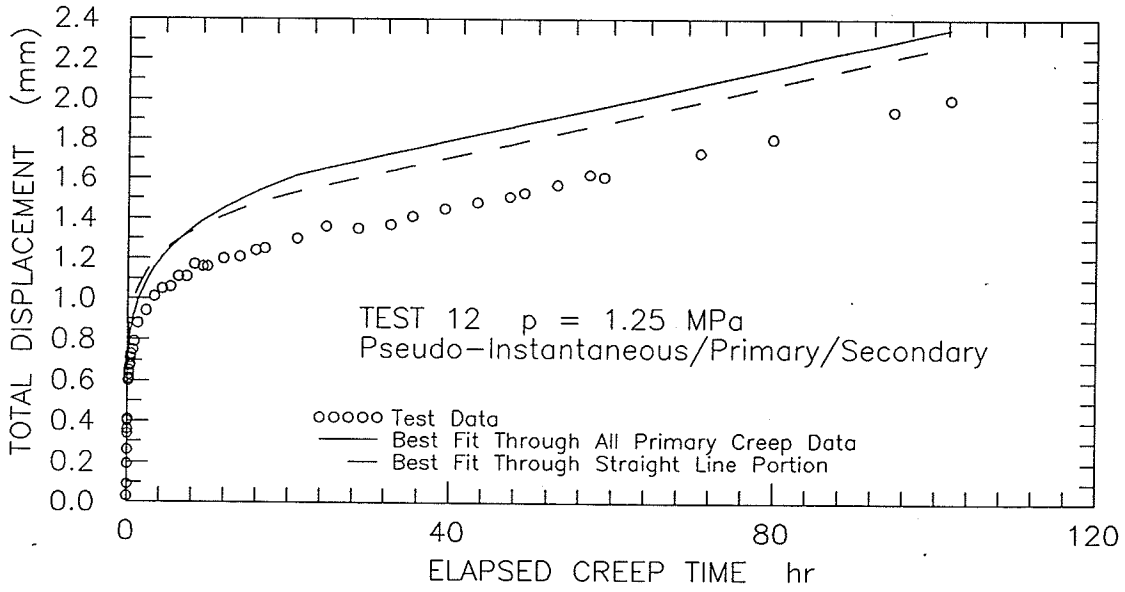


Figure 5.54 Compare pseudo-instantaneous plus primary plus secondary creep model versus test data (p = 1.00 MPa, p = 1.25 MPa) for single stage loaded tests.

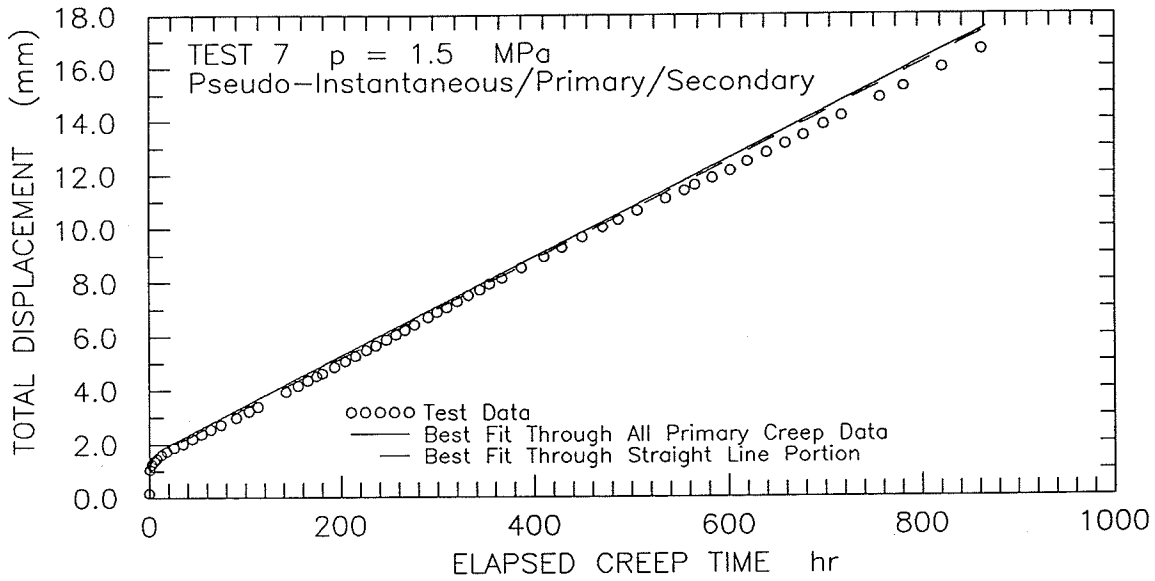


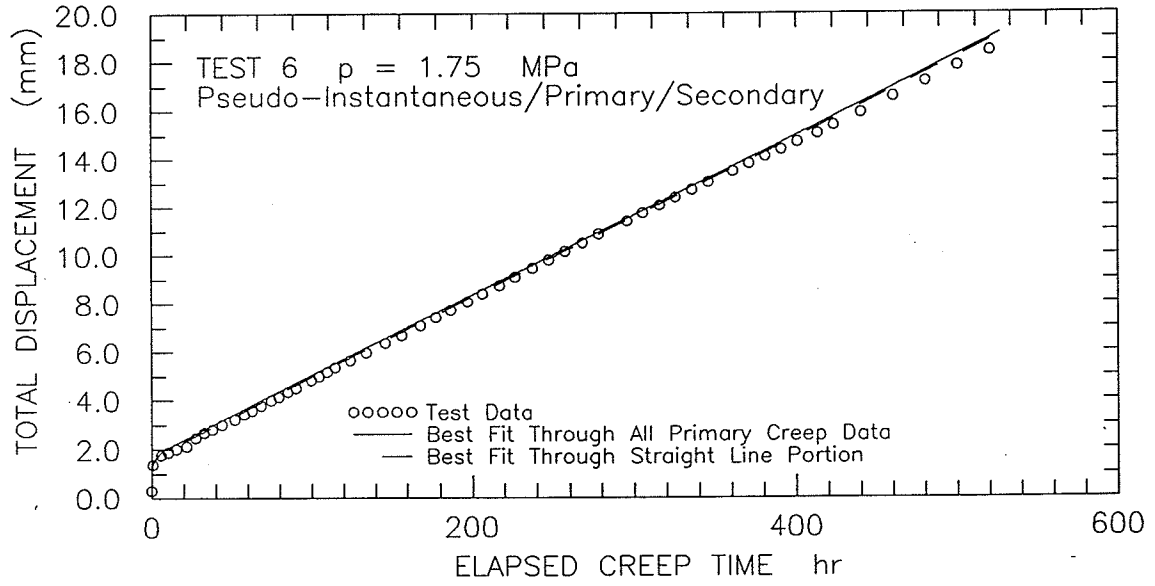


Figure 5.55 Compare pseudo-instantaneous plus primary plus secondary creep model versus test data (p = 1.50 MPa, p = 1.75 MPa) for single stage loaded tests.

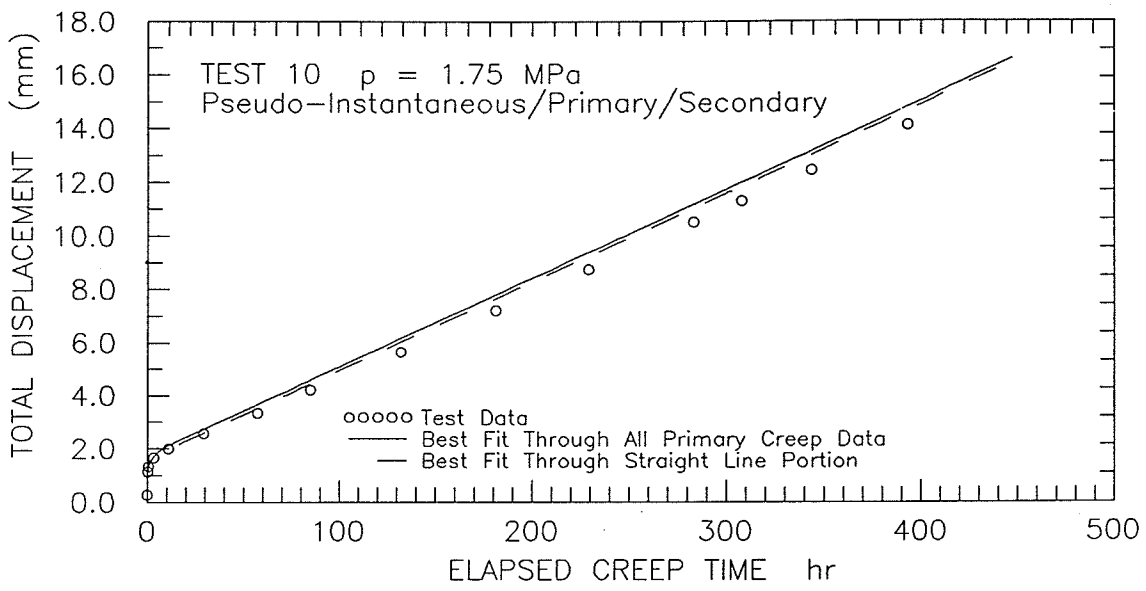


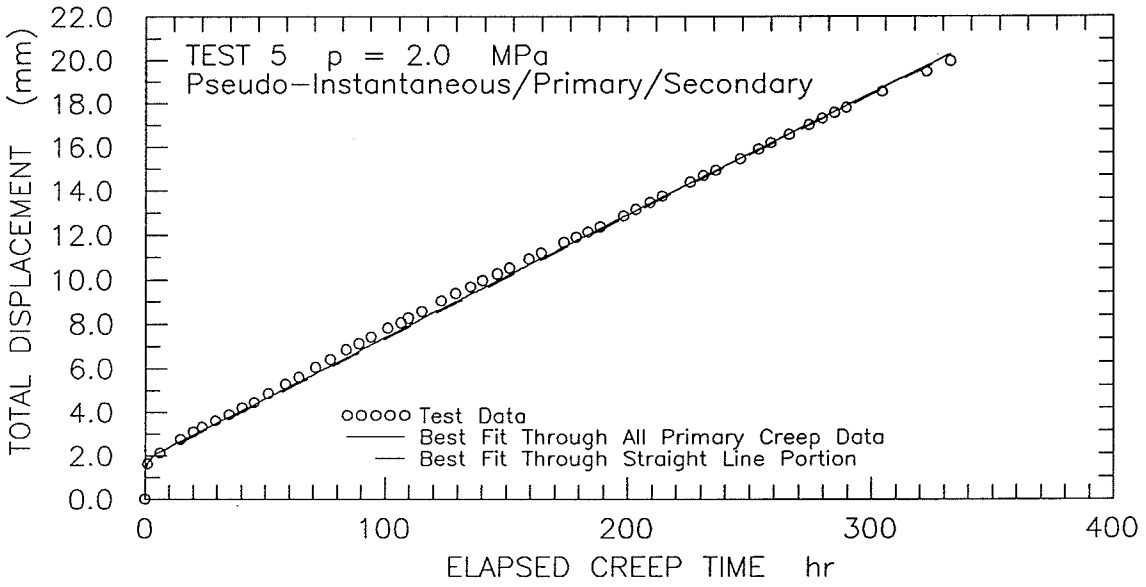


Figure 5.56 Compare pseudo-instantaneous plus primary plus secondary creep model versus test data (p = 1.75 MPa, p = 2.00 MPa) for single stage loaded tests.

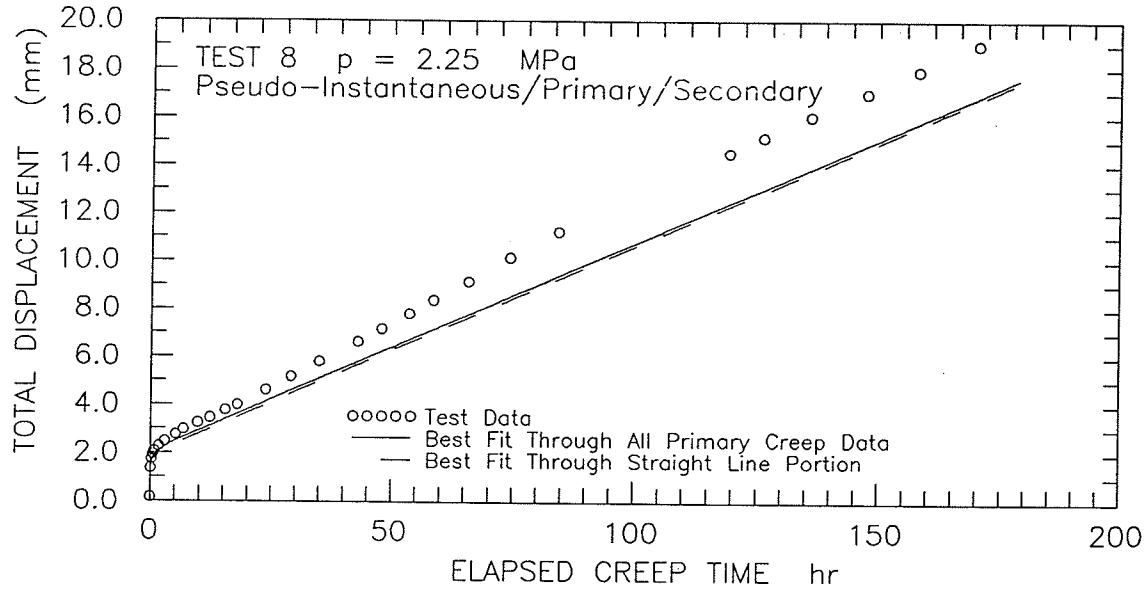


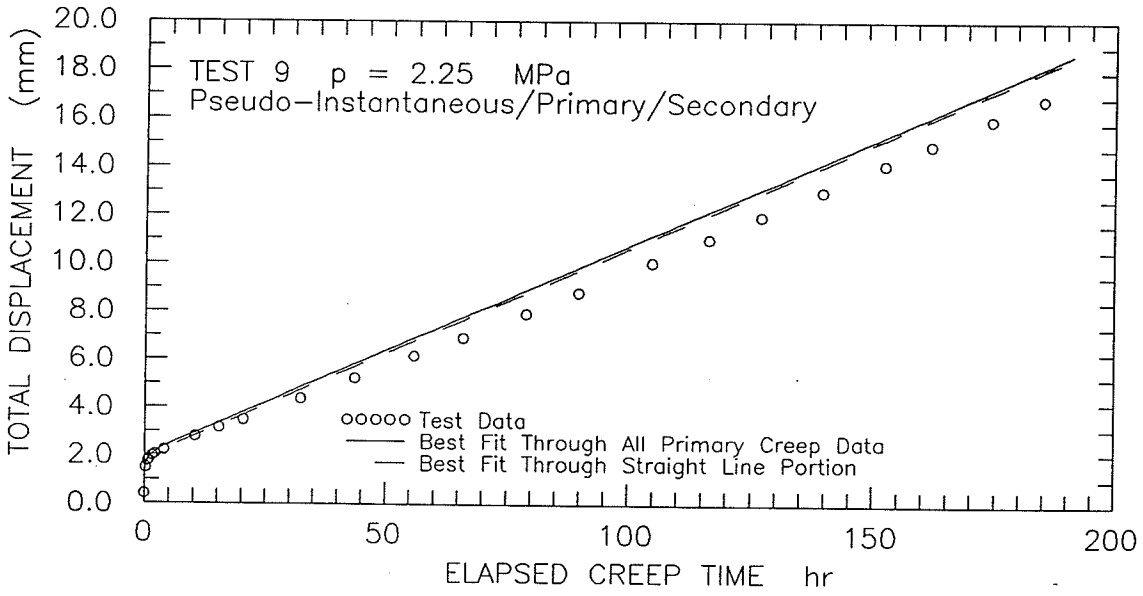


Figure 5.57 Compare pseudo-instantaneous plus primary plus secondary creep model versus test data (p = 2.25 MPa) for single stage loaded tests.

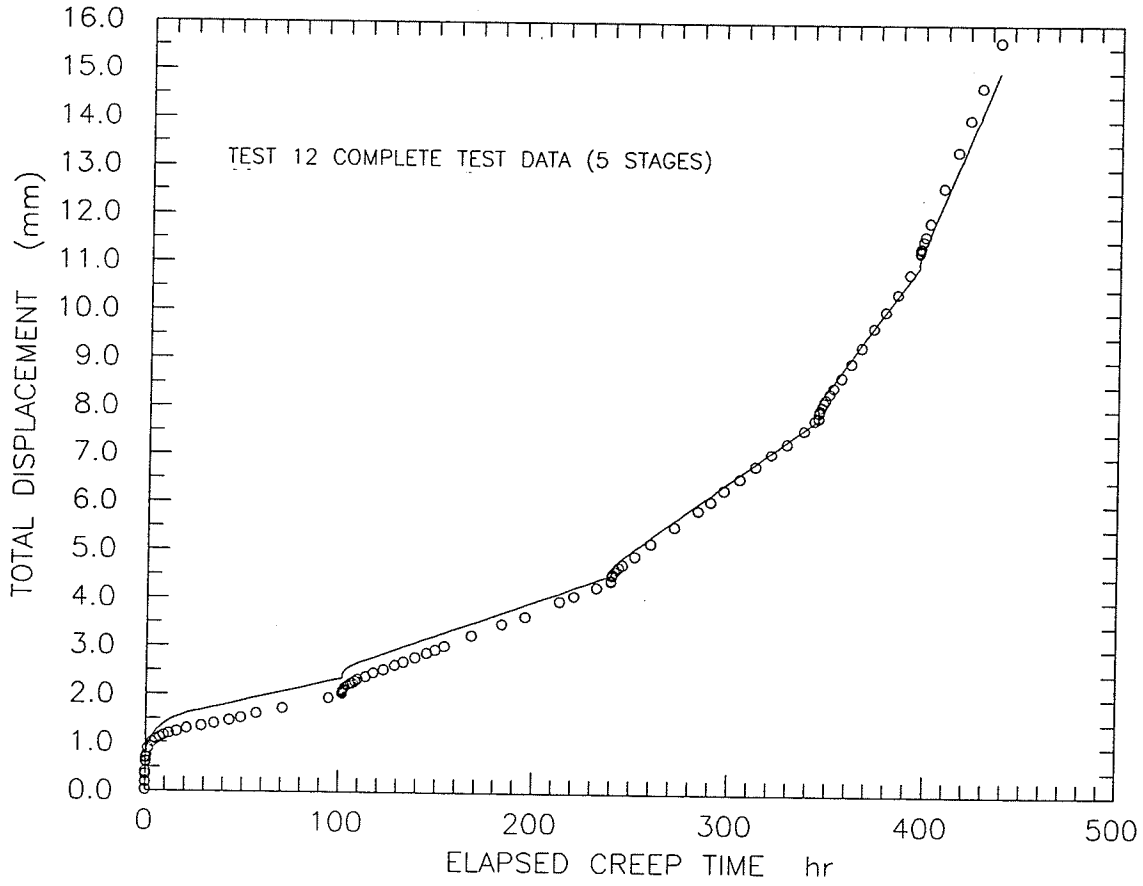


Figure 5.58 Compare pseudo-instantaneous plus primary plus secondary creep model versus test data (multi-stage test).

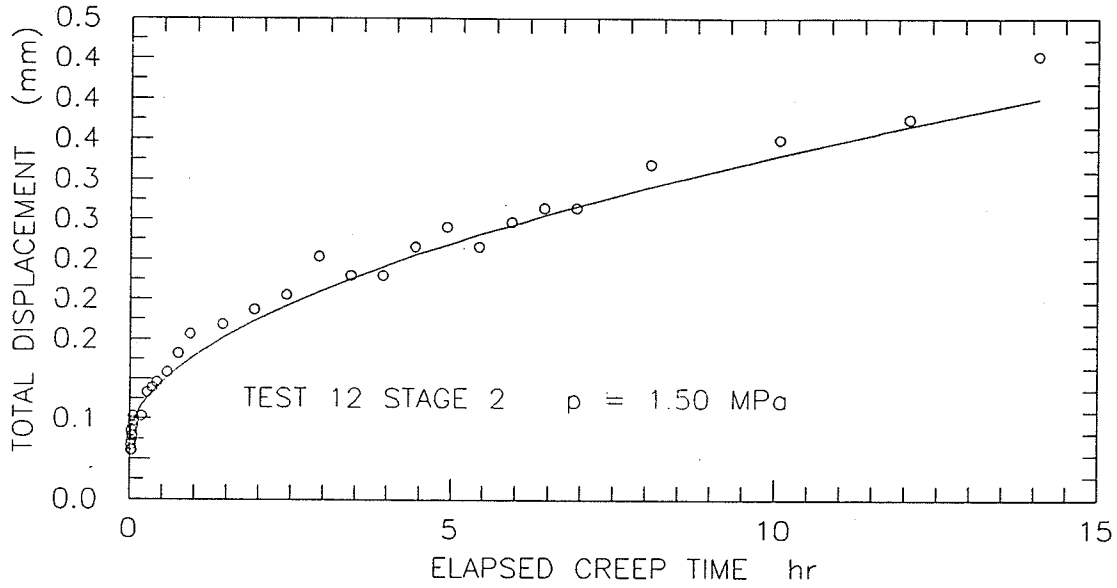


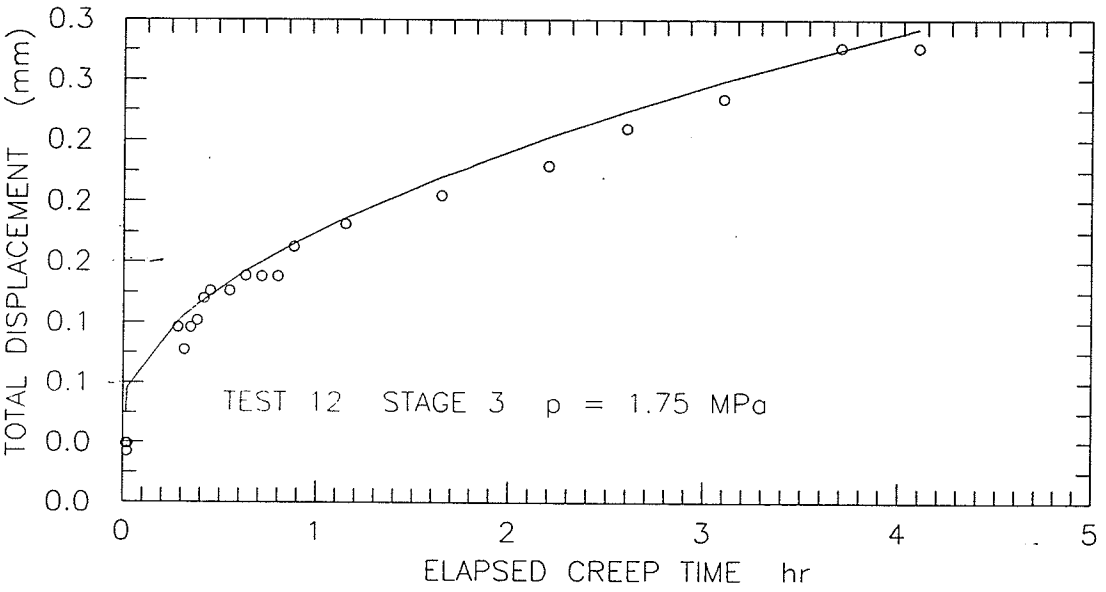


Figure 5.59 Compare pseudo-instantaneous plus primary creep model versus test data (p = 1.50 MPa, p = 1.75 MPa) for multi-stage test.

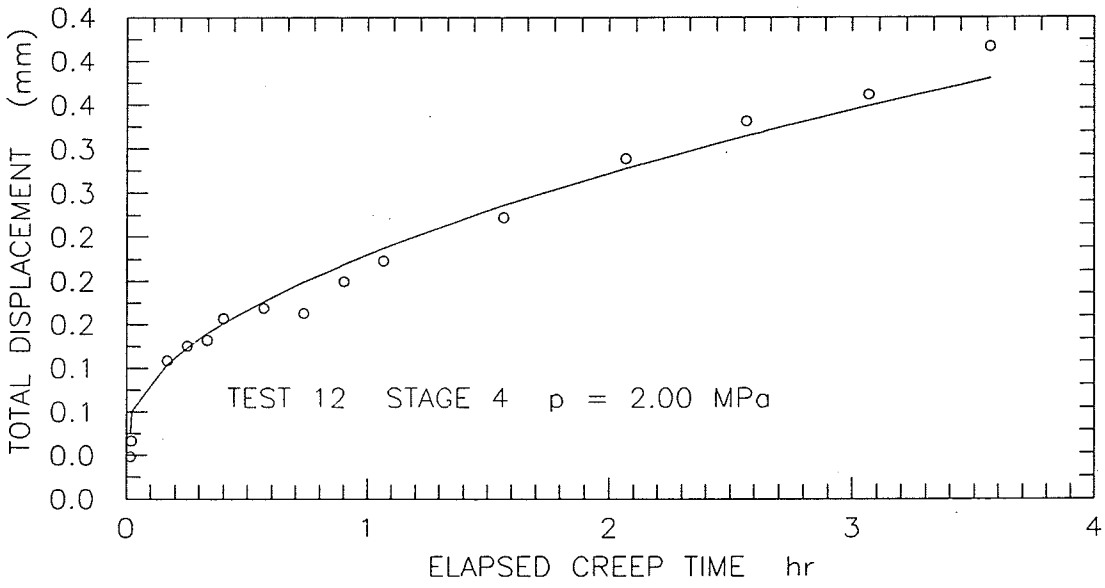


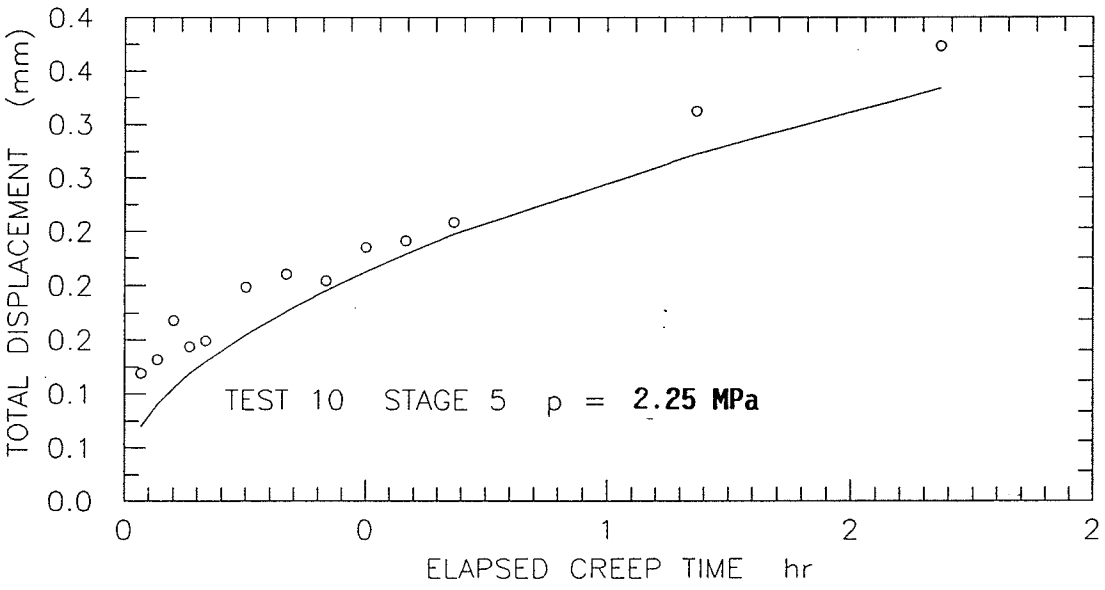


Figure 5.60 Compare pseudo-instantaneous plus primary creep model versus test data (p = 2.00 MPa, p = 2.25 MPa) for multi-stage test.

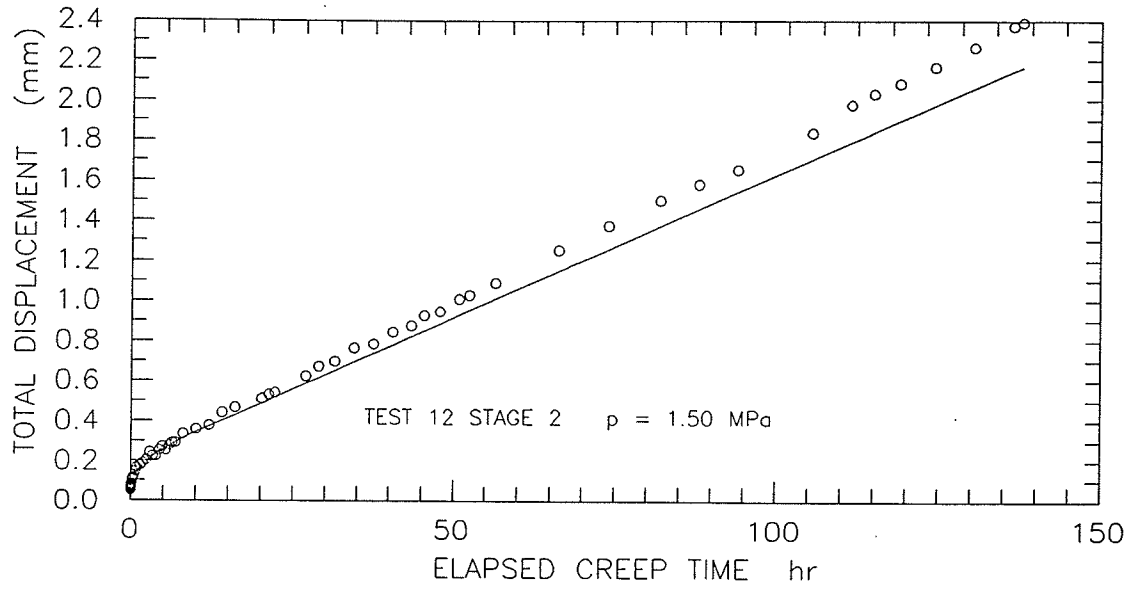


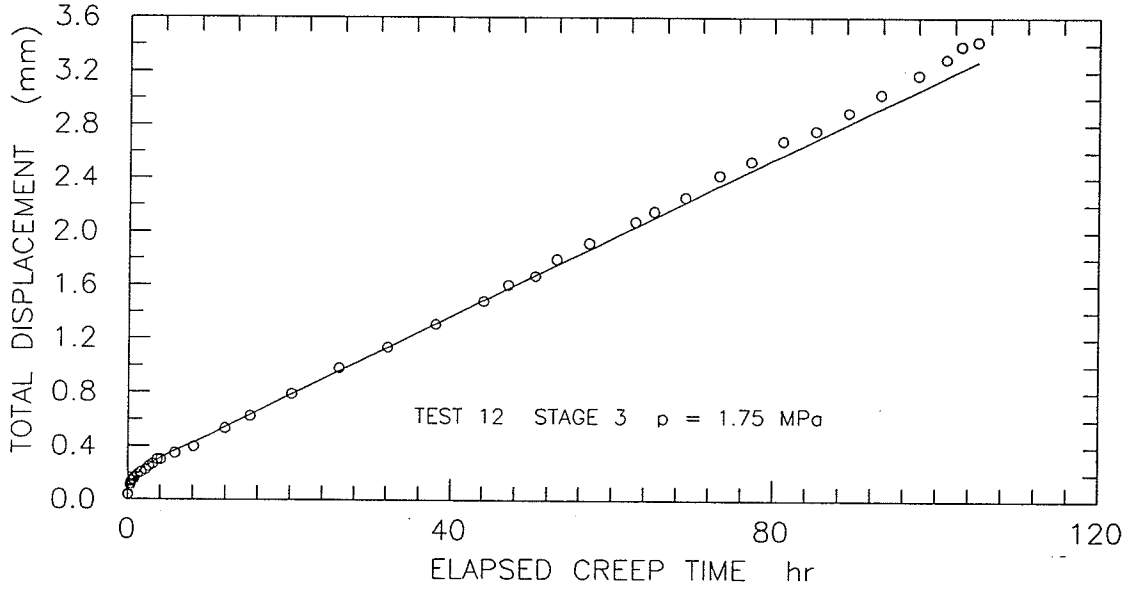


Figure 5.61 Compare pseudo-instantaneous plus primary plus secondary creep model versus test data (p = 1.50 MPa, p = 1.75 MPa) for multi-stage test.

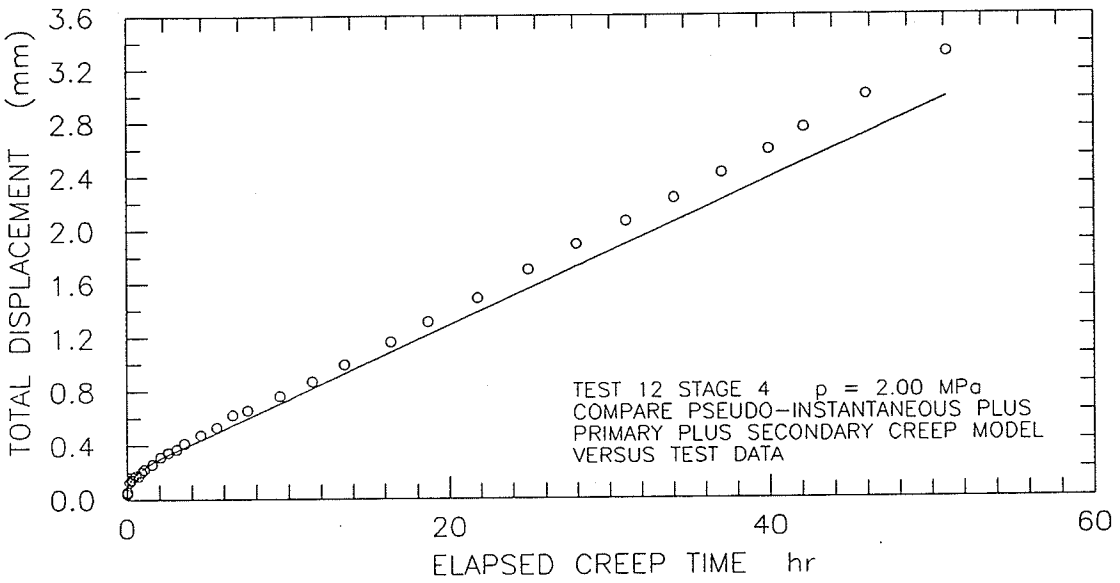


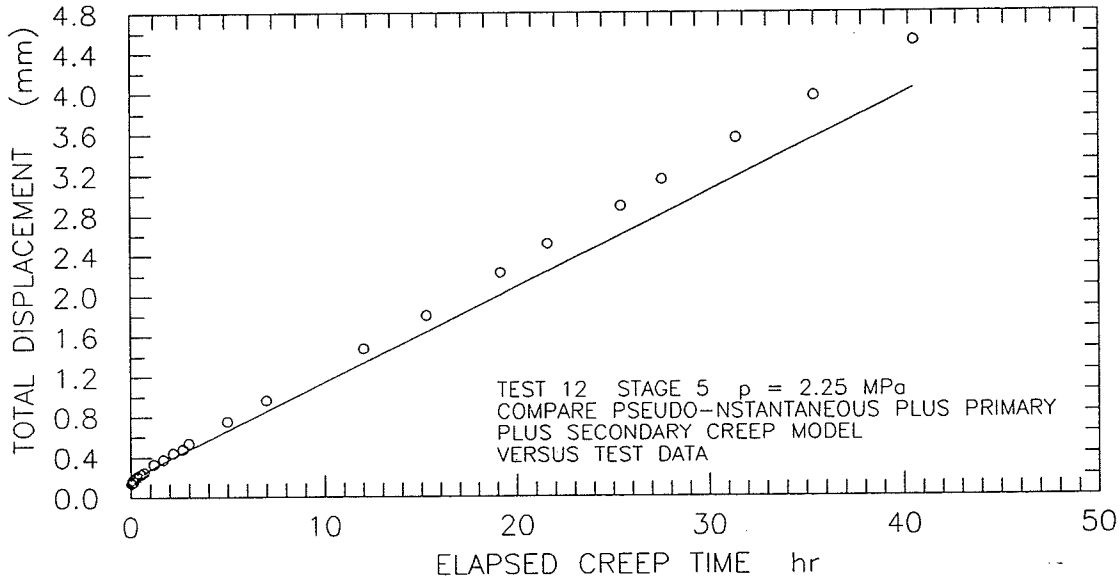


Figure 5.62 Compare pseudo-instantaneous plus primary plus secondary creep model versus test data (p = 2.00 MPa, p = 2.25 MPa) for multi-stage test.

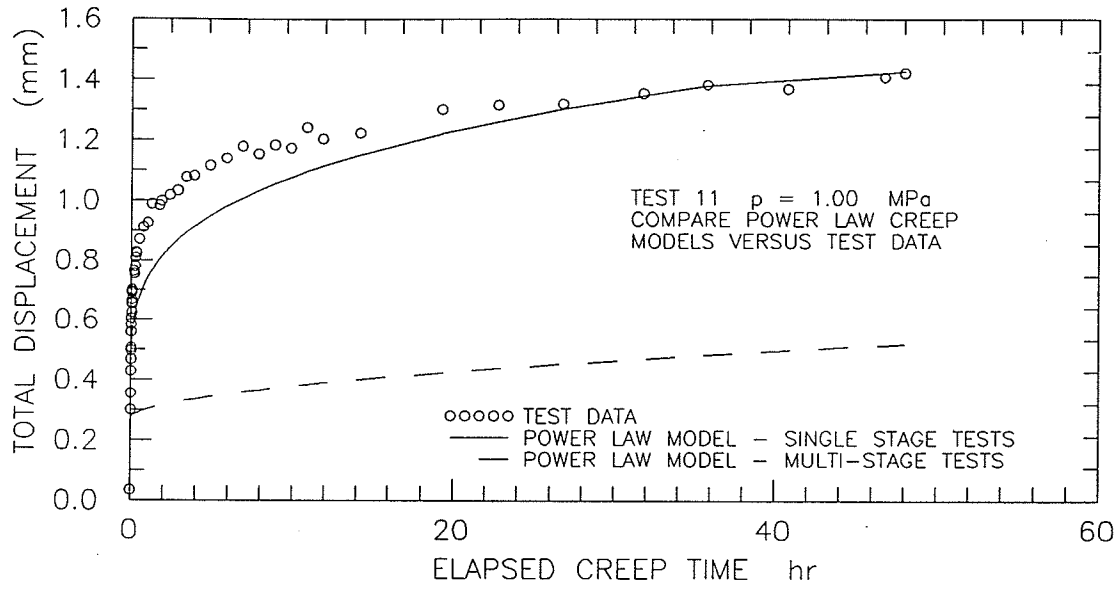


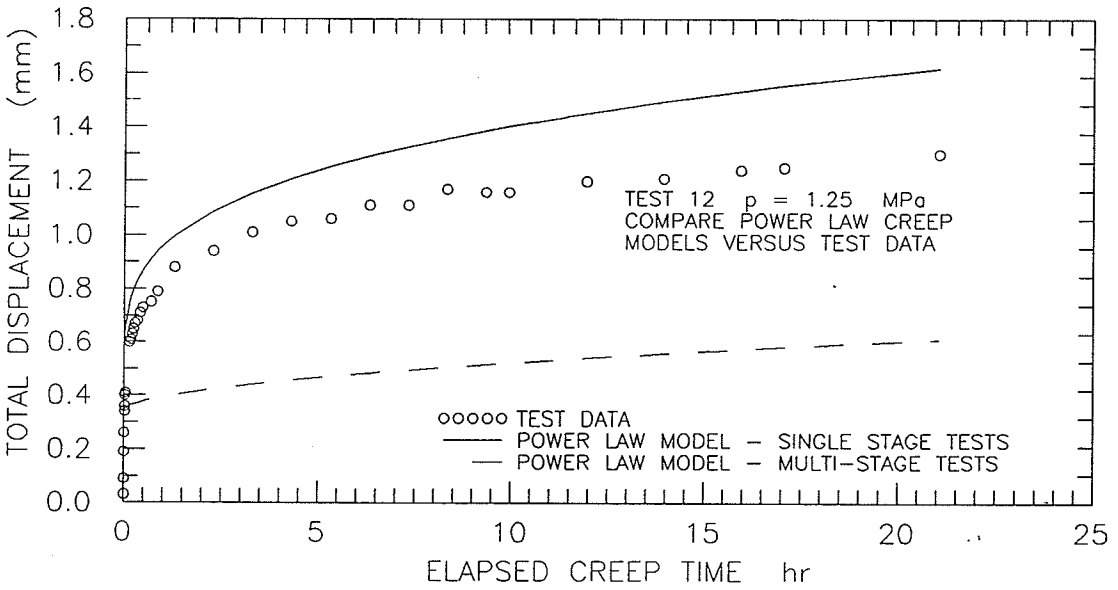


Figure 5.63 Compare pseudo-instantaneous plus primary creep model from multi-stage test versus single stage test data (p = 1.00 MPa, p = 1.25 MPa).

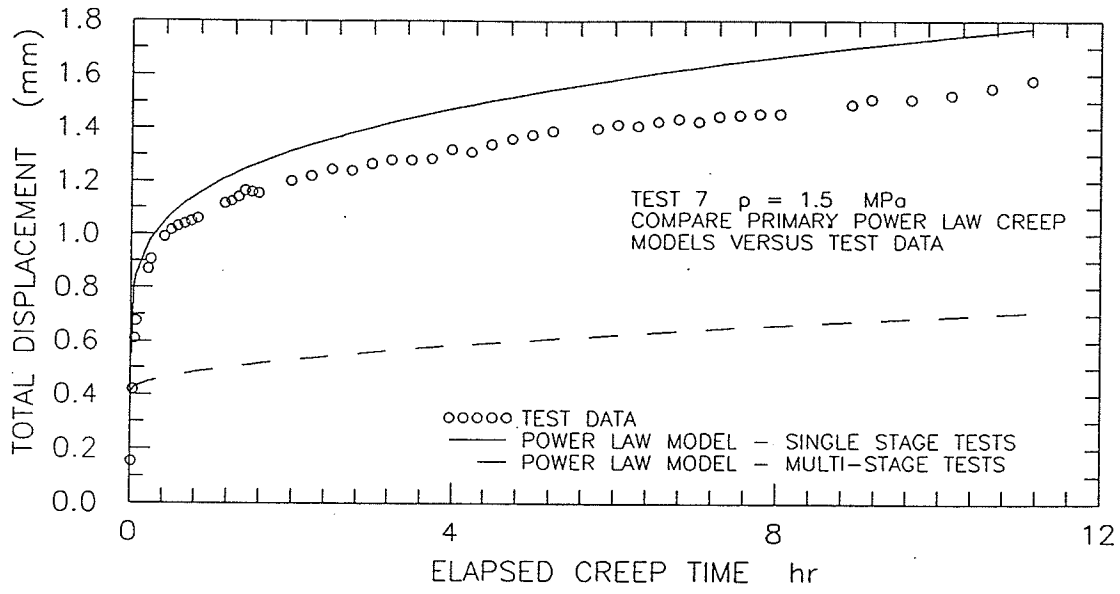


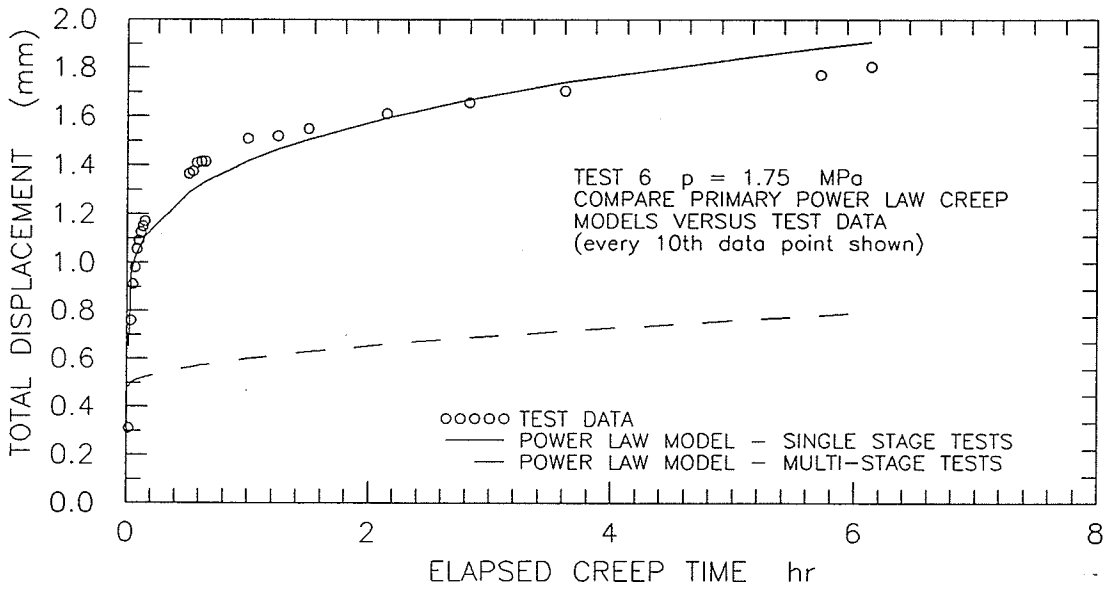


Figure 5.64 Compare pseudo-instantaneous plus primary creep model from multi-stage test versus single stage test data (p = 1.50 MPa, p = 1.75 MPa).

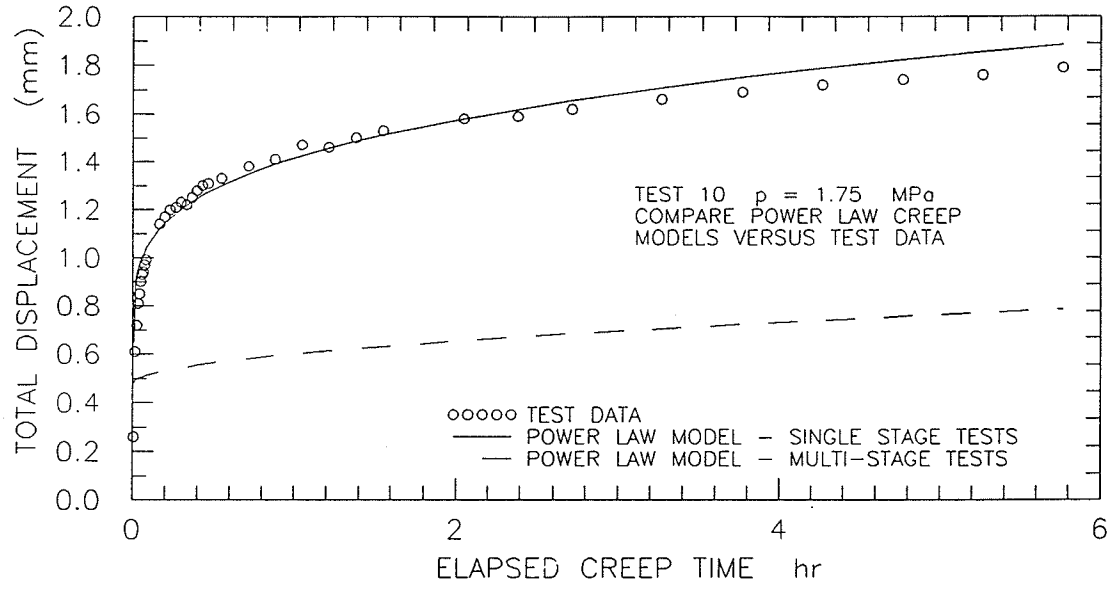


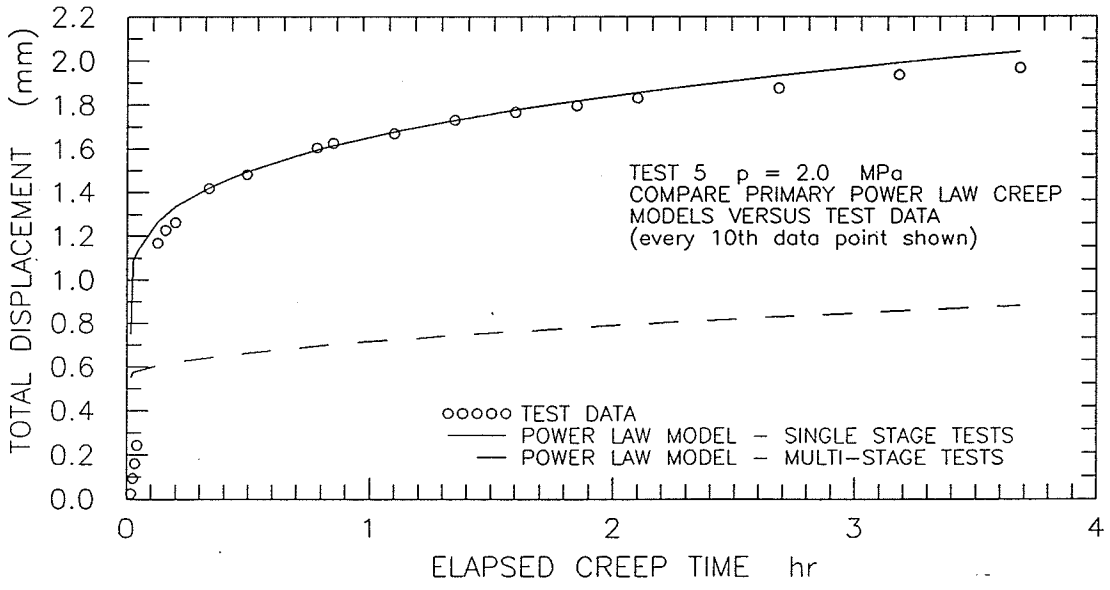


Figure 5.65 Compare pseudo-instantaneous plus primary creep model from multi-stage test versus single stage test data (p = 1.75 MPa, p = 2.00 MPa).

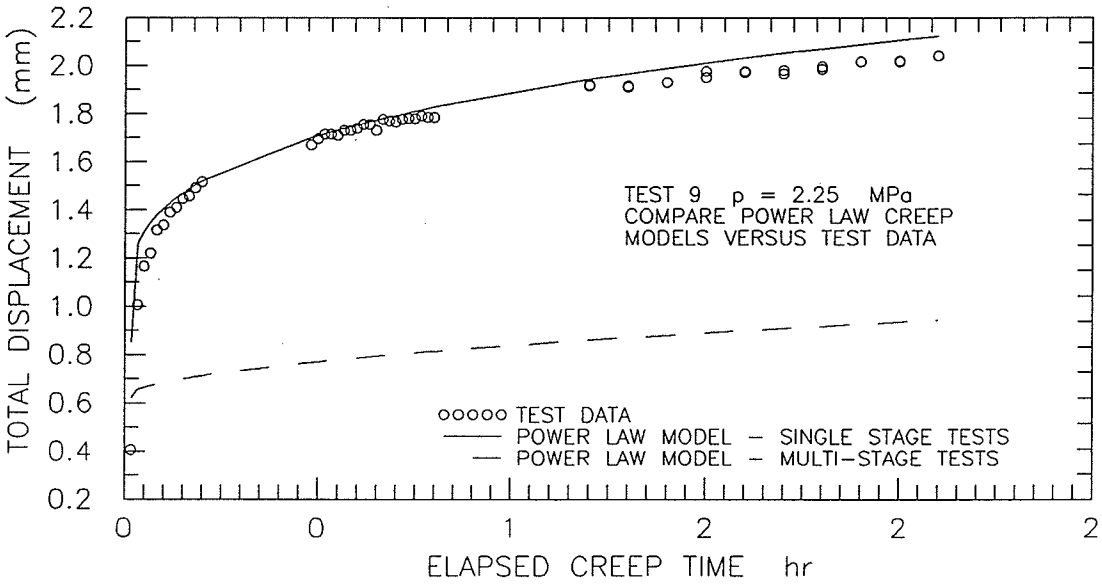


Figure 5.66 Compare pseudo-instantaneous plus primary creep model from multi-stage test versus single stage test data (p = 2.25 MPa).

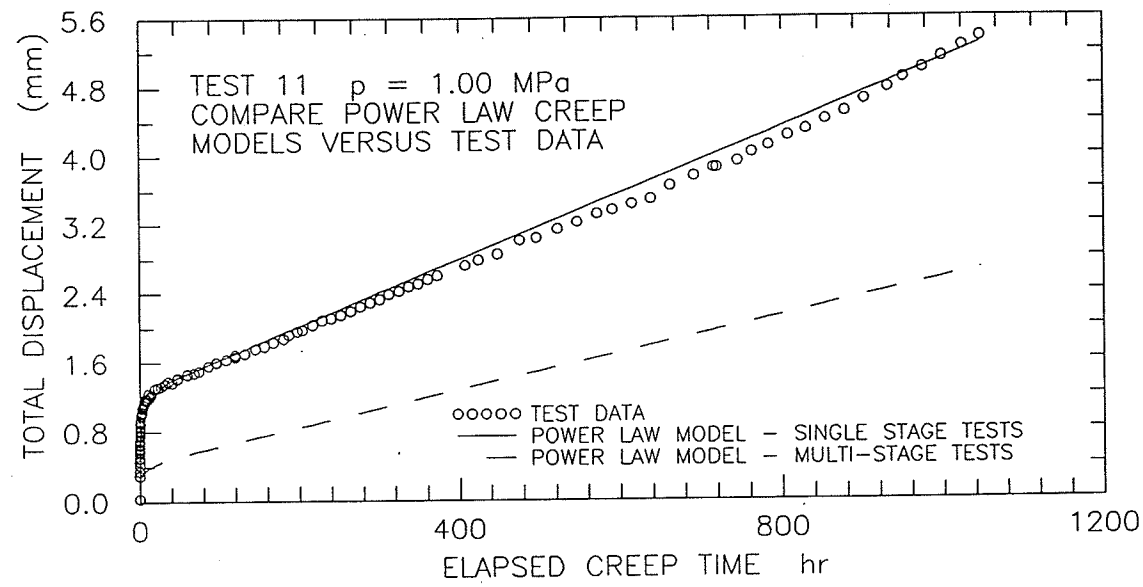


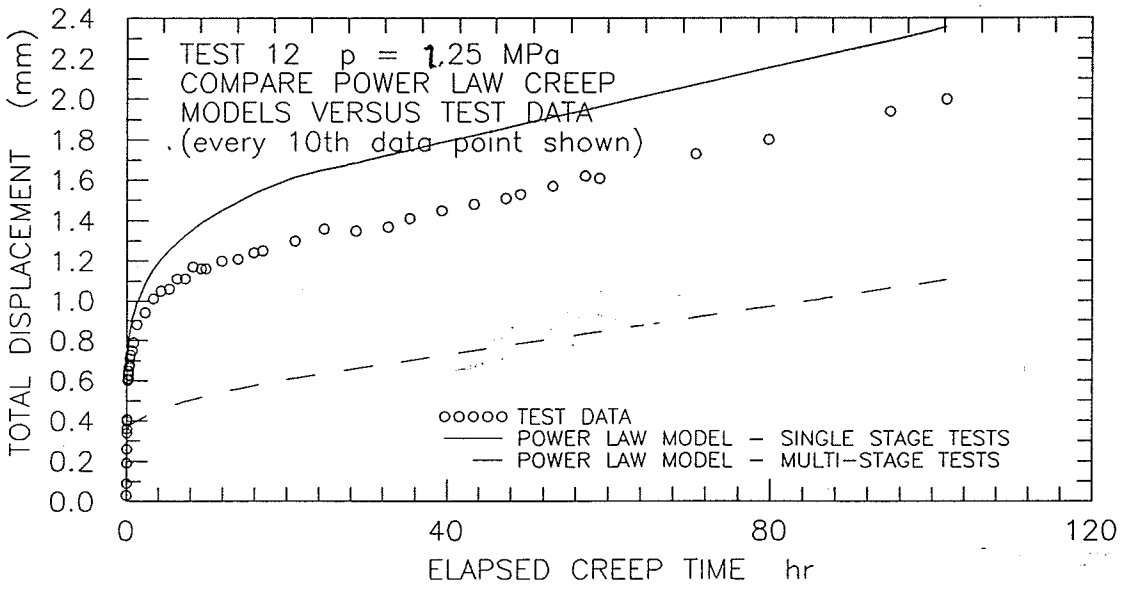


Figure 5.67 Compare pseudo-instantaneous plus primary plus secondary creep model from multi-stage test versus single stage test data (p = 1.00 MPa, p = 1.25 MPa).

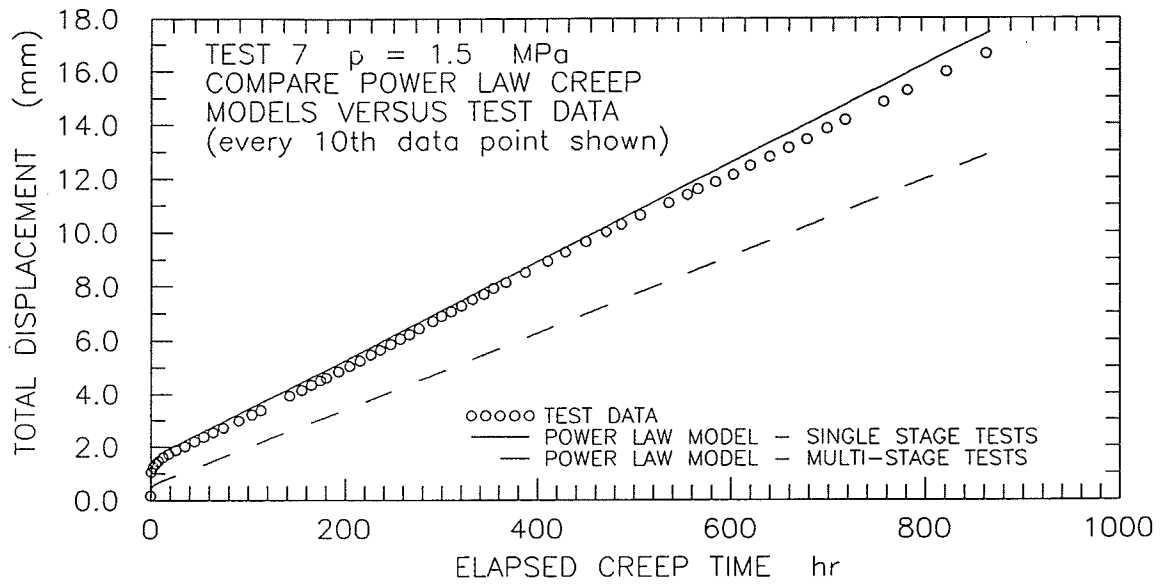


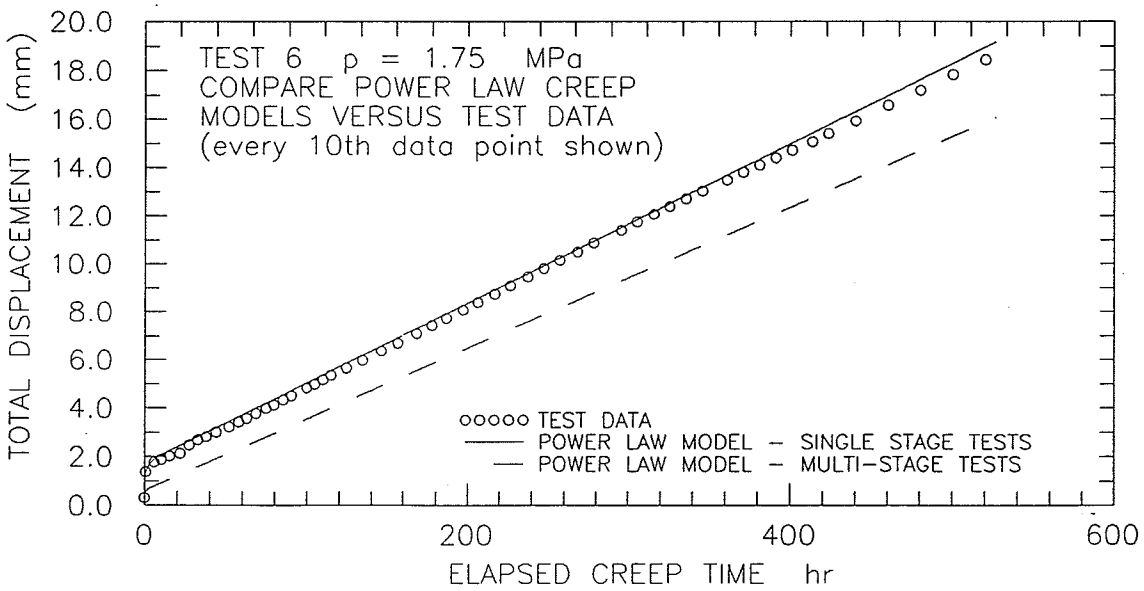


Figure 5.68 Compare pseudo-instantaneous plus primary plus secondary creep model from multi-stage test versus single stage test data (p = 1.50 MPa, p = 1.75 MPa).

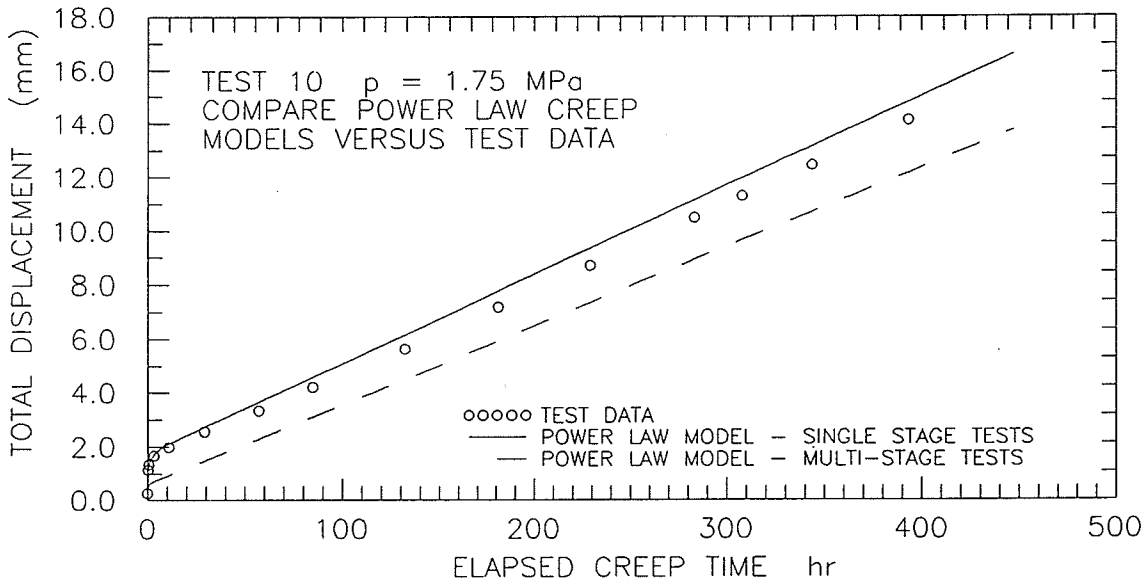


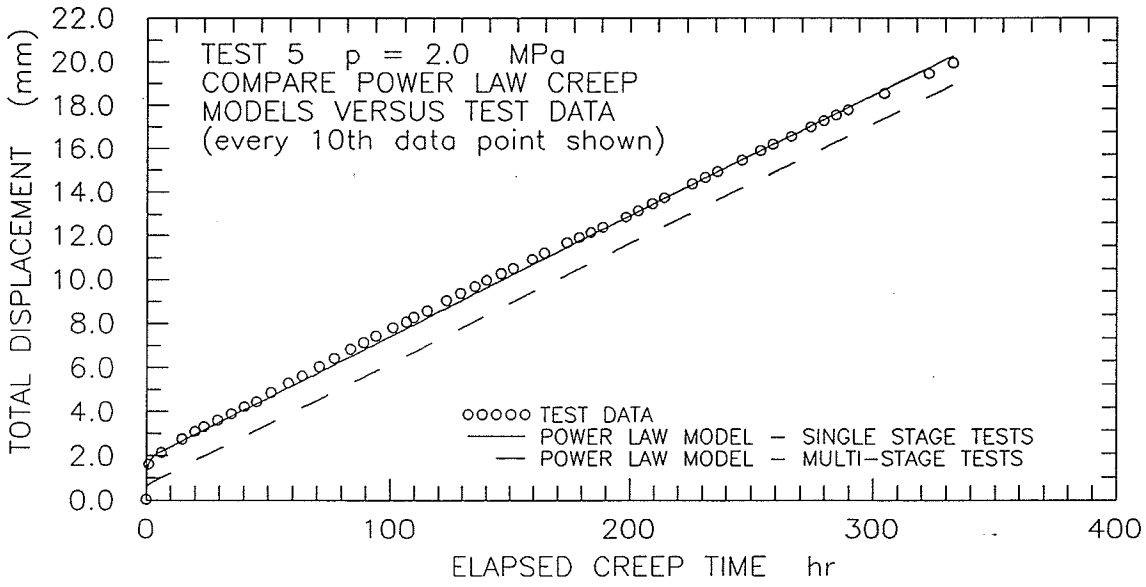


Figure 5.69 Compare pseudo-instantaneous plus primary plus secondary creep model from multi-stage test versus single stage test data (p = 1.75 MPa, p = 2.00 MPa).

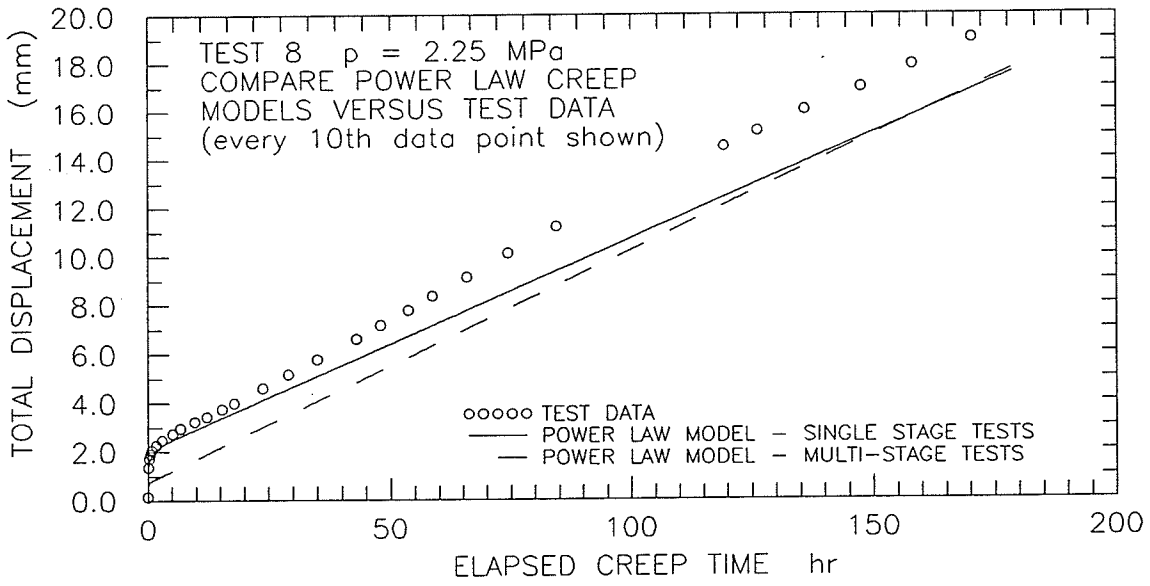


Figure 5.70 Compare pseudo-instantaneous plus primary plus secondary creep model from multi-stage test versus single stage test data (p = 2.25 MPa).

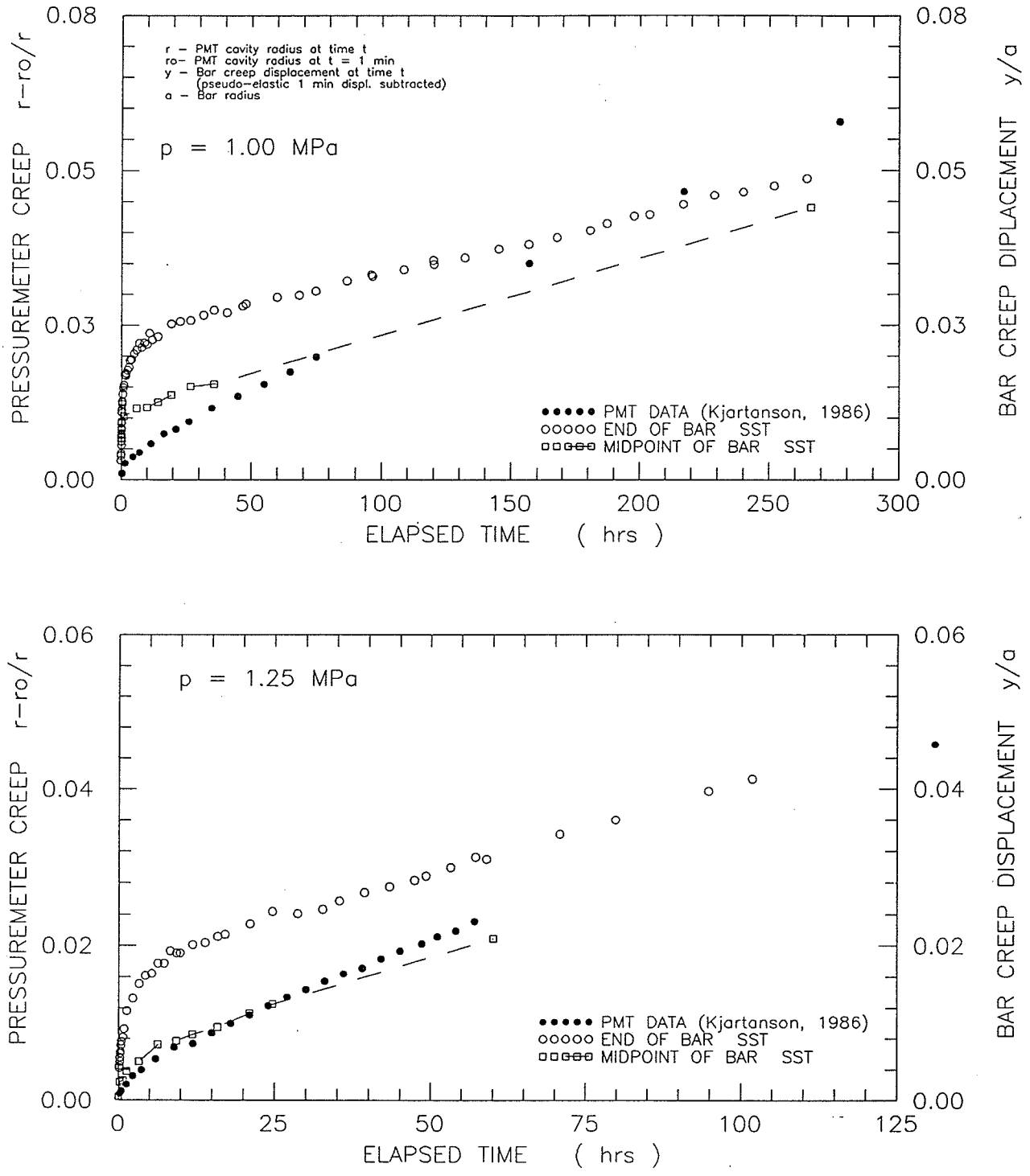


Figure 5.71 Compare bar test data versus pressuremeter test data. Early portions of the tests for p = 1.00 MPa and p = 1.25 MPa.

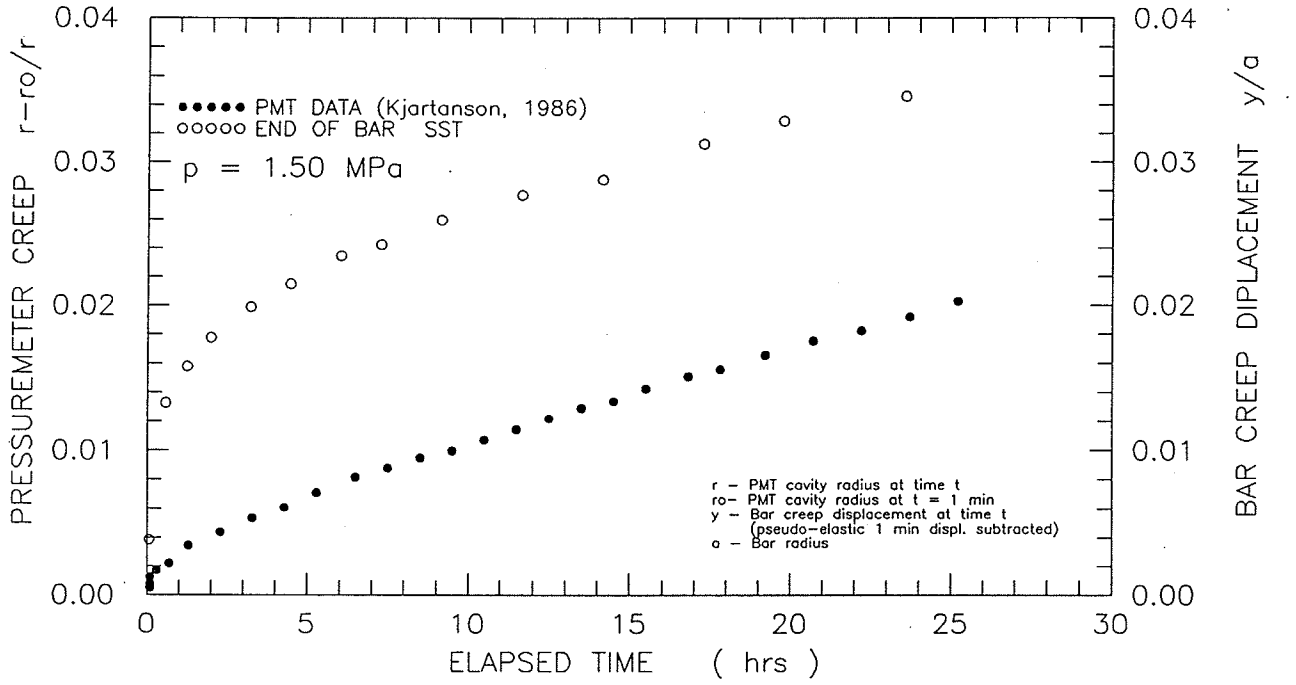


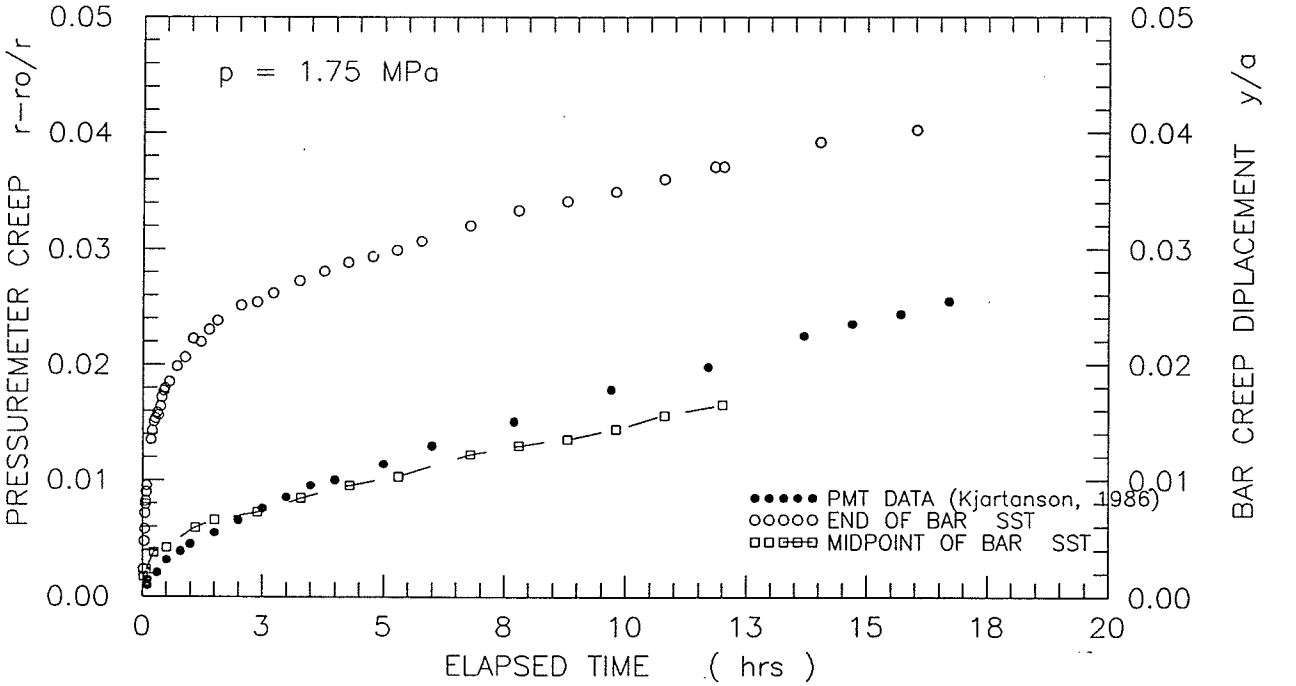


Figure 5.72 Compare bar test data versus pressuremeter test data. Early portions of the tests for p = 1.50 MPa and p = 1.75 MPa.

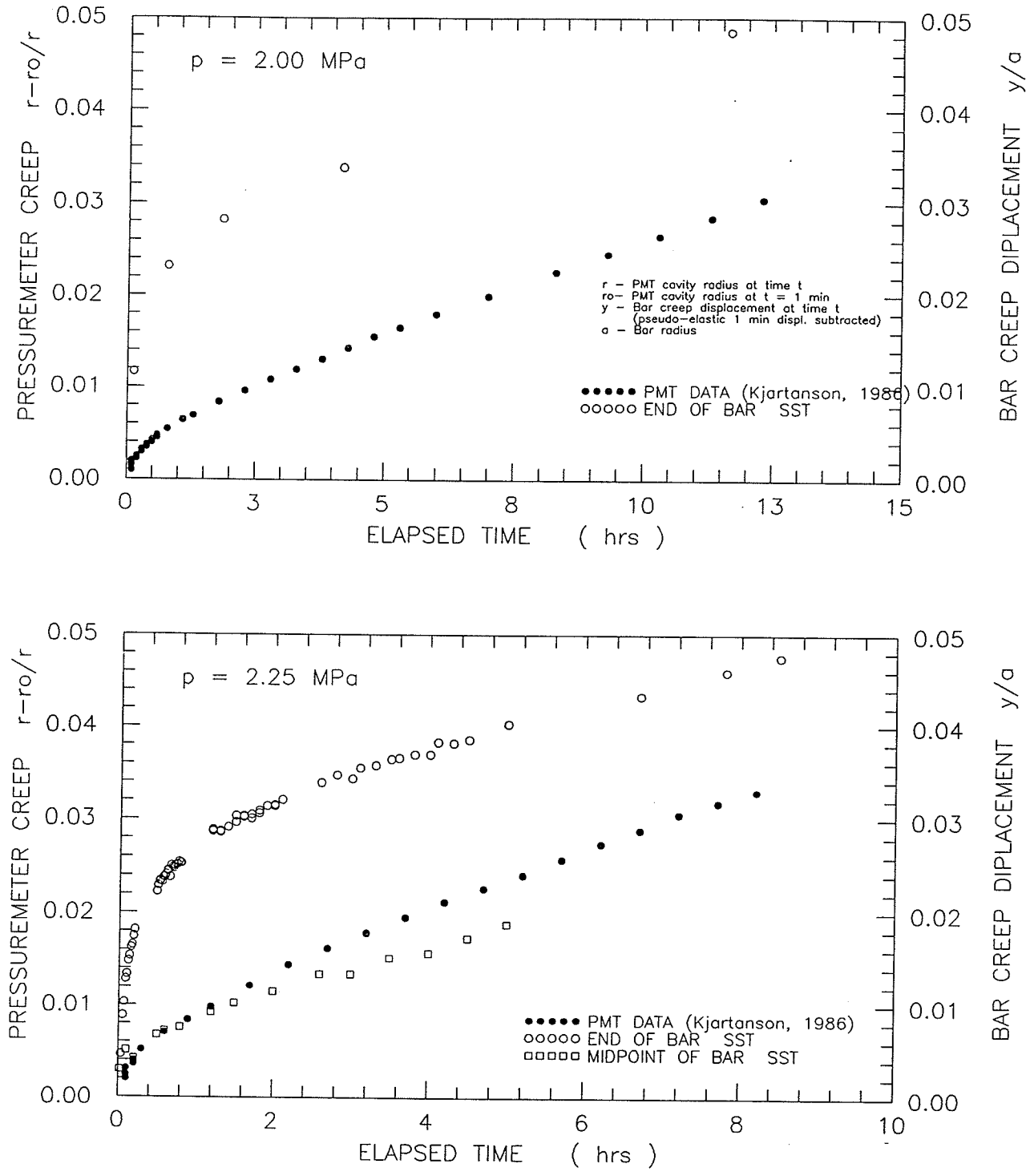


Figure 5.73 Compare bar test data versus pressuremeter test data. Early portions of the tests for p = 2.00 MPa and p = 2.25 MPa.

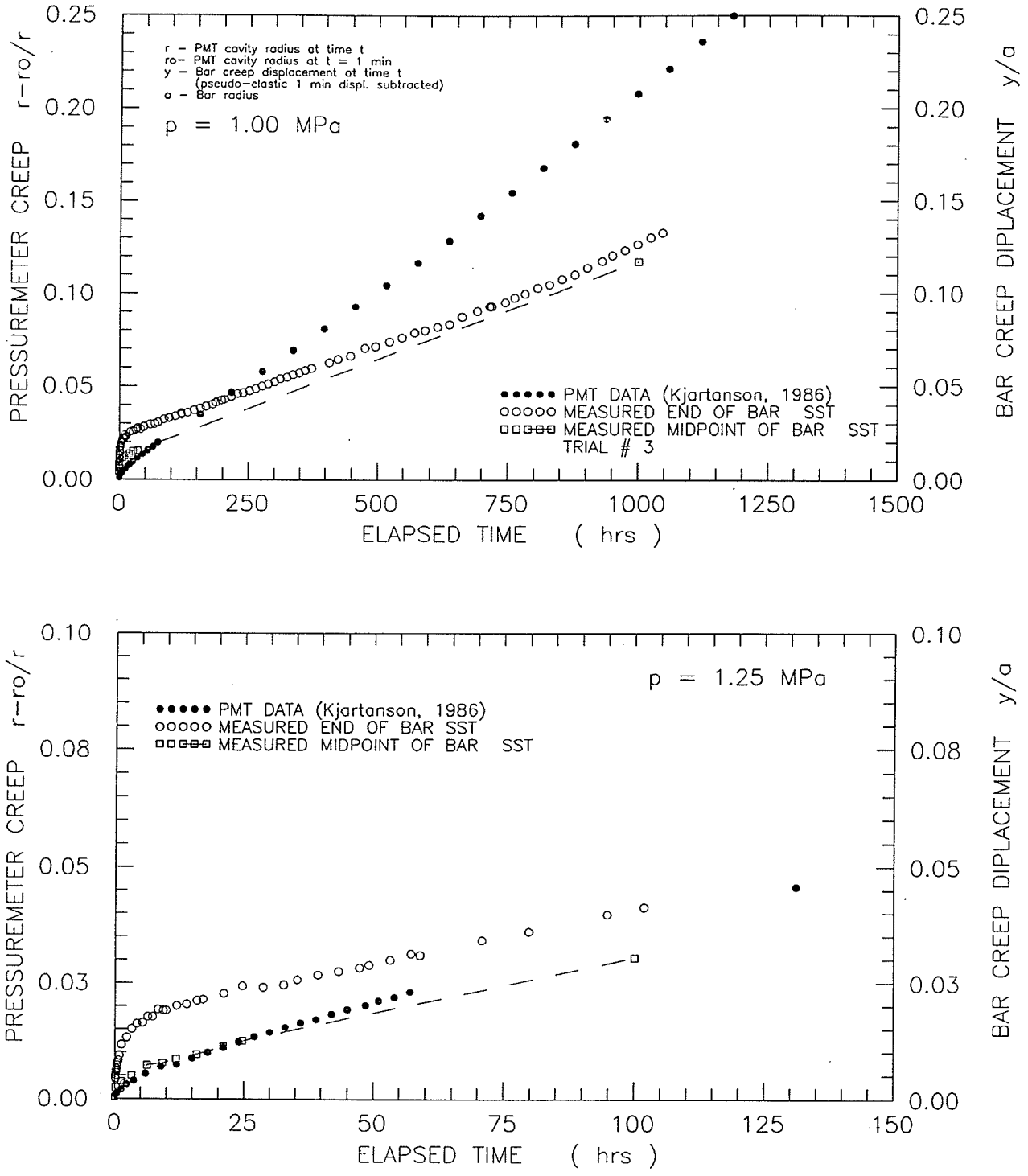


Figure 5.74 Compare bar test data versus pressuremeter test data. Complete test data for p = 1.00 MPa and p = 1.25 MPa.

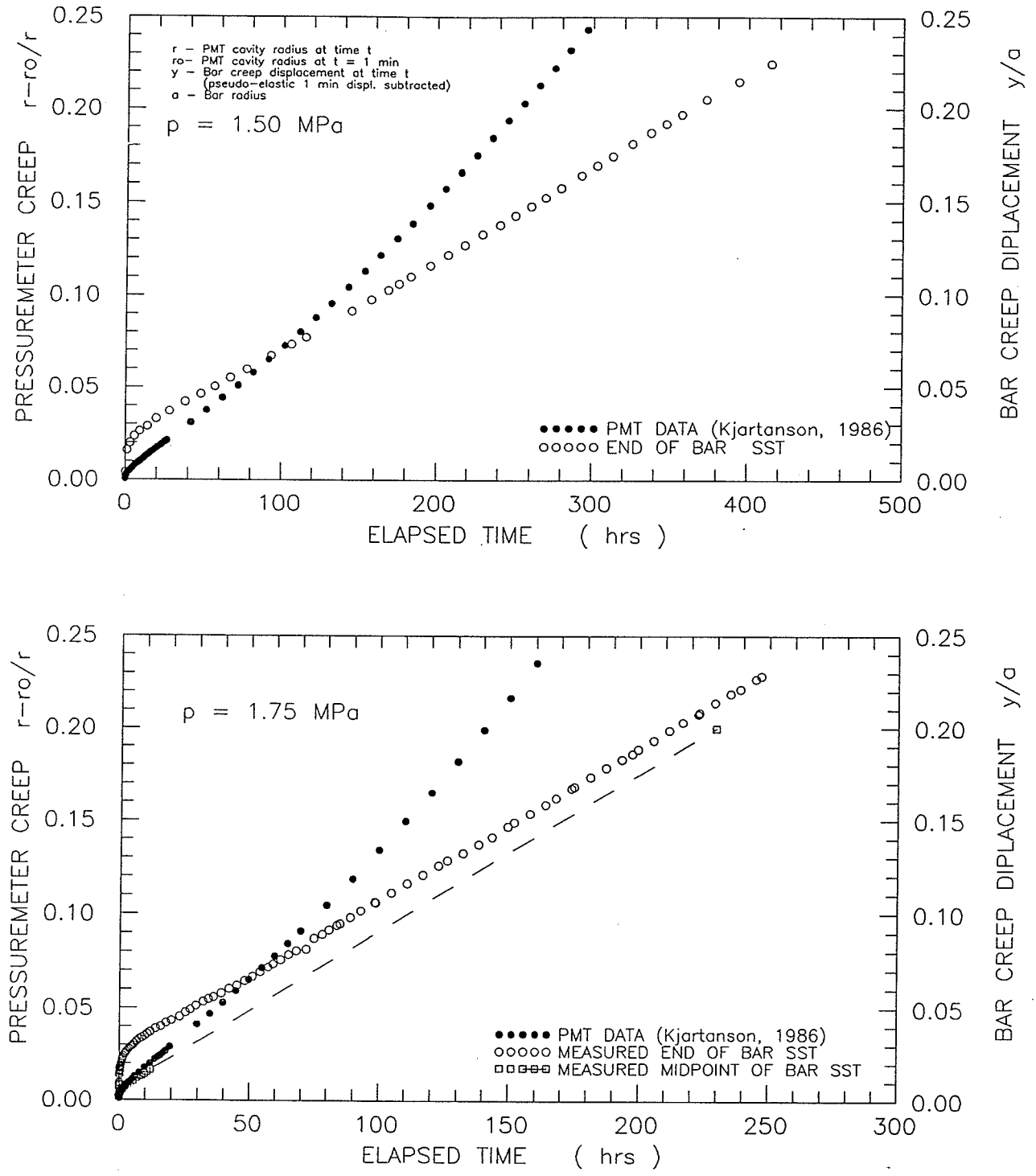


Figure 5.75 Compare bar test data versus pressuremeter test data. Complete test data for p = 1.50 MPa and p = 1.75 MPa.

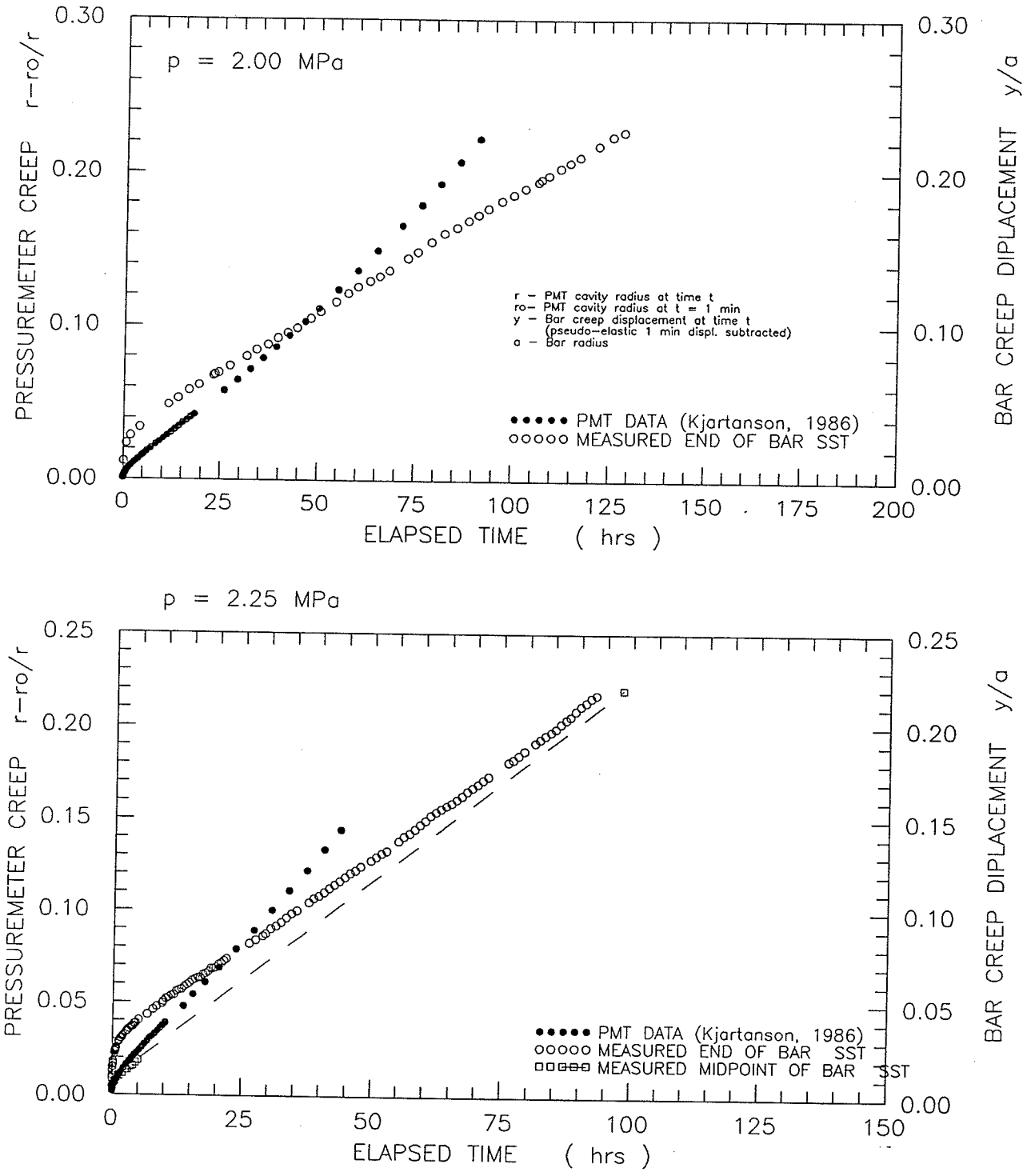


Figure 5.76 Compare bar test data versus pressuremeter test data. Complete test data for p = 2.00 MPa and p = 2.25 MPa.

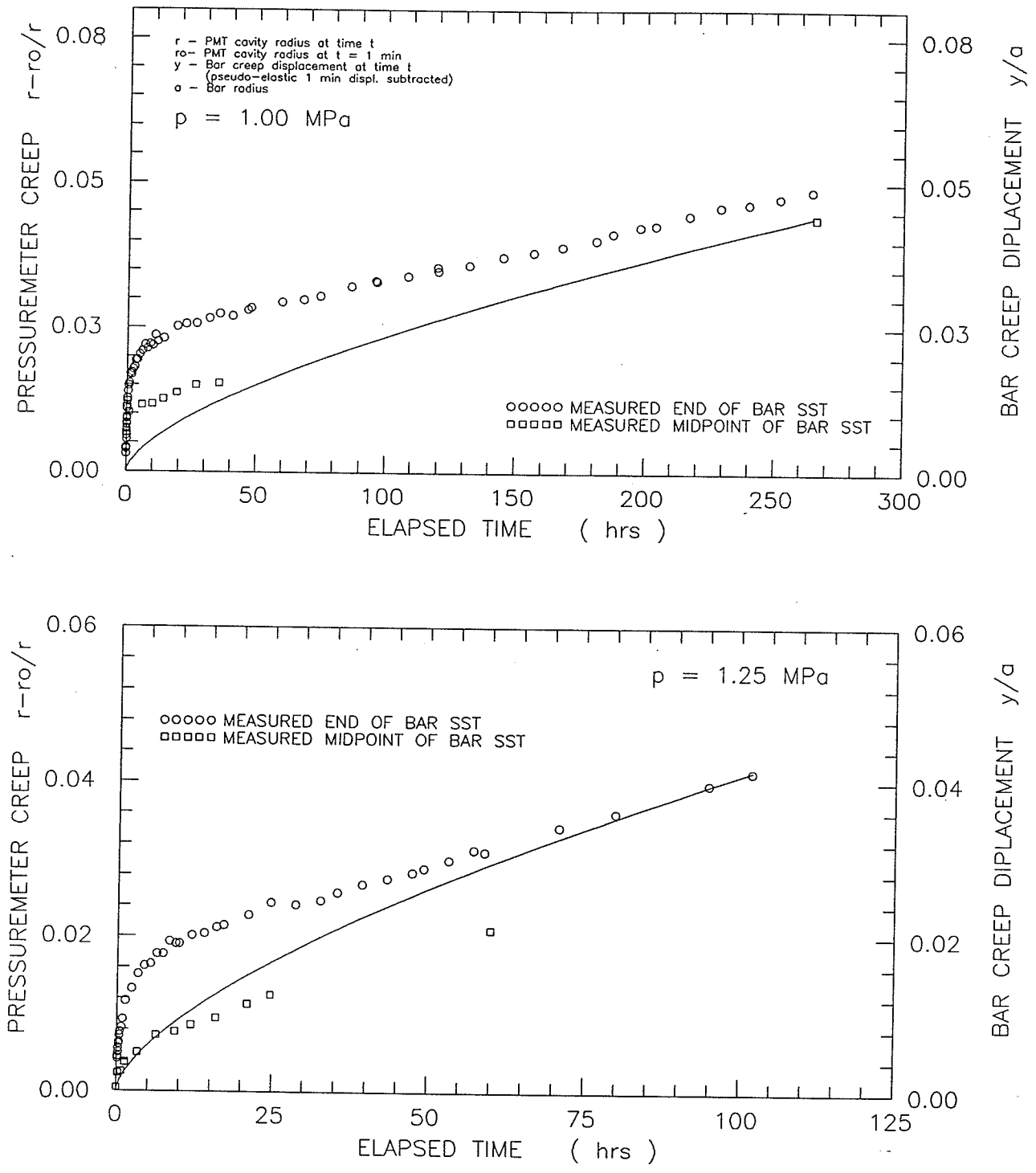


Figure 5.77 Power law creep model using pressuremeter deduced creep parameters versus bar test data for early portions of the tests for p = 1.00 MPa and p = 1.25 MPa.

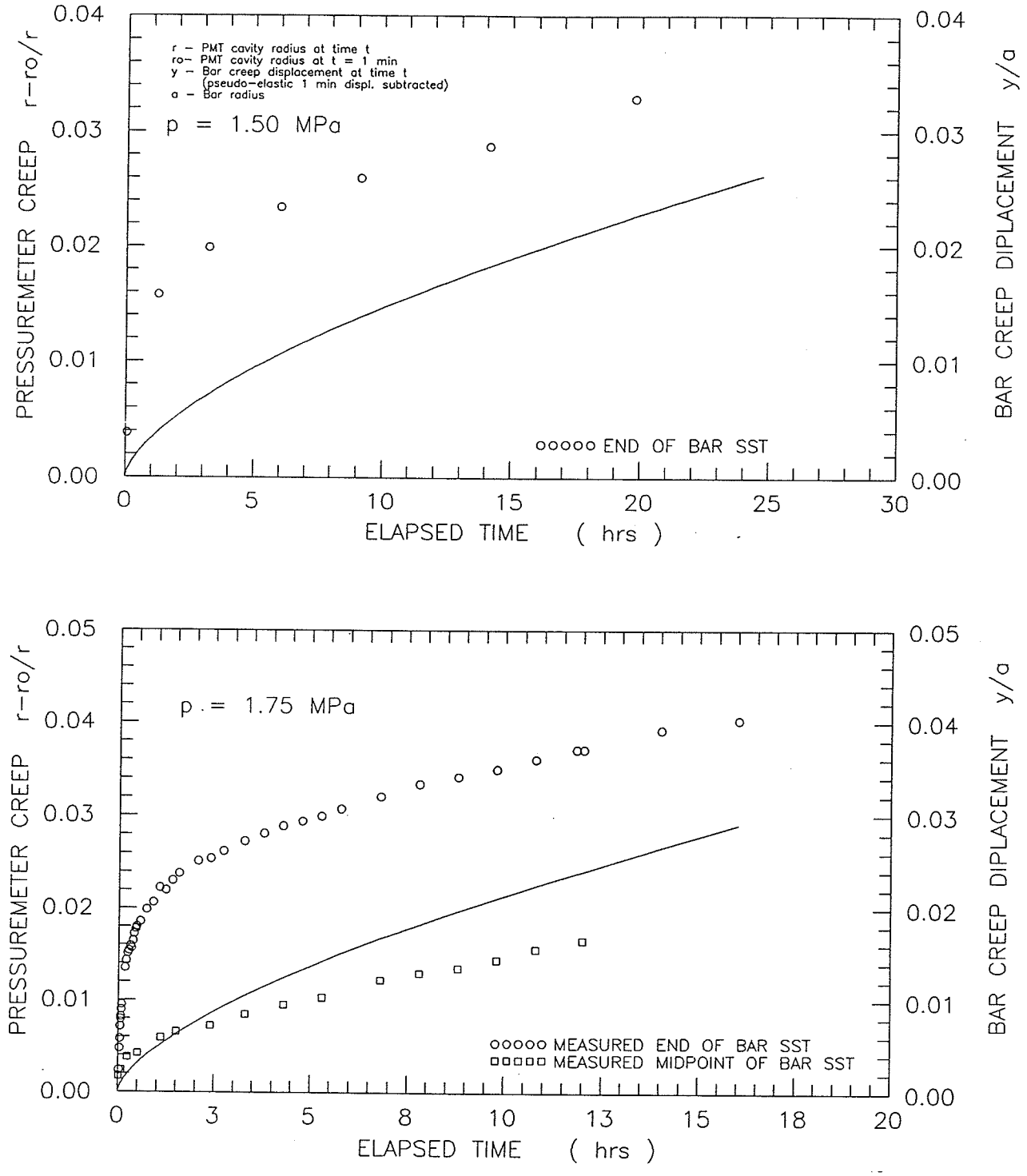


Figure 5.78 Power law creep model using pressuremeter deduced creep parameters versus bar test data for early portions of the tests for p = 1.50 MPa and p = 1.75 MPa.

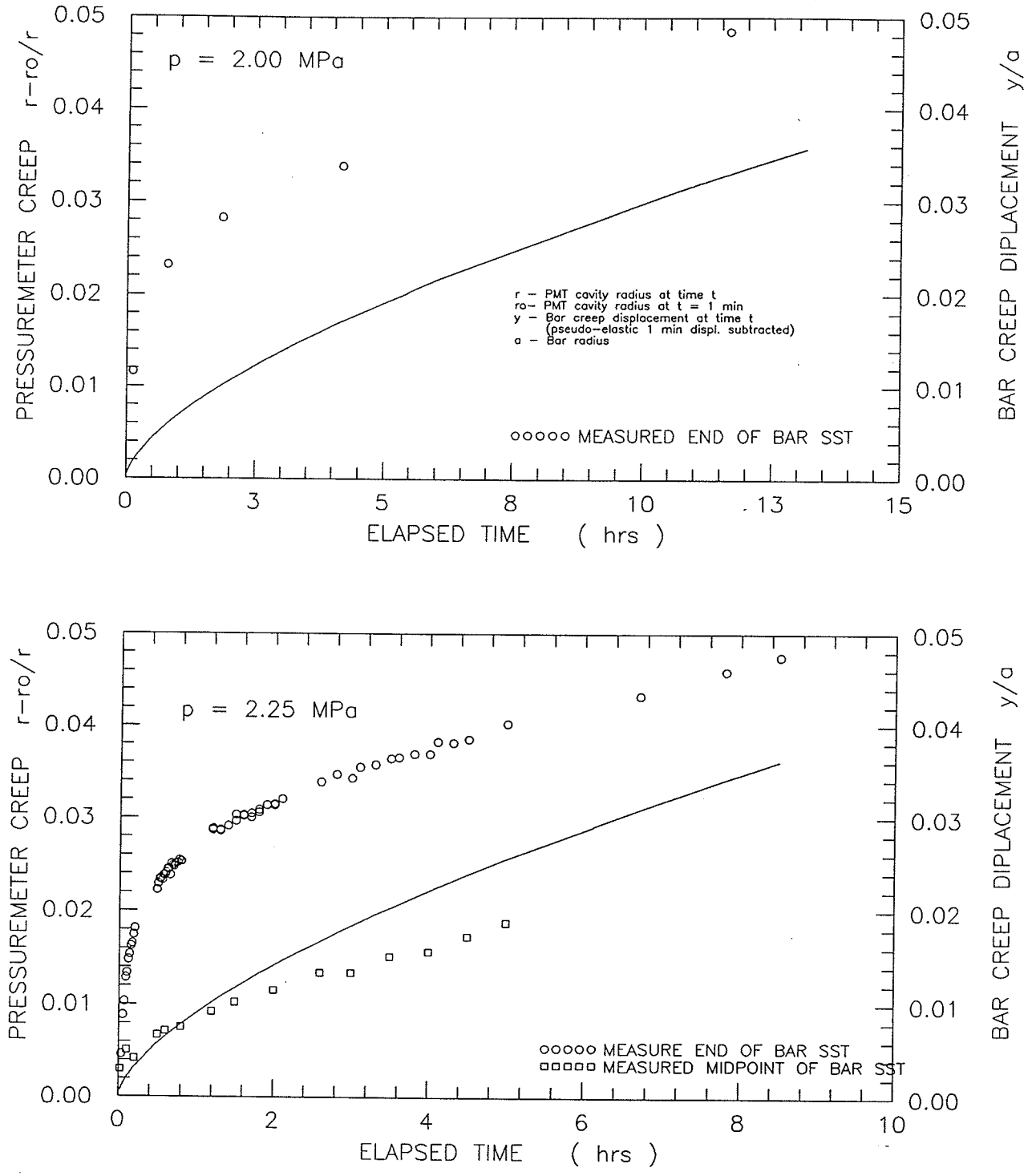


Figure 5.79 Power law creep model using pressuremeter deduced creep parameters versus bar test data for early portions of the tests for p = 2.00 MPa and p = 2.25 MPa.

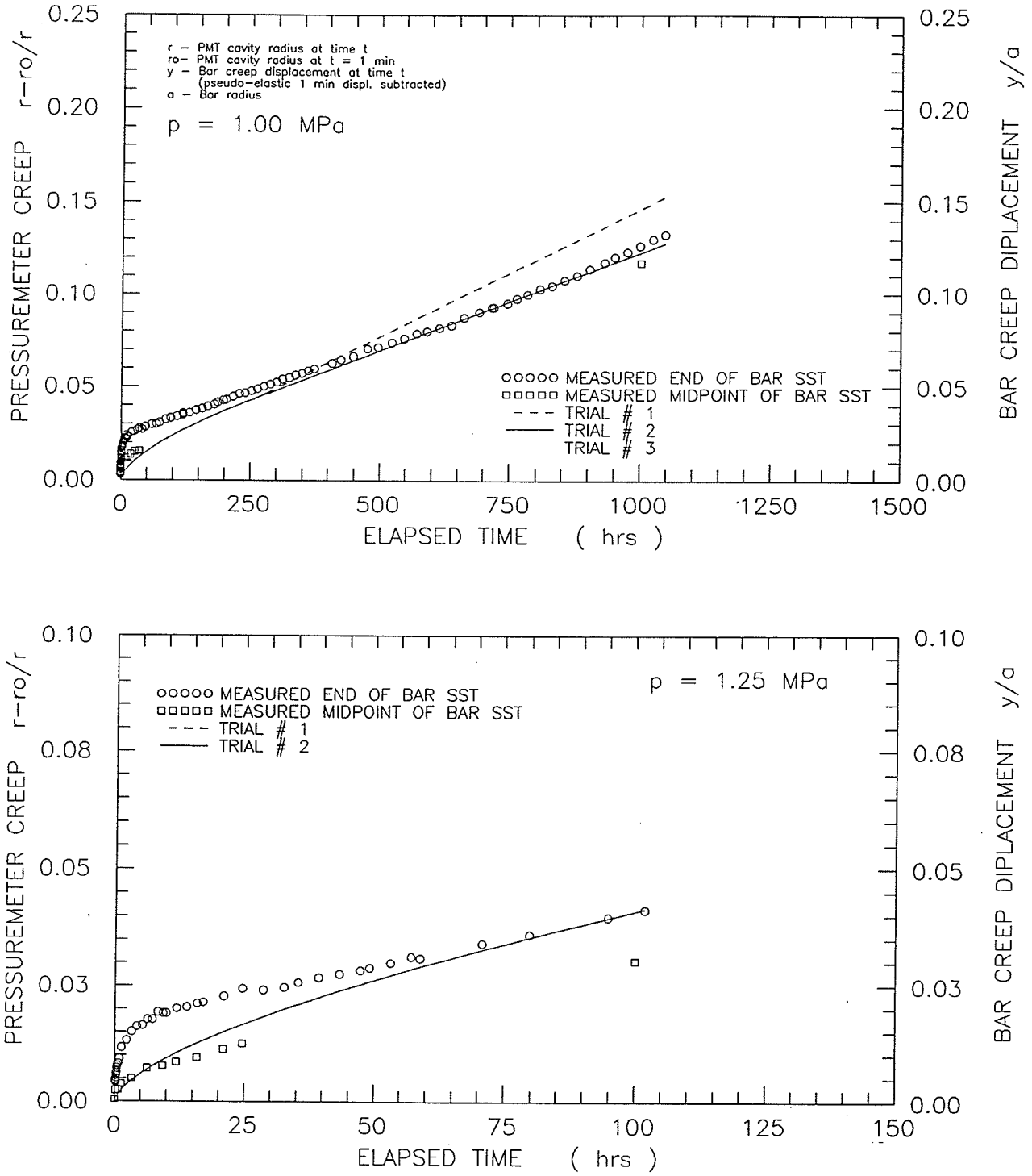


Figure 5.80 Power law creep model using pressuremeter deduced creep parameters versus bar test data for primary creep plus secondary creep of bar at p = 1.00 MPa and p = 1.25 MPa.

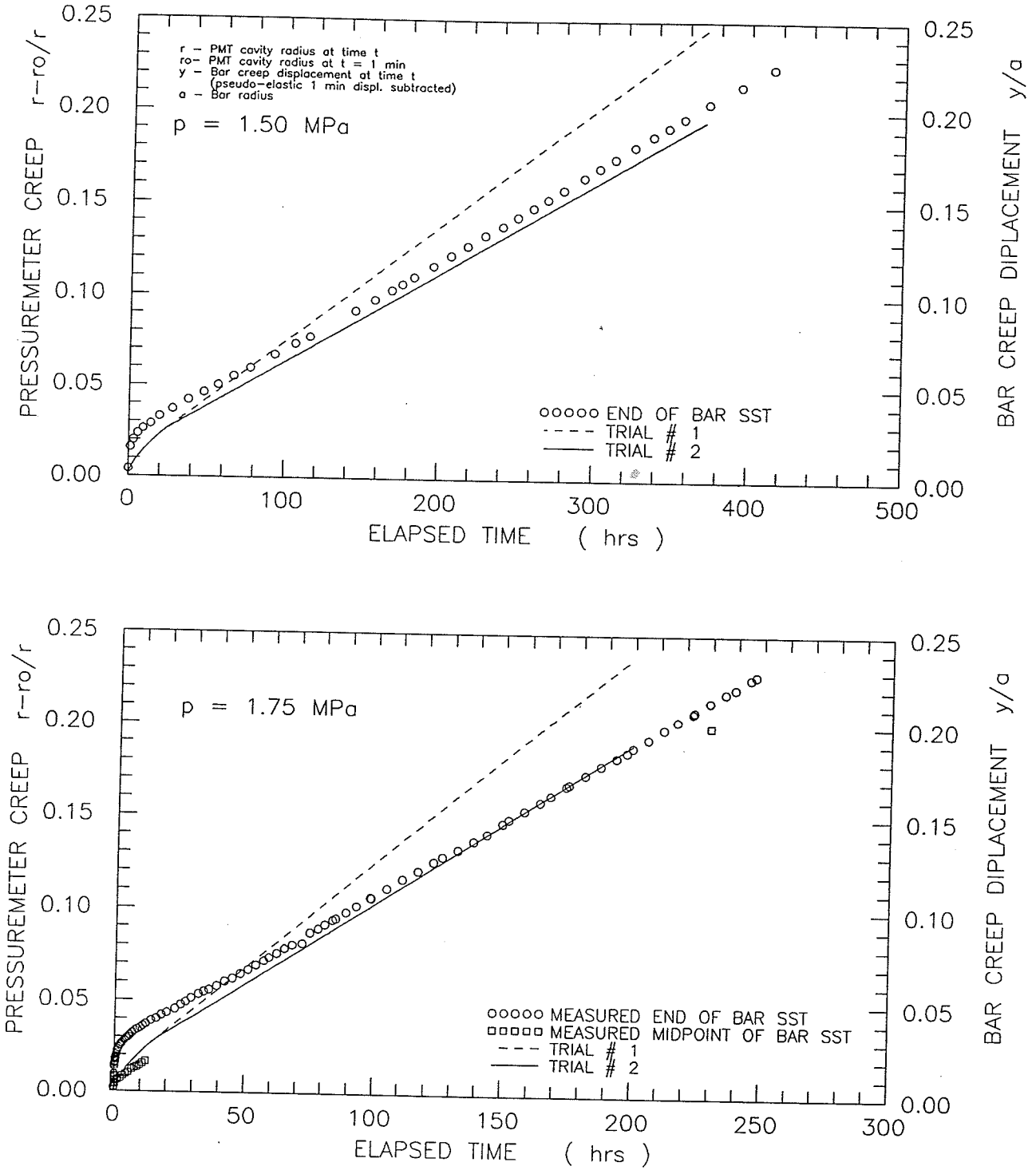


Figure 5.81 Power law creep model using pressuremeter deduced creep parameters versus bar test data for primary creep plus secondary creep of bar at p = 1.50 MPa and p = 1.75 MPa.

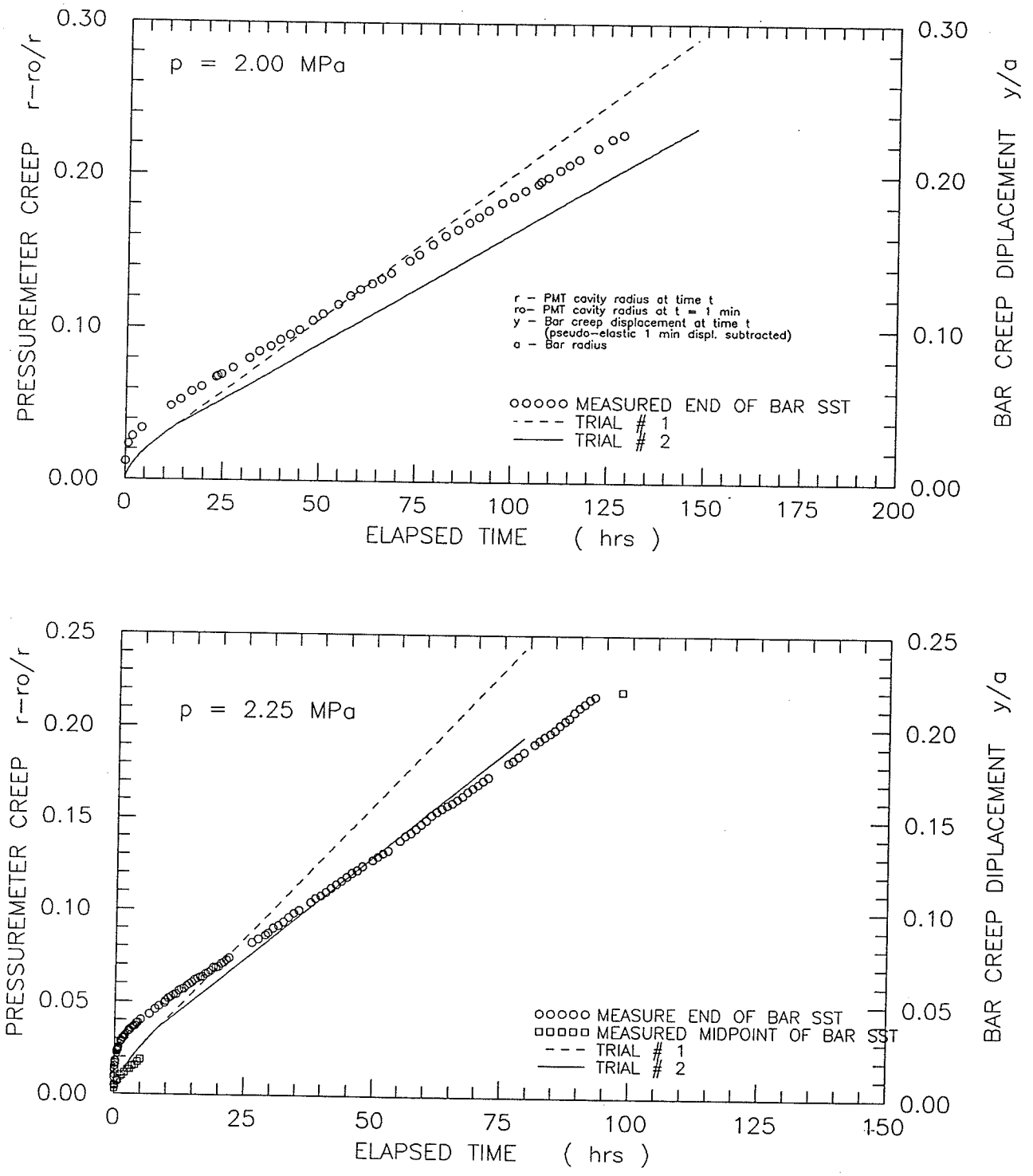


Figure 5.82 Power law creep model using pressuremeter deduced creep parameters versus bar test data for primary creep plus secondary creep of bar at p = 2.00 MPa and p = 2.25 MPa.

# CHAPTER 6

# DISCUSSION OF RESULTS OF BAR CREEP TESTING PROGRAM

## 6.1 INTRODUCTION

This chapter discusses the bar test results presented in Chapter 4 and analyzed in Chapter 5. As in Chapter 5, the discussion is presented in two parts. The discussion focuses first on the applicability of power law creep theory to describe the creep behaviour of the bar creep tests, and by extension to determine how applicable the theory is to describe the creep of laterally loaded piles. The discussion is then completed by examining how well the bar creep data compared to equivalent pressuremeter creep tests (Kjartanson, 1986; Shields et al., 1989). This second component of discussion centres on how the results of carefully conducted pressuremeter creep tests can be interpreted to predict the creep of the bar or of laterally loaded piles.

## 6.2 APPLICABILITY OF POWER LAW CREEP MODEL TO DESCRIBE LATERAL CREEP BEHAVIOUR OF THE BAR

### 6.2.1 Pseudo-Instantaneous Response

This experimental bar program determined a pseudo-instantaneous (1 minute) subgrade reaction modulus K = 215 MPa for the single stage tests, versus K = 290 MPa for the multi-stage test.

Although it is difficult to draw conclusions regarding the larger K values observed for the multi-stage test versus the single stage test results, it is likely that the initial

bending of the bar during the single stage tests (see for example Figure 5.36 versus Figure 5.40) resulted in a larger measured initial displacement at ice surface, and hence a lower (softer) K value.

The pseudo-instantaneous response of ice, is not widely reported in the literature. The convention is more commonly to report on either the elastic characteristics (static or dynamic) of ice (Gold, 1978; Michel, 1979), or alternately to concentrate on its creep behaviour (Mellor, 1979; Mellor and Cole, 1982; Azizi, 1989; Shields et al., 1989), but not to combine both. Researchers have more typically referenced creep calculations to the strain or displacement at the end of some short finite time interval such as 1 minute (Ladanyi and Eckhart, 1983; Shields et al., 1989).

Mellor (1979) in fact argued that applying large stresses "instantaneously" leads to premature damage of the test specimen. It was for this reason that this author chose to apply the initial bar loading over a 1 to 3 minute interval.

### 6.2.2 Primary Creep

**Analysis to Determine the End of Primary Creep**

The method of examining three plots of: creep displacement rates versus time in log-log space, creep displacement versus time in log-log space, and arithmetic plots of creep displacement rates versus time, each gave consistent indicators of when primary creep ended. Tables 5.2 and 5.6 summarized this analysis for the single stage and multi-stage tests, respectively.

It was apparent from these results that examination of the three graphs for each test was redundant. Future researchers might choose any one of the three graphical

methods and expect to determine accurately when primary creep ended.

Based upon Tables 5.2 and 5.6, it appears that at corresponding equivalent frontal pressures, primary creep ended slightly more rapidly during the multi-stage test than during the comparable single stage tests. However when the times to end of primary power law creep are compared in log-log space, as shown on Figure 5.27, there does appear to be some correspondence.

Other published research on laterally loaded piles (Rowley et al., 1973, 1975; Nixon, 1984; Neukirchner and Nixon, 1987) has not addressed this concern, and so the data on Figure 5.27 forms the limited direct experimental basis for engineers to determine whether or not multi-stage test data can be analyzed to predict when a single stage-loaded pile might end primary creep.

Until further research data are available, it is recommended that designers assume that multi-stage test data can be analyzed to predict the approximate end of primary creep of a single stage-loaded bar or pile.

Although the data were limited to three single stage tests plus one multi-stage test, this thesis gives direct experimental confirmation, as presented and discussed in subsection 5.2.2.2 and as summarized on Figure 5.11, that the bar did stop changing shape at a time coincident with the end of primary creep. In other words, the bar began to behave in a rigid fashion at the beginning of secondary creep, thus confirming the hypotheses of other researchers (Rowley et al., 1973, 1975; Nixon, 1984; and Neukirchner and Nixon, 1987).

**Primary Creep Parameters**

The analysis to determine the constitutive primary creep parameters $\sigma_{c_p}$, $n_p$, and $b_p$, was initially completed for both the single stage tests and the multi-stage test using the creep displacements measured at the point of load application very near the ice surface. Subsection 5.2.2 presented this analysis for the single stage tests, and subsection 5.2.3 contained the corresponding analysis for the multi-stage test. Subsequently, in subsection 5.2.4, the analysis was repeated, this time using the calculated creep displacements of the midpoint of the bar.

The analysis of subsections 5.2.2 and 5.2.3 demonstrated clearly that the bar power law creep models, as deduced from the single stage tests and the multi-stage test, respectively, did accurately retrace the bar's behaviour for the respective type of test. For example, Figures 5.13 and 5.15 for the single stage tests showed that when Rowley et al.'s transformed creep displacement was plotted in log-log space versus time, the result was a series of more or less straight and parallel lines. Theoretically, therefore, the value of the primary creep parameter, $b_p$, could be taken as the average slope of these lines. Similarly, the analysis to determine the value of $n_p$, as shown on Figures 5.19 or 5.20, for the single stage tests, satisfied the theoretical requirement that the data plot in a straight line. When the creep parameters determined from either the single stage tests or the multi-stage test were input back into their respective primary power law creep models and compared to the actual test data, the models, as expected, appeared to track the test data very closely. Figures 5.50 through 5.53 presented this comparison for the single stage tests, while Figures 5.59 and 5.60 compared the corresponding multi-

stage test.

Although the form of the power law creep model appeared to describe accurately the primary creep behaviour of the bar, the two types of bar tests did not yield the same constitutive primary creep parameters. The constitutive creep parameters determined for the ice from the single stage bar tests were determined to be $\sigma_{c_p}$ = 12.0 MPa, $b_p$ = 0.206, and $n_p$ = 1.62, if the 1.0 MPa test results were omitted. On the other hand, corresponding creep parameters of $\sigma_{c_p}$ = 3.56 MPa, $b_p$ = 0.53, and $n_p$ = 2.37 were determined from the multi-stage test. At the same time, there was a reasonably strong correspondence between the bar multi-stage test determined constitutive creep parameters for the ice and the pressuremeter test ( $\sigma_{c_p}$ = 1.97 MPa, $b_p$ = 0.64, and $n_p$ = 2.47), or creep tests on unconfined triaxial specimens of ice ( $\sigma_{c_p}$ = 4 MPa, $b_p$ = 0.64, and $n_p$ = 2.43).

In summary it seemed that either the multi-stage bar test, or the pressuremeter test, or triaxial unconfined compression creep testing (stress or strain controlled) yielded comparable primary constitutive creep parameters of the ice. However, the constitutive primary creep parameters deduced from the single stage bar creep tests did not compare with the other forms of testing.

The explanation may be in the bending of the bar. As discussed in subsection 5.2.4, and shown on Figures 5.36 through 5.30, it was noted during single stage tests

that the bar underwent a combination of initial bending plus lateral translation throughout the primary creep phase. The result was that the creep displacement of the midpoint of the bar lagged substantially behind the ends of the bar during the early stages of creep. On the other hand, examination of the deformed shape of the same bar during multi-stage loading, as shown on Figures 5.40 through 5.43, suggested that the same bar did not change shape as appreciably during primary creep.

It was at this point that it was decided to calculate the displacements of the midpoint of the embedded length of the bar, and use these calculated displacements to determine the constitutive creep parameters of the ice. These calculations were completed for both single stage (where bending strain was measured) and multi-stage loadings.

The results of this analysis, also included in Table 5.8, yielded creep parameters $\sigma_{c_p}$ = 1.65 MPa, $b_p$ = 0.67, and $n_p$ = 3.45 for the multi-stage test, versus $\sigma_{c_p}$ = 14.3 MPa, $b_p$ = 0.512, and $n_p$ = 1.32 for the single stage tests. Now $b_p$ values (time creep exponent) determined from both single stage tests and multi-stage tests were somewhat comparable, and they compared more favourably with the pressuremeter determined $b_p$ value of 0.64. The comparison of $\sigma_{c_p}$ values and $n_p$ (stress exponent) values was not, however, significantly improved by this form of the analysis.

It may also be that surface effects, similar to those observed in full-scale pile load tests (where soil resistance within several pile diameters of the ground surface is ignored), account in part for this problem. If so, then perhaps increasing the embedded

length of the same pile section and conducting additional testing would yield some improved understanding of this problem.

It would appear that further research is required to clarify this problem, before practising engineers may utilize the results of multi-stage laterally loaded pile creep tests to predict the behaviour of single stage loaded piles under constant lateral load conditions, at least where it is anticipated that the dominant form of creep will be primary in nature.

### 6.2.3 Secondary Creep

The majority of the creep displacements observed in this experimental program were secondary creep displacements. Here there was excellent agreement between the secondary creep rates measured during single stage bar tests and those measured during the multistage test. There was also a strong correlation with the minimum strain rates observed during equivalent pressuremeter tests (discussed in the following subsection). Figure 5.35 demonstrated this comparison. Actual rates were listed on Table 5.5.

The conclusion of the secondary creep analysis was that the secondary creep phase of multi-stage bar creep test results can be used to predict the secondary creep behaviour of single stage loaded bar tests.

## 6.3 COMPARISON OF BAR TEST RESULTS VERSUS PRESSUREMETER CREEP TEST RESULTS

Although the pressuremeter test is routinely used to predict the behaviour of laterally loaded piles in unfrozen soils, this thesis marks the first attempt to compare

experimentally the creep behaviour of pressuremeter tests to the lateral creep of a bar or pile segment which has virtually the same dimensions as the pressuremeter. The intent in doing so was to obtain direct observations and comparisons of the behaviour of the two types of test, and hopefully to obtain a clearer understanding of how to use the pressuremeter to design laterally loaded piles in a creeping medium such as permafrost.

The analysis to compare the bar test results to equivalent pressuremeter test results, as presented in subsection 5.4, consisted first of a direct visual comparison of test data. This comparison was followed by substituting the constitutive creep parameters of ice, as determined by the pressuremeter test, back into the power law creep model for the bar test and comparing the results to the test data.

Figures 5.71 through 5.73 compared directly the early portions of the single stage bar tests to equivalent pressuremeter tests of Kjartanson (1986). Both the measured creep displacements of the ends of the bar and the calculated creep displacements of the midpoint (where available) of the bar were plotted. Typically the calculated creep of the midpoint of the bar tracked very closely to the measured creep strain of the pressuremeter test. On the other hand, the measured creep displacement of the ends of the bar were always tracking well in advance (usually double) of the pressuremeter tests.

Although there were only four tests where the comparison between the creep of the midpoint of the bar could be compared to the pressuremeter test, these preliminary tests do intuitively suggest that there may indeed be some direct correspondence between the pressuremeter test and the behaviour of a perfectly rigid bar.

Figures 5.75 through 5.76 compared primary plus secondary plus tertiary creep of the pressuremeter test to primary plus secondary creep of the bar. Now there is a

fundamental difference in observed behaviour between the bar and the pressuremeter in that the pressuremeter test proceeds directly from a minimum creep strain rate directly into accelerating or tertiary creep. On the other hand, the bar maintained its minimum creep displacement rate as a steady rate of displacement.

There was, nevertheless, a correspondence between the minimum creep rate of the pressuremeter test and the minimum or secondary displacement rate of the bar. This comparison, summarized on Table 5.4 concluded that the minimum pressuremeter creep strain rate was approximately 1.3 times faster than the equivalent normalized secondary displacement rate of the bar.

The second part of the pressuremeter versus bar comparison consisted of substituting the constitutive creep parameters for ice determined by Shields et al. (1989) from Kjartanson's (1986) pressuremeter tests, back into the power law creep models detailed in Chapter 2 for the bar.

Figures 5.77 through 5.79 summarized the accuracy of this predictive model versus the early portions of the bar test results. The results of the analysis are encouraging in that the model typically appeared to track between the calculated creep of the midpoint of the bar and the measured creep of the ends of the bar.

Finally, Figures 5.80 through 5.82 summarize the accuracy of this model versus the complete primary plus secondary bar test results. If the pressuremeter minimum creep strain rates are reduced by 1\1.3 (Trial 2), then the model very closely predicts the overall bar behaviour.

## 6.4 THE RECOMMENDED APPROACH TO PREDICTING THE BEHAVIOUR OF LATERALLY LOADED PILES IN CREEP

The bar test results, as analyzed in Chapter 5 and discussed in subsections 6.2 and 6.3, considered three approaches to predicting the creep behaviour of a single stage loaded bar. They were :

1. Conduct a series of single stage loaded bar creep tests and analyze the resulting data in terms of power law creep theory for the bar.
2. Conduct multi-stage loaded bar creep tests and analyze the multi-stage creep data in terms of power law creep theory.
3. Conduct a series of single stage loaded pressuremeter creep tests, analyze the pressuremeter creep data to determine the constitutive creep parameters of ice, and back-substitute the creep parameters for the ice back into the creep model for the bar.

Based upon the discussions in the previous two subsections, it is concluded that either the results of a series of single stage loaded bar creep tests, or the results of a series of single stage pressuremeter tests may be analyzed to predict the behaviour of the laterally loaded bar.

Either method appears to yield results which adequately predict the overall behaviour of the bar. Analysis of the pressuremeter tests to predict the early primary creep behaviour of the bar tended to yield predicted bar behaviour somewhere between that measured at its ends and the creep displacement calculated at its midpoint. Attempts to analyze the results of the multi-stage creep test were not as encouraging, possibly due to the differences in observed bending of the bar during multi-stage loading and single

stage loading.

In engineering geotechnique of unfrozen ground, it is routine to conduct pressuremeter testing to aid in preliminary analysis and design of laterally loaded piles. Given the very high costs of conducting full-scale pile load tests (short-term pile load tests in unfrozen soils routinely cost $50,000.00 in 1993 to complete), pile load tests are normally completed only for larger sized projects requiring hundreds of piles, and even then are carried out to confirm a design which was typically based upon the much less expensive pressuremeter tests.

It was encouraging to find the agreement between the pressuremeter derived creep model of ice versus the measured creep of the bar. Although preliminary in nature, this thesis suggests that such an approach is valid in ice or ice-rich frozen soils.

# CHAPTER 7

# CONCLUSIONS

The objectives of this experimentally based thesis were:

1. To test the validity of using power law creep theory to model the creep behaviour of laterally loaded piles (in frozen soils).
2. To test directly the validity of using the pressuremeter creep test to predict the behaviour of a rigid bar, of similar shape and dimensions, which is forced to translate laterally through the same creep sensitive medium; i.e., to compare cylindrical cavity creep expansion versus cylindrical cavity creep translation.

The conclusions of this thesis, after testing these objectives, are presented below.

Chapter 2 reviewed power law creep theory, as applied to the laterally translating bar and the pressuremeter. The chapter also reviewed previously published studies of laterally loaded piles in ice or ice-rich frozen soils. The review concluded that there has been a progressive increase in the sophistication in applying power law creep theory to model the creep behaviour of laterally loaded piles. Modelling efforts have included: the analytic solution by Rowley et al. (1973, 1975), the analytic model of Nixon (1984), the numerical (finite difference) modelling by Neukirchner and Nixon (1987), and more recently the finite element modelling by Foriero and Ladanyi (1990). At the same time, there is virtually no high quality laterally loaded pile test data for the modellers to test and calibrate their models.

This thesis concludes that the full-scale field test data by Rowley el al., (1973, 1975) is difficult to analyze because of problems in the field regarding temperature

conditions in the permafrost, and the method of installing the piles. The remaining data consists of three small-scale laboratory tests on "pencil" piles embedded in ice, plus the results of one large-scale model pile test by Domaschuk (1991). Therefore there is a clear need for additional high quality experimental research regarding the creep behaviour of laterally loaded piles.

The experimental program worked well to test the creep behaviour of a laterally loaded bar. Large, relatively homogeneous samples of polycrystalline ice, were produced by modifying Kjartanson's (1986) technique of making ice. Ice sample temperatures were carefully controlled to maintain a steady -2°C temperature. Instrumentation to measure load, temperature, displacement, and bending strain were carefully calibrated, and the instrumentation performed as required.

The load frame allowed the top and bottom lateral loads to be maintained separately. This was required because it was necessary to apply a very slight differential loading in order to maintain the bar translating uniformly through the ice. This thesis does not establish conclusively why this differential loading was required.

The bar test results of Chapter 4 indicated clearly that the bar did undergo some bending during the pseudo-instantaneous and primary creep phase. In the single stage tests, in particular, this bending was occurring progressively during primary creep while the bar was also undergoing lateral creep translation. This thesis did demonstrate clearly, for the first time, that the bar does stop changing shape at the end of primary creep, and it does translate in a rigid fashion through secondary creep. On the other hand, when the bar was subjected to multi-stage loading, it remained more or less rigid during both the primary and secondary creep phase of the second and successive load

stages of the test.

The analysis of the test data concluded first that the power law creep model accurately describes the creep behaviour of the laterally loaded bar in all phases of creep. In a "class z" type of prediction, where the constitutive creep model determined from the test results was then compared to the test data, the fit of the model was excellent.

Unfortunately, the results of the multistage bar creep test could not be used to predict accurately the creep behaviour of a single stage loaded bar during primary creep, particulary when the creep displacements of the ends (ice surface) of the bar were considered. On the other hand, both the single stage loaded bar and the multi-stage loaded bar translated at the same rates during secondary creep. Although not proved conclusively, it is suspected that the progressive bending of the single stage loaded bar during primary creep may have contributed to the lack of agreement.

The constitutive primary creep parameters of the ice, as deduced from the creep displacements of the ends (ice surface) of the bar during single stage bar tests, did not compare well to the constitutive creep parameters determined by pressuremeter testing, or as determined by unconfined compression testing. There was some better agreement if the calculated creep displacements of the midpoint of the bar were used instead of the creep at the end of the bar ($b_p$ values), but the possible influence of the bending of the bar requires further research. On the other hand, the creep parameters deduced from the multi-stage test were in good agreement with those deduced from either pressuremeter creep tests or compression tests.

During primary creep, there was strong agreement between the observed behaviour of the single stage loaded pressuremeter creep tests and the calculated primary

creep of the midpoint of the single stage loaded bar tests. Only half of the bar tests were instrumented to measure bending, so this conclusion is based upon only four of the eight single stage tests.

During secondary creep, there was a clear correspondence between the normalized (displacement/radius) steady creep rate of the bar, and the minimum strain rate from the pressuremeter. Based upon this testing, it appears that the minimum strain rate of the pressuremeter test was 1.3 times faster than the normalized creep displacement rate of the bar.

# CHAPTER 8

# RECOMMENDATIONS FOR FURTHER RESEARCH

It is important that the influence of the bending of the bar be further investigated experimentally. Additional testing should maintain the present bar diameter, and vary its embedded length. All bars should be instrumented to define the deformed shape of the bar.

Additional bar testing should focus equally on multi-stage testing and on single stage loaded testing until a clearer understanding of the correspondence between the experimental behaviour of the two types of tests is achieved. In engineering practise, multi-stage full-scale pile load tests are much less expensive to conduct than a series of equivalent single stage loaded tests.

Both Kjartanson's pressuremeter tests and the bar tests of this thesis were conducted at much higher equivalent pressure levels (1.0 to 2.25 MPa) than is used in routine foundation engineering. At the present time there is very little direct experimental evidence to support extrapolating the results of such high pressure testing of ice down to more conventional foundation engineering stress levels. It is of importance, therefore, to conduct lower stress range tests (i.e., pressures ranging from say 0.25 to 1.0 MPa) to either confirm or refute the use of such high pressure tests to predict creep behaviour at much lower corresponding pressures. Such lower stress tests would necessarily be of much longer durations, of say 1 year or more.

This experimental program was designed to eliminate scale effects when

comparing the pressuremeter and bar tests. Full-scale piles are typically several orders of magnitude larger than either this bar or the pressuremeter. Future experimental studies should consider the influence of larger bar or pile diameters.

There is also a need to conduct similar pressuremeter and bar tests at different ice temperatures, both closer to the melting point of ice, and also at colder temperatures.

Finally, although ice is an important constituent of frozen soils, and massive ice layers or lenses do frequently occur as part of the permafrost stratigraphy, there is also a need to conduct additional lateral pile load and pressuremeter creep testing in other ice-rich frozen soils. The results of such tests could be compared to testing in polycrystalline ice to assess the influence of the matrix of particulate matter on overall creep behaviour.

## REFERENCES


Andersland, O.B., Sayles, F.H. and Ladanyi, B. 1978. Mechanical properties of frozen ground. Geotechnical Engineering for Cold Regions, edited by O.B. Andersland and D.M. Anderson, McGraw-Hill, Chapter 5, pp. 216-275.

Andrade, E.N. da C. 1910. The viscous flow in metals and allied phenomena. Proc. Royal Society of London, Vol. A84, pp. 1-12.

Azizi, F. 1989. Primary creep of polycrystalline ice under constant stress. Cold Regions Science and Technology, Vol. 16, No. 2, pp. 159-165.

Baguelin, F., Frank, R. and Said, Y.H. 1977. Theoretical study of lateral reaction mechanism of piles. Géotechnique, Vol. 27, No. 3, pp. 405-434.

Bailey, R.W. 1929. Trans. World Power Conference, Tokyo, p. 1089.

Bailey, R.W. 1935. Proceedings, Institute Mechanical Engineers, 131, pp. 131-349.

Baker, T.H.W. 1976. Transportation, preparation and storage of frozen soil samples for laboratory testing. ASTM Special Technical Publication 599, pp. 88-112.

Bankratz, J.L., Frank, R. and Kutniak, M. 1985. PILATE programme de calcul d'un pieu isolé soumis à des efforts de flexion en tête et à des poussées laterales de sol. Notice d'Utilisation, Laboratoire Central des Ponts et Chaussées, Division Géotechnique Mécanique des Sols, Section des Fondations. Copies available by mailing to 58 Boulevard Lefebvre, 75732 Paris, Cedex 15.

Broms, B.B. 1964. Lateral resistance of piles in cohesive soils. ASCE Journal of the Soil Mechanics and Foundations Division, Vol. 90, No. SM3, pp. 123-156.

Cole, D.M. 1979. Preparation of polycrystalline ice specimens for laboratory experiments. Cold Regions Science and Technology, Vol. 1, pp. 153-159.

Domaschuk, L., Fransson, L. and Shields, D.H. 1988. Interaction between a laterally loaded pile and frozen sand. Proc. 5th Intl. Conf. on Permafrost, Trondheim, Norway, pp. 1060-1065.

Domaschuk, L., Shields, D.H. and Kenyon, R. 1989. Penetration of rods and spheres in ice. Proc. 10th Intl. Conf. on Ports and Ocean Engineering Under Arctic Conditions (POAC), Lulea, Sweden.

Domaschuk, L., Shields, D.H. and Fransson, L. 1991. Reactive soil pressures along pile in frozen sand. Journal of Cold Regions Engineering, Vol. 5, No. 4, pp. 174-194.

Domaschuk, L., Ji, Zhanliang, and Shields, D.H. 1992. A creep analysis of a laterally loaded pile in frozen sand. Proc. of the 11th Conf. on Offshore and Arctic Engineering, American Society of Mechanical Engineering, Calgary, Alberta, pp. 389-394.

Eckardt, H. 1981. Laboratory borehole creep and relaxation tests in thick-walled cylinder samples of frozen sand. Report 222, Northern Engineering Centre, Ecole Polytechnique, Montreal, 125 p.

Fensury, H. 1985. Determination of creep parameters of frozen soil using the pressuremeter test. M.Sc. Thesis, University of Manitoba, Winnipeg, Manitoba, 209 pp.

Finnie, I. and Hellor, W.R. 1959. Creep of engineering materials. McGraw-Hill Book Company, Inc., New York.

Foriero, A. and Ladanyi, B. 1989. A streamline solution for rigid laterally loaded piles in permafrost. Canadian Geotechnical Journal, Vol. 26, pp. 568-574.

Foriero, A. and Ladanyi, B. 1990. Finite element simulation of behaviour of laterally loaded piles in permafrost. ASCE Journal of Geotechnical Engineering, Vol. 116, No. 2, pp. 266-284.

Foriero, A. and Ladanyi, B. 1991. Design of piles in permafrost under combined lateral and axial load. Journal of Cold Regions Engineering, Vol. 5, No. 3, pp. 89-105.

Frank, R. 1993. Personal communication.

Fransson, 1986. Personal communication.

Glen, J.W. 1955. The creep of polycrystalline ice. Proc. Royal Society of London, Vol. A228, pp. 519-539.

Glen, J.W. 1975. The mechanics of ice. U.S. Army Cold Regions Research and Engineering Laboratory, Hanover, N.H., Monograph II-2cb, 47 p.

Gold, L.W. 1978. Ice pressures and bearing capacity. Geotechnical Engineering for Cold Regions, edited by O.B. Andersland and D.M. Anderson, McGraw-Hill, Chapter 10, pp. 505-552.

Gold, L.W. and Sinha, N.K. 1980. The rheological behaviour of ice at small strains. Proc. of Intl. Union of Theoretical and Applied Mechanics Symp. on Physics and Mechanics of Ice, edited by Per Tryde, Springer-Verlag, pp. 117-128.

Goodman, R. 1992. Calibrating a large steel tank for use with pressuremeters in ice. B.Sc. Thesis, University of Manitoba, Civil Engineering Dept.

Hetenyi, M. 1946. Beams on elastic foundations. University of Michigan Press, Ann

Arbor, Michigan.

Hult, J.A.H. 1966. Creep in engineering structures. Blaisdell Publishing Company, Waltham, Mass., 115 pp.

Huneault, P. 1984. Étude paramétrique d'un essai pressiométrique à long terme dans la glace. Mémoire de maitrise, École Polytechnique de Montréal.

Johnston, G.H. and Ladanyi, B. 1972. Field tests of grouted rod anchors in permafrost. Canadian Geotechnical Journal, Vol. 9, pp. 176-194.

Kenyon, R., Shields, D.H., Domaschuk, L. and Frank, R. 1991. Lateral creep behaviour of discrete pile segments in ice. Proc. Intl. Colloquium on Creep Foundations, "Fondations Profondes", Paris, pp. 209-216.

Kjartanson, B. 1986. Pressuremeter creep testing in laboratory ice. Unpublished Ph.D. Thesis, University of Manitoba, Winnipeg, Manitoba, 400 pp.

Kjartanson, B.H., Shields, D.H., Domaschuk, L. and Man, C.S. 1988. The creep of ice measured with the pressuremeter. Canadian Geotechnical Journal, Vol. 25, No. 2, pp. 250-261.

Ladanyi, B. 1972. An engineering theory of creep of frozen soils. Canadian Geotechnical Journal, Vol. 9, pp. 63-80.

Ladanyi, B. 1975. Bearing capacity of strip footings in frozen soils. Canadian Geotechnical Journal, Vol. 12, pp. 393-407.

Ladanyi, B. 1981. Mechanical behaviour of frozen soils. Proc. of the Intl. Symp. on the Mechanical Behaviour of Structured Media, Ottawa, Part B, pp. 205-245.

Ladanyi, B. 1982. Borehole creep and relaxation tests in ice-rich permafrost. Proc. 4th Canadian Permafrost Conference, the R.J.E. Brown Memorial Volume, National Research Council of Canada, Ottawa, pp. 406-415.

Ladanyi, B. 1983. Shallow foundations on frozen soil: creep settlement. ASCE, Journal of Geotechnical Engineering, Vol. 109, No. 11, November, pp. 1434-1448.

Ladanyi, B. and Eckardt, H. 1983. Dilatometer testing in thick cylinders of frozen sand. Permafrost: Proc. 4th Intl. Conf., Fairbanks, Alaska, Nat. Acad. Press, Washington, D.C., pp. 677-682.

Ladanyi, B. and Johnston, G.H. 1973. Evaluation of in situ creep properties of frozen soils with the pressuremeter. In: Permafrost, the North American Contribution to the 2nd International Permafrost Conference, Yakutsk, NAS, Washington, D.C., pp. 310-318.

Ladanyi, B. and Johnston, G.H. 1975. Behaviour of circular footings and plat anchors embedded in permafrost. Canadian Geotechnical Journal, Vol. 11, pp. 531-553.

Ladanyi, B. and Johnston, G.H. 1978. Field investigations in frozen ground. Geotechnical Engineering for Cold Regions, edited by O.B. Andersland and D.M. Anderson, McGraw-Hill, Chapter 9, pp. 459-504.

Ladanyi, B. and Paquin, J. 1978. Creep behaviour of frozen sand under a deep circular load. Proc. 3rd Intl. Conf. on Permafrost, Vol. 1, Edmonton, Canada, pp. 679-686.

Ladanyi, B. and Saint-Pierre, R. 1978. Evaluation of creep properties of sea ice by means of a borehole dilatometer. Proc. IAHR Symp. on Ice Problems, Luleä, Sweden, Vol. 1, pp. 97-115.

Ladanyi, B. Barthelemy, E. and Saint-Pierre, R. 1979. In situ determination of creep properties of ice covers by means of borehoole creep and relaxation tests. Proc. Workshop on Bearing Capacity of Ice Covers, Winnipeg, NRCC-ACGR Technical Memo., No. 123, pp. 44-64.

Mellor, M. 1979. Mechanical properties of polycrystalline ice. Proc. of Intl. Union of Theoretical and Applied Mechanics Symp. on Physics and Mechanics of Ice, edited by Per Tryde, Springer-Verlag, pp. 217-245.

Mellor, M. and Cole, D.M. 1982(a). Deformation and failure of ice under constant stress or constant strain-rate. Cold Regions Science and Technology, Vol. 5, pp. 201-219.

Mellor, M. and Cole, D.M. 1982(b). Stress/strain/time relations for ice under uniaxial compression. Cold Regions Science and Technology, Vol. 6, pp. 207-230.

Mellor, M. and Testa, R. 1969. Effect of temperature on the creep of ice. Journal of Glaciology, Vol. 8, pp. 131-145.

Michel, B. 1978. Ice mechanics. Les Presses de l'Université Laval, Laval, Quebec, 499 pp.

Morgenstern, N.R., Roggensack, W.D. and Weaver, J.S. 1980. The behaviour of friction piles in ice and ice-rich soils. Canadian Geotechnical Journal, Vol. 17, pp. 405-415.

Morin, P.J. 1992. Discussion on finite element simulation of behaviour of laterally loaded piles in permafrost by Foriero and Ladanyi. Journal of Geotechnical Engineering, ASCE, Vol. 118, No. 1, pp. 171-173.

Morin, P., Shields, D.H., Frank, R. 1992. Modelling laterally loaded piles in permafrost: relative importance of computer methods and physical properties. Intl. Colloq. Geotechnique et Informatique, Paris, France.

Morin, P., Shields, D.H., Kenyon, R., Domaschuk, L. and Frank, R. 1991. Predicting creep displacements of laterally loaded piles in ice and ice-rich materials. Proc. 1st Intl. Offshore and Polar Engineering Conference, Edinburgh, United Kingdom, pp. 535-542.

Murat, J.R., Huneault, P. and Ladanyi, B. 1986. Effect of stress redistribution on creep parameters determined by borehole dilatometer tests. Proc. 5th Intl. Symp. on Offshore Mechanics and Arctic Engineering, Tokyo, Vol. 4,, pp. 58-64.

Nadia, A. 1963. Theory of flow and fracture of solids. Vol. II. McGraw-Hill Book Company, New York, N.Y.

Neukirchner, R.J. and Nixon, J.F. 1987. Behaviour of laterally loaded piles in permafrost. ASCE Journal of Geotechnical Engineering, Vol. 113, No. 1, pp. 1-14.

Neukirchner, R.J. 1987. Analysis of laterally loaded piles in permafrost. ASCE Journal of Geotechnical Engineering, Vol. 113, No. 1, pp. 15-29.

Nixon, J.F. 1978. First Canadian Geotechnical Colloquium: Foundation design approaches in permafrost areas. Canadian Geotechnical Journal, Vol. 15, pp. 96-112.

Nixon, J.F. 1984. Laterally loaded piles in permafrost. Canadian Geotechnical Journal, Vol. 21, pp. 431-438.

Nixon, J.F. and McRoberts, E.C. 1976. A design approach for pile foundations in permafrost. Canadian Geotechnical Journal, Vol. 13, pp. 40-57.

Norton, F.H. 1929. Creep of steel at high temperatures. McGraw-Hill Book Co., New York.

Odqvist, F.K.G. 1933. Plasticity theory with applications. (Monograph in Swedish), Royal Swedish Academy of Engineering Sciences, Stockholm.

Odqvist, F.K.G. 1962. Creep in metallic structures. (In German), Springer, Berlin.

Odqvist, F.K.G. 1966. Mathematical theory of creep and creep rupture. Oxford Mathematical Monograph, Clarendon Press, Clarendon, Texas, 168 pp.

Reese, L.C. 1971. The analysis of piles under lateral loading. Proc. of the Symp. on the Interaction of Structures and Foundations, University of Birmingham, Birmingham, U.K.

Rowley, R.K., Watson, G.H. and Ladanyi, B. 1973. Vertical and lateral pile load tests in permafrost. Proc. 2nd Intl. Conf. on Permafrost, Yakutsk, North American Contribution, pp. 712-721.

Rowley, R.K., Watson, G.H. and Ladanyi, B. 1975. Prediction of pile performance in permafrost under lateral load. Canadian Geotechnical Journal, Vol. 12, pp. 510-523.

Sego, D.C. 1980. Deformation of ice under low stresses. Unpublished Ph.D. Thesis, University of Alberta, Edmonton, 500 p.

Sego, D.C. and Morgenstern, N.R. 1983. Deformation of ice under low stresses. Canadian Geotechnical Journal, Vol. 20, pp. 587-602.

Sego, D.C. and Morgenstern, N.R. 1985. Punch indentation of polycrystalline ice. Canadian Geotechnical Journal, Vol. 22, pp. 226-233.

Shields, D.H., Domaschuk, L., Azizi, F. and Kjartanson, B. 1989. Primary creep parameters for ice as measured in-situ. Cold Regions Science and Technology, Vol. 16, pp. 281-290.

Sun, Q.-X. 1987. On two special Rivlin-Ericksen fluid models generalizing Glen's flow law for polycrystalline ice. Unpublished Ph.D. Thesis, University of Manitoba, Winnipeg, Canada.

Thompson, D.B. 1987. The influence of entrained air on ice crystallography: a microscopic study. Unpublished B.Sc. Thesis, Geological Engineering Department, University of Manitoba, Winnipeg, Manitoba, 87 pp.

Vesic, A.S. 1961. Bending of beams resting on isotropic elastic solid. ASCE Journal of the Soil Mechanics and Foundations Divisions, Vol. 87, No. SM2, pp. 35-53.

Vivatrat, V., Chen, V. and Bruen, F.J. 1984. Ice load prediction for Arctic nearshore zone. Cold Regions Science and Technology, Vol. 10, pp. 75-88.

Von Mises, R. 1928. Z. angew. Math. Mech., Vol. 8, p. 161.

Weaver, J.S. 1979. Pile foundations in permafrost. Unpublished Ph.D. Thesis, University of Alberta, Edmonton, 225 pp.

Weaver, J.S. and Morgenstern, N.R. 1981. Pile design in permafrost. Canadian Geotechnical Journal, Vol. 18, pp. 357-370.

Winkler, E. 1867. Die Lehre der Elastizität und Festigheit. Dominicas, Prague, (in German).

# APPENDIX A

# THE PRELIMINARY FOUR TESTS

## A.1 INTRODUCTION

This appendix documents the results of the 4 preliminary Winkler Bar tests, and synthesizes the results of an undergraduate thesis (Thompson, 1987) which was a detailed crystallographic study on representative ice cores from Tests 1 and 2.

The problem which occurred during the preliminary tests, and the reason the test results are not included in the analysis, was that the two ends of the bar did not translate at the same rate when equal loads were applied to both ends of the bar. At the conclusion of this preliminary testing, this differential rate of movement was attributed to a systematic variation in the crystallography of the ice; hence the crystallographic study.

Each of the 4 preliminary tests differed either in how the ice sample was prepared, or in how the ice was frozen, but not in the procedures which were used to move the bar. The variations in sample preparation and freezing were:

- **Test 1.** The ice was prepared and frozen following Kjartanson's adaptation of the seed crystal technique for the pressuremeter test samples. Two hundred and forty kilograms of seed ice crystals were saturated using ordinary tap water, and the sample was frozen unidirectionally from the bottom upward.
- **Test 2.** The seed ice cubes were saturated using de-aired pore water (Glen, 1955; Mellor and Testa, 1969; Sego, 1980) rather than the ordinary tap water used in Test 1. The sample was frozen from the bottom upward.

- **Test 3.** The seed ice cubes were pre-wetted (Fransson, 1986) and then saturated using de-aired pore water. This time the direction of sample freezing was reversed, and the sample was **frozen from the top downward.**
- **Test 4.** The sample was prepared as in Test 3, but this time it was **frozen from the bottom upward.**

For these 4 tests, the magnitude of the lateral loads was maintained equal at the top and bottom surfaces of the ice.

**Test 1**

The results of Test 1, are shown in Figure A.1. For the first 20 hours, both ends of the bar translated more or less uniformly. After that, however, the bottom end began to translated significantly more rapidly than the top end. At the time, this result was unexpected, and the question as to why this had occurred had to be answered.

The possible causes of this differential movement were considered to be:

1. Experimental error in calibrating the load cells or the LVDTs, or in mounting same.
2. Non-uniform boundary conditions imposed by the ends of the tank.
3. The ice was not homogeneous.

The load cells and LVDTs were recalibrated; the accuracy of the applied loads was confirmed; and this cause was ruled out.

Preliminary calculations, following the solution by Baguelin (1977), to calculate the far field stress imposed by a Winkler element in an elastic disc, had suggested that the stresses imposed at the tank boundaries was insignificant. Both ends of the tank were

similarly confined by an 11.5 mm thick end plate. The possibility of non-uniform boundary conditions was not ruled out at this stage, but was considered to be less likely than non-uniformity of the ice.

When the ice from Test 1 was cored and examined visually under ordinary white light, it appeared that there was a systematic variation in the ice structure. Ice cored from near the bottom of the tank appeared nuggety, but further up the sample (from approximately the mid-depth up to the top) the ice appeared more cloudy than nuggety. Near the bottom of the tank, tiny air bubbles were concentrated around the individual seed ice cubes giving the ice this nuggety appearance. The cubes were clear, as was the pore ice. As one examined ice from further up the sample, the air bubbles appeared to become fewer in number, larger in diameter, and more randomly situated throughout the ice mass. At the time, it was decided to repeat the test using de-aired water.

### Test 2 Results

It was anticipated that the use of de-aired water as the saturating fluid for this test might reduce the air bubbles in the ice, and result in the bar translating more uniformly.

The results of Test 2 (see Figure A.2) were discouraging in that more differential movement was observed than had occurred during Test 1.

At this time, a crystallographic examination of the ice was initiated. The results are presented and discussed in the following subsection.

## A.3 THE CRYSTALLOGRAPHIC EXAMINATION OF TEST 1 ICE

Following Test 2, an examination of the ice crystallography and structure was

initiated. The study is documented in an undergraduate thesis (Thompson, 1987). The study considered:

1. Systematic variations in ice density.
2. Variations in crystal size.
3. Variations in distribution of air bubbles within the core.

Thompson examined ice cored from Tests 1 and 2. He also cored ice from an ice sample which he prepared in a taller barrel, i.e. in thicker ice. His work consisted of:

1. Density measurements of all cores from the 3 barrels.
2. Preparing thin sections from representative top and bottom cores from Test 1 ice, and from individual ice seed cubes. A total of 19 thin sections were prepared, and the average crystal diameter in each thin section was determined.
3. Visually inspecting ice cores under ordinary white light from all three barrels of ice. It was under white light that the variations in distribution and size of the entrained air bubbles was most apparent.

Thompson's density measurements were consistent with the density measurements reported by Kjartanson. Thompson's average ice density for the three ice samples was 0.900 $Mg/m^3$ versus an average density reported by Kjartanson of 0.901 $Mg/m^3$. Densities were consistent in all 3 barrels of ice. Within individual barrels, densities were also consistent, both laterally from borehole to borehole, and vertically in the boreholes. It was concluded that the ice densities were the same in the tanks of Tests 1 and 2 and in the taller tank. Using de-aired water in Test 2 did not change the measured density.

Variation in crystal diameter was examined by measuring crystal diameters from thin sections prepared from Test 1 ice cores. The thin sections were photographed under cross-polarizing light, and the average crystal diameters were determined. A total of 19 thin sections were prepared from the Test 1 ice including:

1. Nine thin sections taken near the top of the disc of ice.
2. Eight thin sections taken near the bottom of the disc of ice.
3. Two thin sections were prepared from the seed ice cubes.

From the thin section photographs it was first concluded there was a random orientation of the c-axis of the crystals, and hence the ice could be considered polycrystalline in structure. There was, however, a systematic variation in the average diameter of the crystals. The average crystal diameter near the top of the ice was 1.24 mm, while the average crystal size at the bottom of the ice was 1.46 mm. In other words, the average crystal diameter at the bottom was 18.5% larger than at the top. For comparison, the individual ice cubes used as seed crystals had an average crystal diameter of 1.43 mm.

The third component consisted of a visual logging and description of the intact ice cores as viewed under ordinary white light. Plates A.1, A.2, and A.3 are photographs of core samples which are representative of the bottom, middle, and top of the ice in Test 2. In Plate A.1 the ice core is nuggety in appearance. The individual nuggets are the individual ice cubes or seed crystals, which are highlighted under white light by tiny (typically less than 1 mm) bubbles concentrated along the outside surface of the seed cubes. As the ice further up the core was examined (Plate A.2 from the middle of the tank), it was observed that ice became less nuggety and more cloudy in appearance. In

most cores, visual definition of the seed ice cubes was lost by about the midpoint of the disc of ice. Air bubbles remained, but became more randomly distributed throughout the ice, giving the ice a cloudier appearance. At the top of the ice, virtually all definition of the seed ice cubes was lost. The air bubbles became fewer in number, but larger in size (typically 4 to 6 mm versus about 1 mm at the bottom).

Thompson observed that the seed ice cubes delivered to the laboratory in the 20 kg bags were quite often covered with a thin dusting of hoar frost and powdered ice crystals. He hypothesized that the air bubbles remained attached to the lattice points of the hoar frost crystals, and that the surface tension of the individual bubbles held them in place as the ice froze. He suggested that during the several days it took for the freezing front to advance up from the bottom of the sample, the hoar frost crystals higher up in the sample may have melted.

Thompson's recommendation was that more homogeneous ice may result if the ice seed crystals were pre-wetted (Fransson, 1986), for just long enough to melt the light dusting of hoar frost and powdered ice crystals. This technique was employed in preparing the samples for Tests 3 and 4.

**Tests 3**

Following Thompson's recommendation, the sample for Test 3 was prepared by pre-wetting the ice cubes. This was accomplished by letting the pore water in the reservoir cool to approximately 4°C, and then saturating the seed ice cubes with the water for approximately 5 minutes, before pumping the water back into the reservoir. The water in the reservoir was then cooled to 0°C; the pre-wetted seed crystals were

saturated; and the sample was frozen.

In addition to pre-wetting the ice cubes, the direction of freezing was reversed (as compared to Tests 1 and 2), so that the ice froze from the top down. If Thompson's hypothesis regarding the pre-wetting of the crystals was correct, then a homogeneous distribution of entrained air bubbles would result, regardless of the direction of freezing. If, however, other factors associated with the freezing direction of the ice were producing a variation in ice properties, then reversing the freezing direction would also reverse the differential movements of the two ends of the bar.

In order to freeze the sample from the top downward, a drainage line was placed through the bottom of the tank. This line allowed excess porewater to drain as the freezing front advanced. Drainage was controlled by maintaining the top of the drain hose at the same elevation as the freezing front. After the freezing was more than 50% complete the lid at the top of the tank was loosened to allow for sample expansion.

The test results, as shown in Figure A.3, suggest that reversing the freezing direction did reverse the differential translation of the bar. For the first 1,000 hours, the top of the pile did indeed move faster than the bottom. This behaviour was the reverse of Tests 1 and 2. From that point onward, the slope of the displacement curve for the bottom end of the bar became curvilinear upwards in shape (the deflection rate was increasing steadily). Examination of the experiment at the conclusion of the test, revealed, however, that at least 75 mm of ice had sublimated away from around the bottom end of the bar. The plastic seal placed around the bar at the bottom of the tank had been torn away. The gradual increase in displacement rate to the point where the bottom end caught up with the top end was attributed to this gradual, continuous

reduction in support as the ice disappeared. Nevertheless, the evidence during the initial stages of the test, when sublimation would not have been a factor, was indeed that the differential movement had been reversed.

The ice cores for Test 3 were noted to be very nearly uniform in appearance from top to bottom. A nuggety structure was slightly visible, now near the top, as compared to near the bottom of the ice in Tests 1 and 2. However, the overall appearance was of a clear ice; the air bubbles were far fewer, and more uniformly distributed throughout the ice than had been observed for Tests 1 and 2.

**Test 4**

The ice sample for Test 3 was also prepared by pre-wetting the seed ice cubes, but this sample was frozen, conventionally, from the bottom upward.

The results, shown in Figure A.4, confirmed that the differential movement of the bar was somehow related to the direction of freezing of the sample. The two ends of the bar moved more or less uniformly for the first half of the test (50 hours), but after that the bottom moved more rapidly than the top. This behaviour was opposite to Test 3 but the same as for Tests 1 and 2.

**Conclusions of Preliminary Testing**

The principal observation of the preliminary tests (including the 4 bar tests, and Thompson's study of the ice crystallography) was that there was a systematic vertical variation in both ice crystal size, and in the distribution of entrained air bubbles within the discs of ice. It is believed that the variations in ice crystal size and air bubbles

created variations in the creep properties of the ice. This, in turn, led to one end of the bar moving faster than the other when both ends were under the same load.

It was concluded that a detailed examination of the role that crystallography could have in determining creep properties should be made at some time in the future. This study could couple crystallographic information with creep testing of the ice. The creep testing could consist either of uniaxial creep, or pressuremeter creep testing, using, say, a small pavement pressuremeter to conduct in situ creep tests at varying depths within the sample.

The principal conclusion drawn was that while it was obviously possible to "force" the two ends of the bar to translate at the same rate, it was not clear that it was going to be possible to produce ice samples that were truly homogeneous so that the ends would translate at the same rate under equal end loads. By forcing the ends to translate at the same rate it was thought that displacement conditions would be uniform throughout the thickness of the ice.

Furthermore, as was suggested by M. François Baguelin (personal communication, 1987), because the creep rate of ice is approximately a cubic function of applied stress, only a very small differential in the loads would "force" the bar to translate uniformly. This suggestion was accepted and proved to be correct.

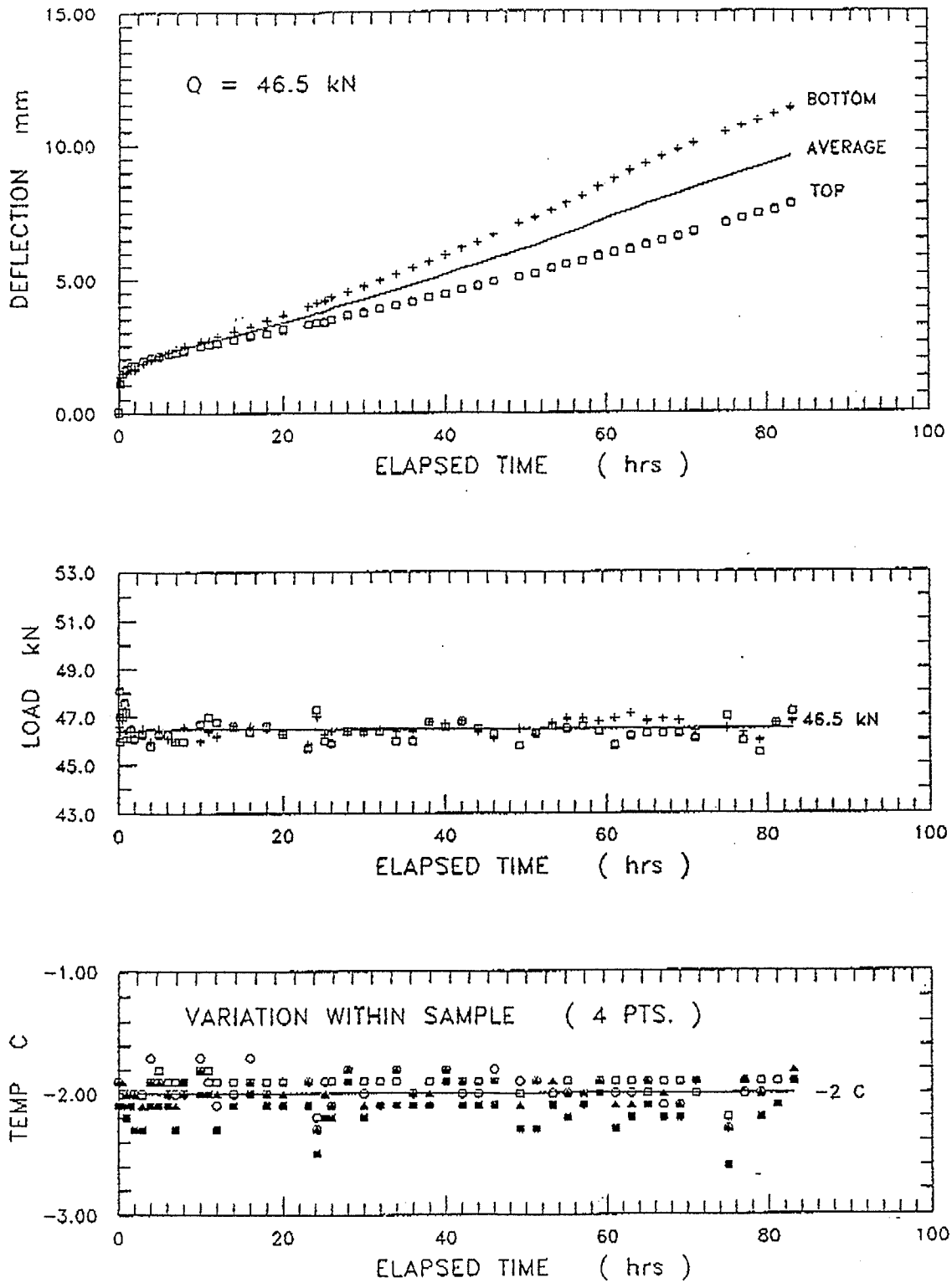


Figure A.1 Test 1 results

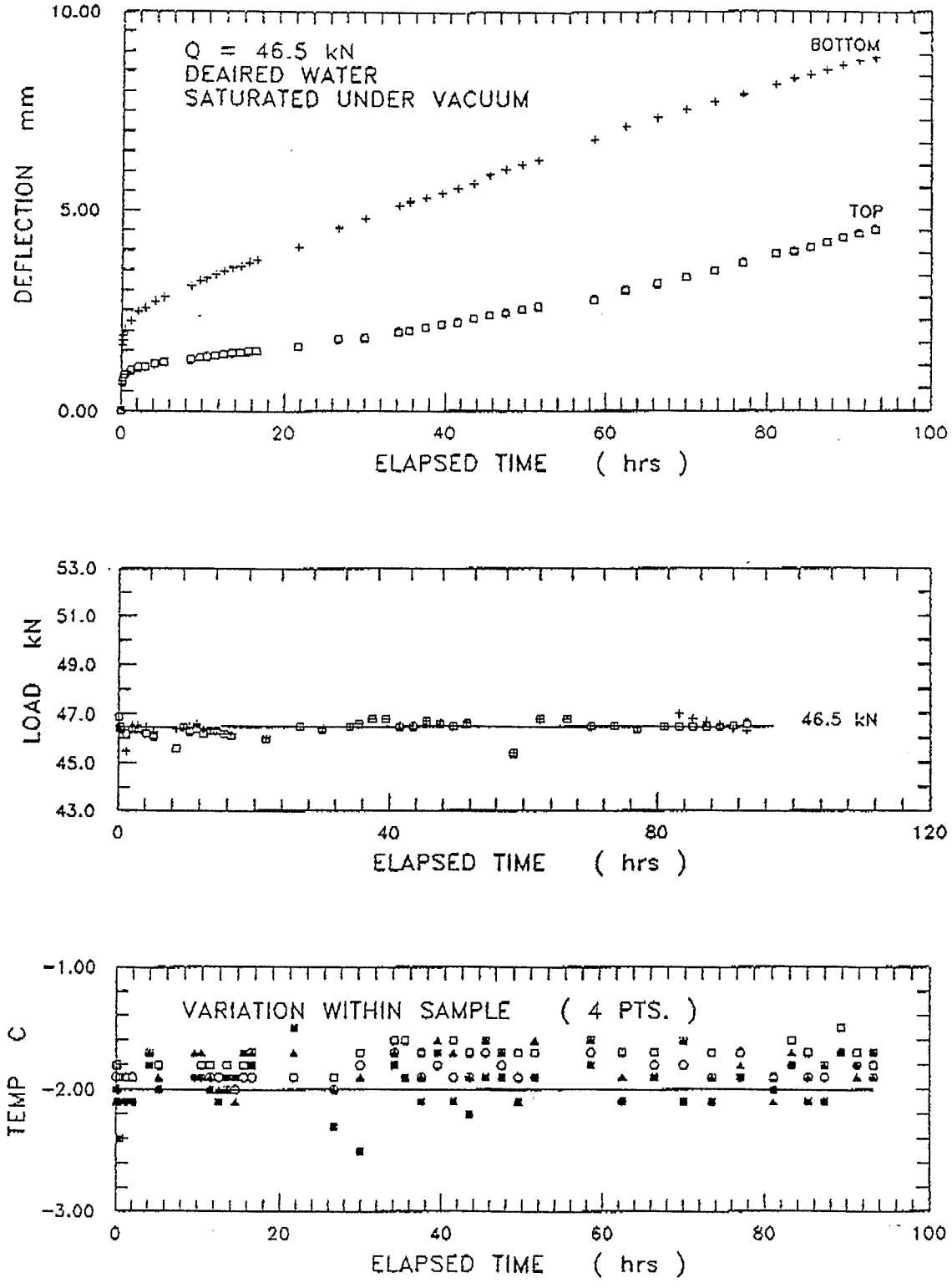


Figure A.2 Test 2 results

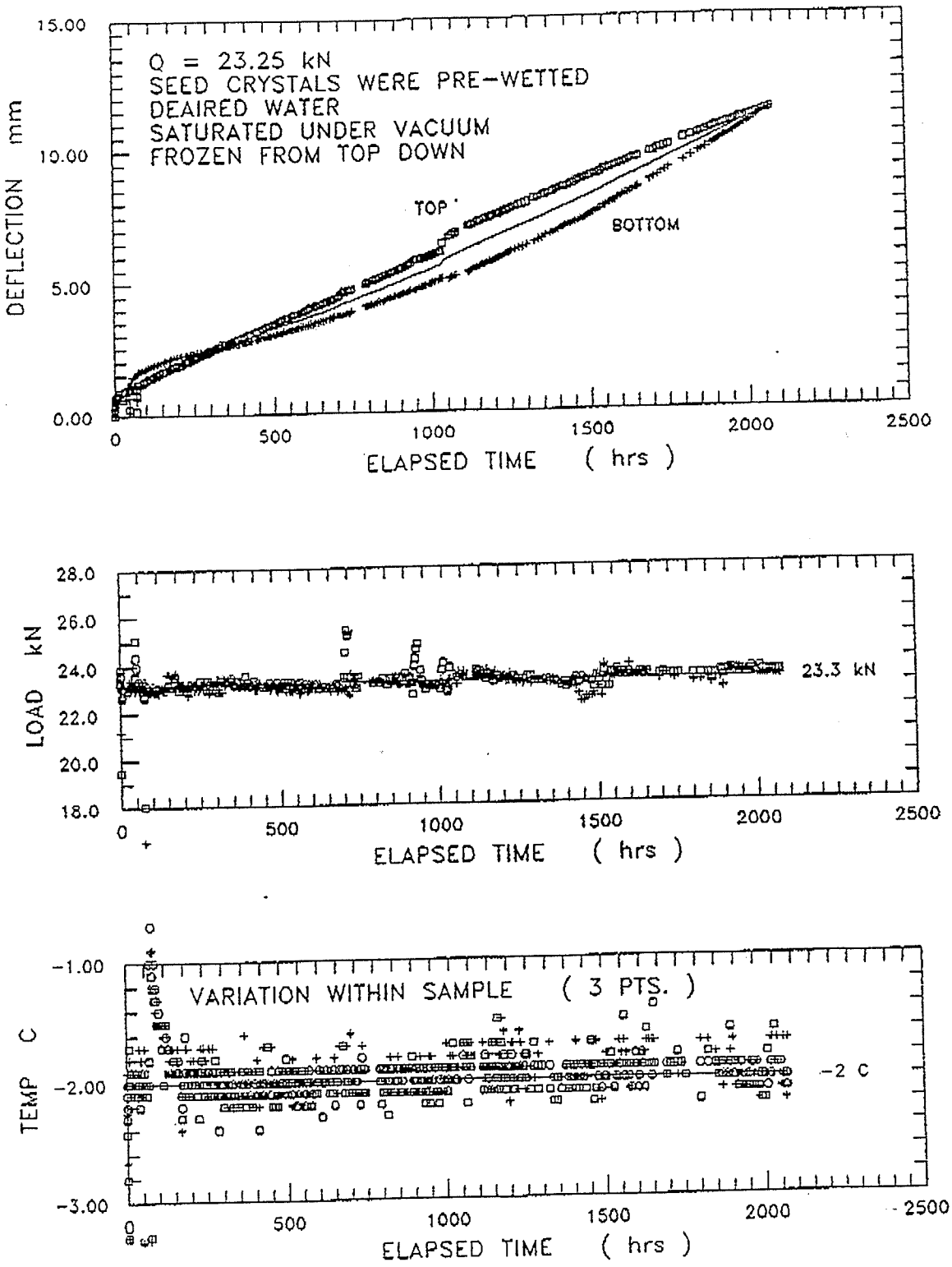


Figure A.3 Test 3 results

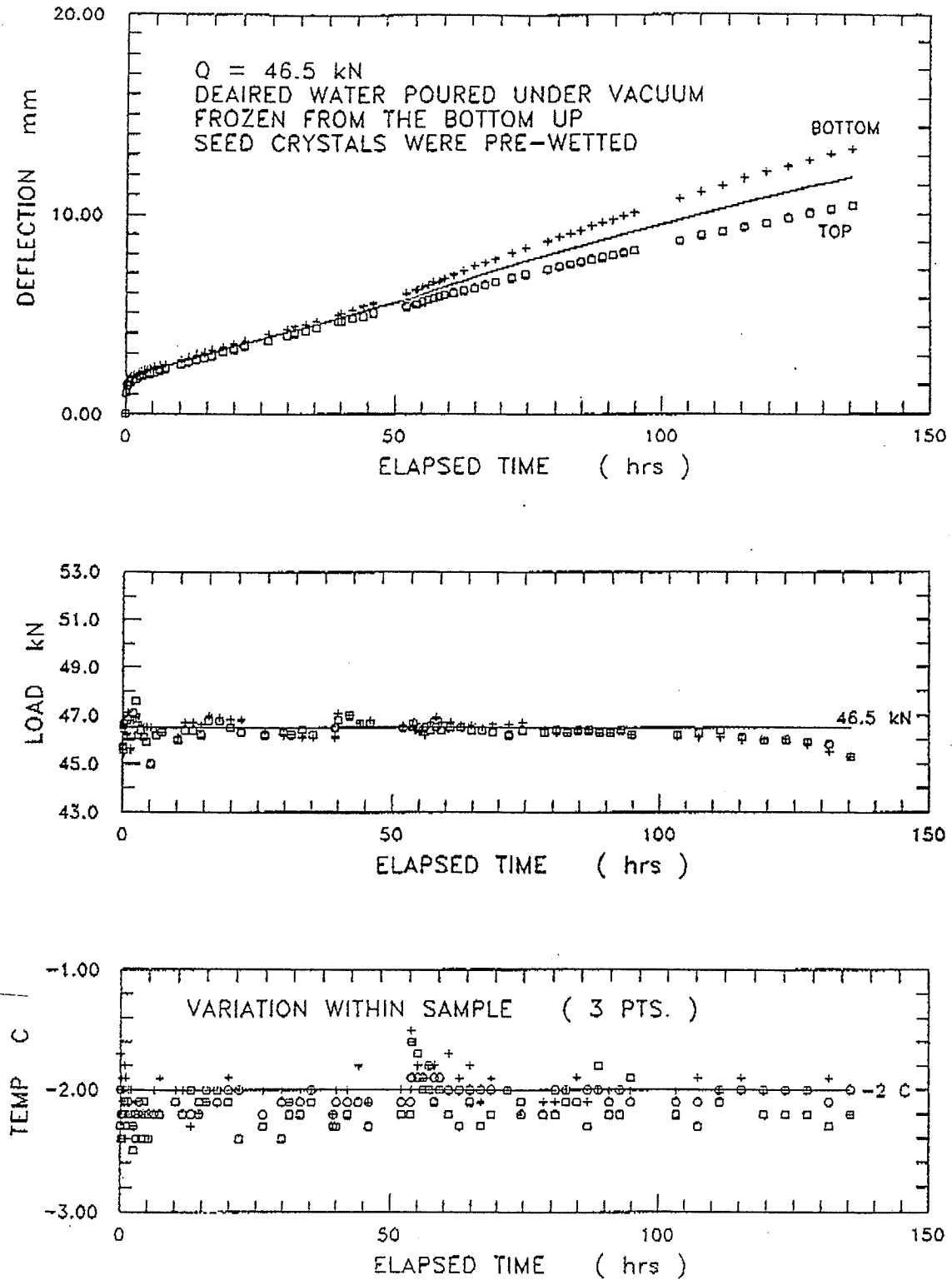


Figure A.4 Test 4 results


Photo A.1 Typical ice core from near the bottom of the ice sample (Test 1).

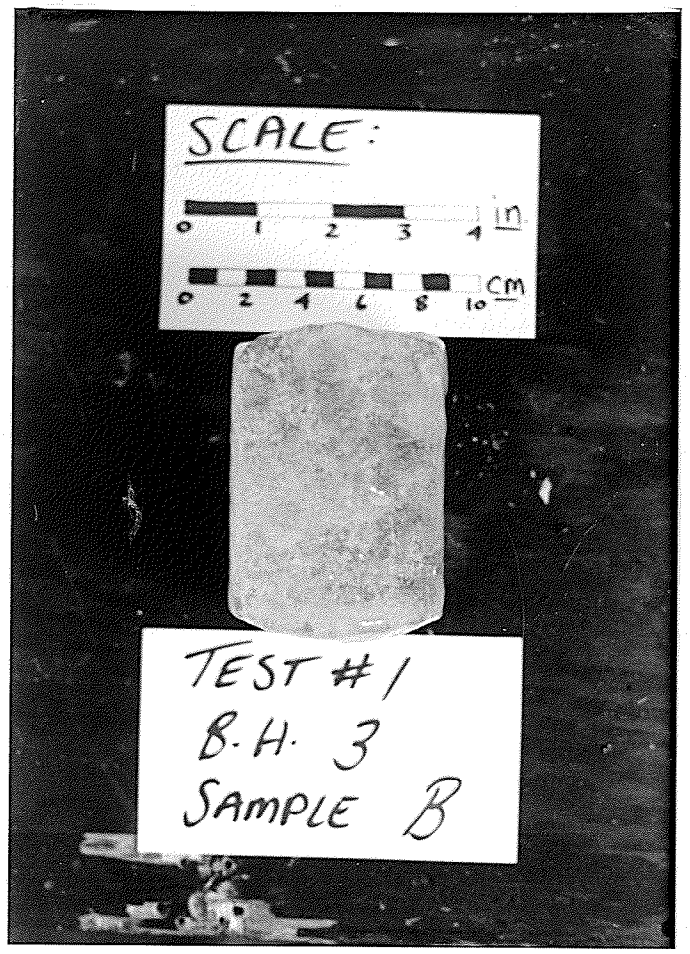


Photo A.2 Typical ice core from near the middle depth of the ice sample (Test 1).

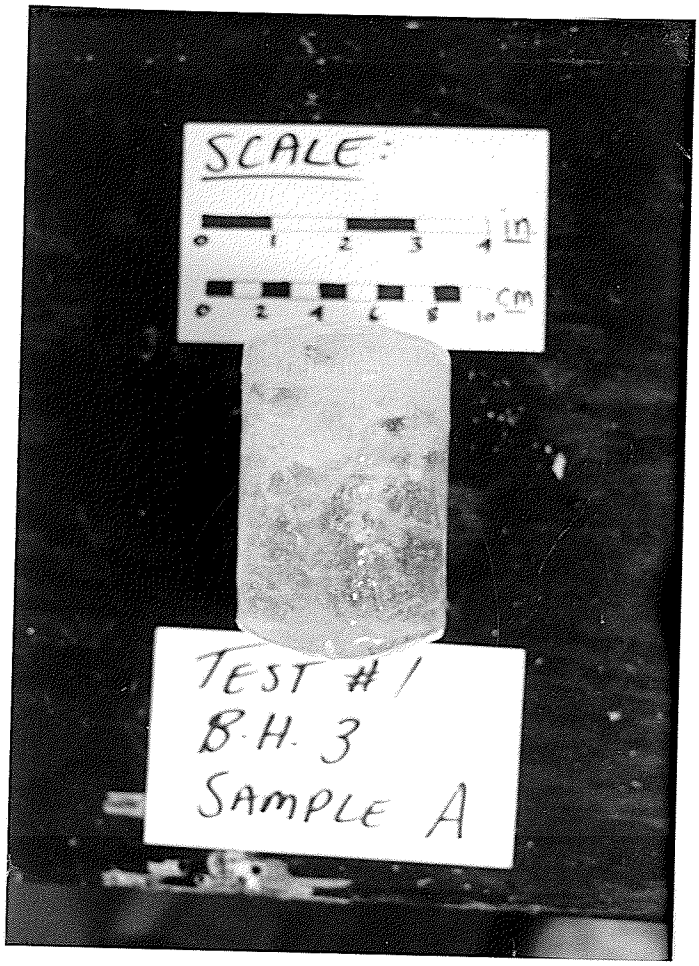


Photo A.3 Typical ice core from near the top of the ice sample (Test 1).

# APPENDIX B

# COMPLETE TEST RESULTS

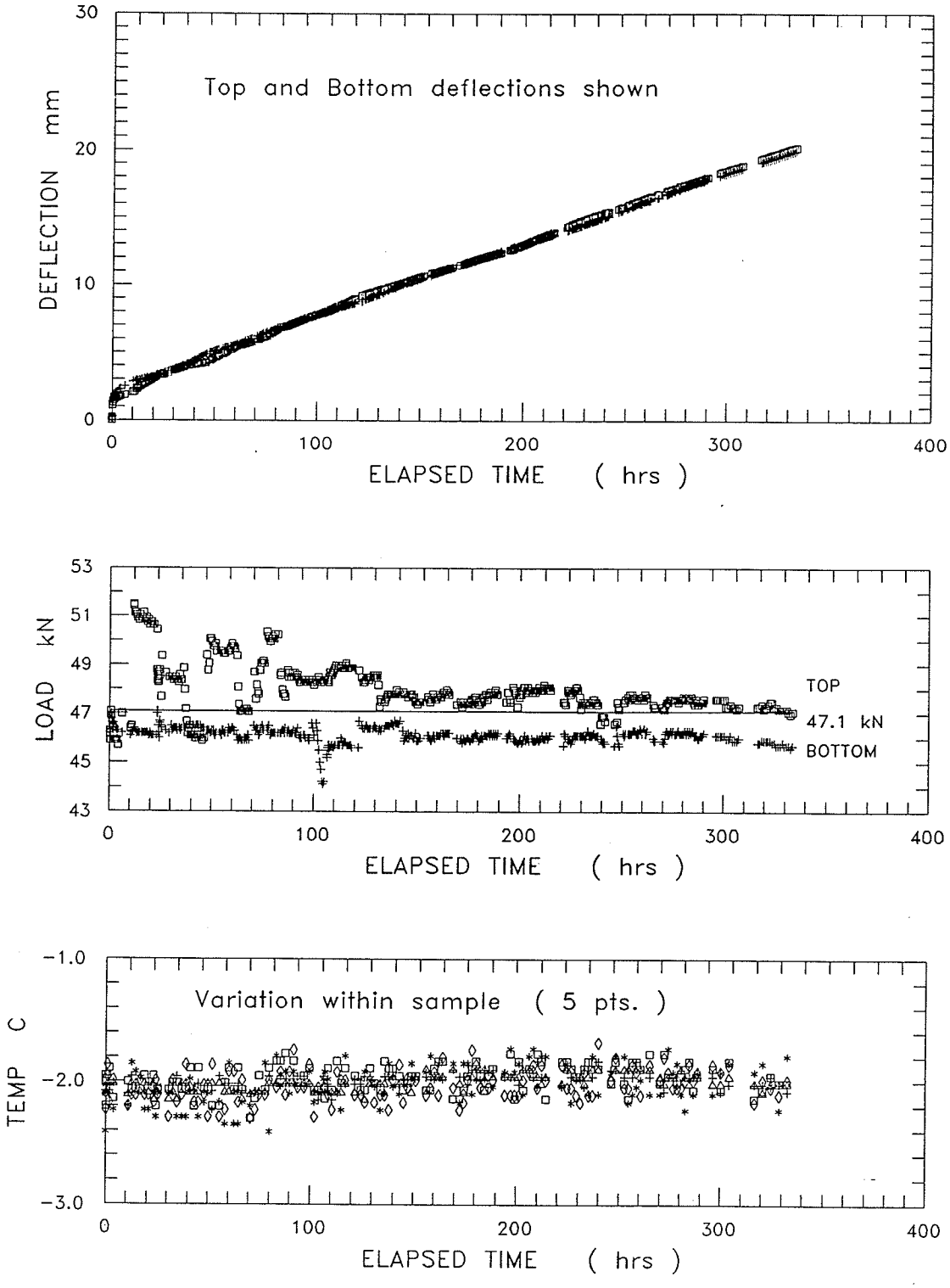


Figure B.1 Single stage Test 5: displacement, load, and sample temperature versus elapsed time.

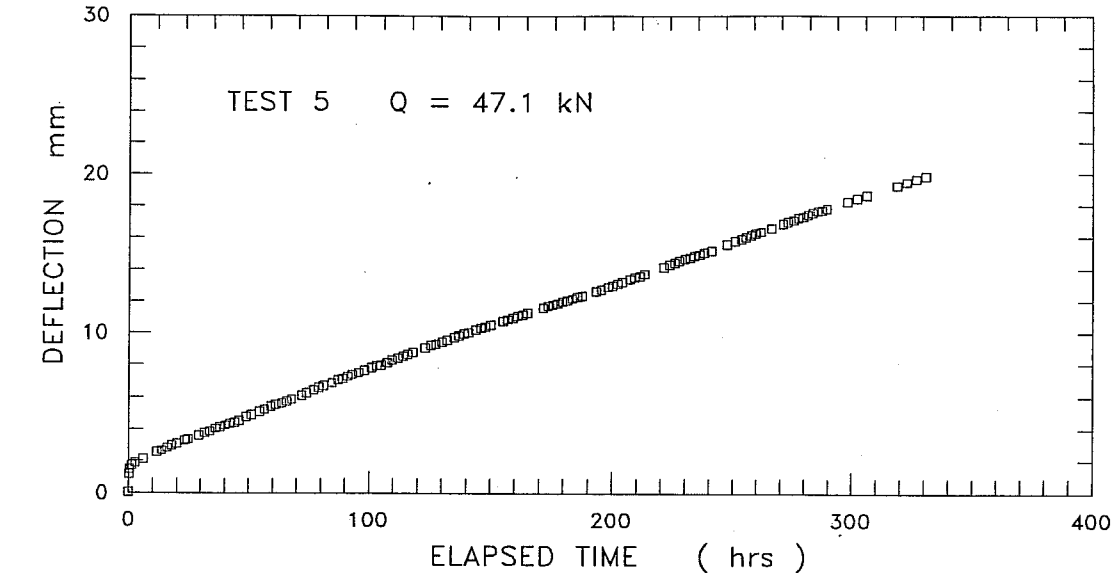


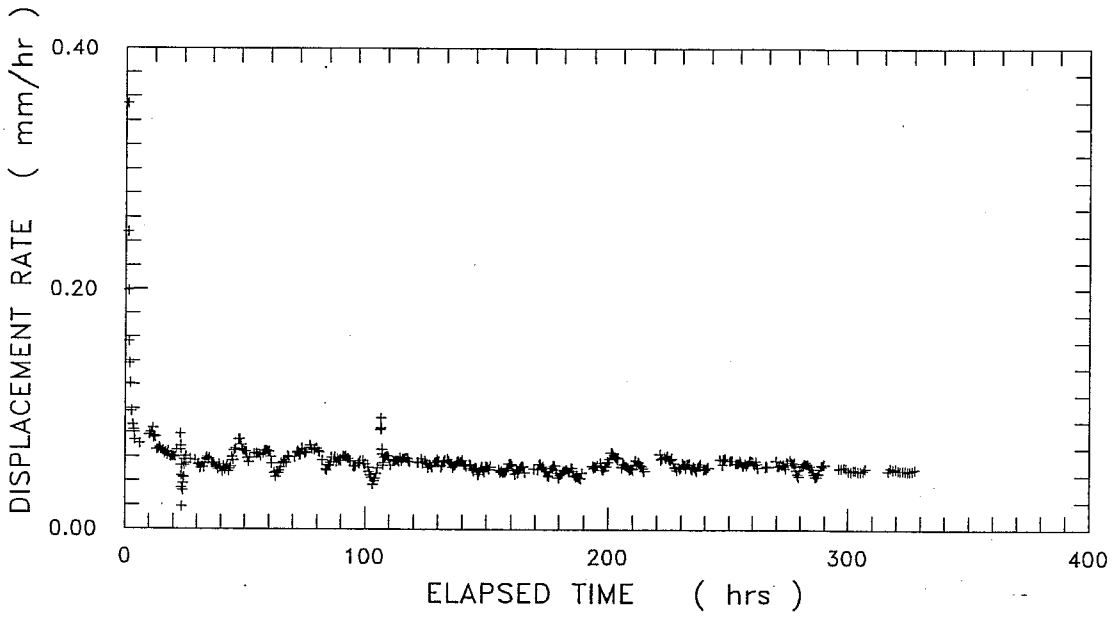


SST 5 Pile displacement rate variation with time

Figure B.2 Single stage Test 5: displacement, and displacement rate versus elapsed time.

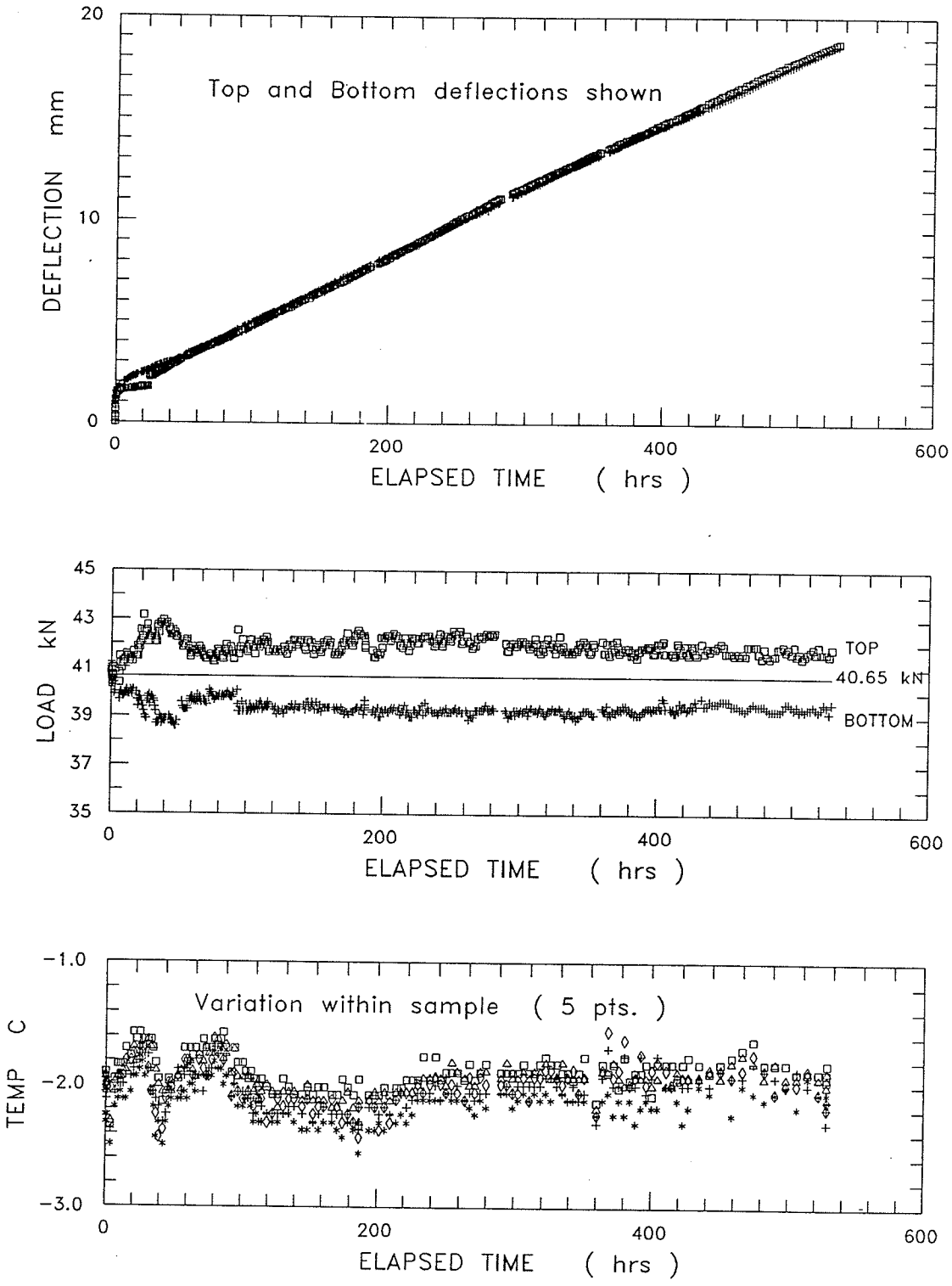


Figure B.3 Single stage Test 6: displacement, load, and sample temperature versus elapsed time.

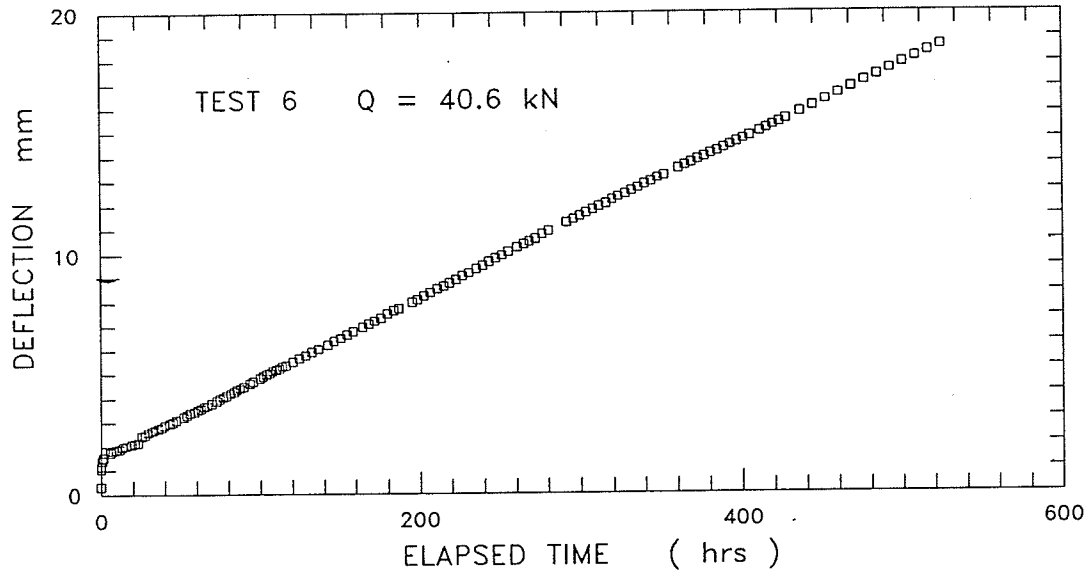


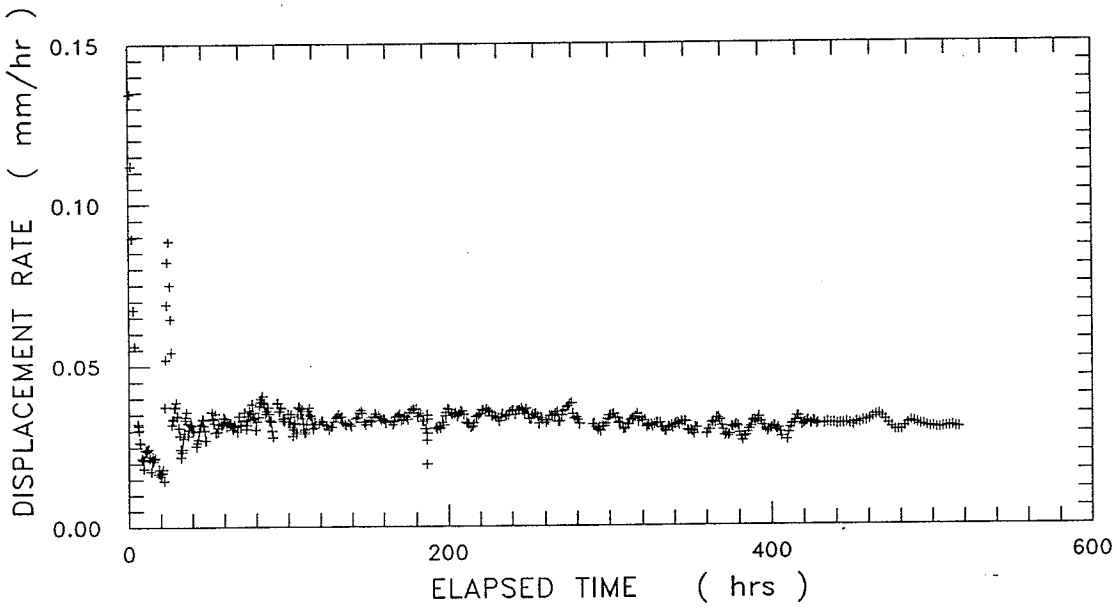


Figure B.4 Single stage Test 6: displacement, and displacement rate versus elapsed time.

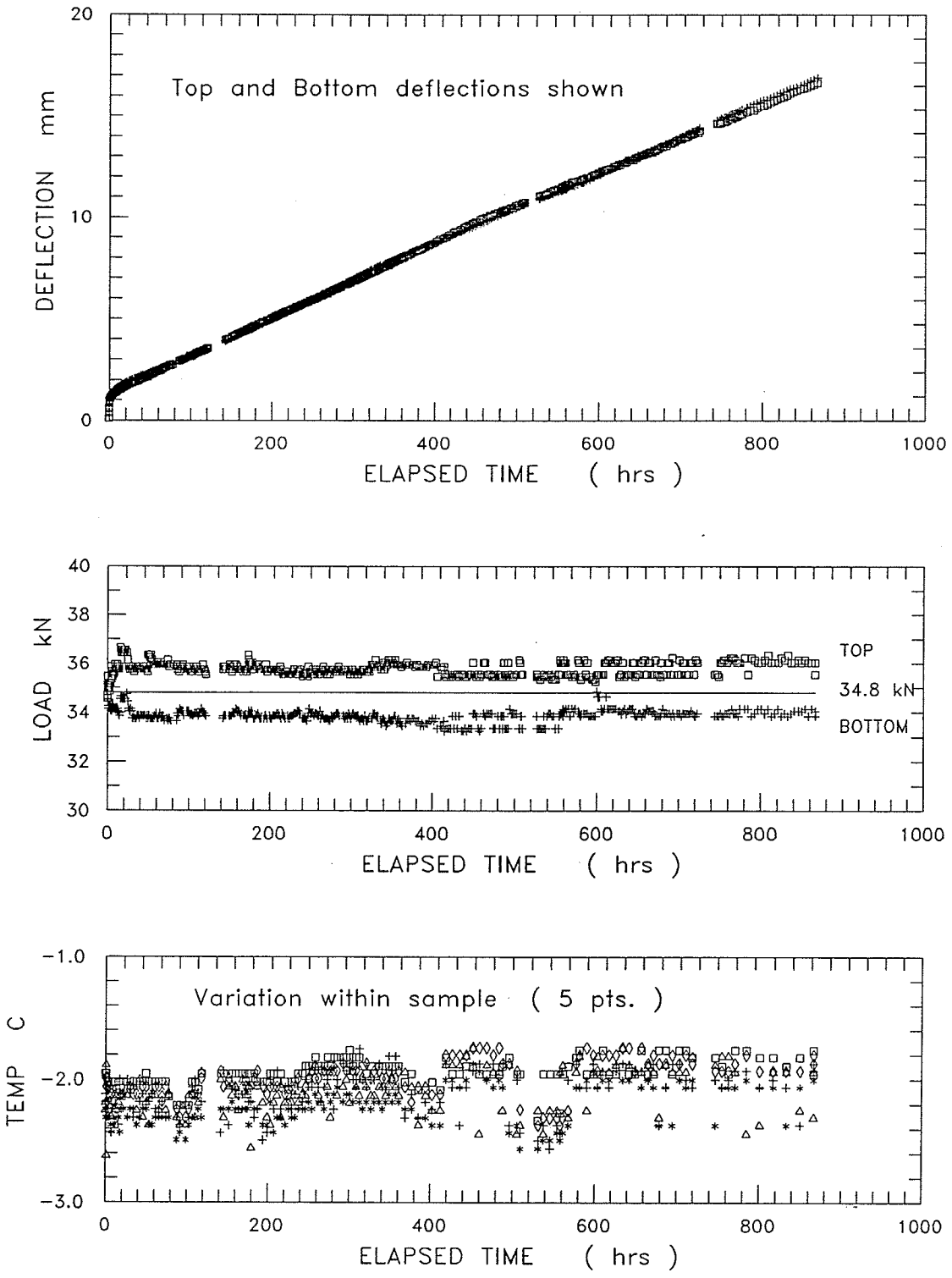


Figure B.5 Single stage Test 7: displacement, load, and sample temperature versus elapsed time.

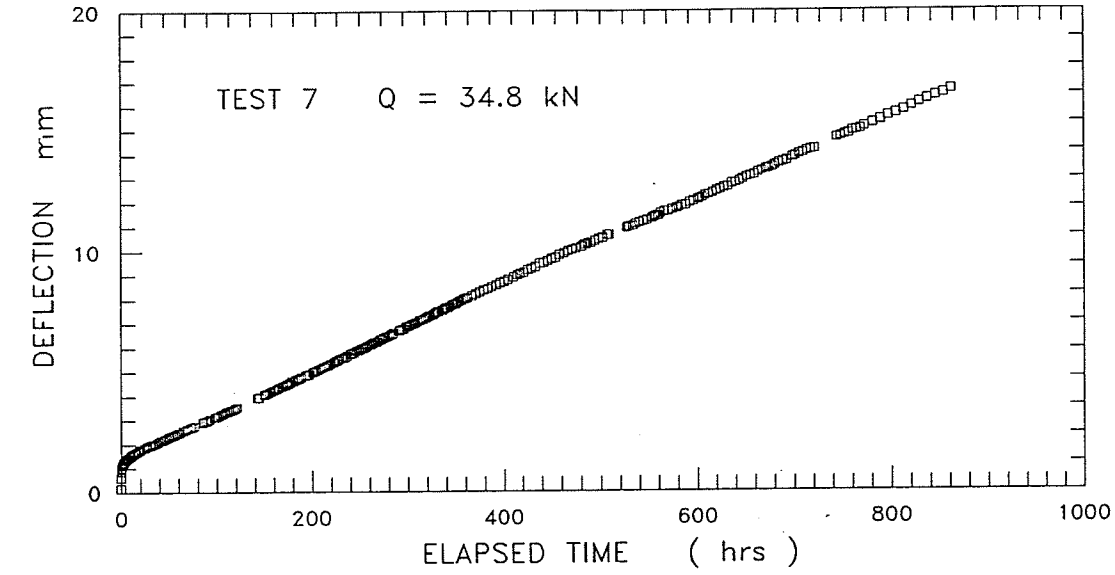


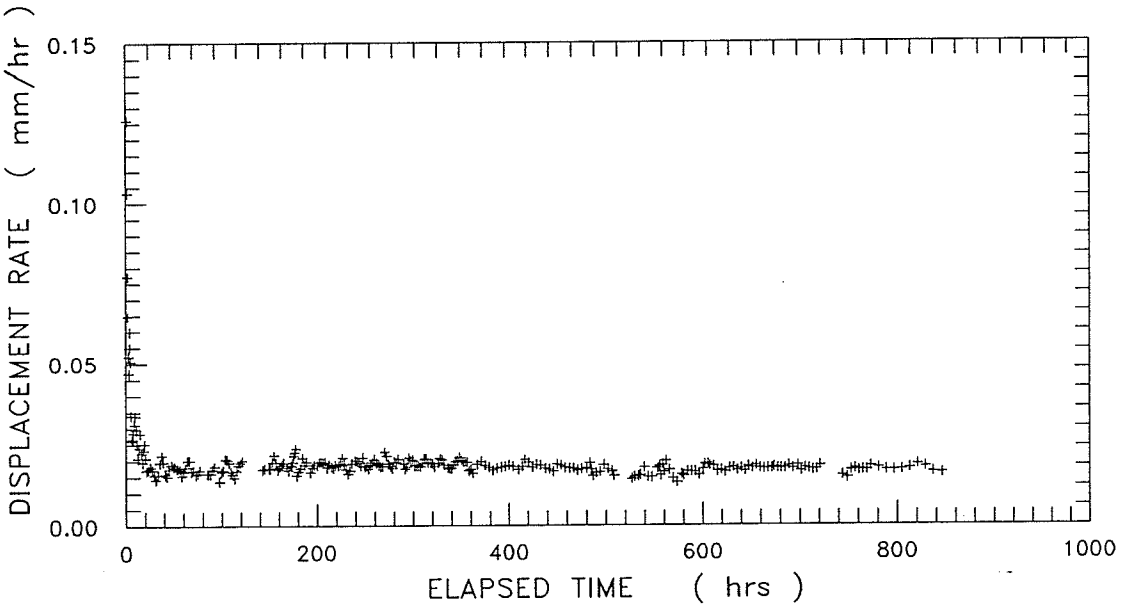


Figure B.6 Single stage Test 7: displacement, and displacement rate versus elapsed time.

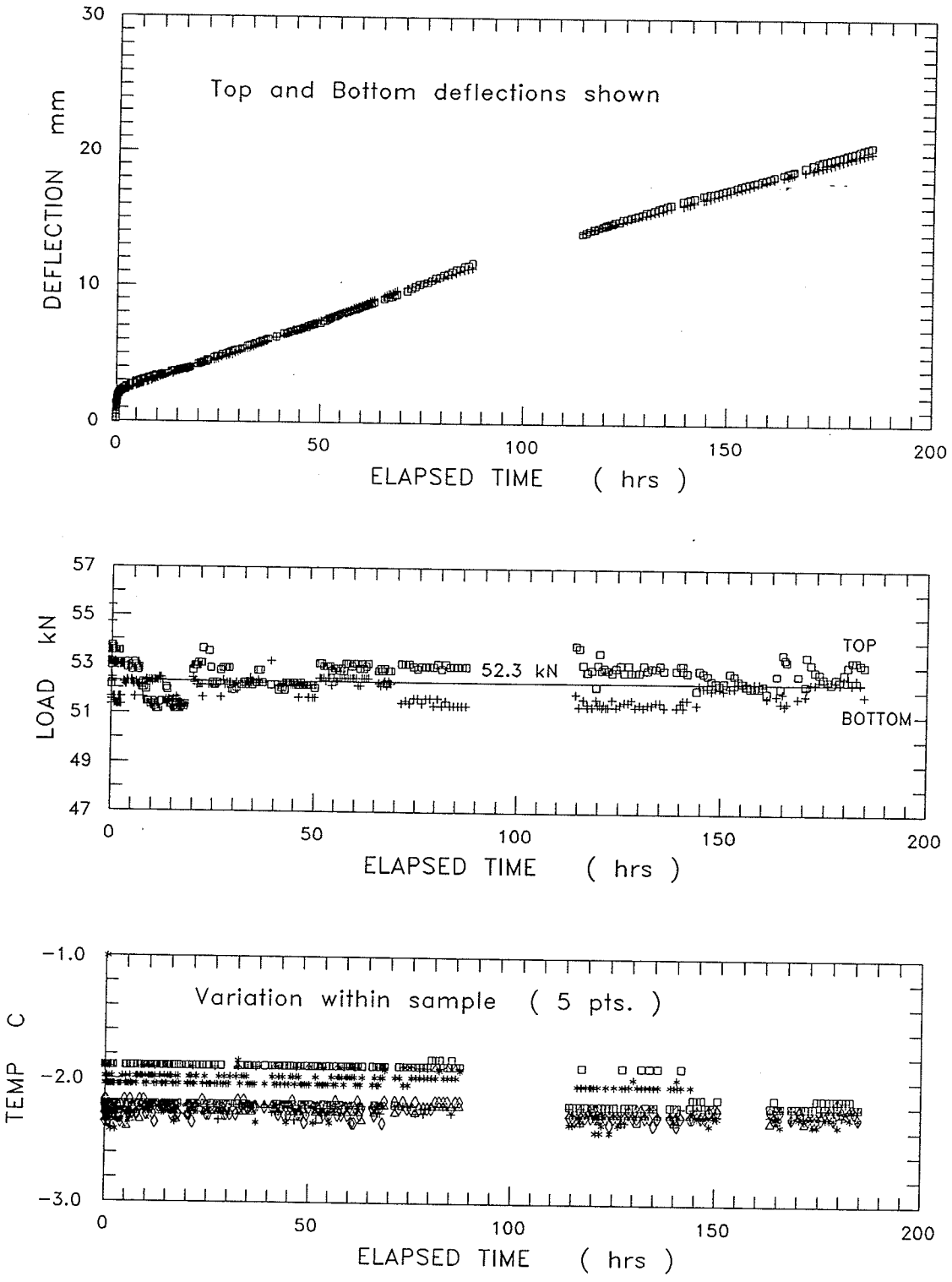


Figure B.7 Single stage Test 8: displacement, load, and sample temperature versus elapsed time.

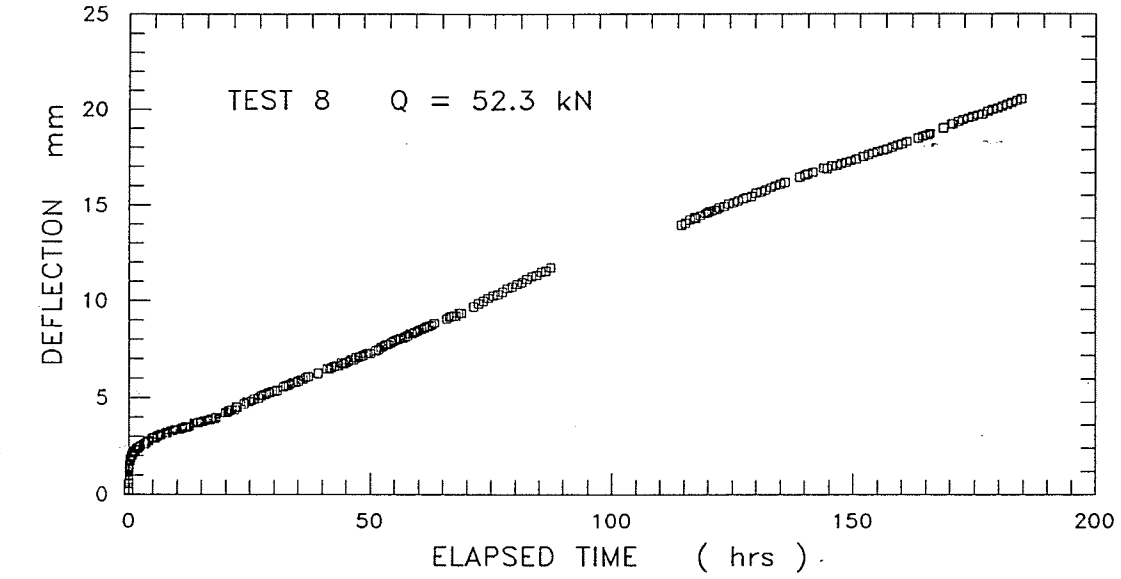


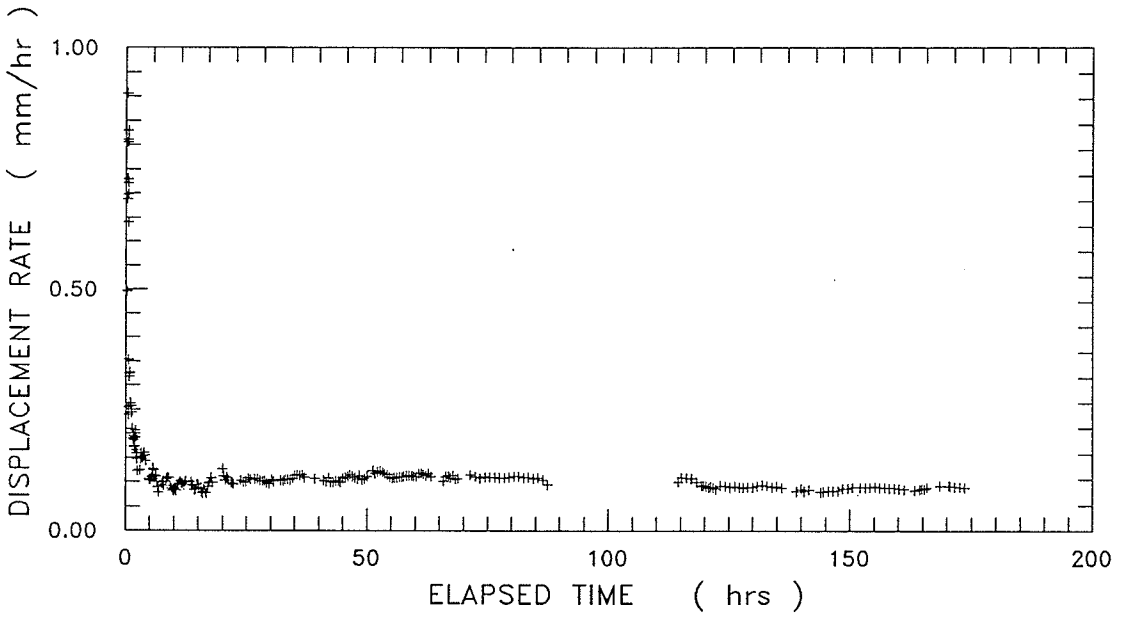


SST 8 Pile displacement rate variation with time

Figure B.8 Single stage Test 8: displacement, and displacement rate versus elapsed time.

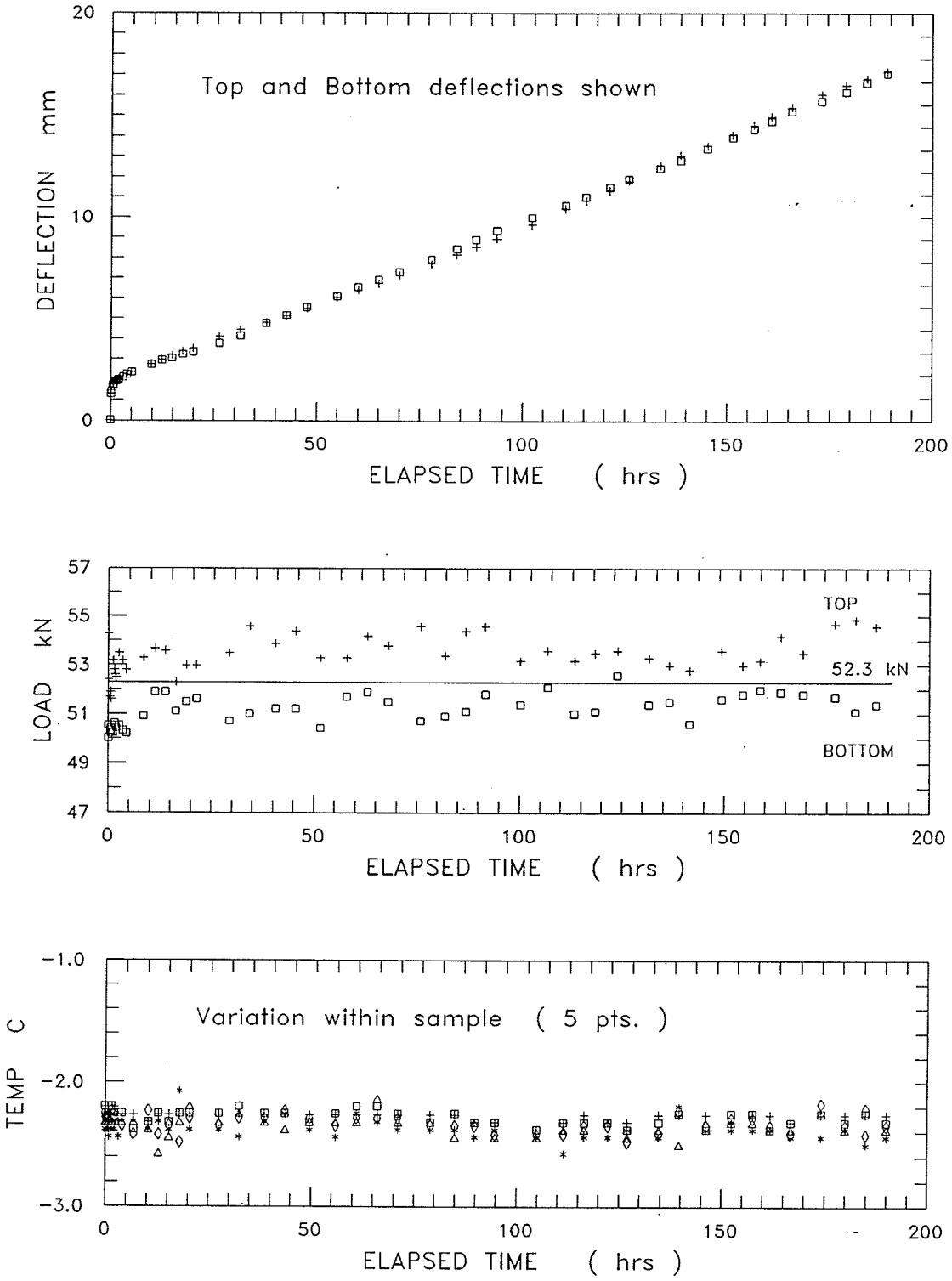


Figure B.9 Single stage Test 9: displacement, load, and sample temperature versus elapsed time.

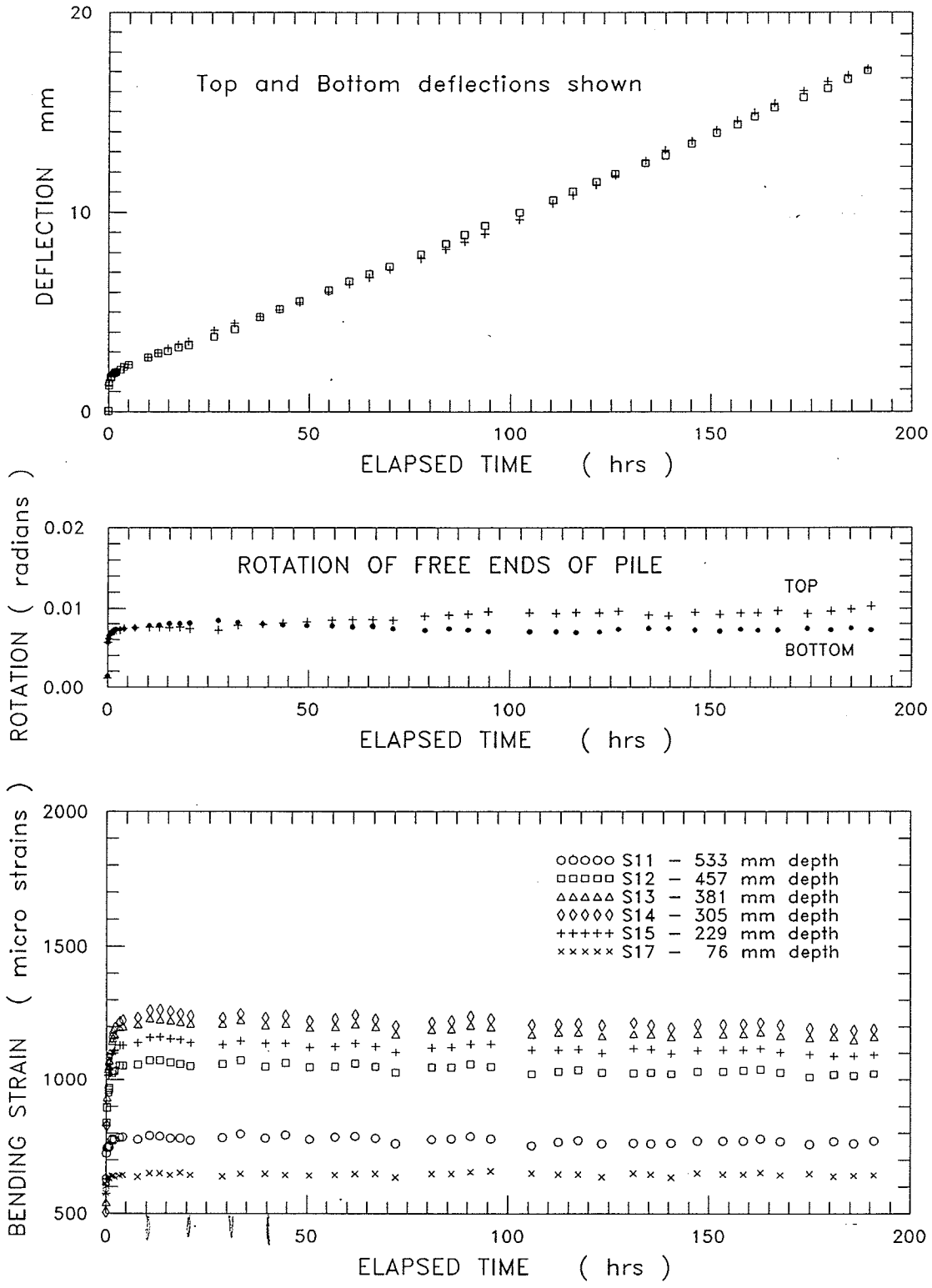


Figure B.10 Single stage Test 9: displacement, rotation of free ends of the bar, and bending strain versus time.

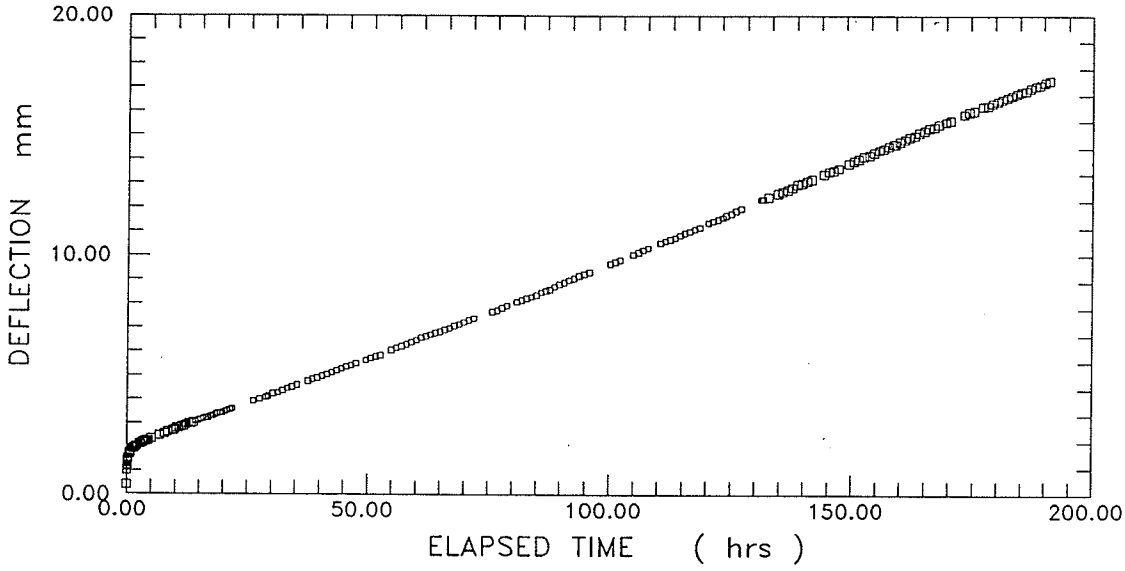


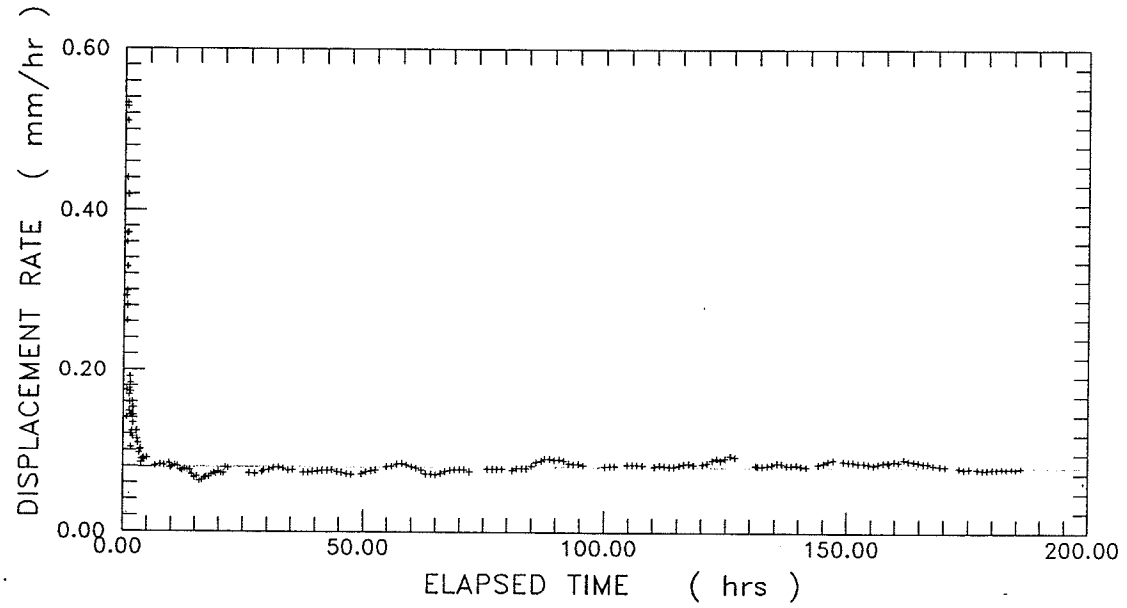


SST 9 Pile displacement rate variation with time

Figure B.11 Single stage Test 9: displacement, and displacement rate versus elapsed time.

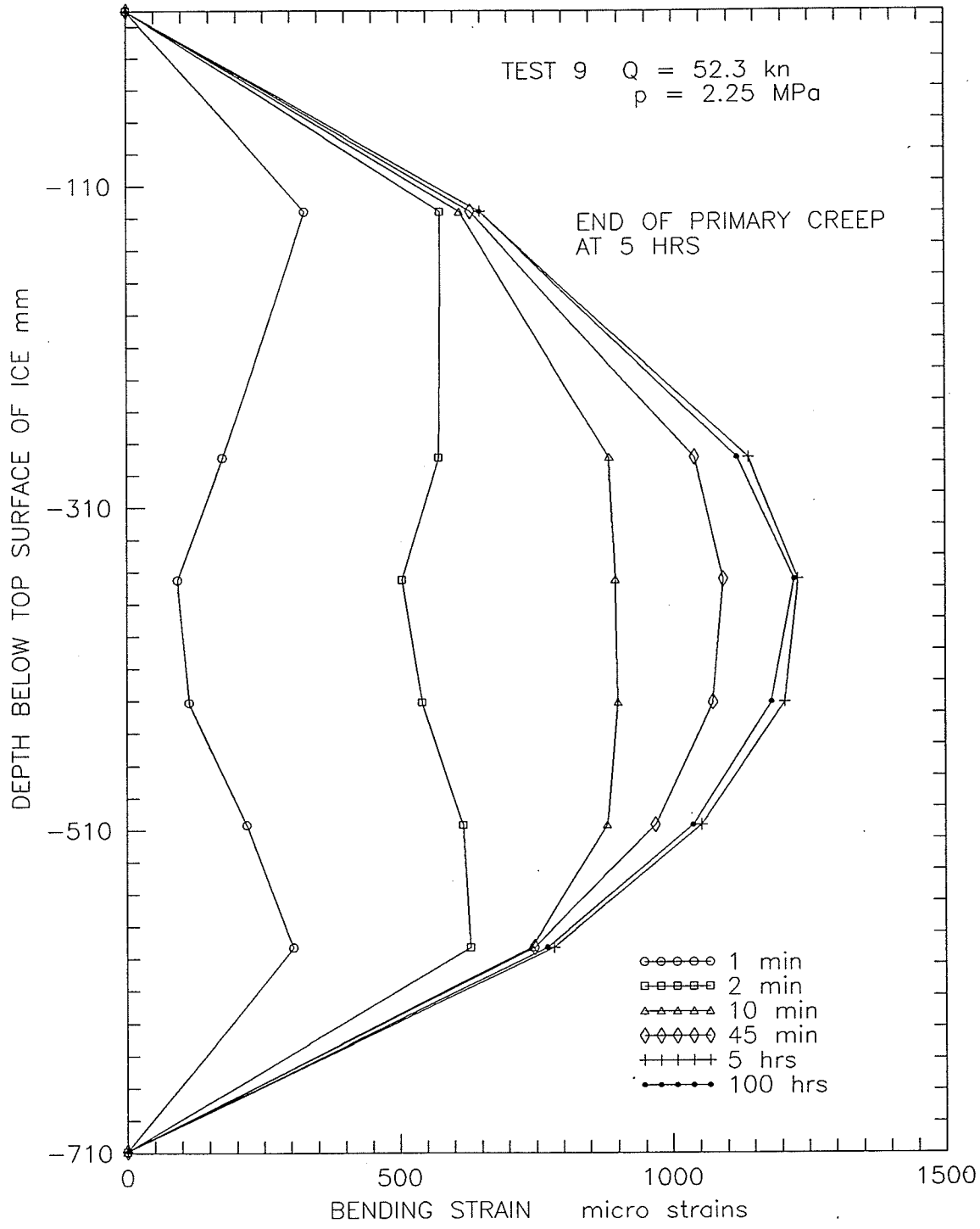


Figure B.12 Single stage Test 9: redistribution of bending strains during Test 9.

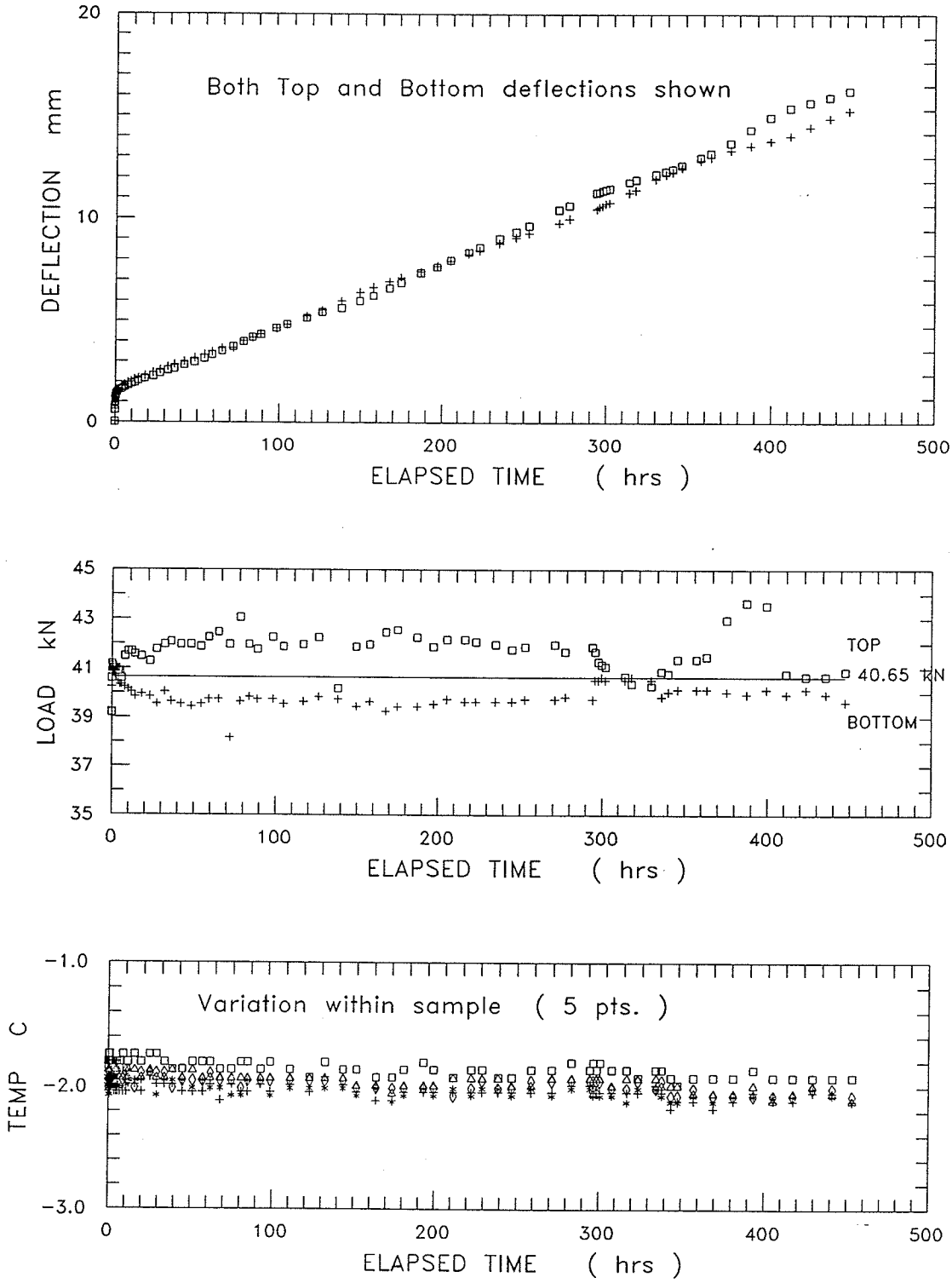


Figure B.13 Single stage Test 10: displacement, load, and sample temperature versus elapsed time.

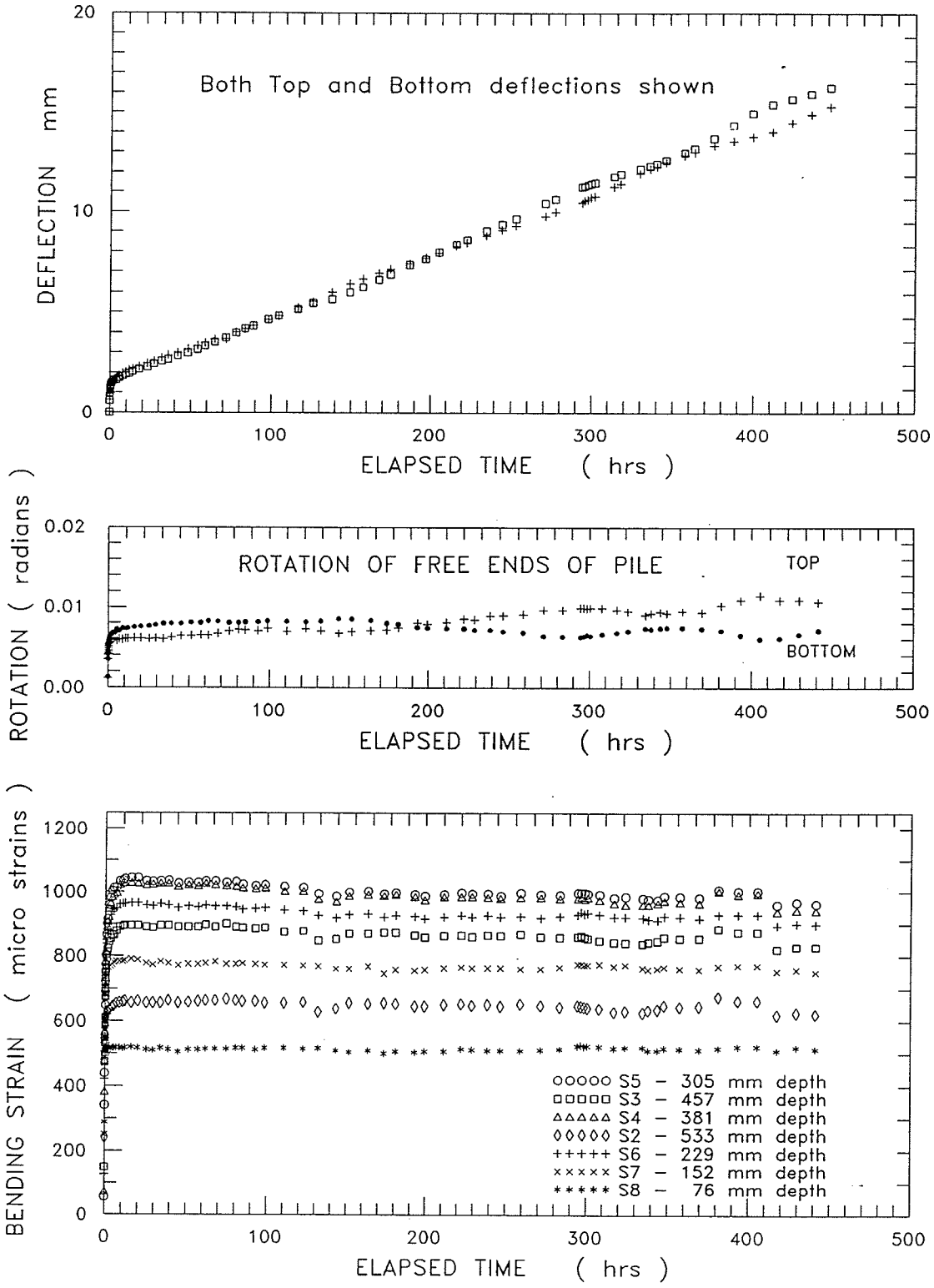


Figure B.14 Single stage Test 10: displacement, rotation of free ends of the bar, and bending strain versus time.

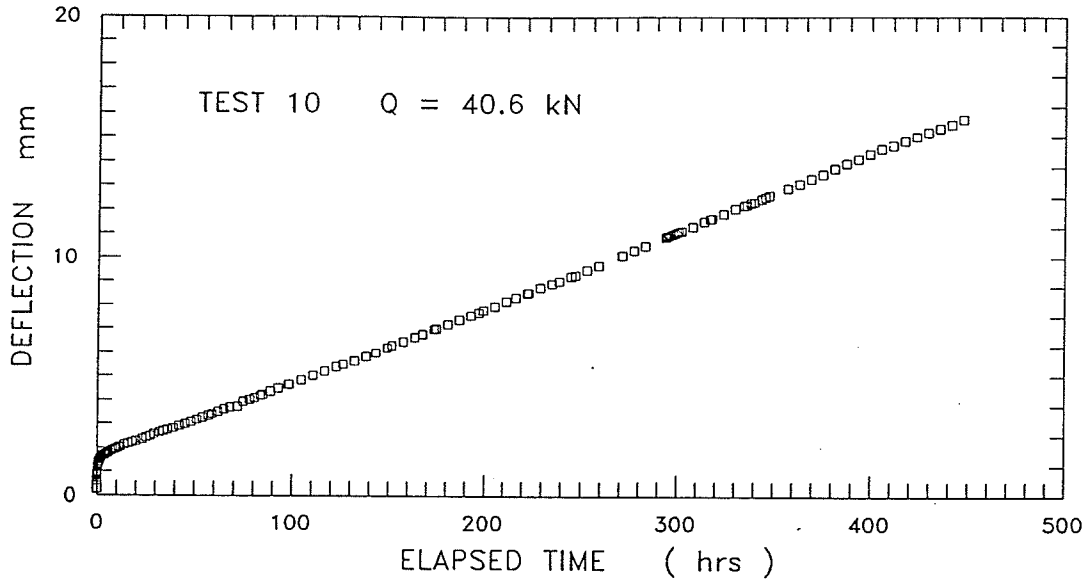


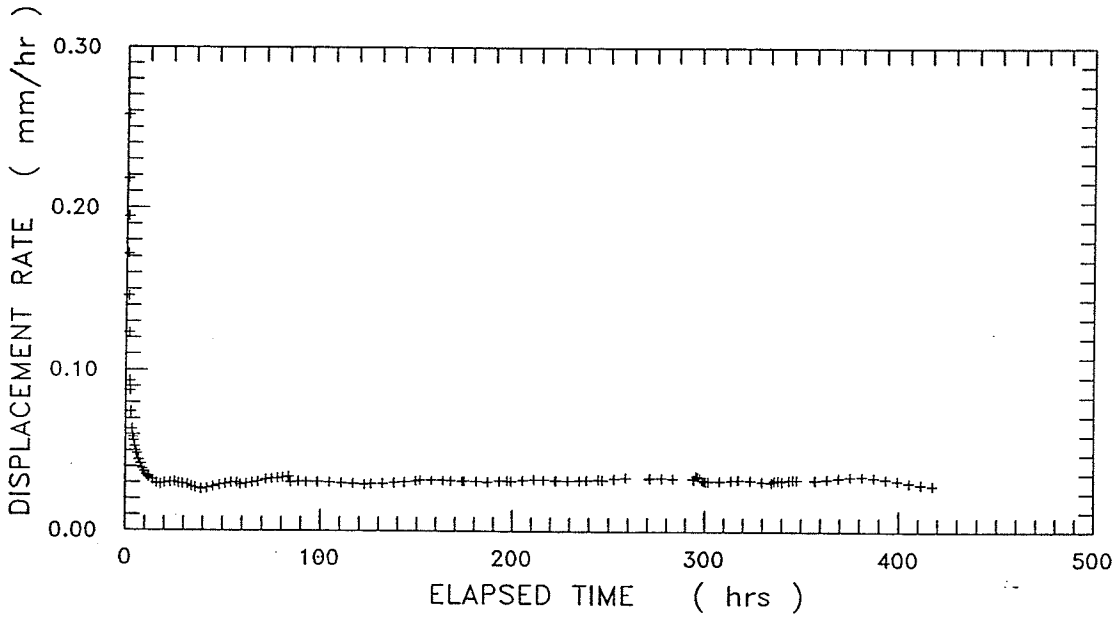


SST 10 Pile displacement rate variation with time

Figure B.15 Single stage Test 10: displacement, and displacement rate versus elapsed time.

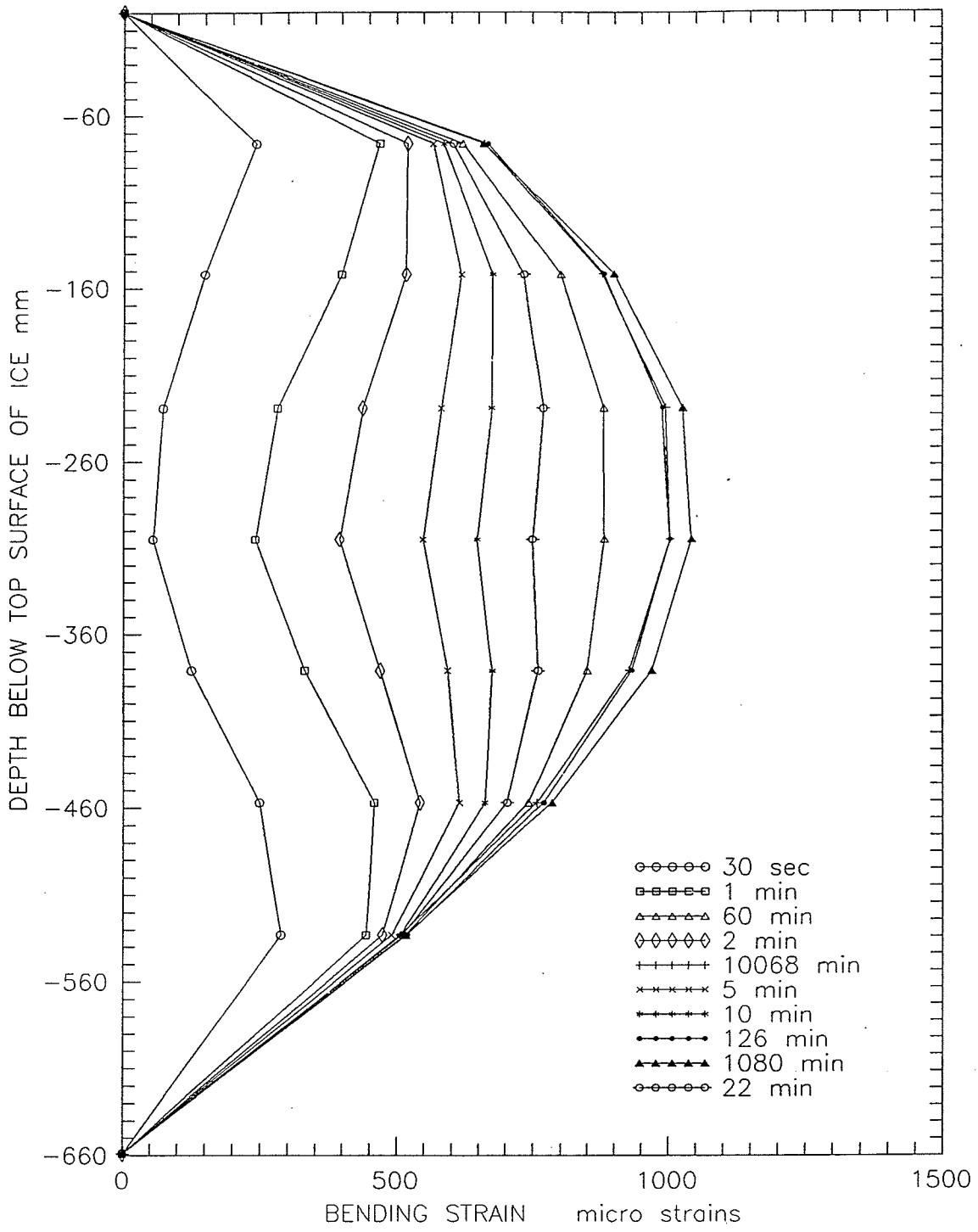


Figure B.16 Single stage Test 10: redistribution of bending strains during Test 10.

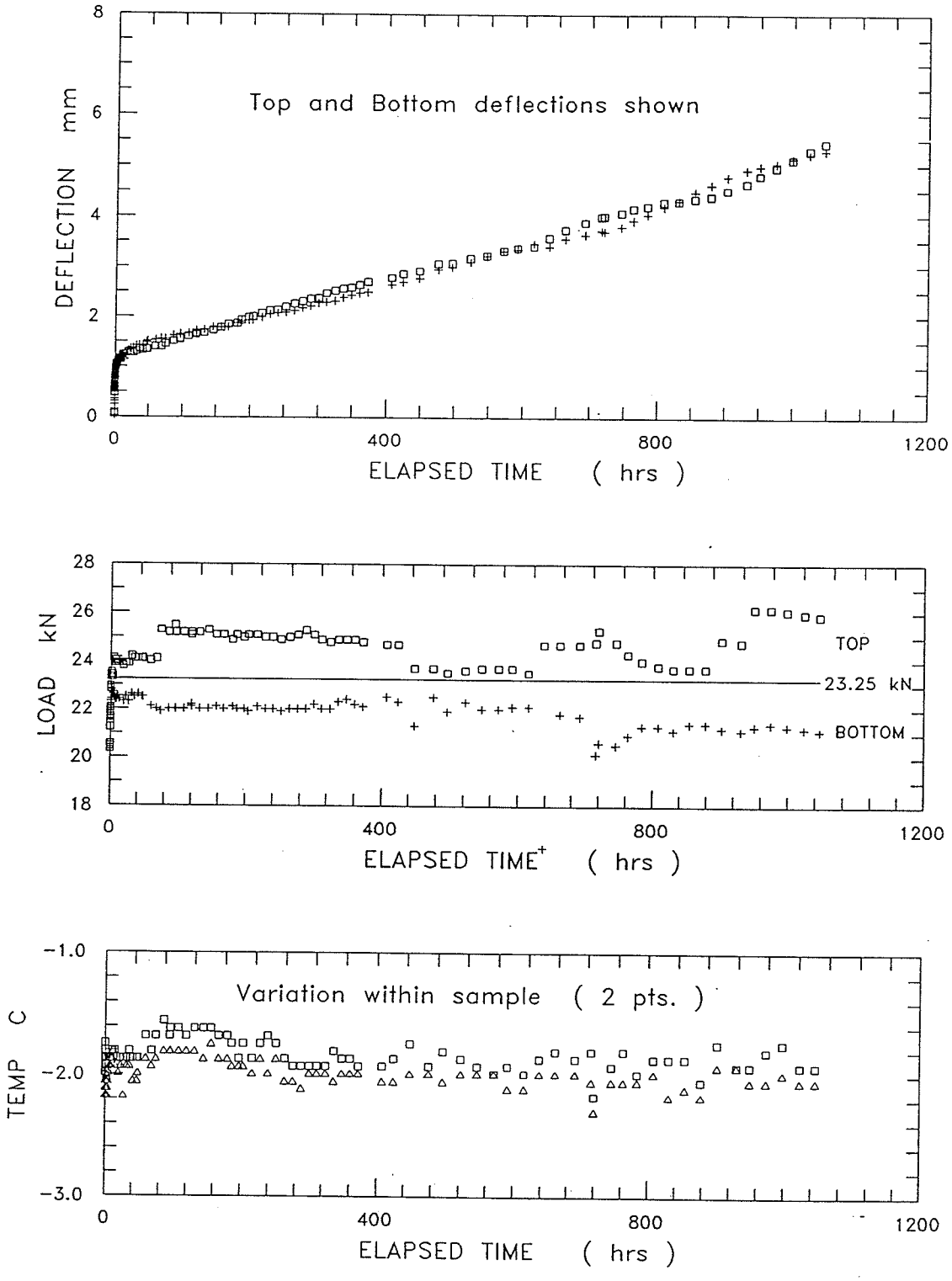


Figure B.17 Single stage Test 11: displacement, load, and sample temperature versus elapsed time.

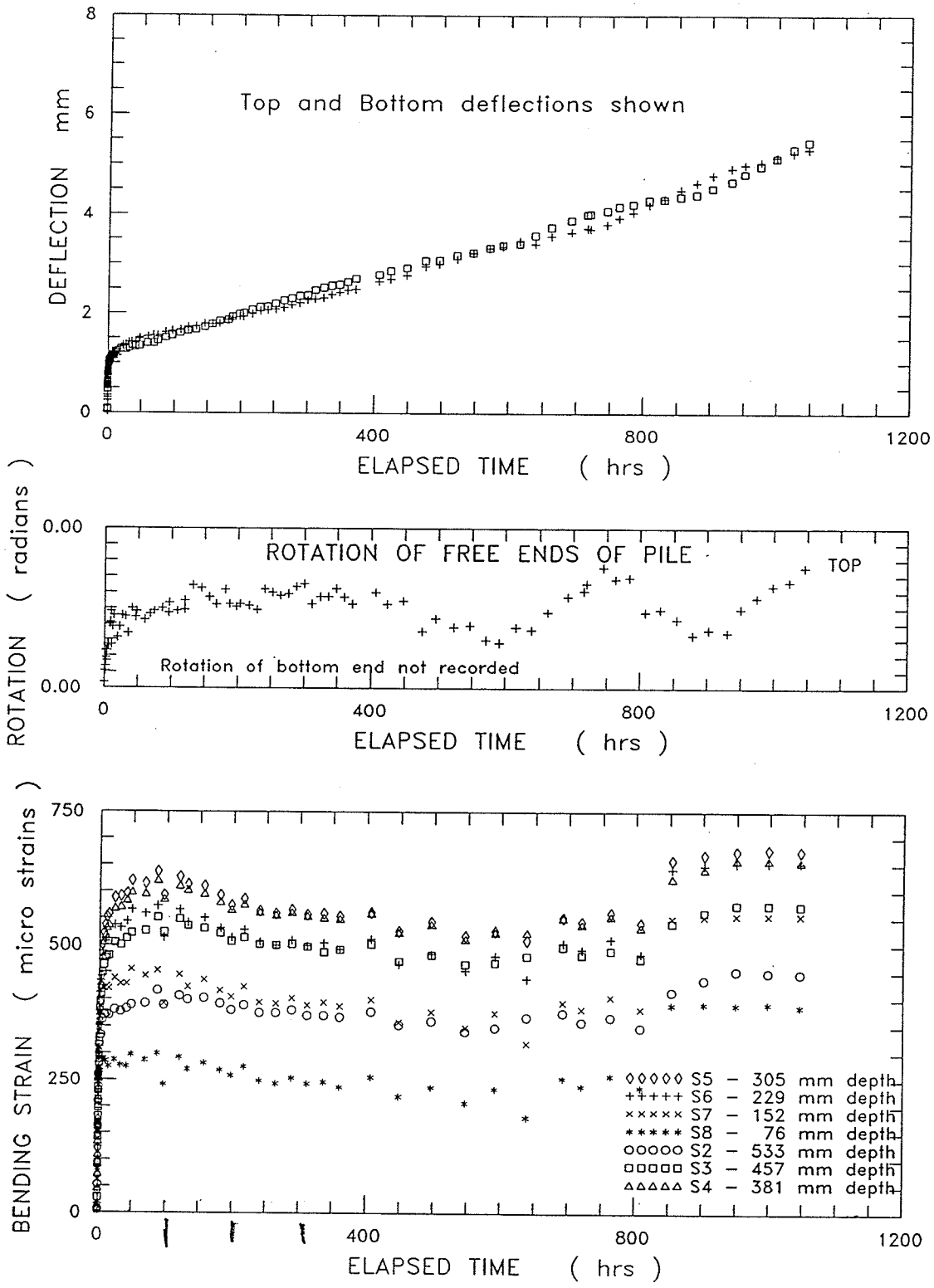


Figure B.18 Single stage Test 11: displacement, rotation of free ends of the bar, and bending strain versus time.

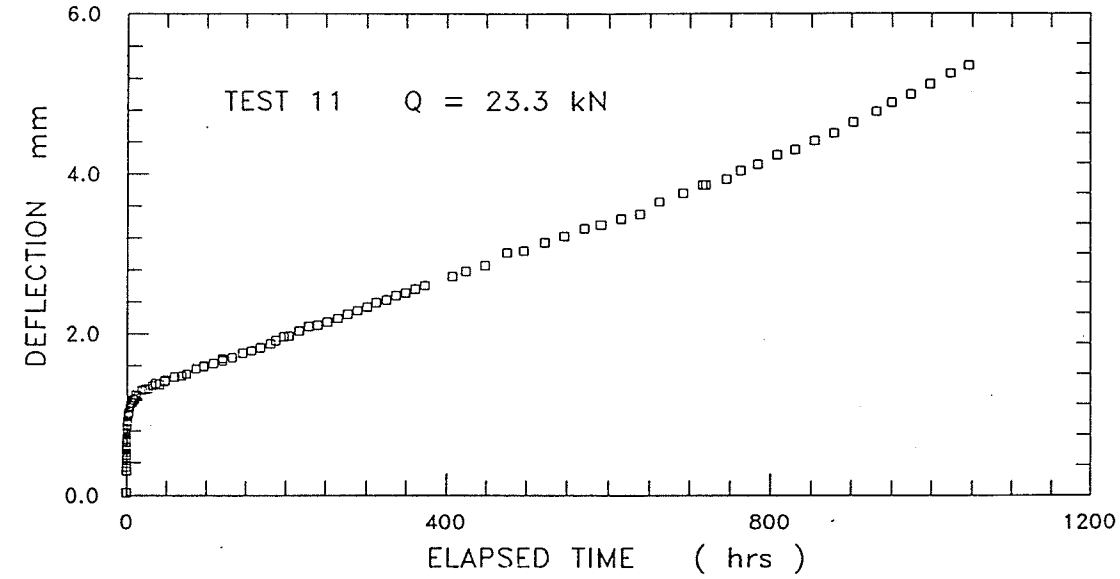


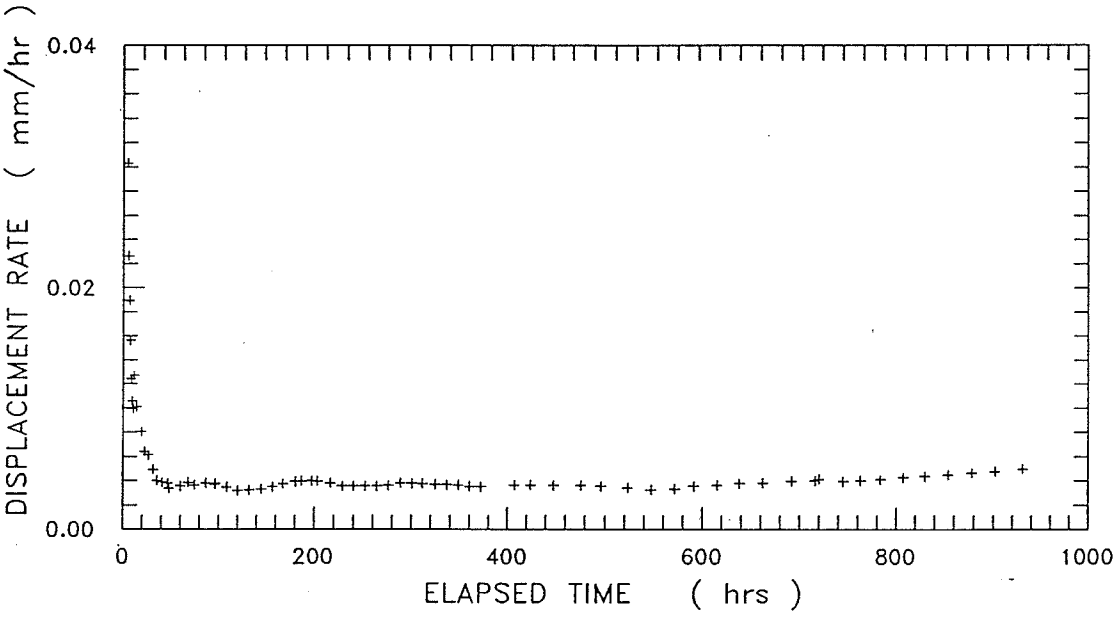


SST 11 Pile displacement rate variation with time

Figure B.19 Single stage Test 11: displacement, and displacement rate versus elapsed time.

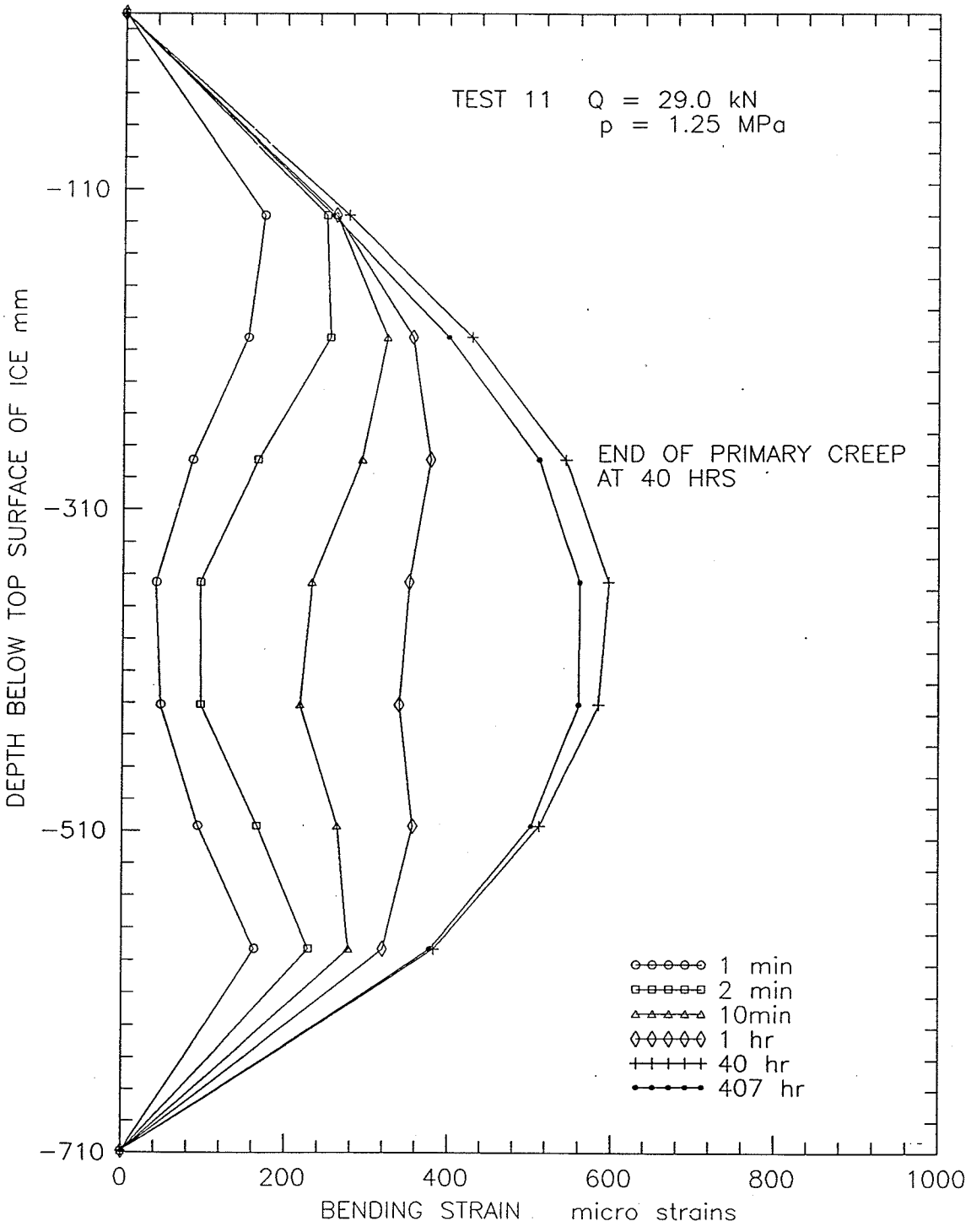


Figure B.20 Single stage Test 11: redistribution of bending strains during Test 10.

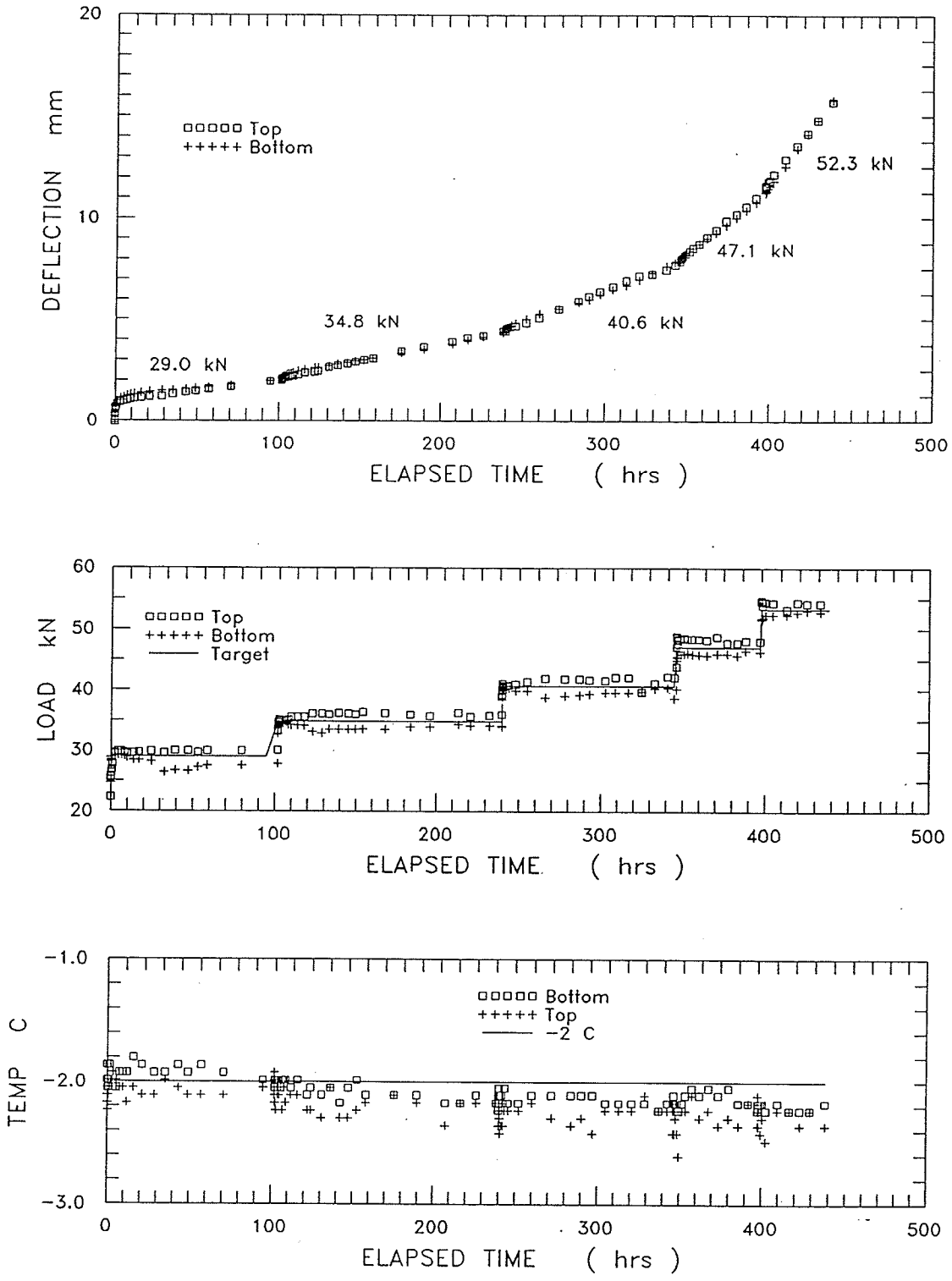


Figure B.21 Multi-stage Test 12: displacement, load, and sample temperature versus elapsed time.

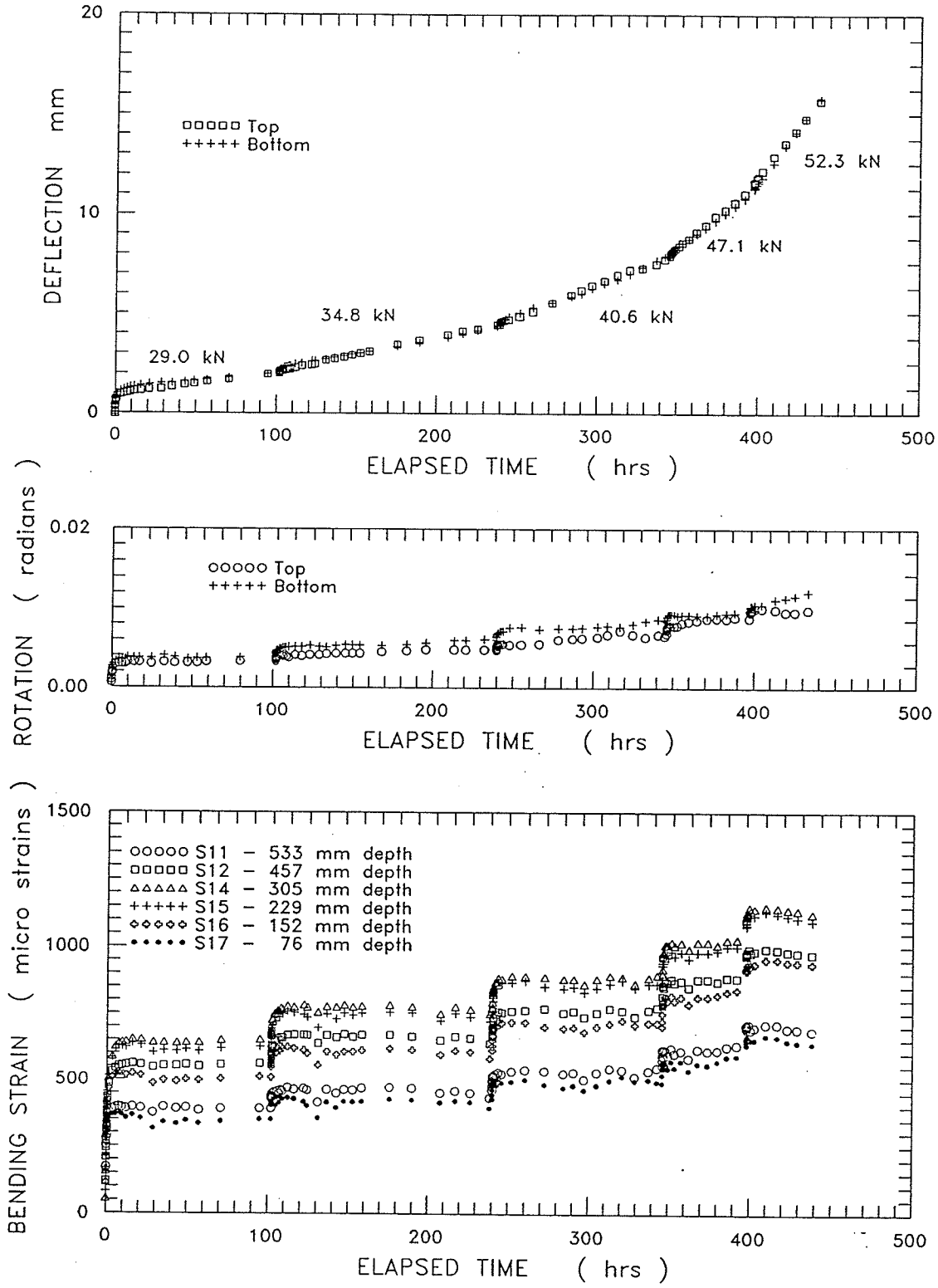


Figure B.22 Multi-stage Test 12: displacement, rotation of free ends of the bar, and bending strain versus time.

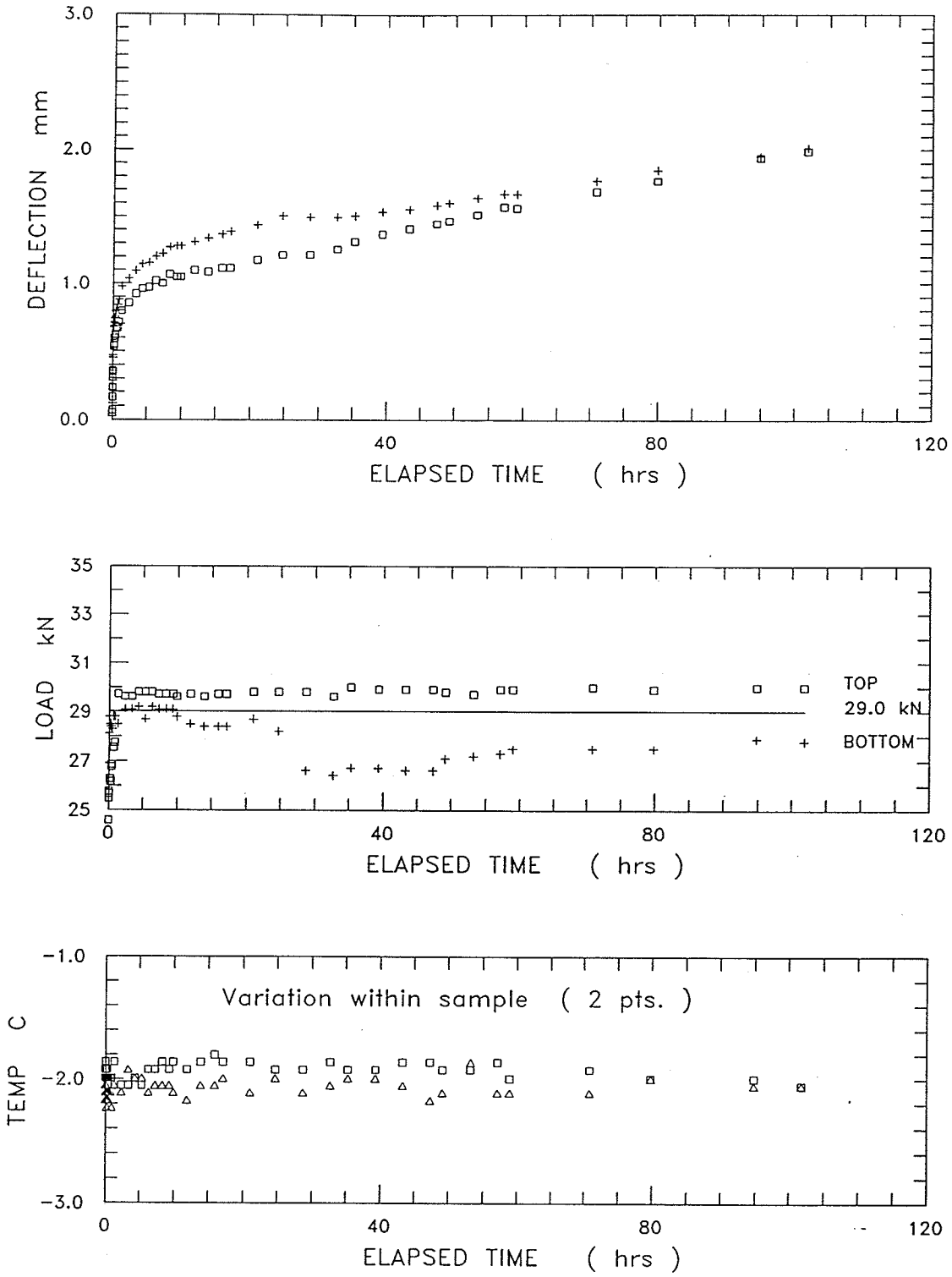


Figure B.23 Multi-stage Test 12, Stage 1: displacement, load, and sample temperature versus elapsed time.

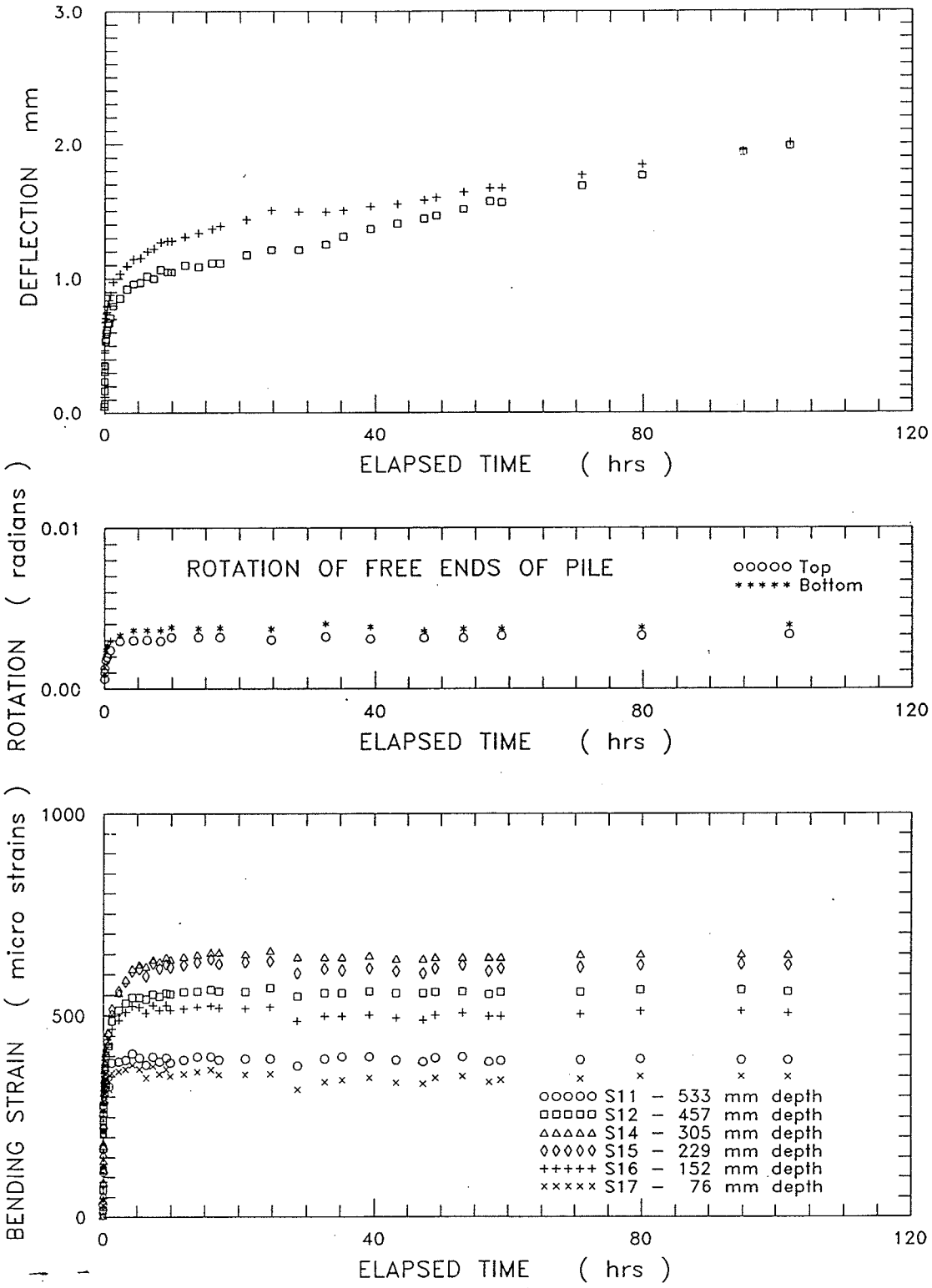


Figure B.24 Multi-stage Test 12, Stage 1: displacement, rotation of free ends of the bar, and bending strain versus time.

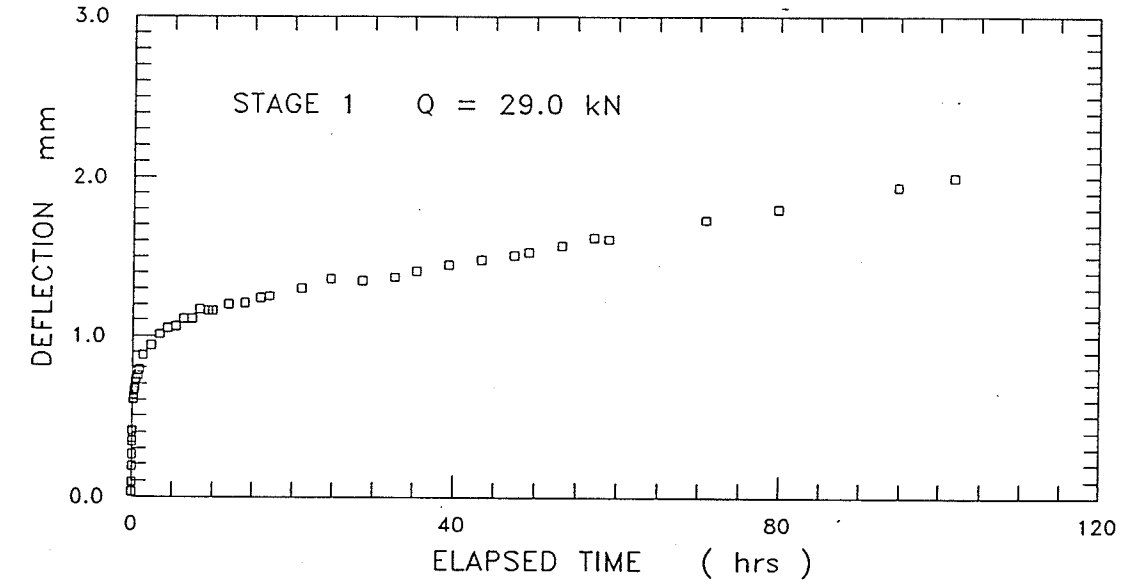


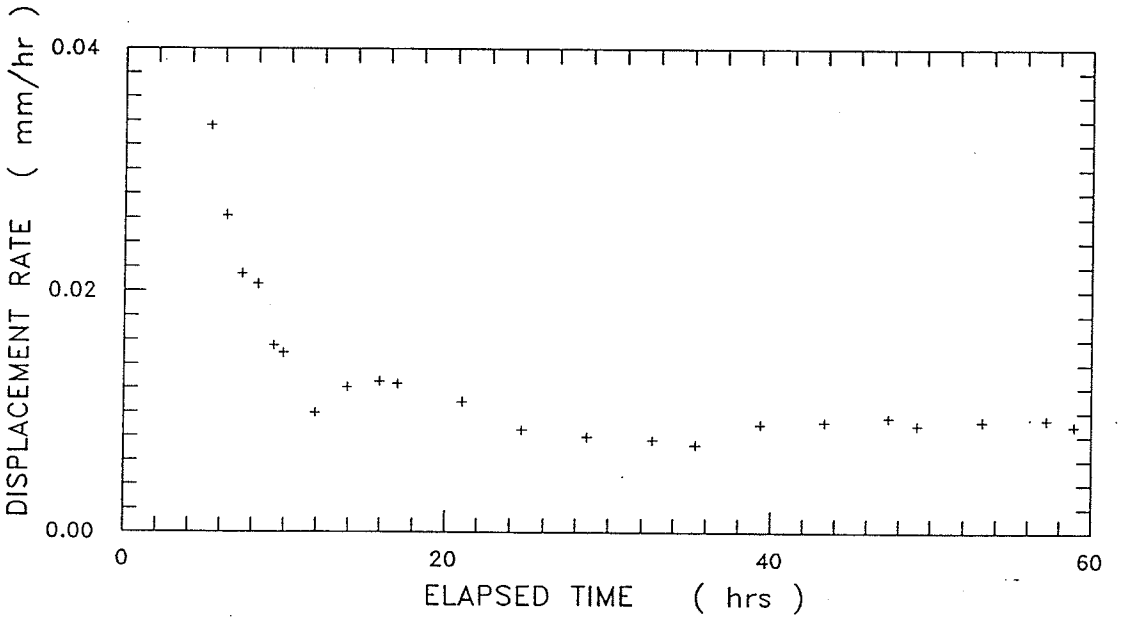


Figure B.25 Multi-stage Test 12, Stage 1: displacement, and displacement rate versus elapsed time.

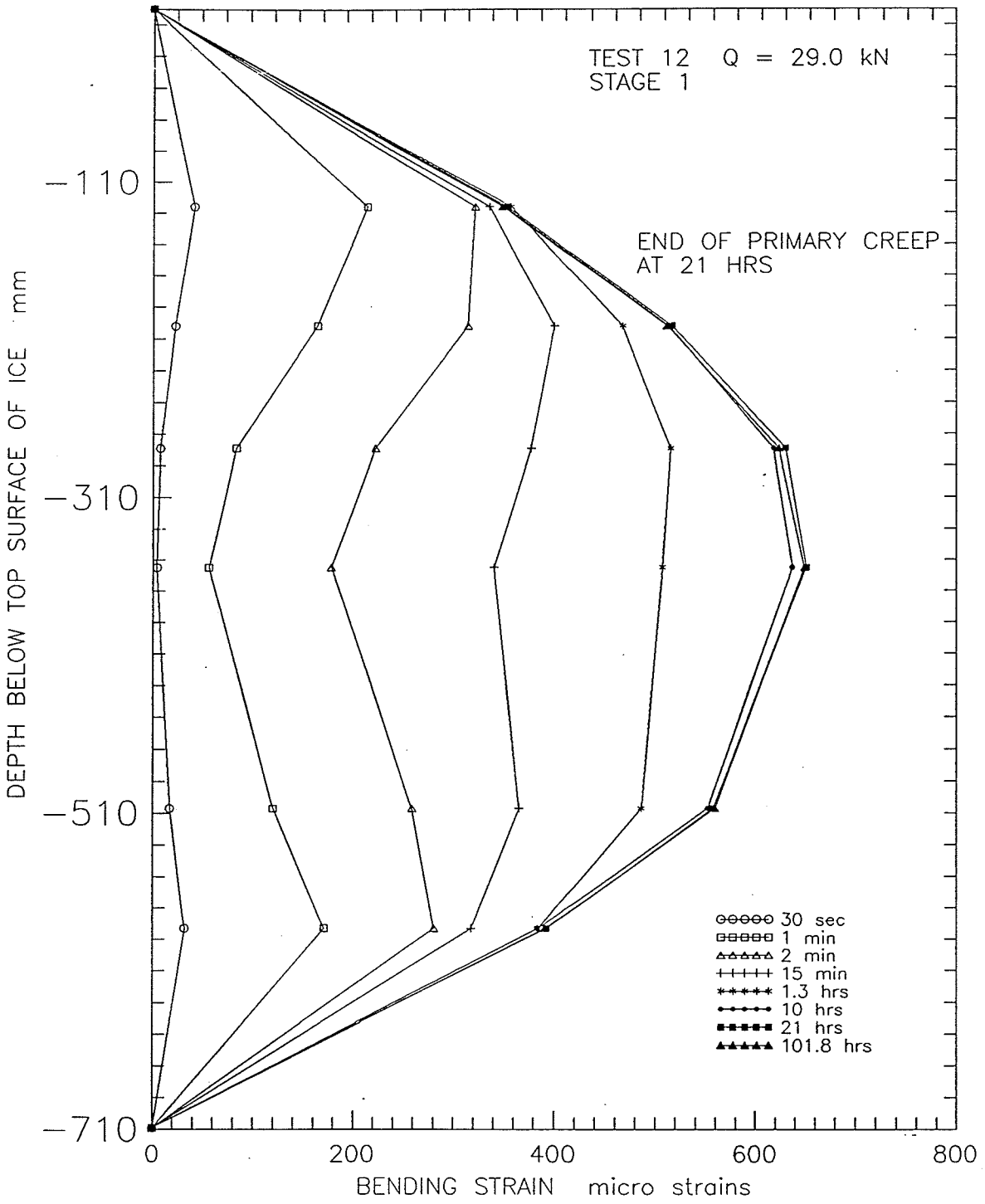


Figure B.26 Multi-stage Test 12, Stage 1: redistribution of bending strains during Stage 1.

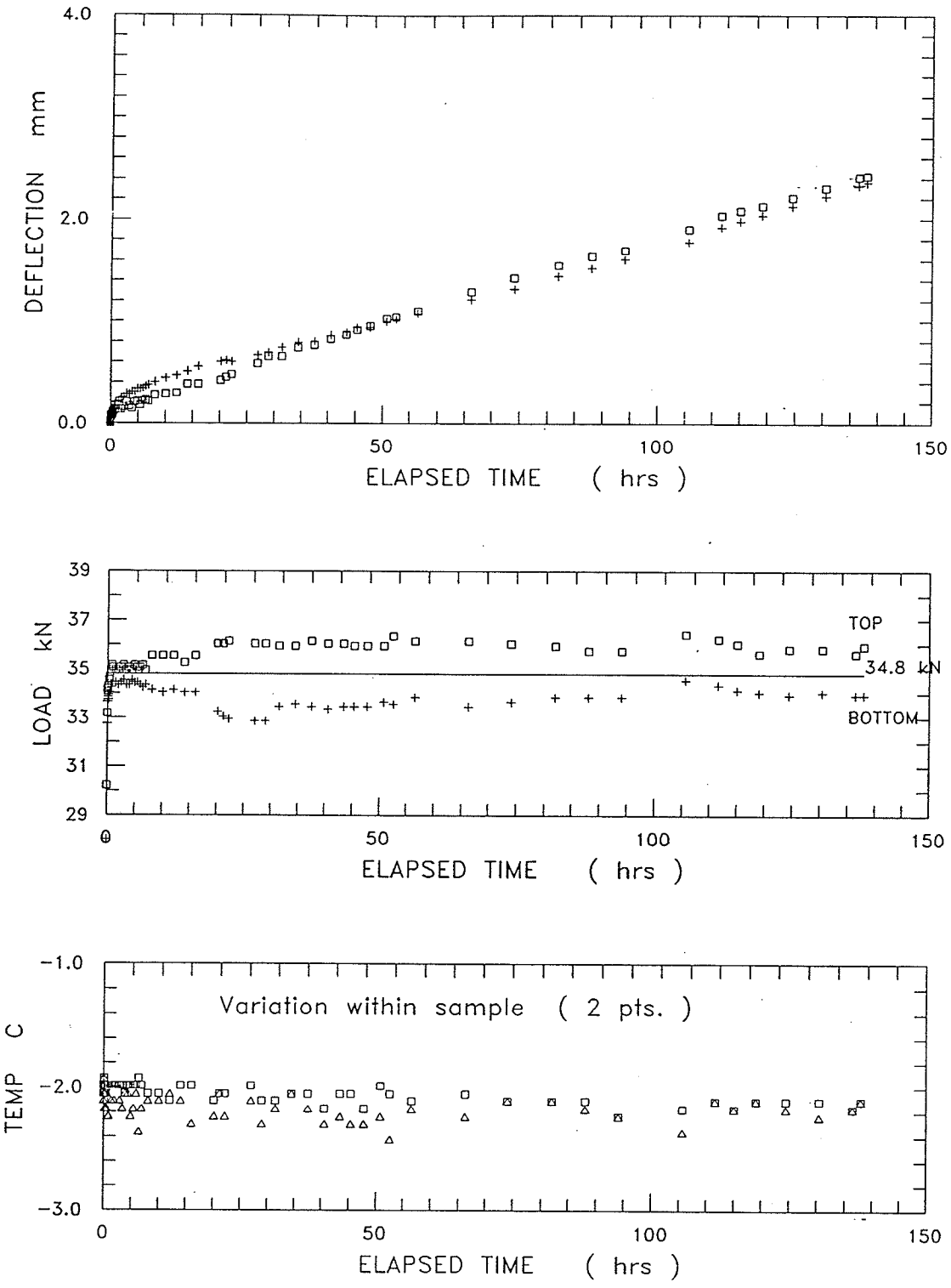


Figure B.27 Multi-stage Test 12, Stage 2: displacement, load, and sample temperature versus elapsed time.

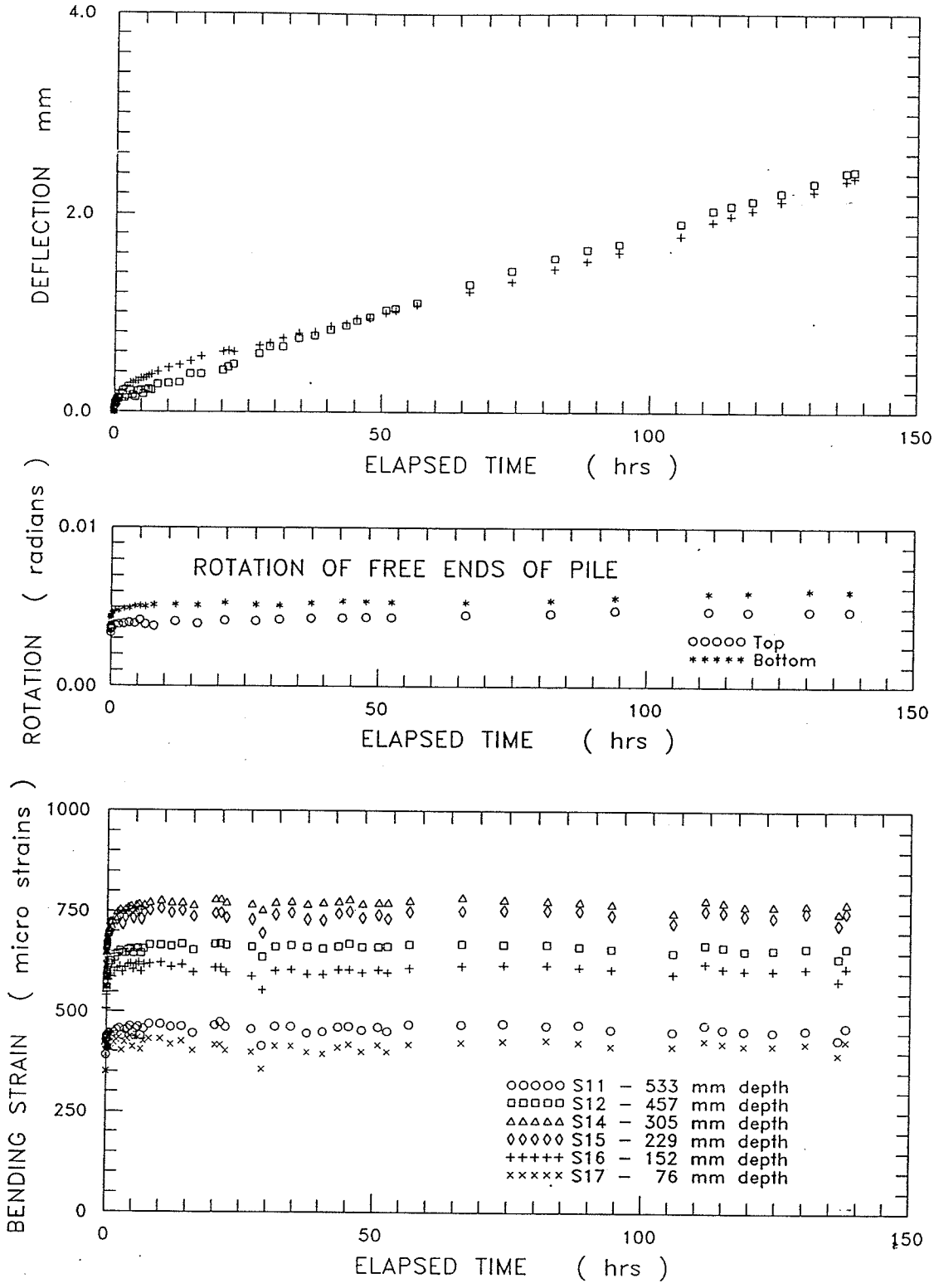


Figure B.28 Multi-stage Test 12, Stage 2: displacement, rotation of free ends of the bar, and bending strain versus time.

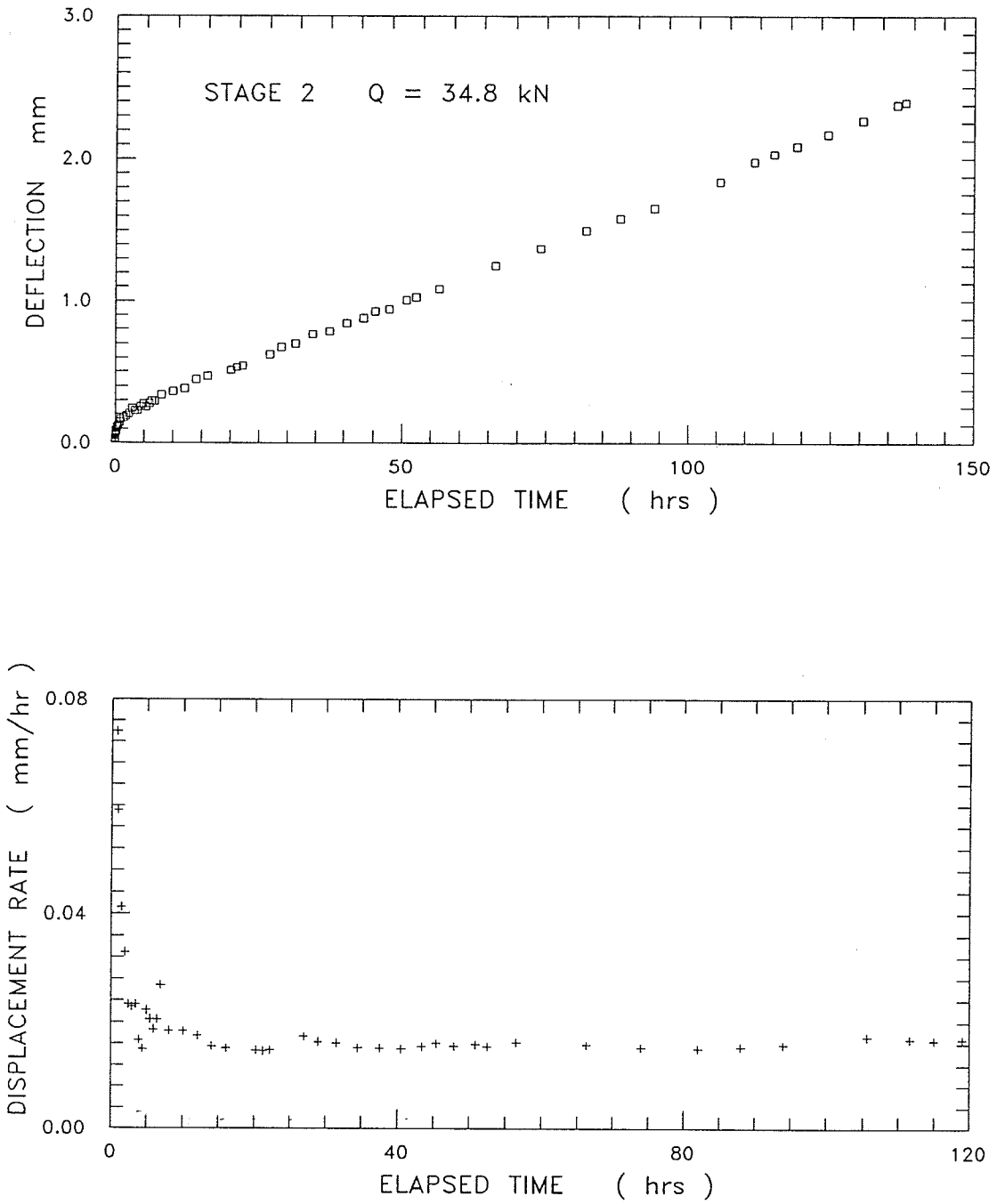


Figure B.29 Multi-stage Test 12, Stage 2: displacement, and displacement rate versus elapsed time.

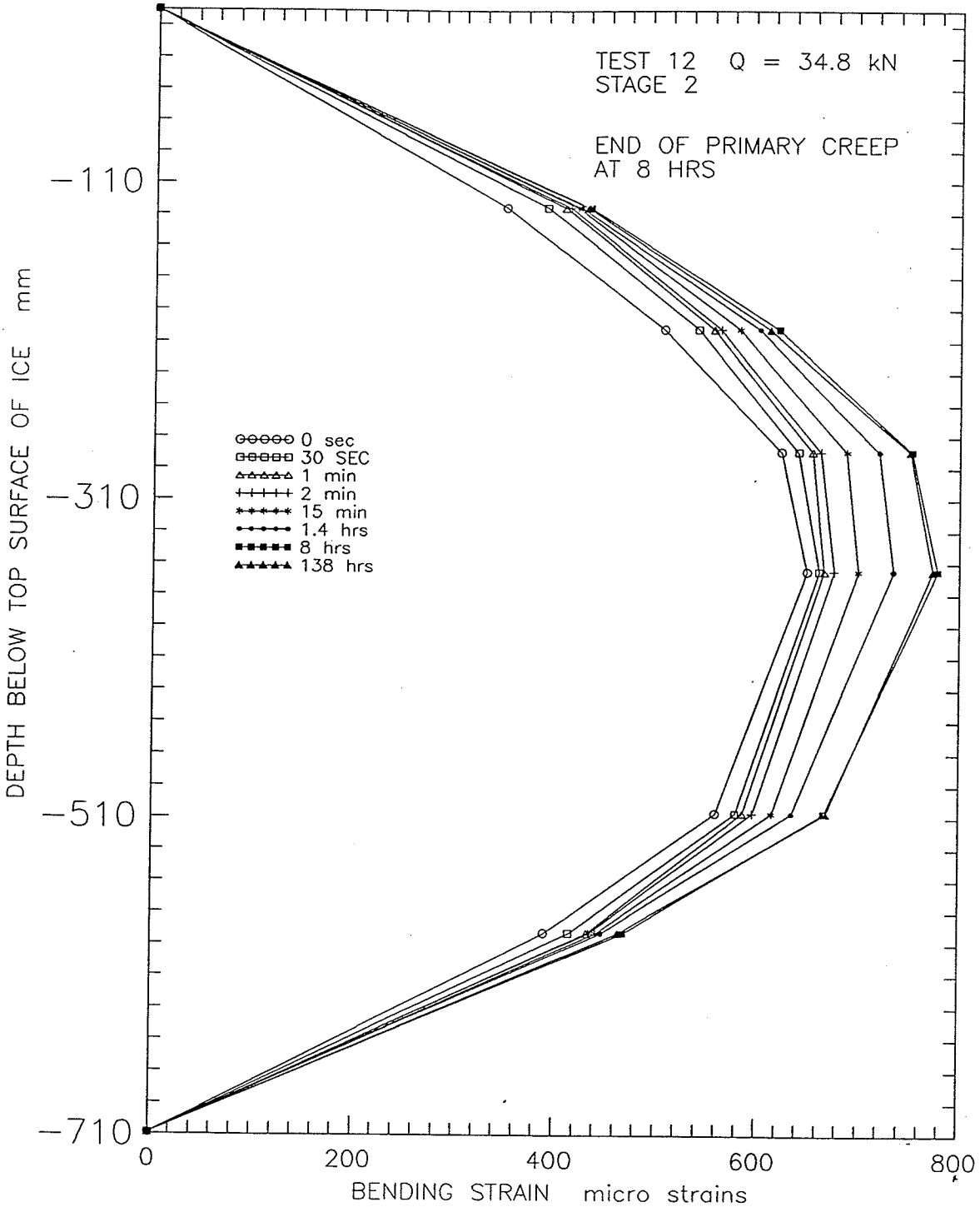


Figure B.30 Multi-stage Test 12, Stage 2: redistribution of bending strains during Stage 2.

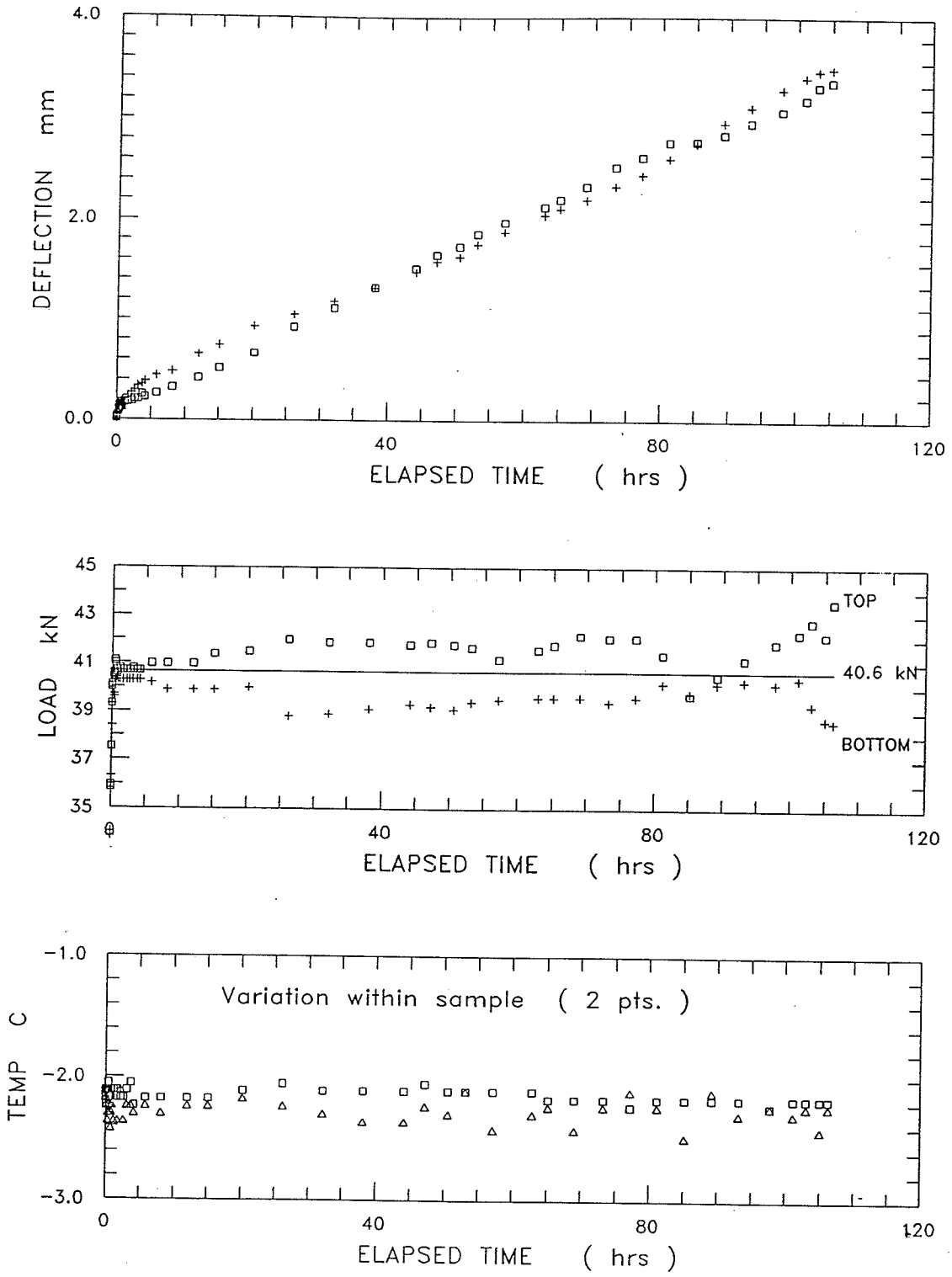


Figure B.31 Multi-stage Test 12, Stage 3: displacement, load, and sample temperature versus elapsed time.

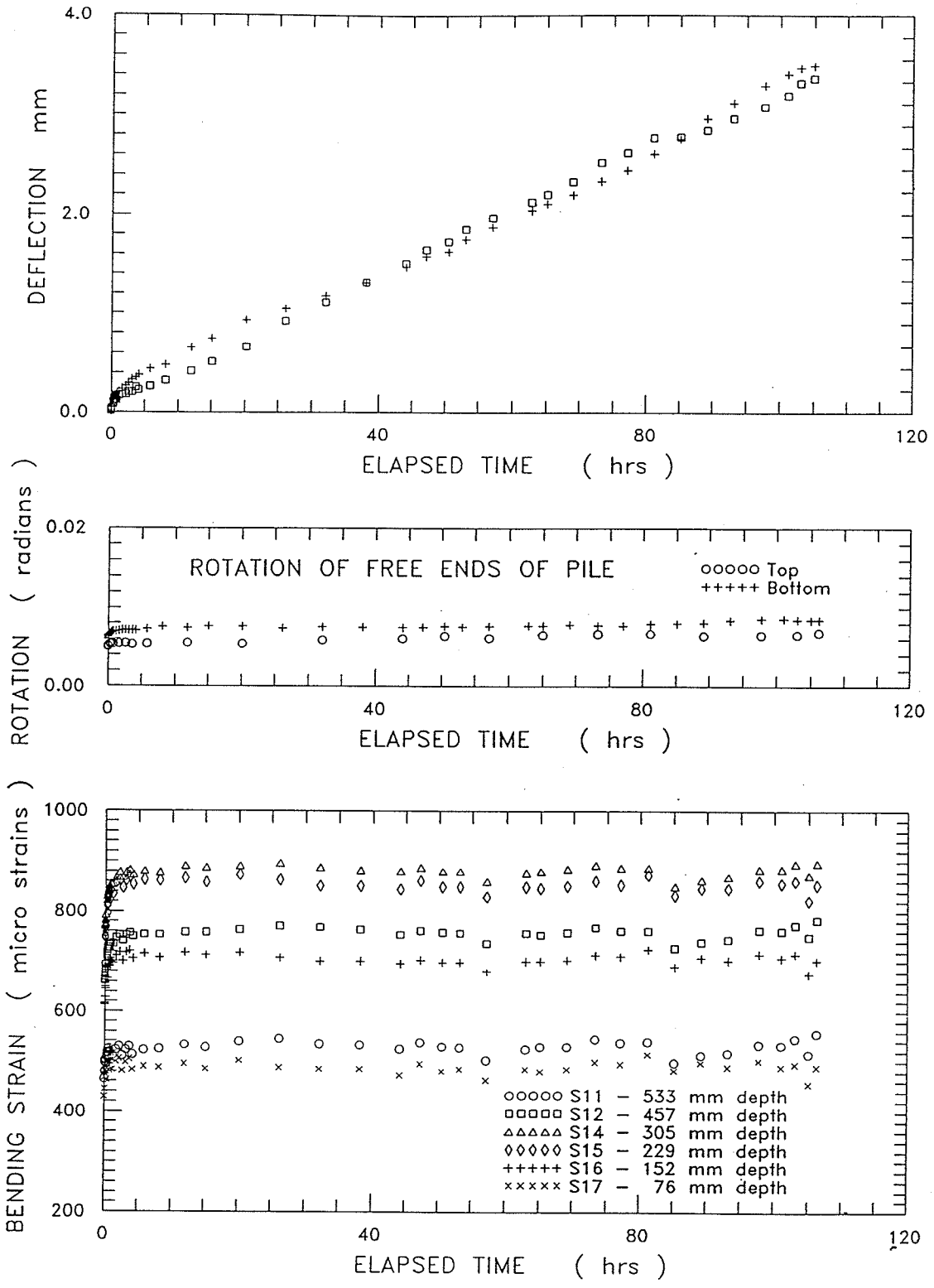


Figure B.32 Multi-stage Test 12, Stage 3: displacement, rotation of free ends of the bar, and bending strain versus time.

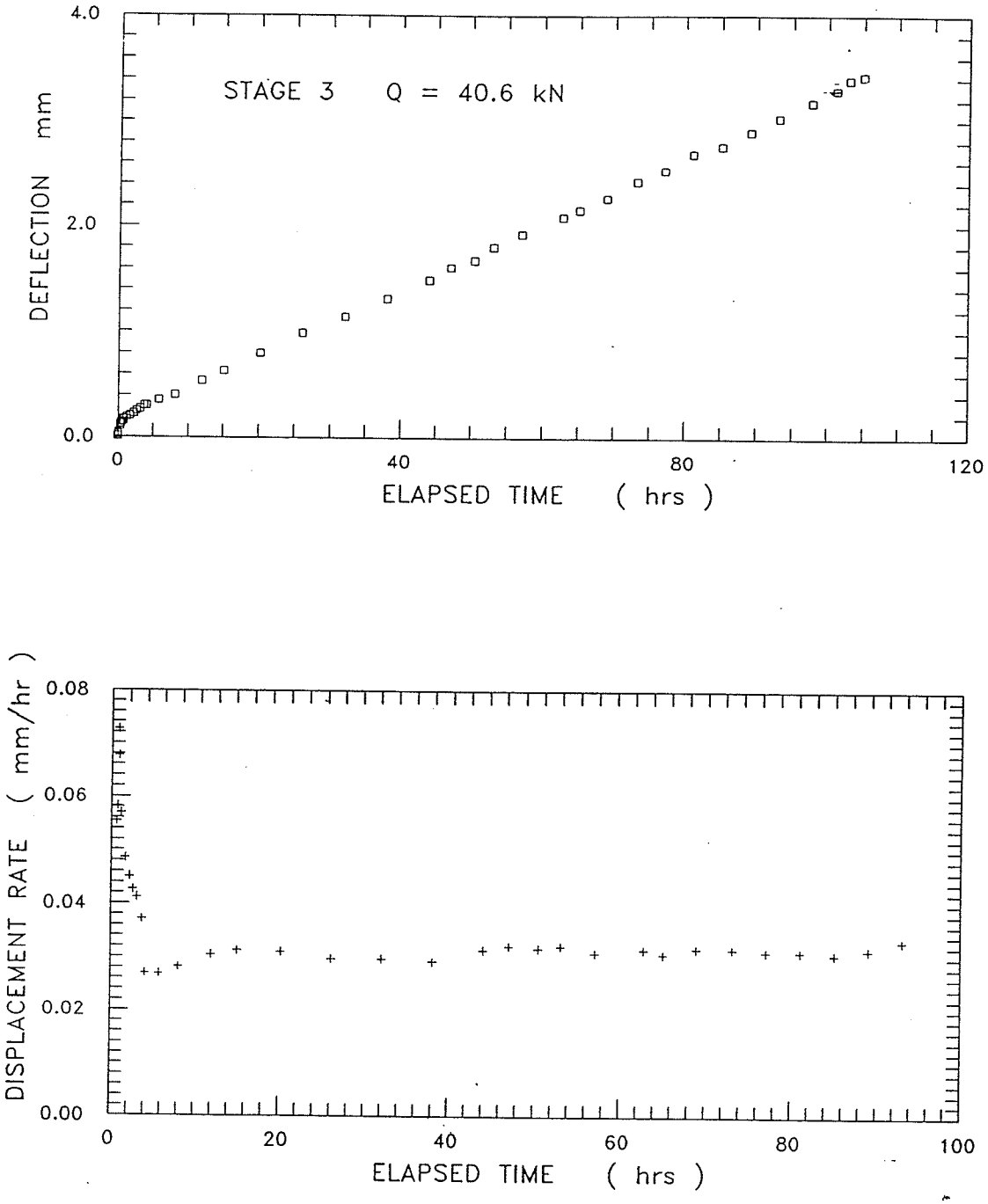


Figure B.33 Multi-stage Test 12, Stage 3: displacement, and displacement rate versus elapsed time.

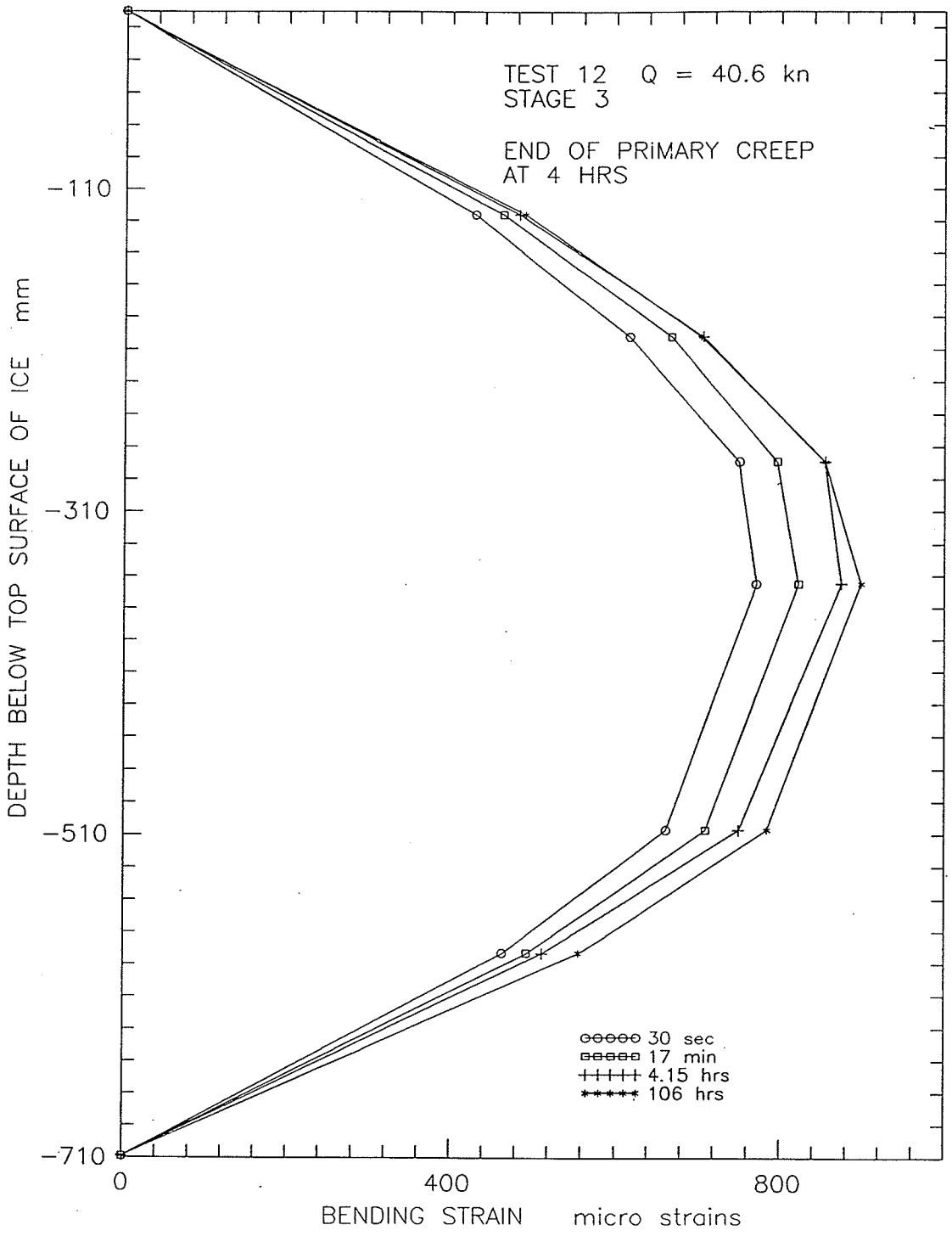


Figure B.34 Multi-stage Test 12, Stage 3: redistribution of bending strains during Stage 3.

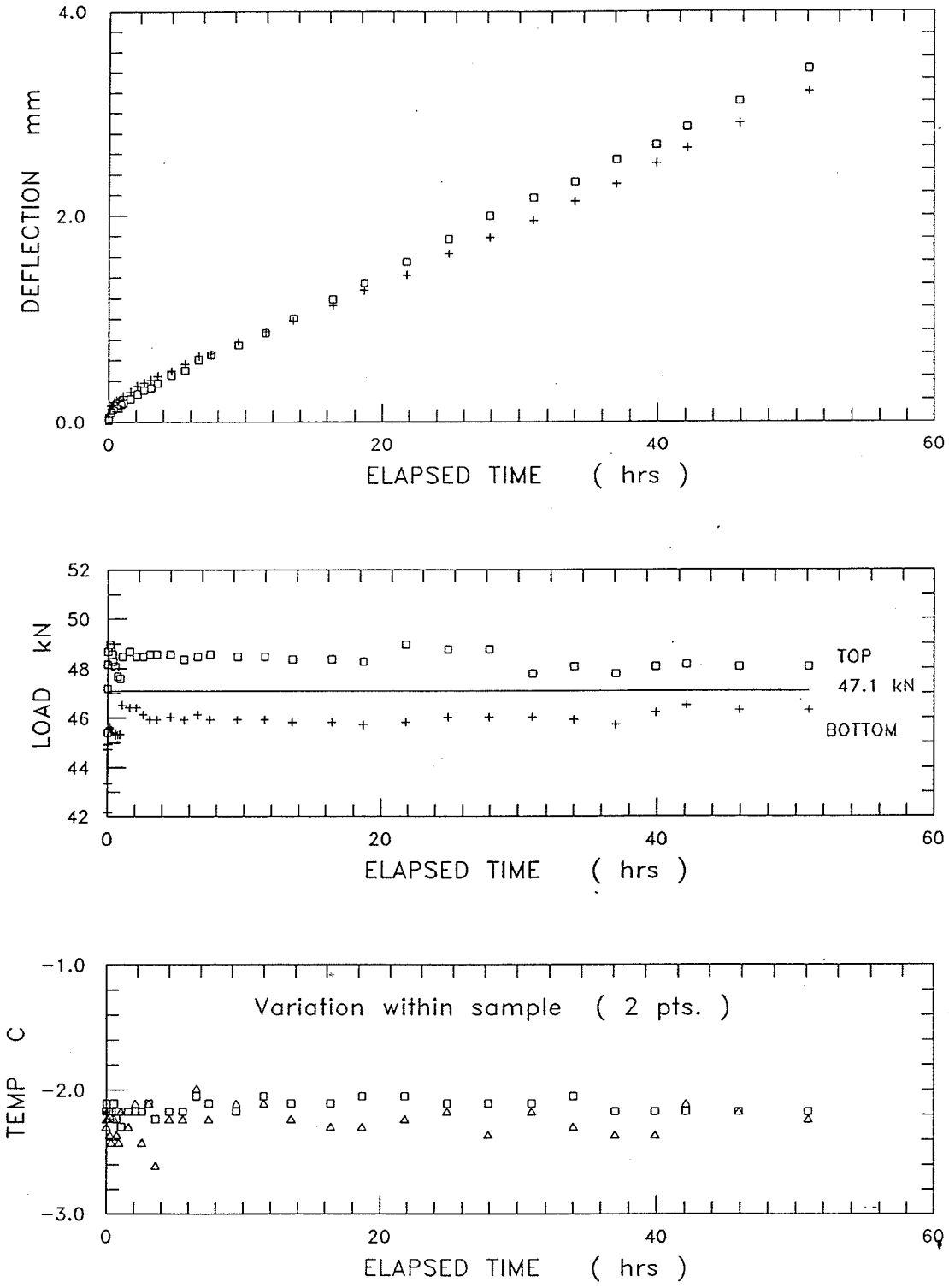


Figure B.35 Multi-stage Test 12, Stage 4: displacement, load, and sample temperature versus elapsed time.

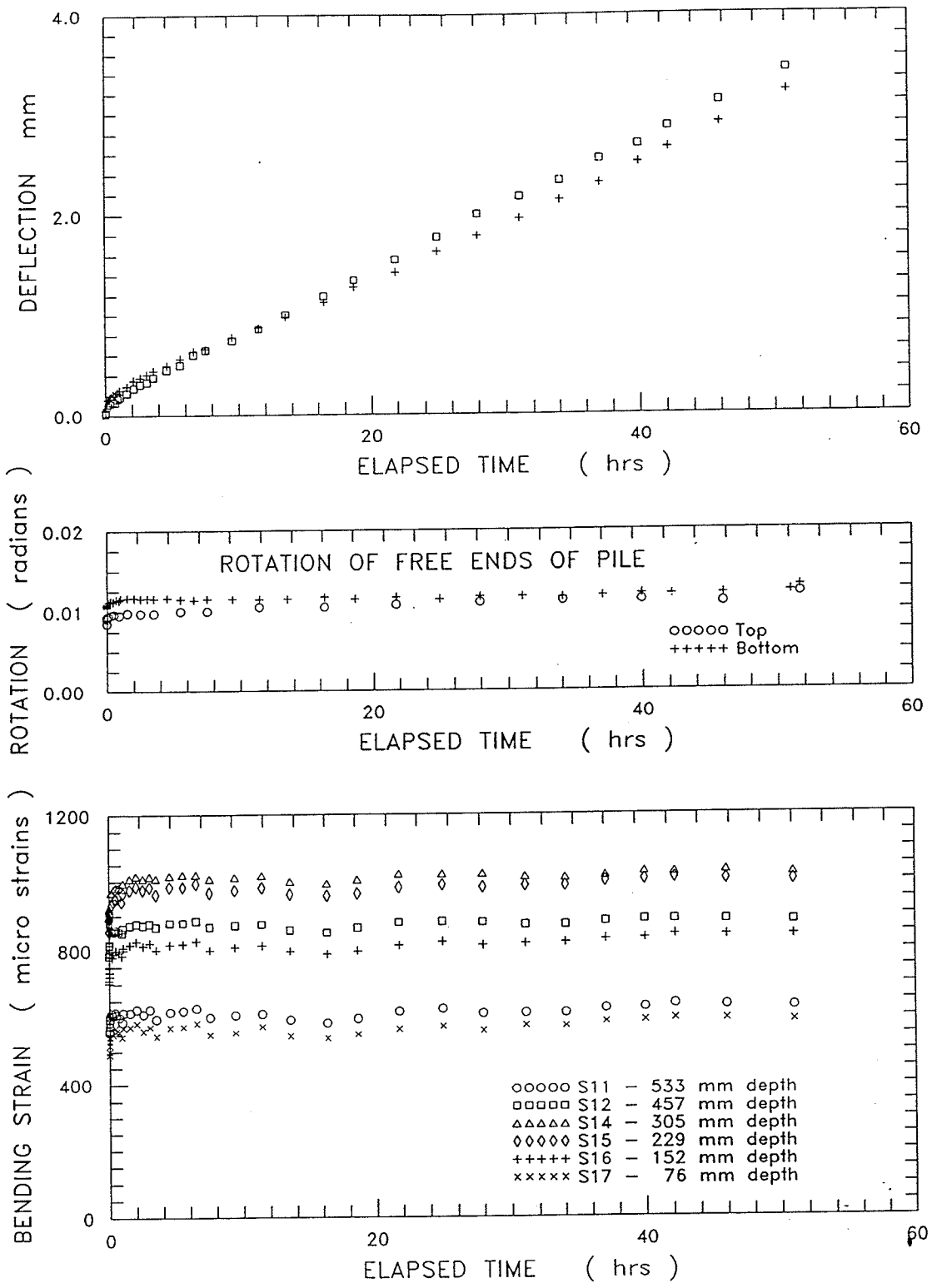


Figure B.36 Multi-stage Test 12, Stage 4: displacement, rotation of free ends of the bar, and bending strain versus time.

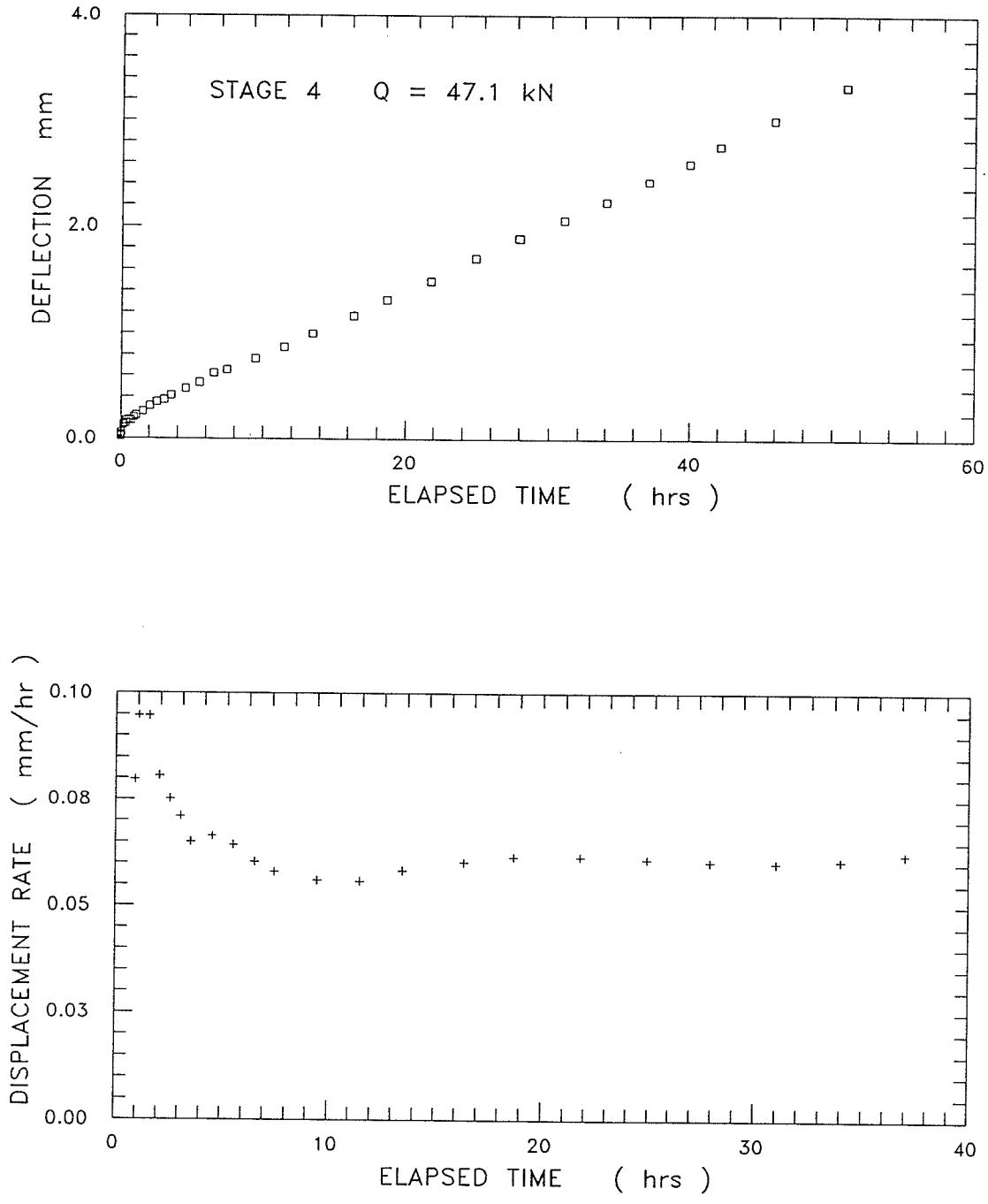


Figure B.37 Multi-stage Test 12, Stage 4: displacement, and displacement rate versus elapsed time.

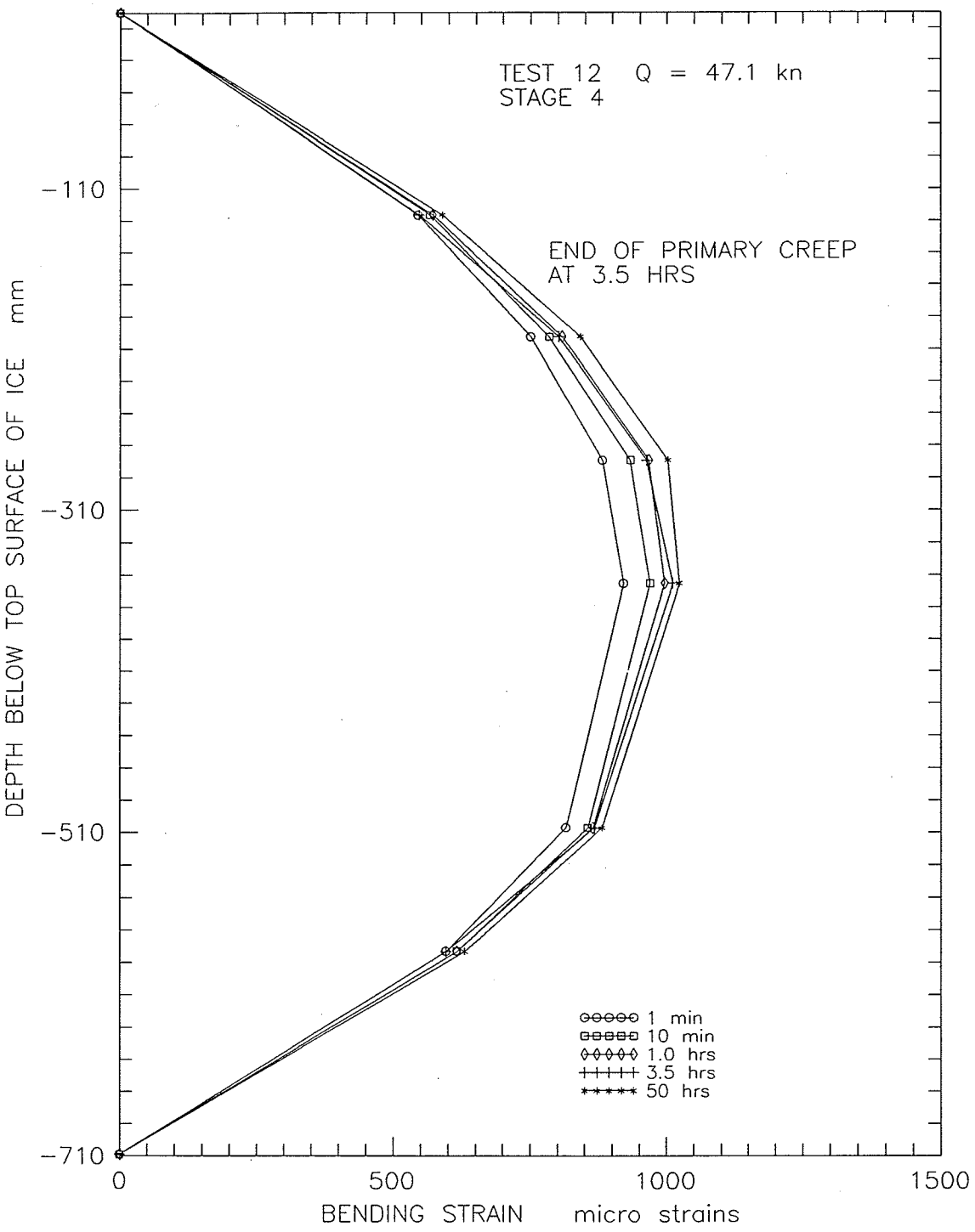


Figure B.38 Multi-stage Test 12, Stage 4: redistribution of bending strains during Stage 4.

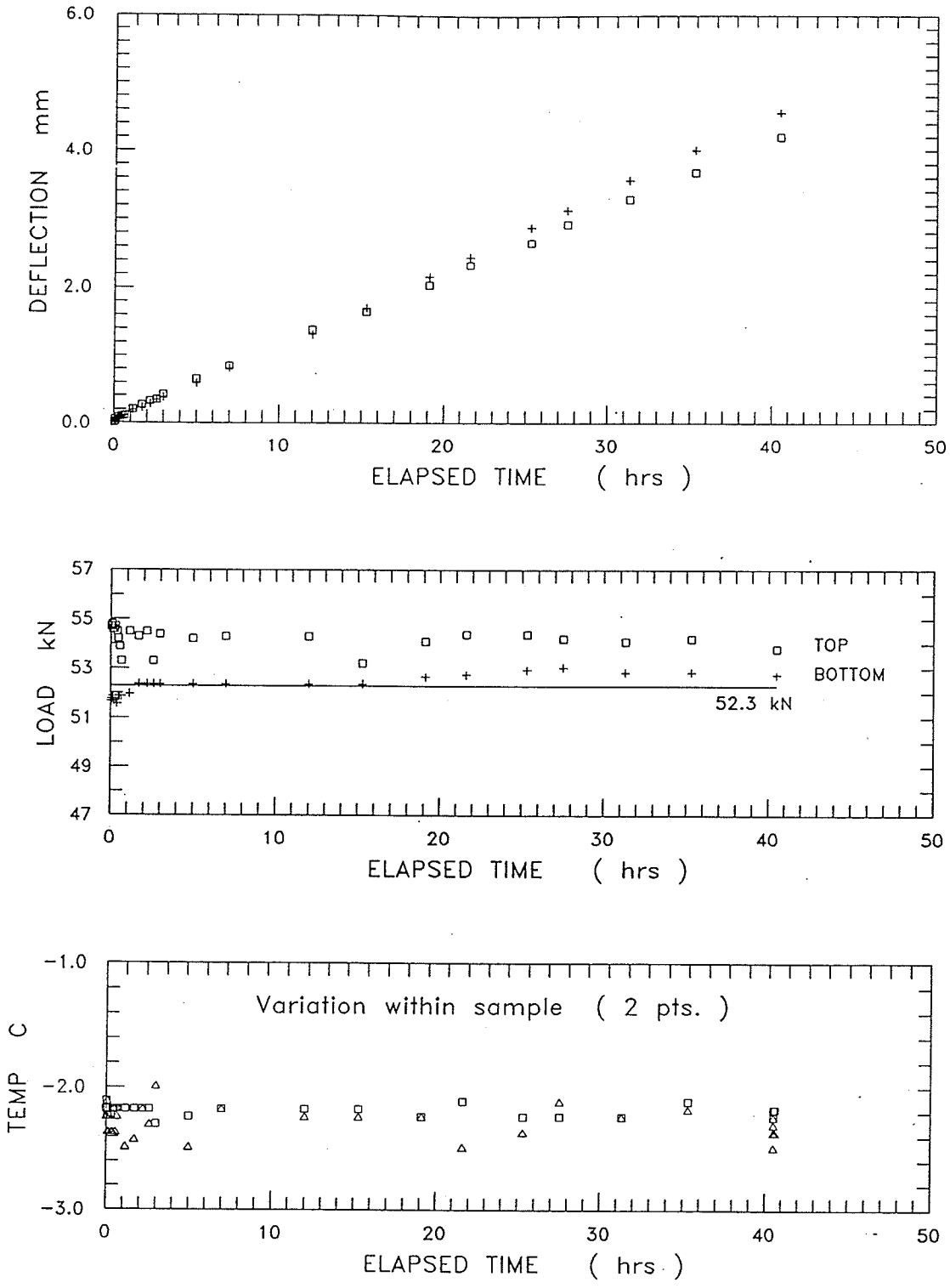


Figure B.39 Multi-stage Test 12, Stage 5: displacement, load, and sample temperature versus elapsed time.

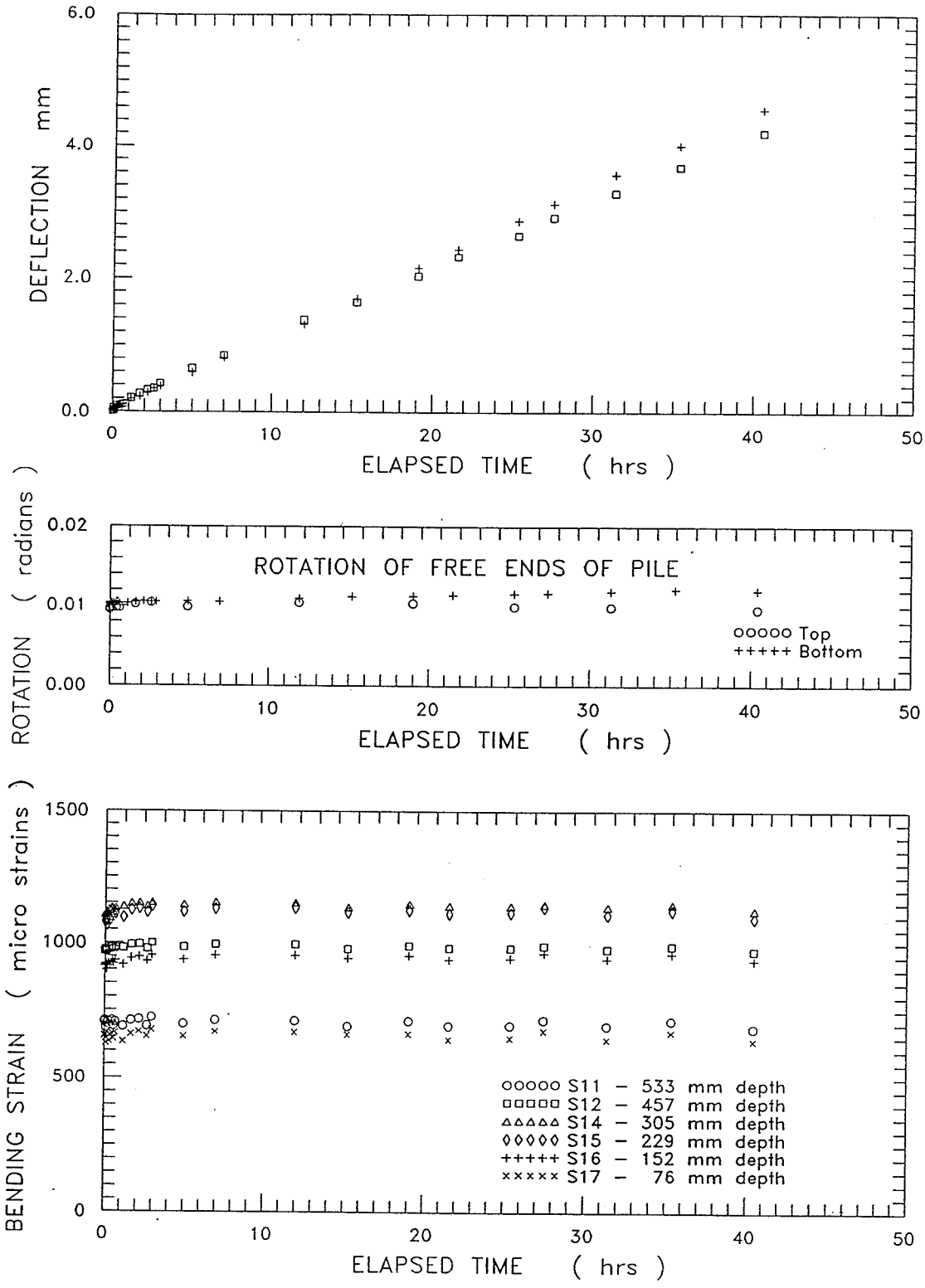


Figure B.40 Multi-stage Test 12, Stage 5: displacement, rotation of free ends of the bar, and bending strain versus time.

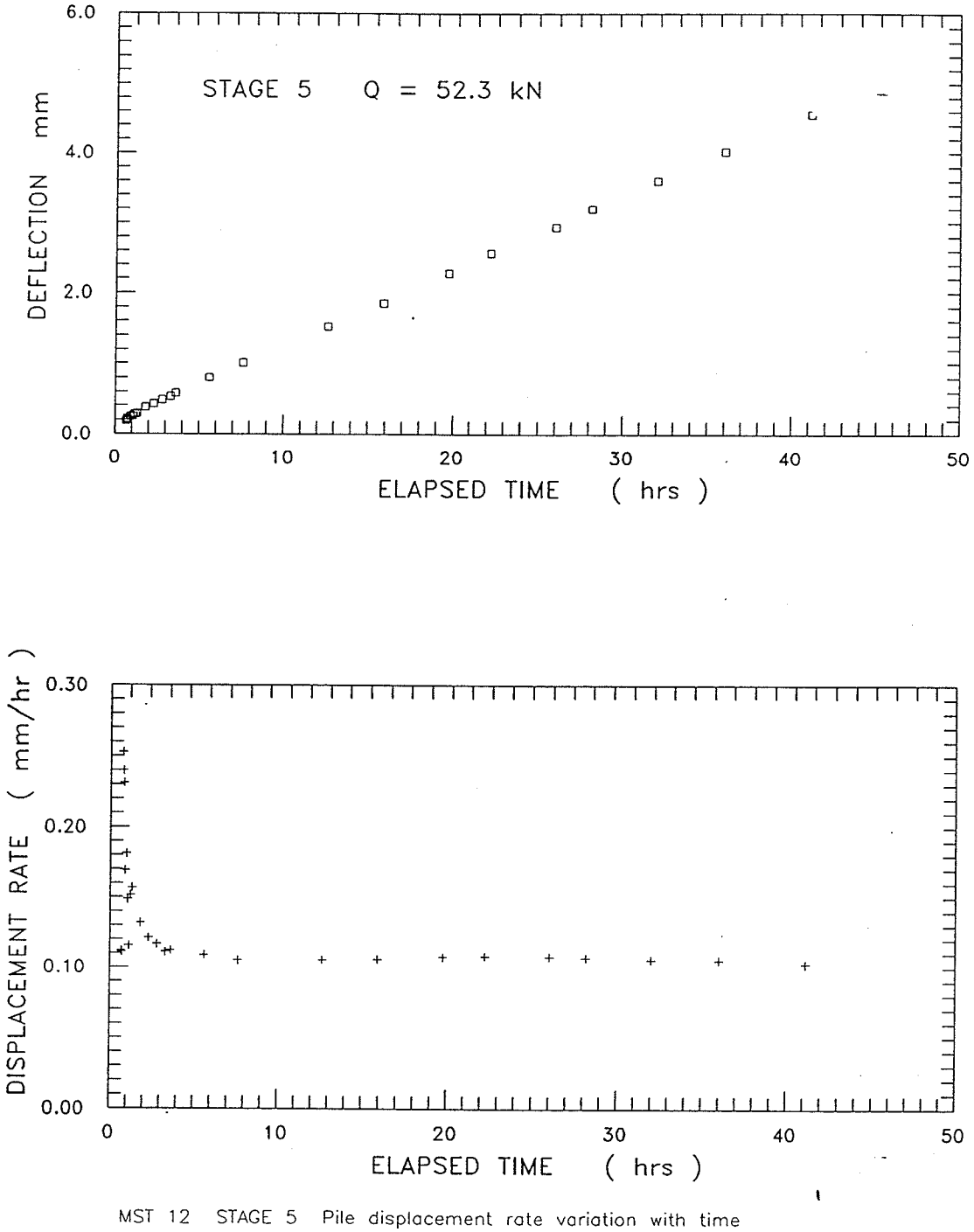


Figure B.41 Multi-stage Test 12, Stage 5: displacement, and displacement rate versus elapsed time.

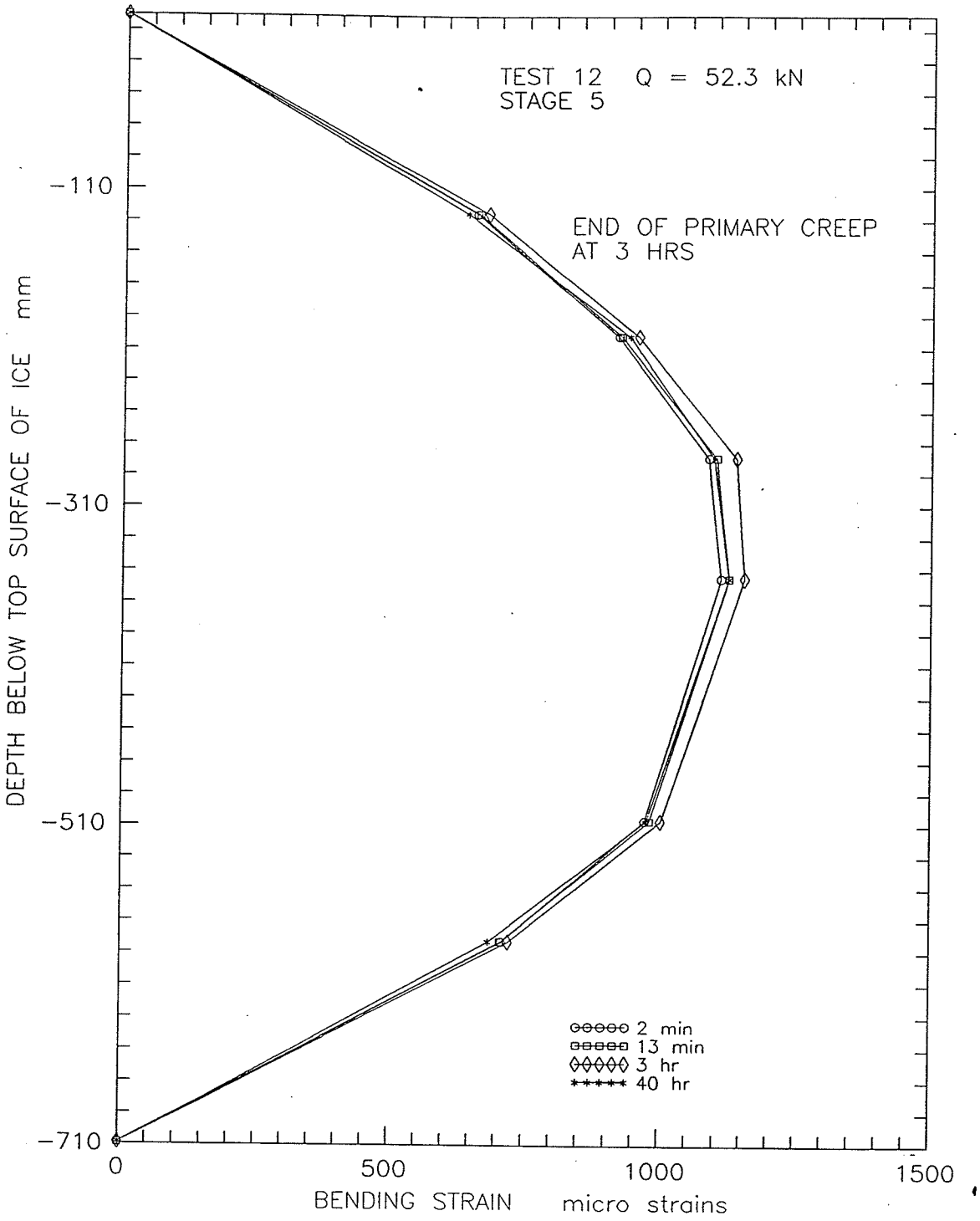


Figure B.42 Multi-stage Test 12, Stage 5: redistribution of bending strains during Stage 5.

# APPENDIX C

# PLOTS USED TO DETERMINE END OF PRIMARY CREEP

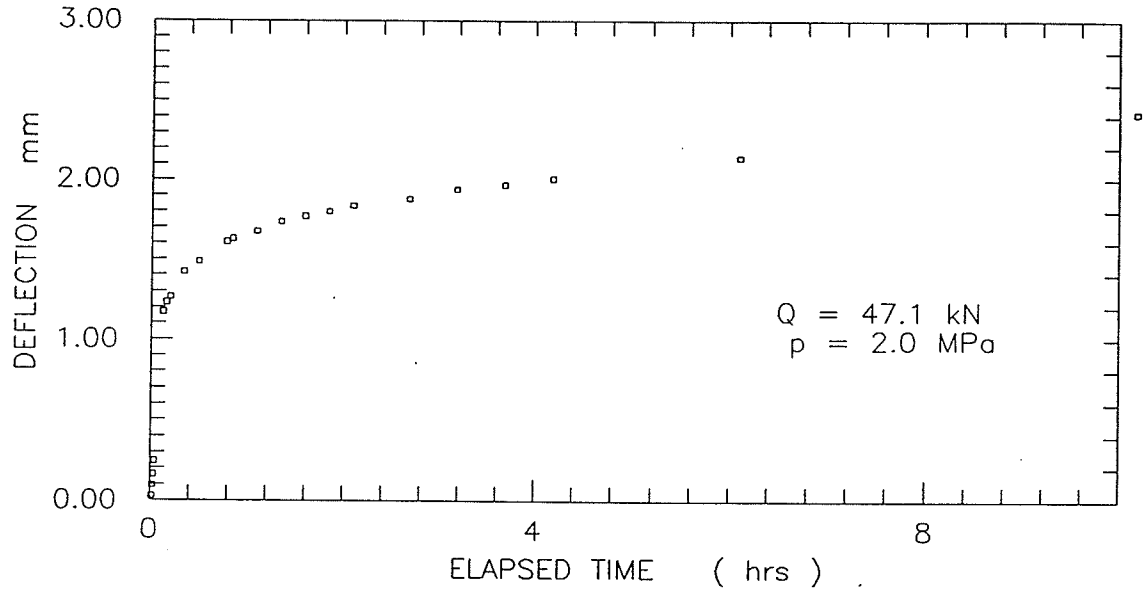


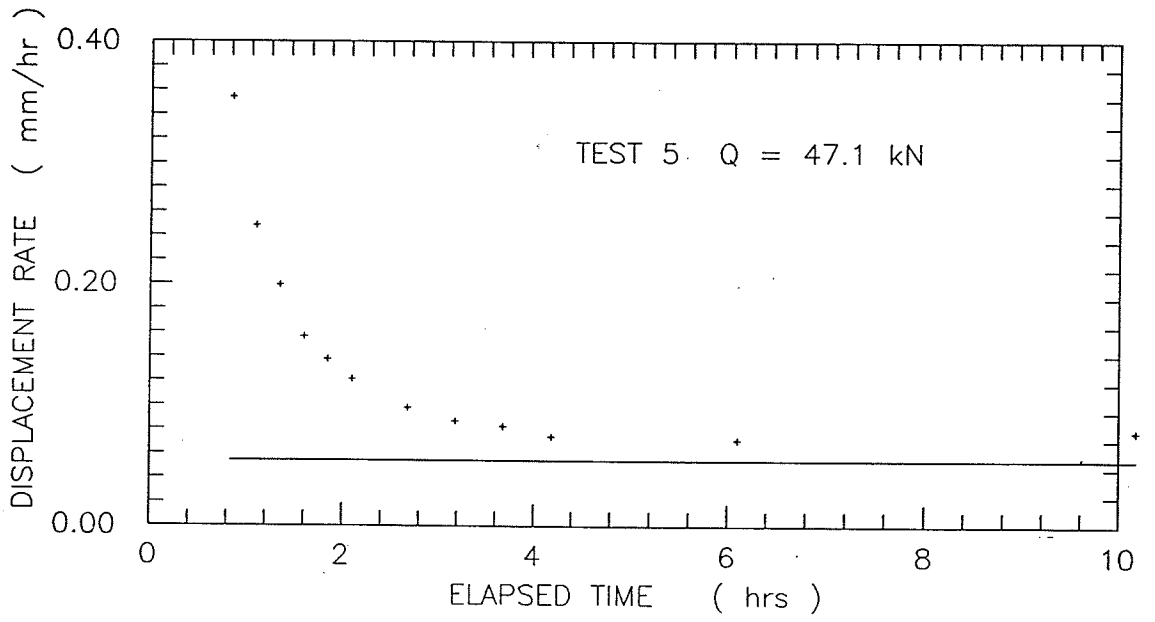


Figure C.1 Single stage Test 5: displacement and displacement rate versus time.

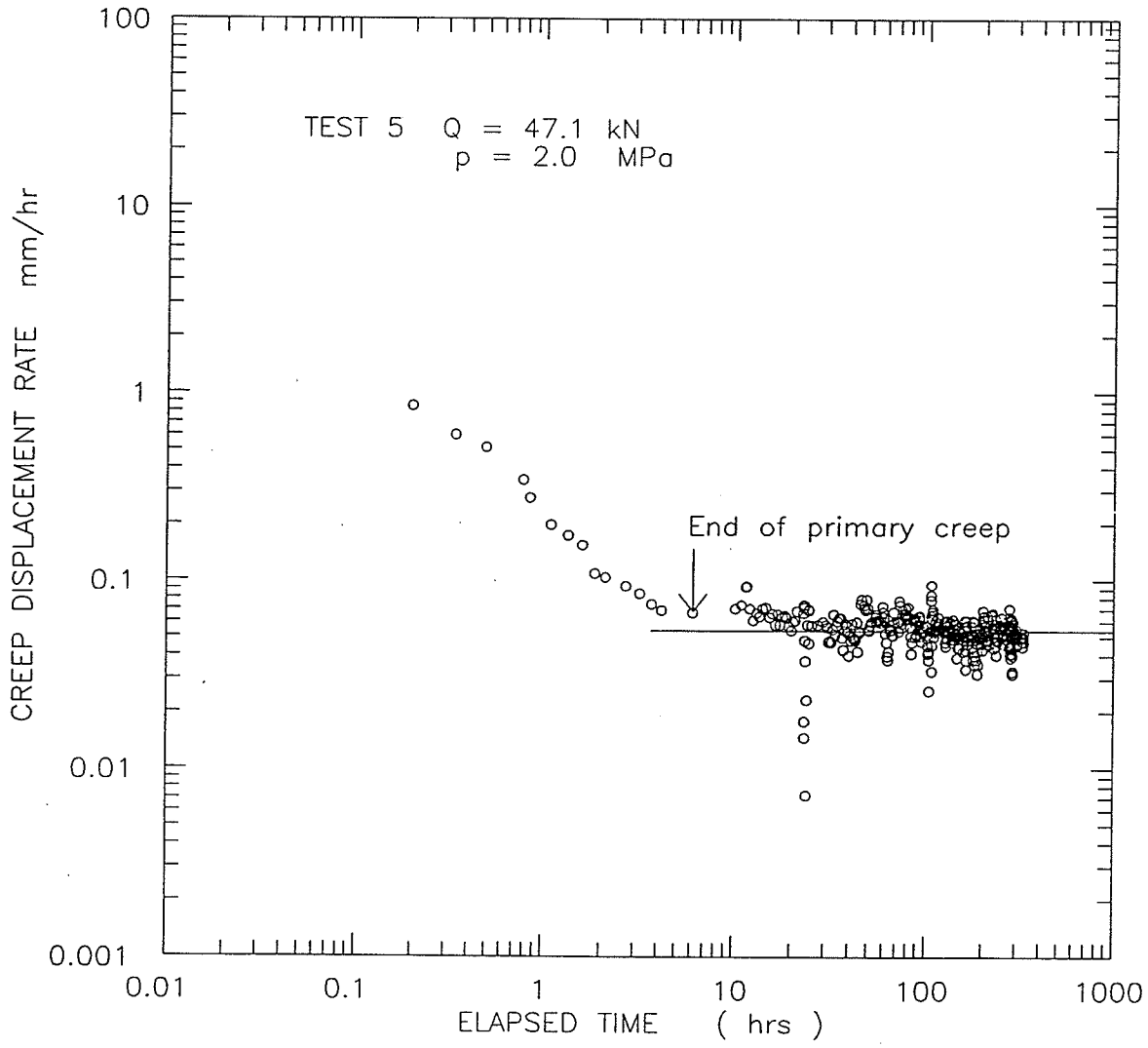


Figure C.2 Single stage Test 5: creep displacement rate versus time (log-log).

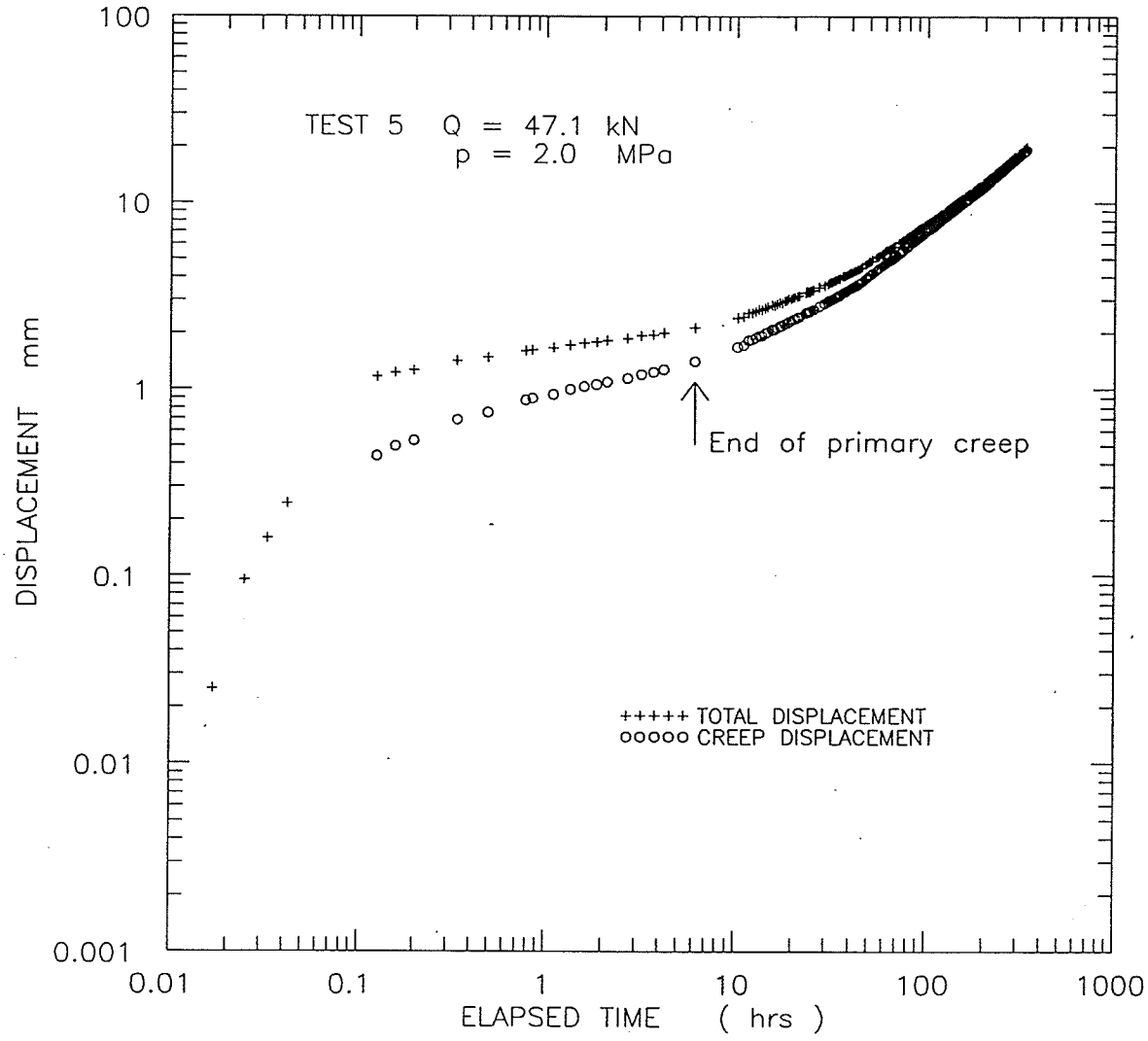


Figure C.3 Single stage Test 5: total and creep displacements versus time (log-log).

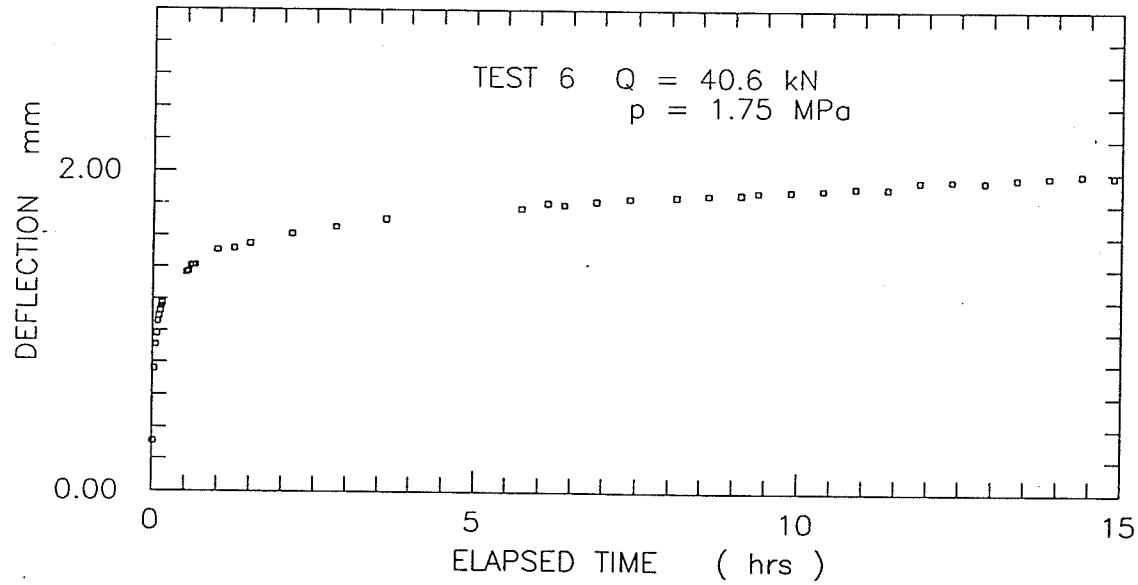


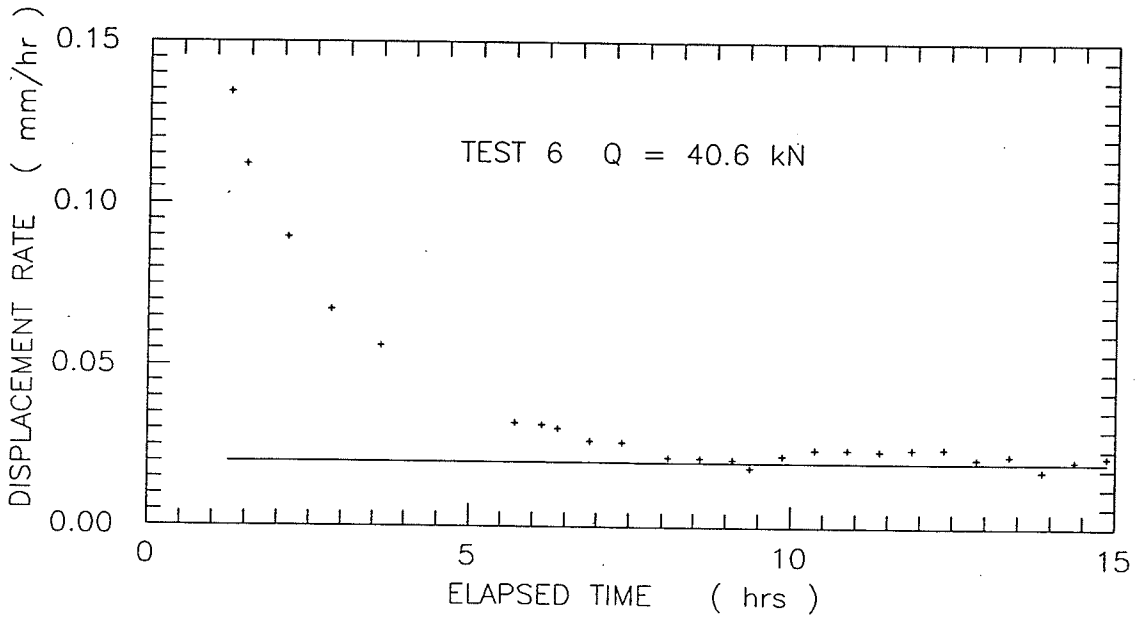


Figure C.4 Single stage Test 6: displacement and displacement rate versus time.

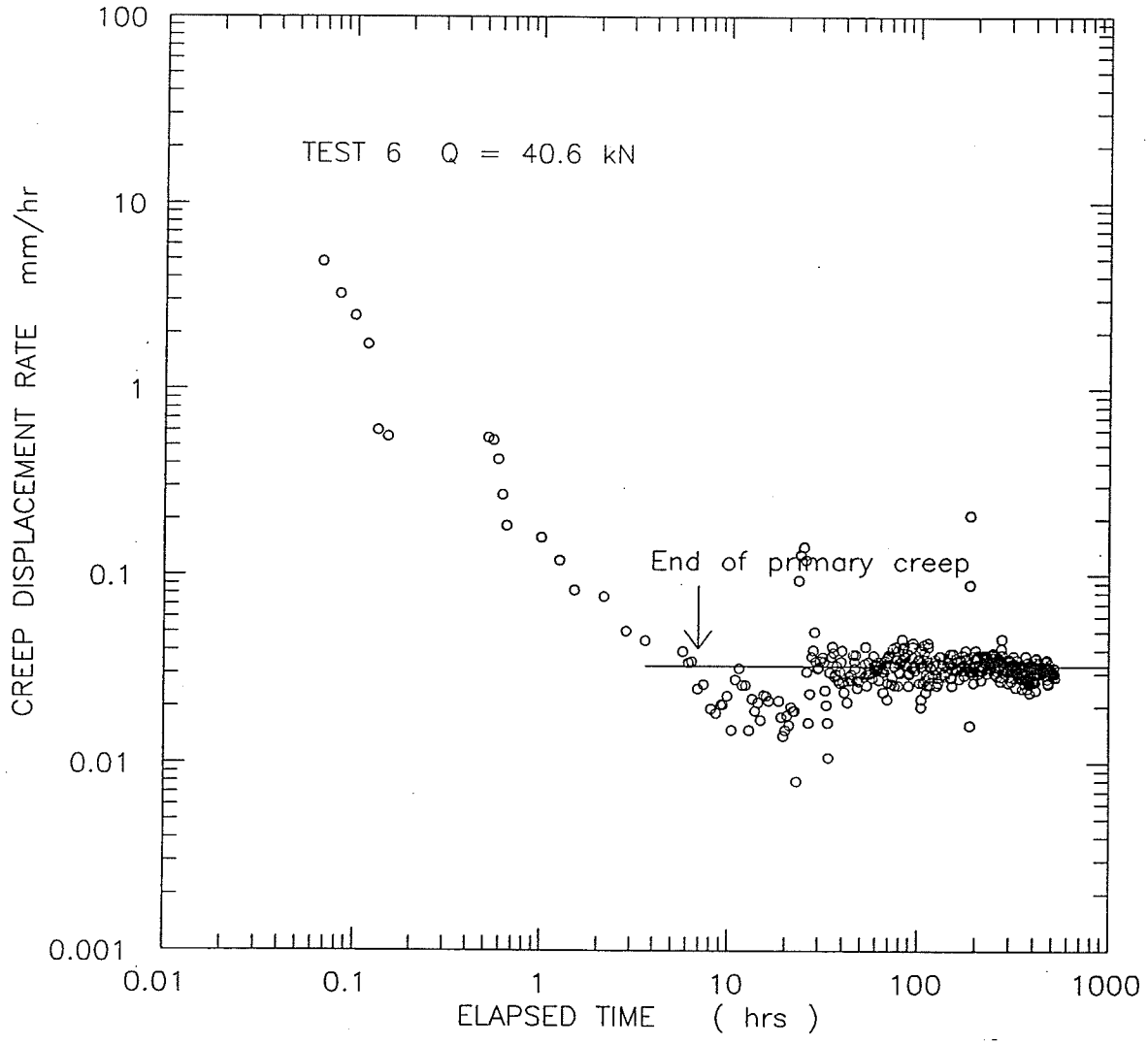


Figure C.5 Single stage Test 6: creep displacement rate versus time (log-log).

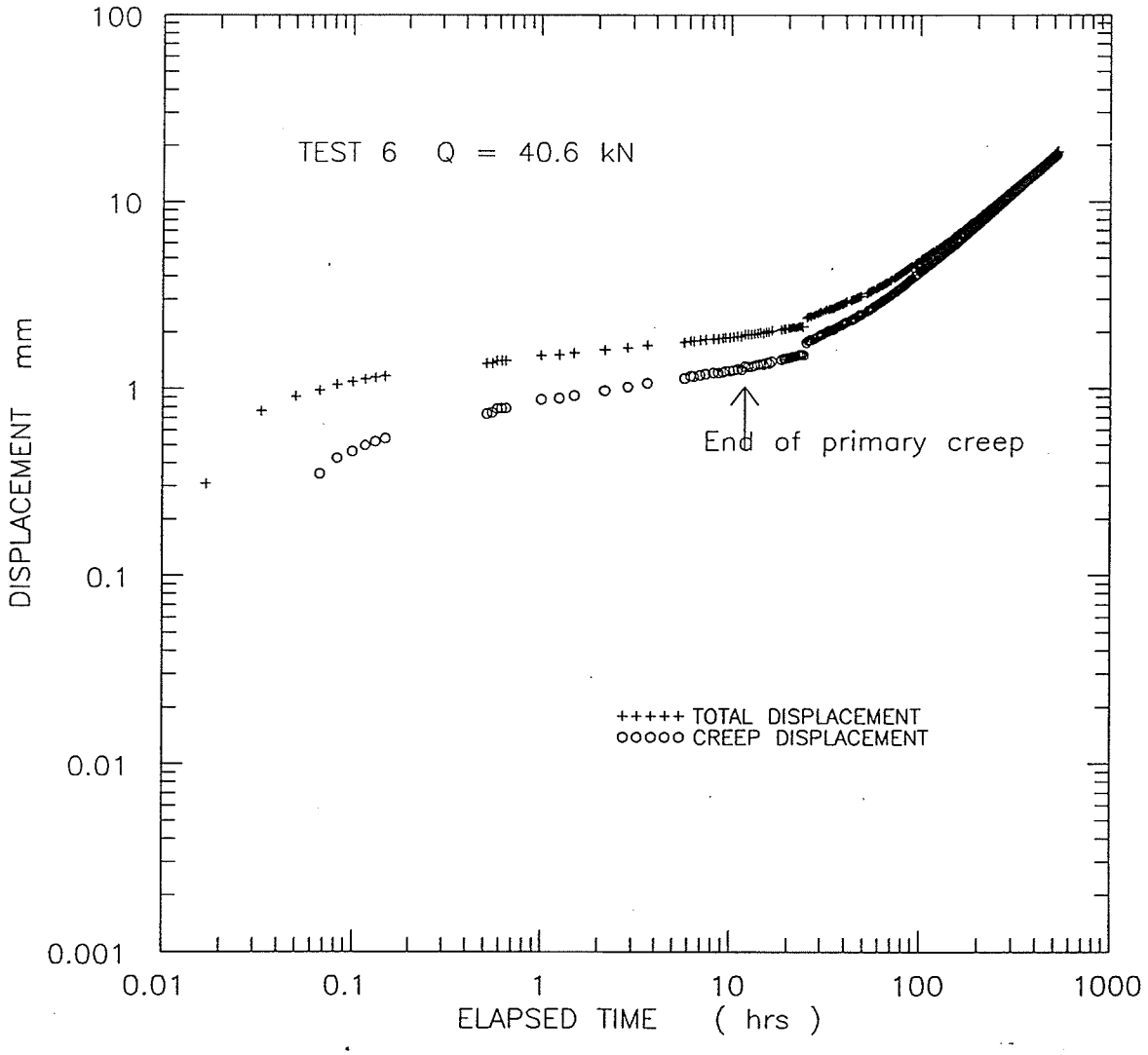


Figure C.6 Single stage Test 6: total and creep displacement versus time (log-log).

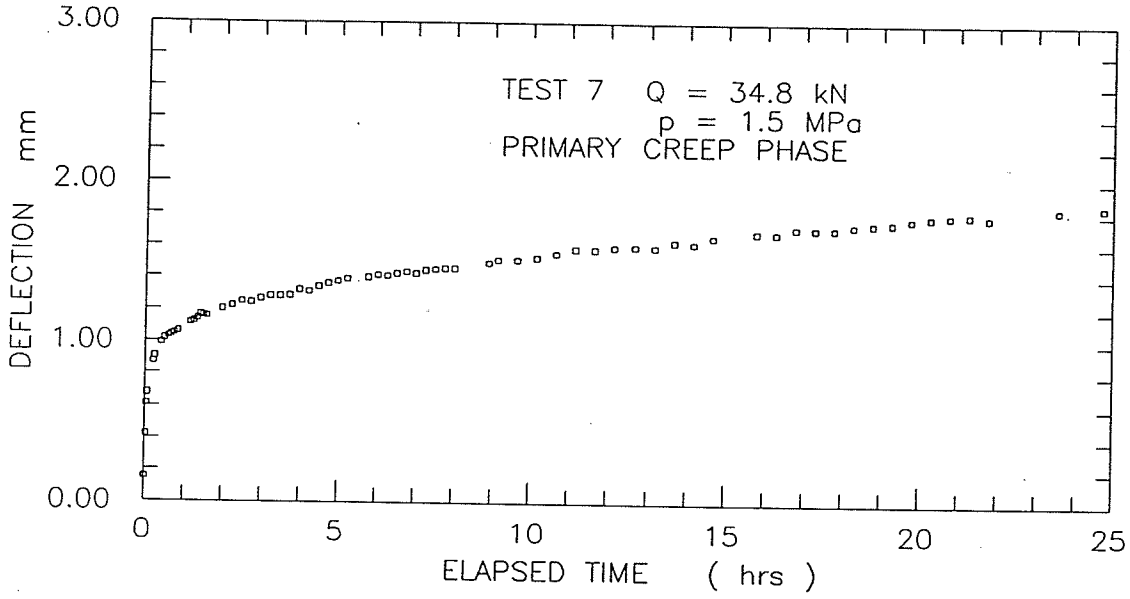


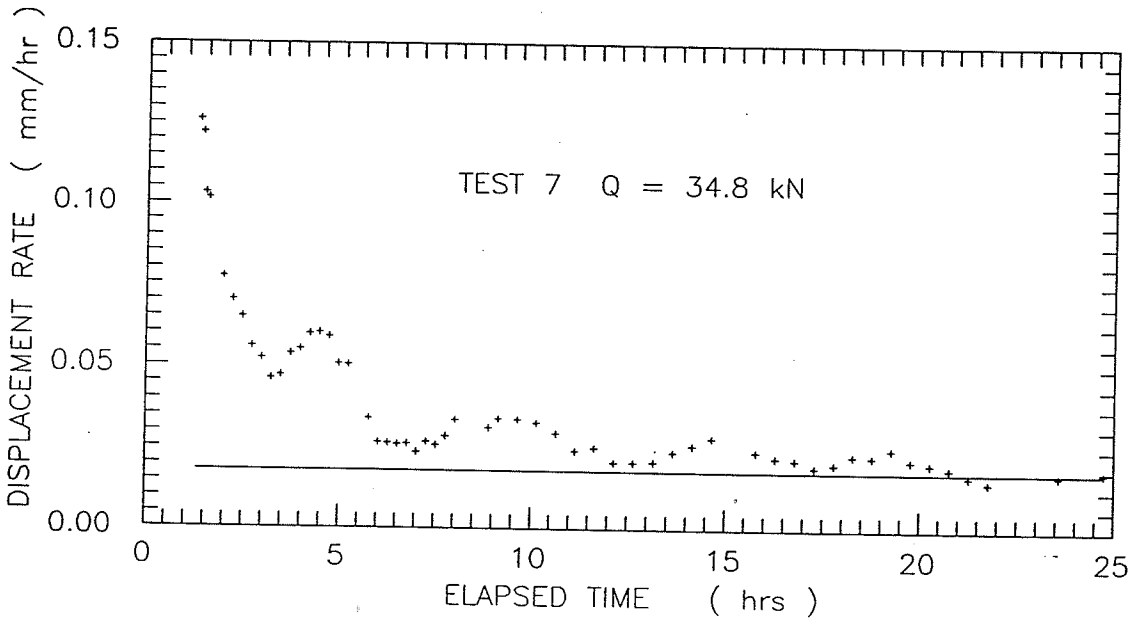


Figure C.7 Single stage Test 7: displacement and displacement rate versus time.

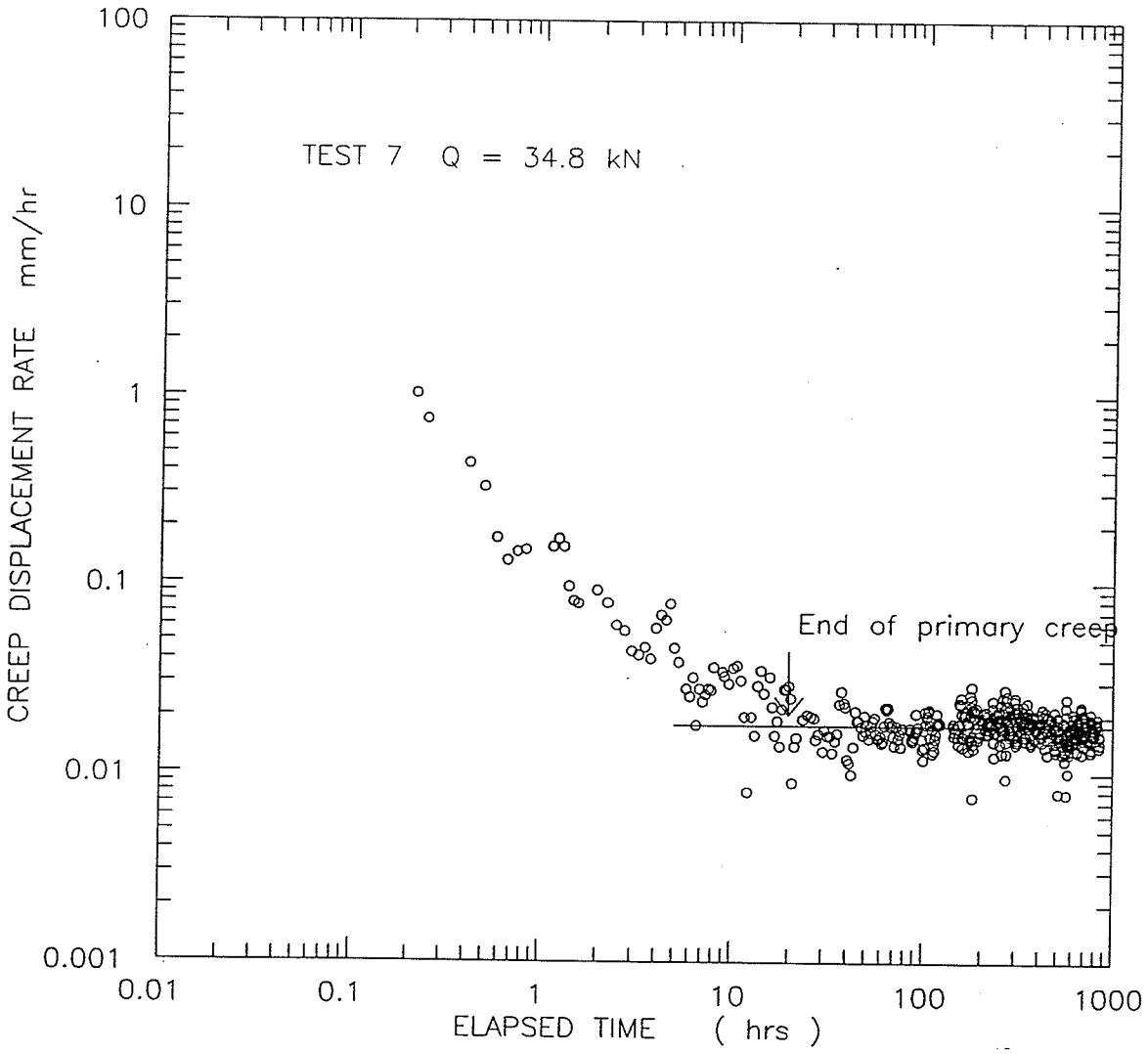


Figure C.8 Single stage Test 7: creep displacement rate versus time (log-log).

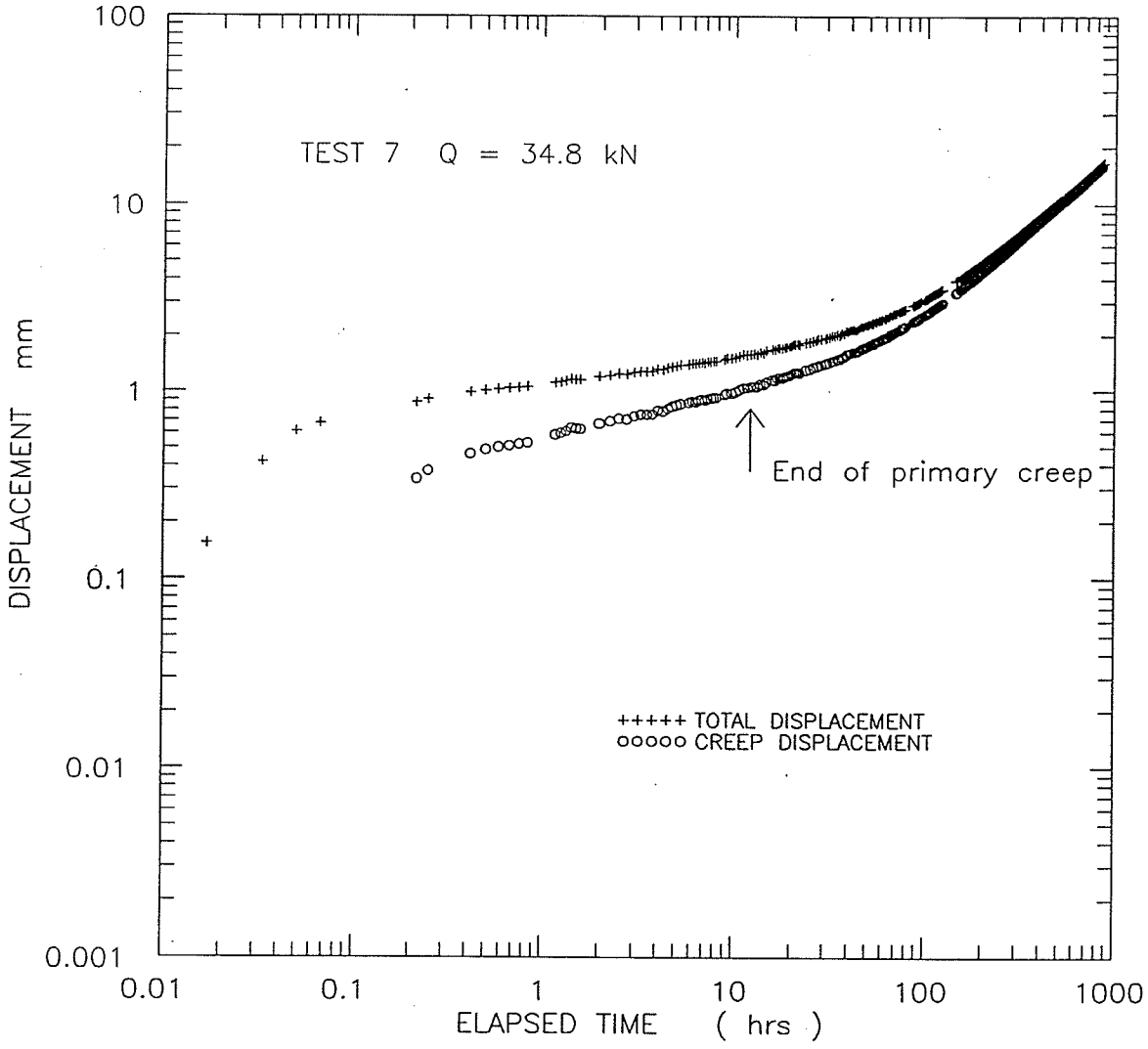


Figure C.9 Single stage Test 7: total and creep displacement versus time (log-log).

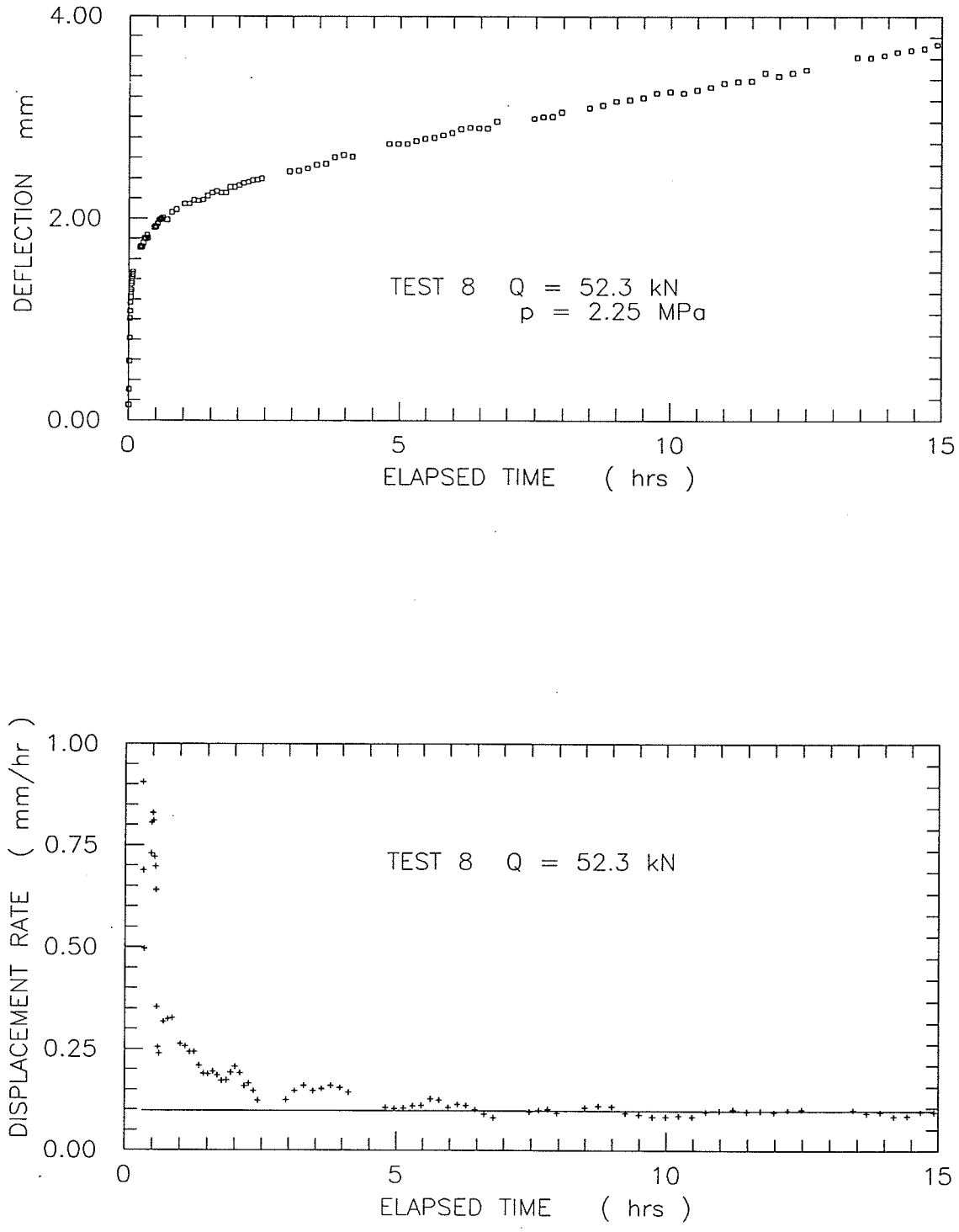


Figure C.10 Single stage Test 8: displacement and displacement rate versus time.

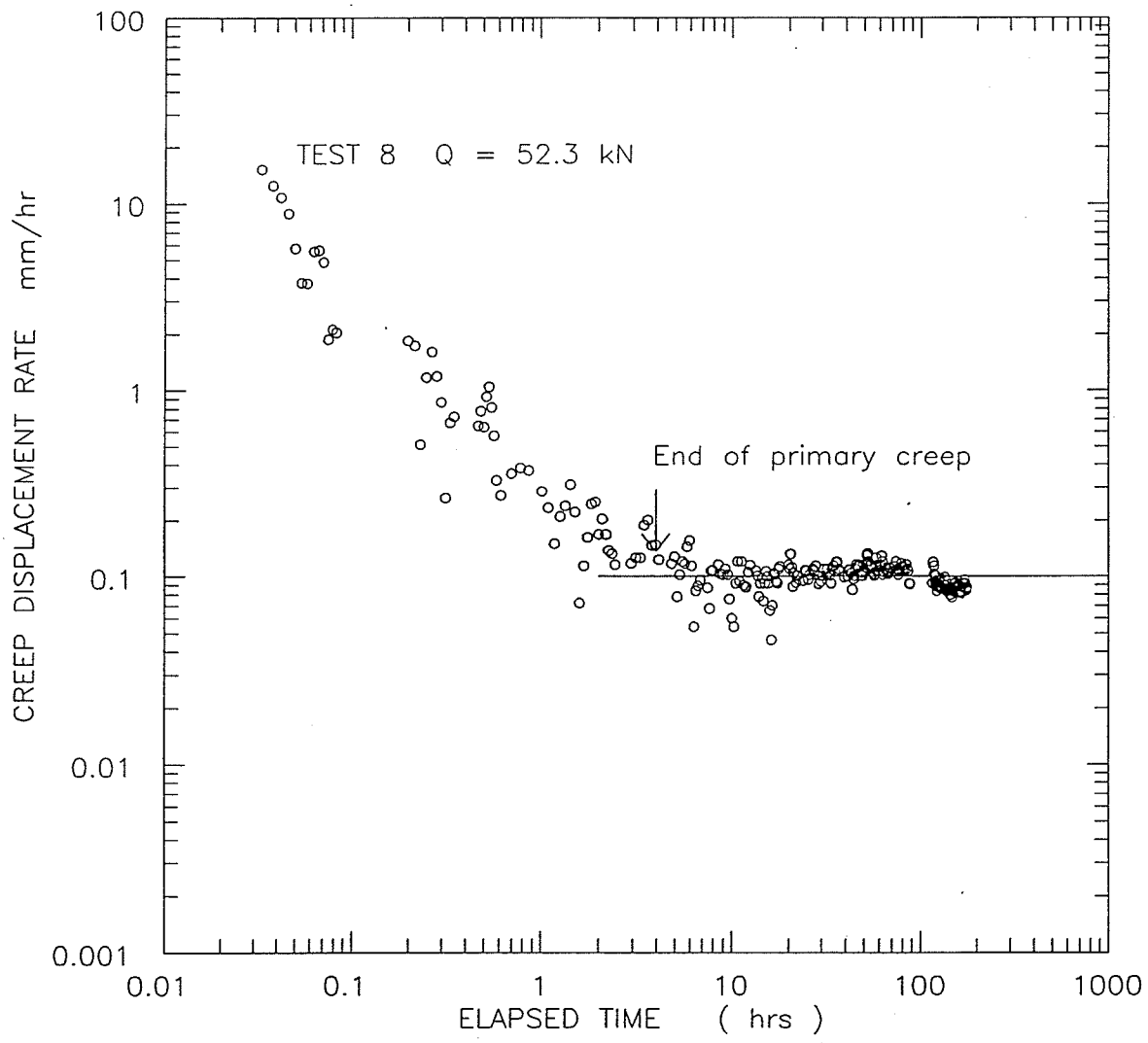


Figure C.11 Single stage Test 8: creep displacement rate versus time (log-log).

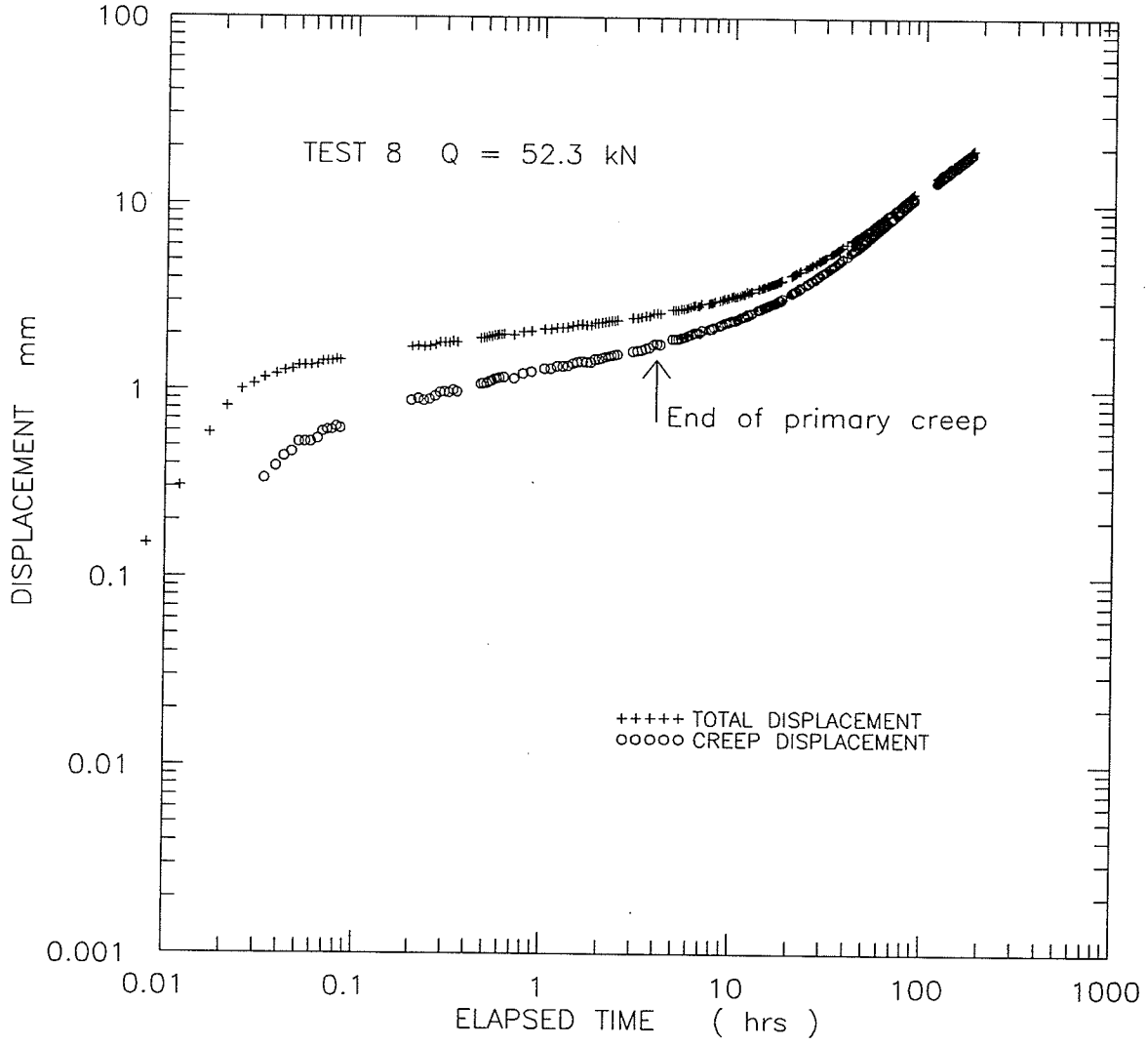


Figure C.12 Single stage Test 8: total and creep displacement versus time (log-log).

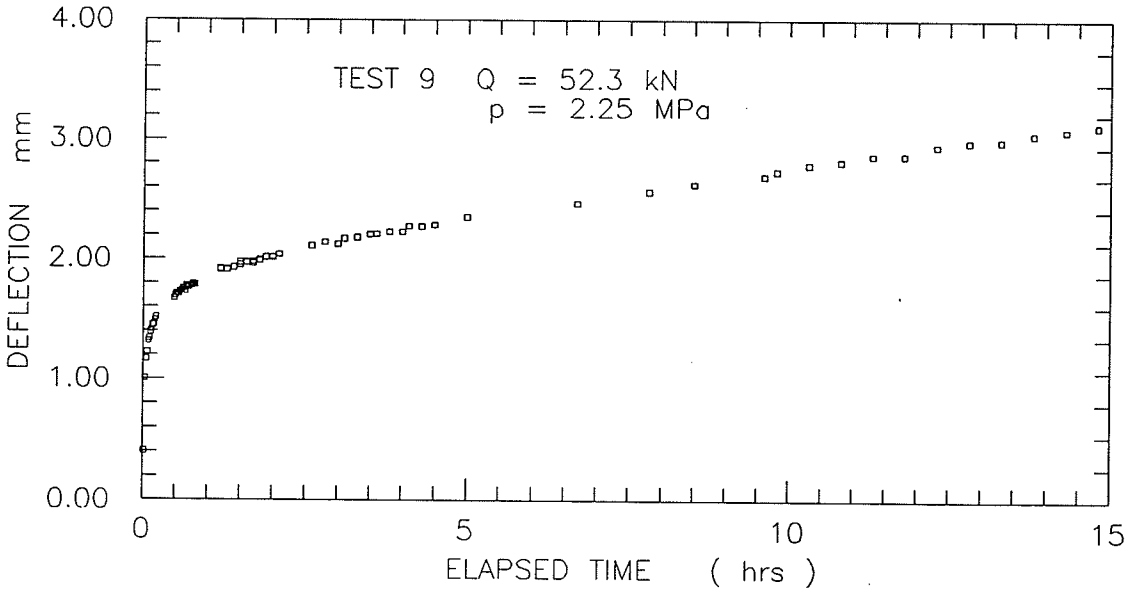


Figure C.13 Single stage Test 9: displacement versus time.

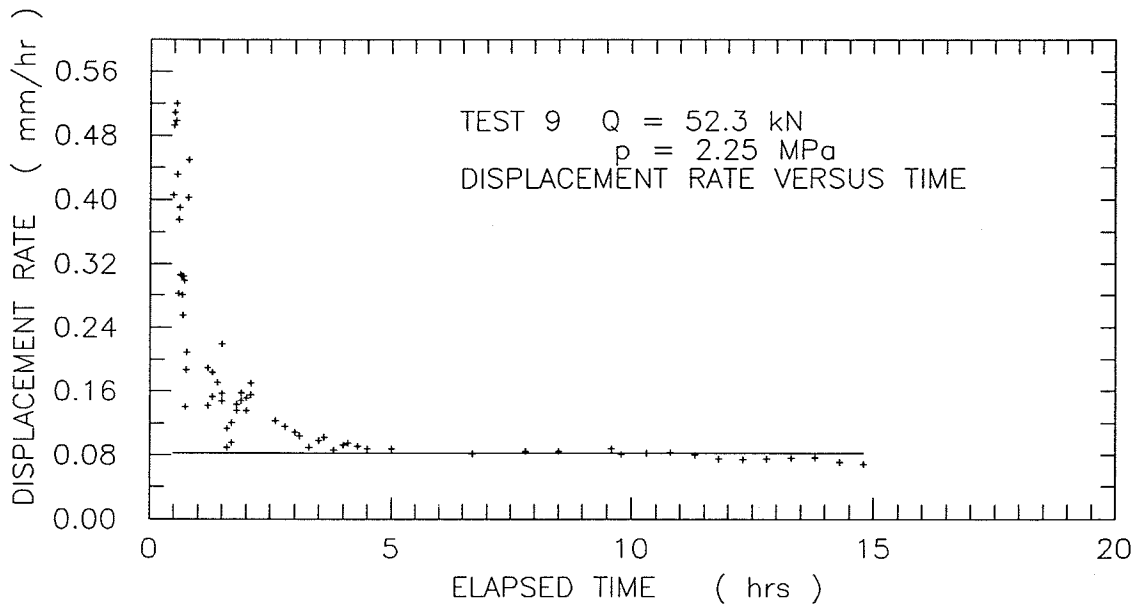


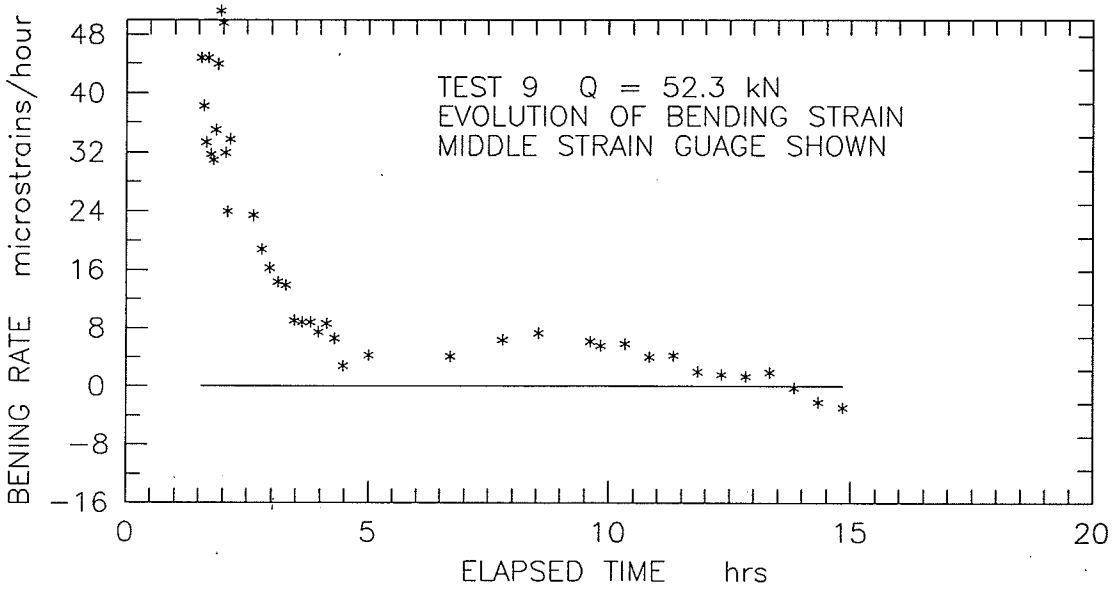


Figure C.14 Single stage Test 9: displacement rate and evolution of bending strain (middle strain gauge) versus time.

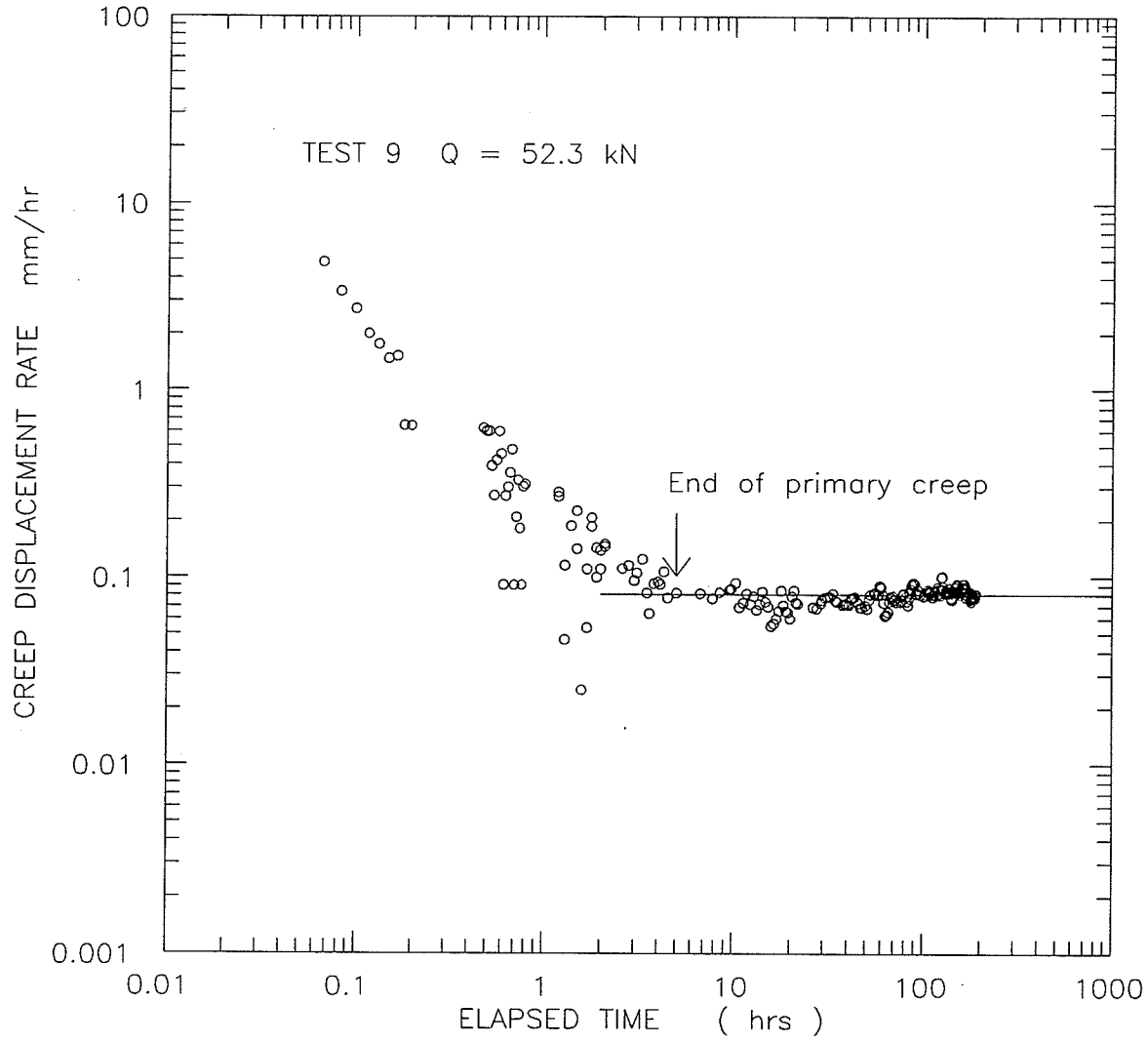


Figure C.15 Single stage Test 9: creep displacement rate versus time (log-log).

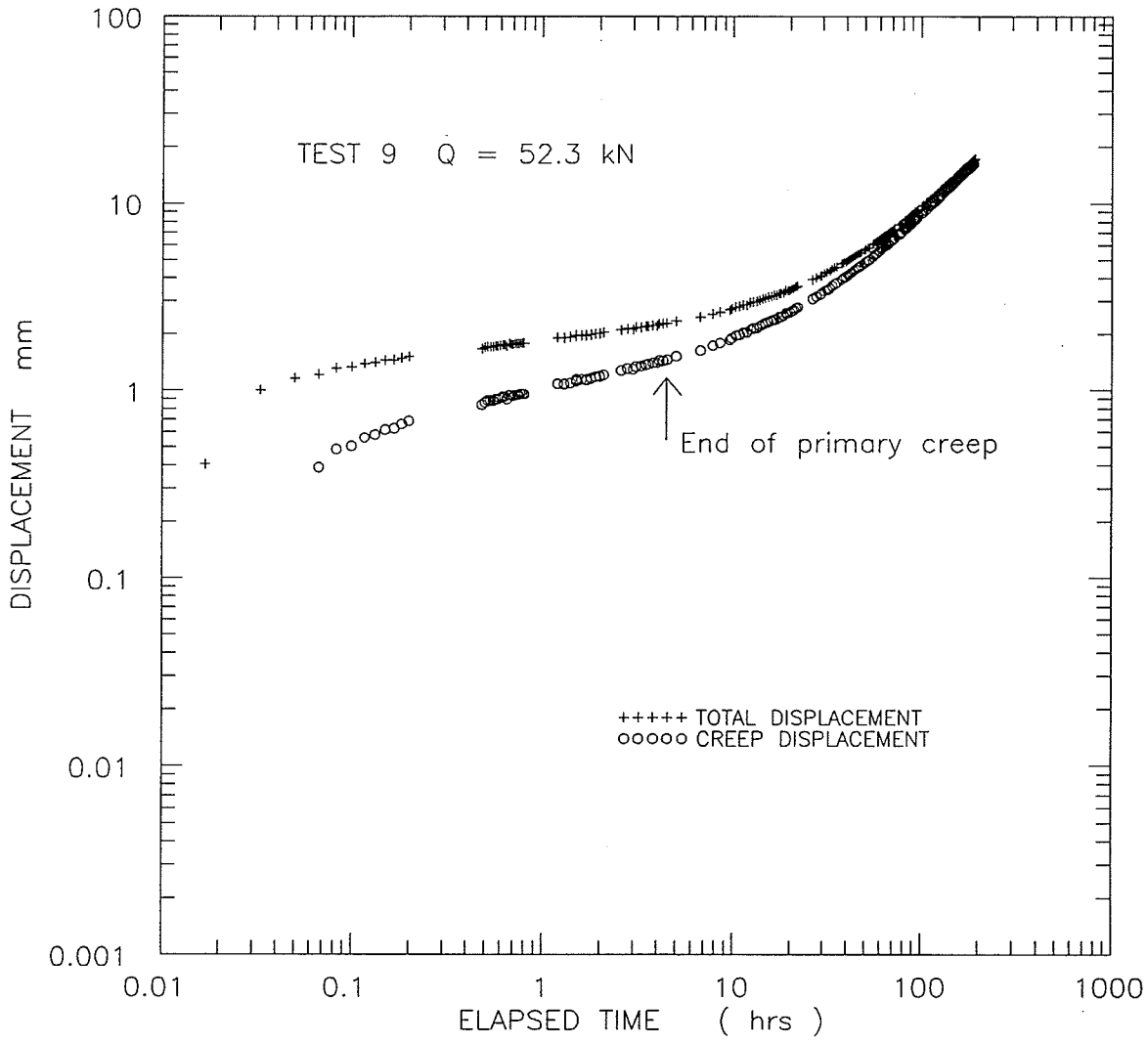


Figure C.16 Single stage Test 9: total and creep displacement versus time (log-log).

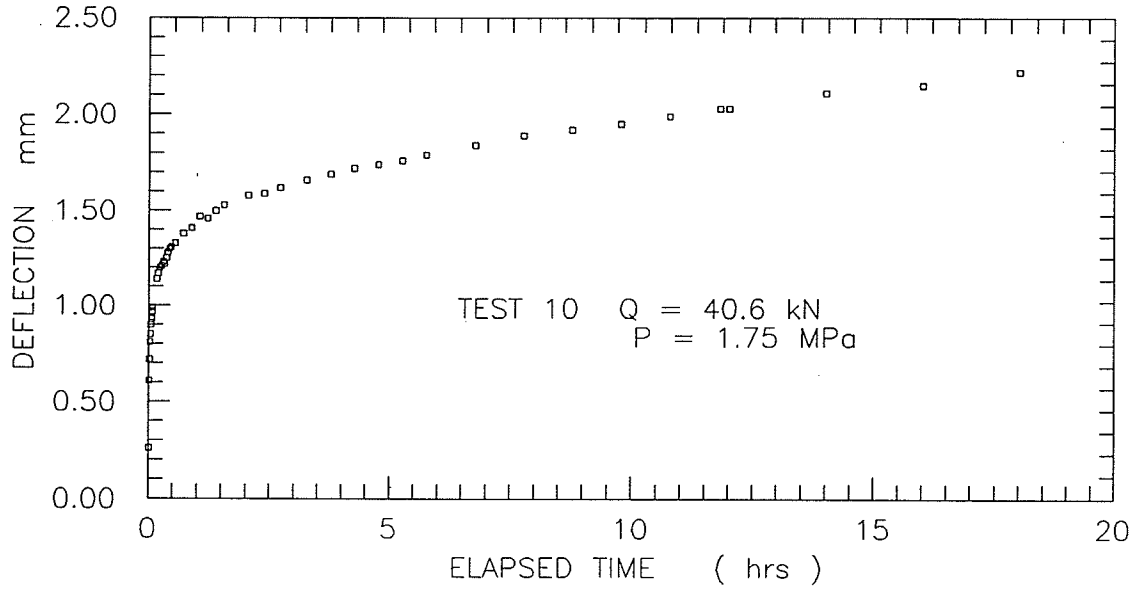


Figure C.17 Single stage Test 10: displacement versus time.

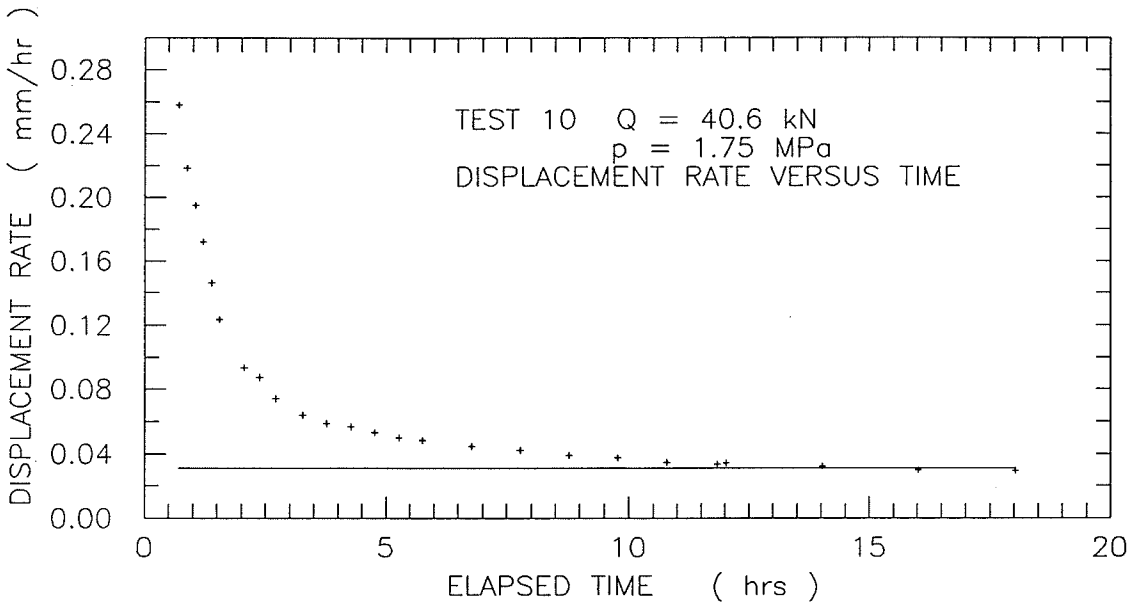


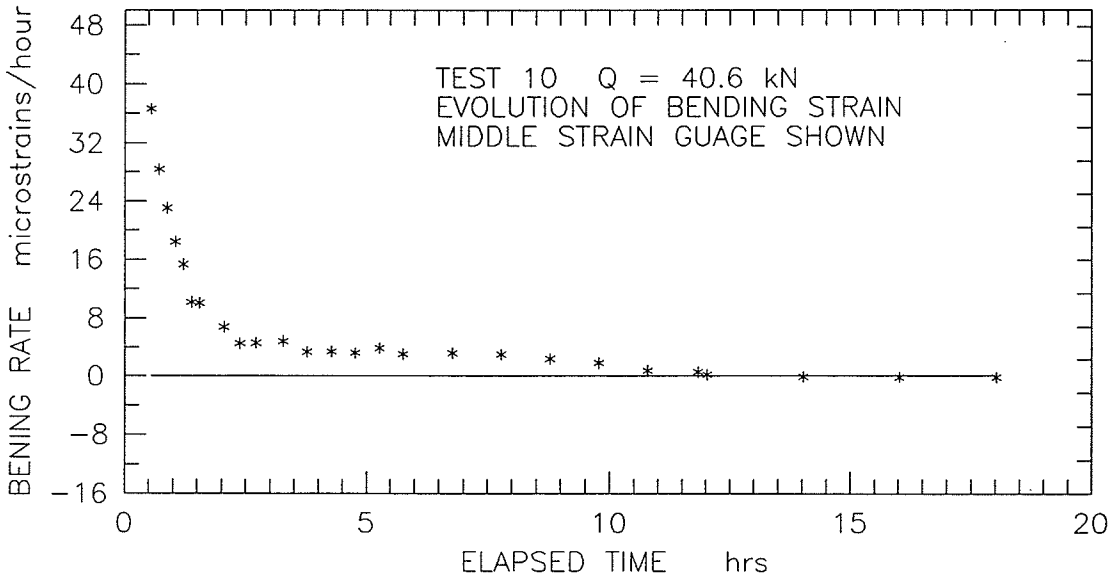


Figure C.18 Single stage Test 10: displacement rate and evolution of bending strain (middle strain gauge) versus time.

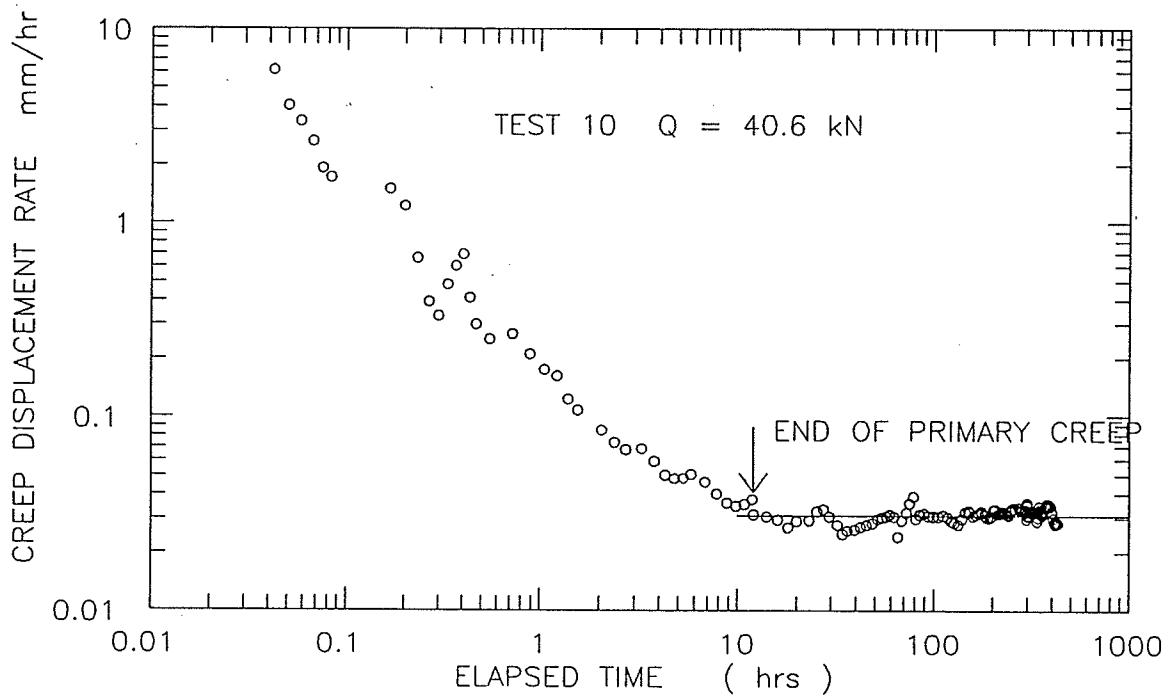


Figure C.19 Single stage Test 10: creep displacement rate versus time (log-log).

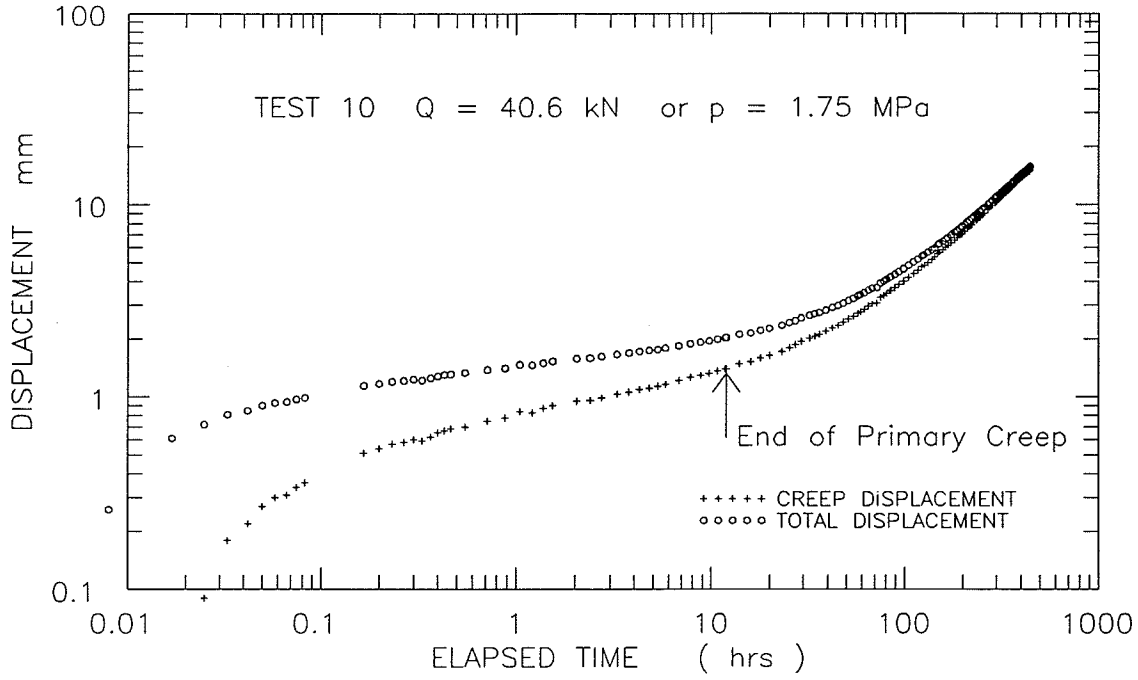


Figure C.20 Single stage Test 10: total and creep displacement versus time (log-log).

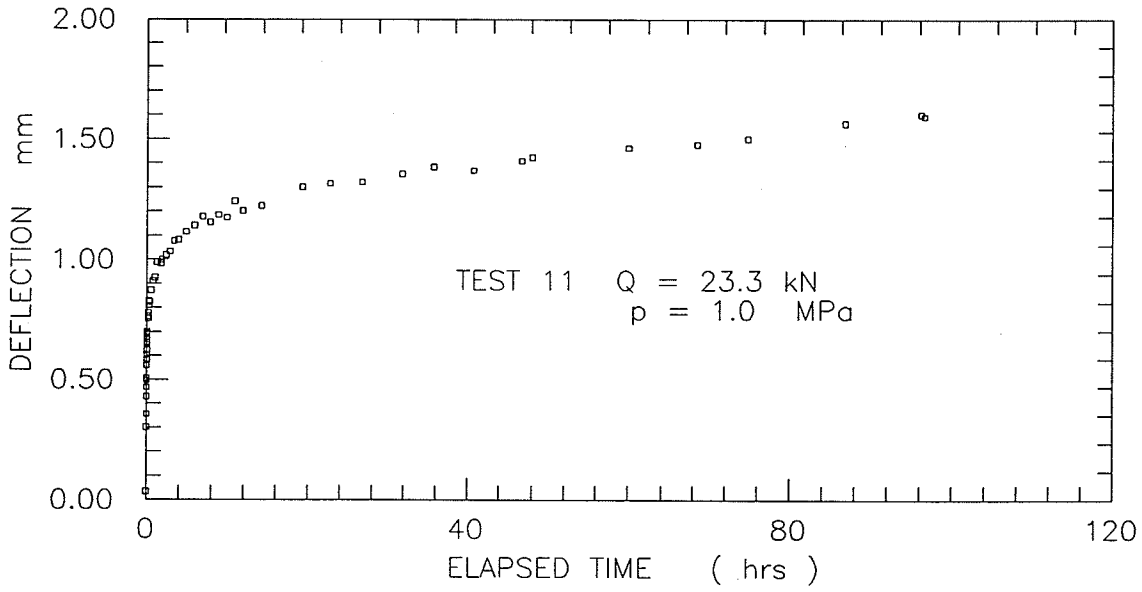


Figure C.21 Single stage Test 11: displacement versus time.

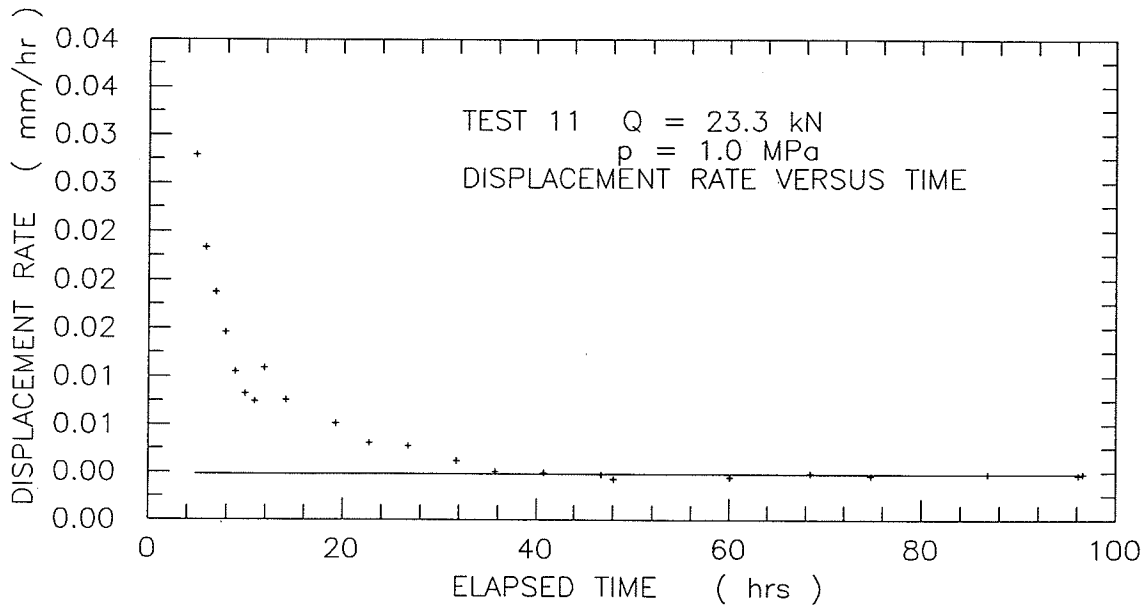


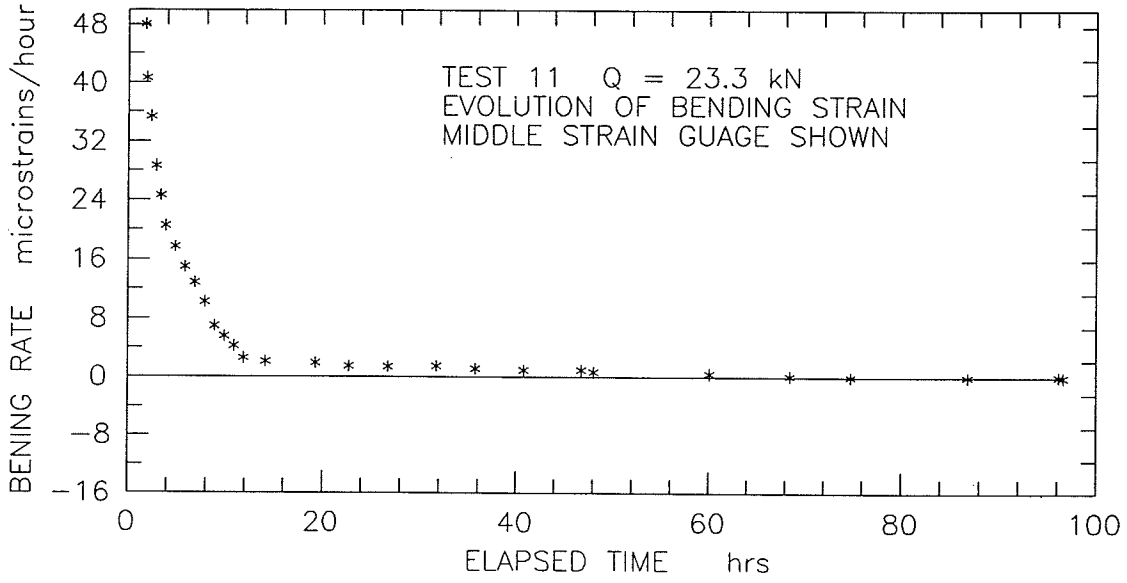


Figure C.22 Single stage Test 11: displacement rate and evolution of bending strain (middle strain gauge) versus time.

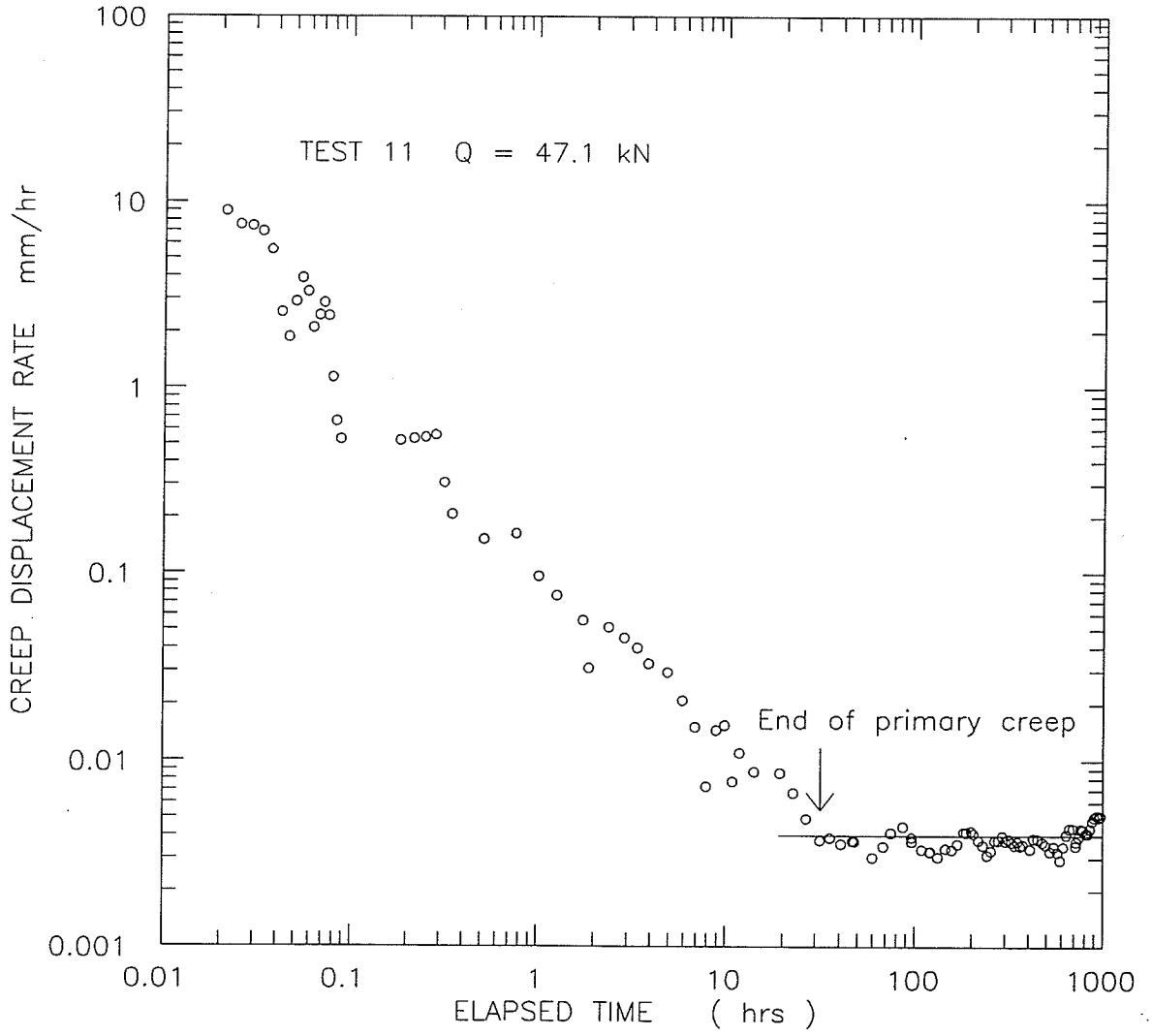


Figure C.23 Single stage Test 11: creep displacement rate versus time (log-log).

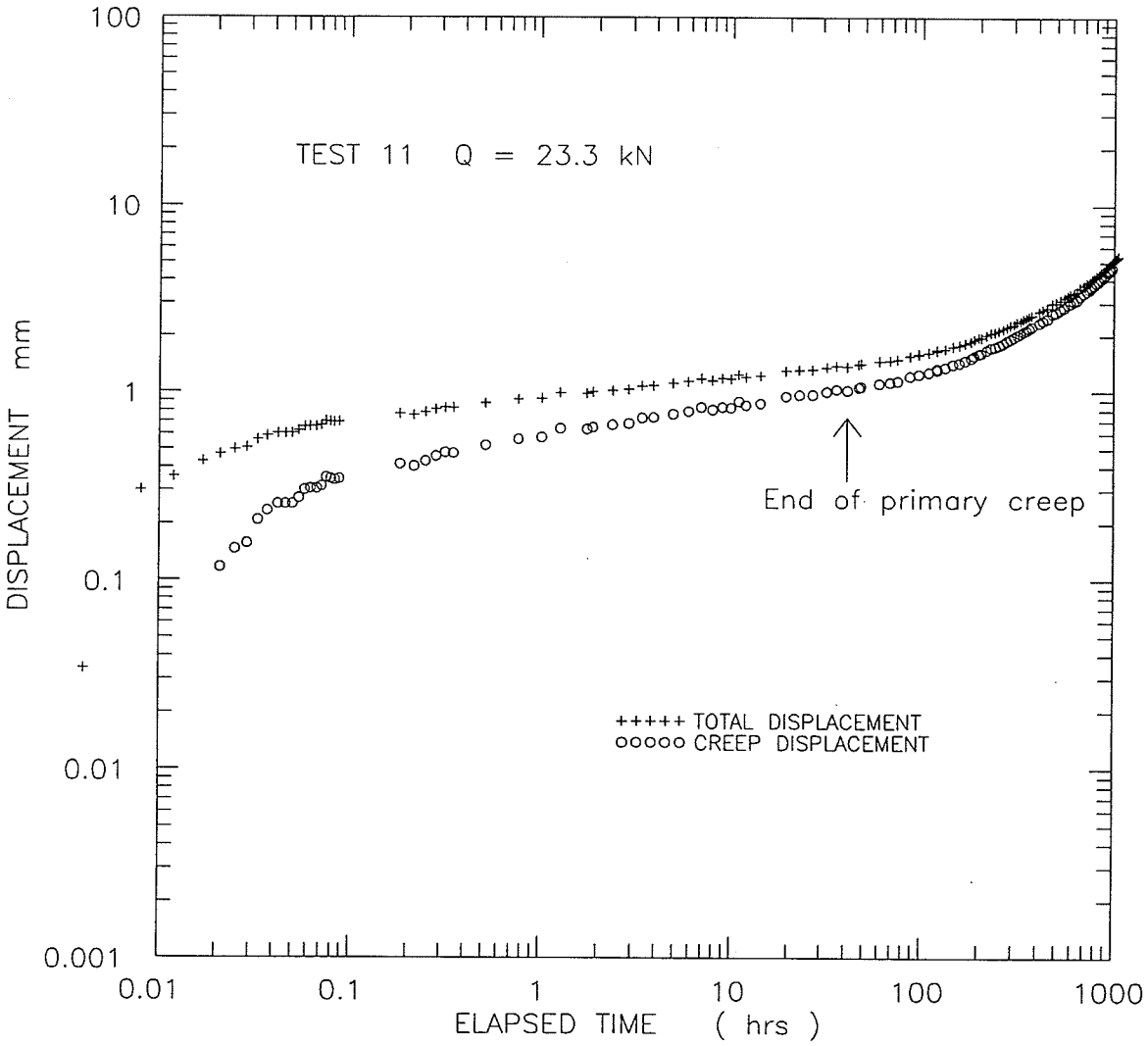


Figure C.24 Single stage Test 11: total and creep displacement versus time (log-log).

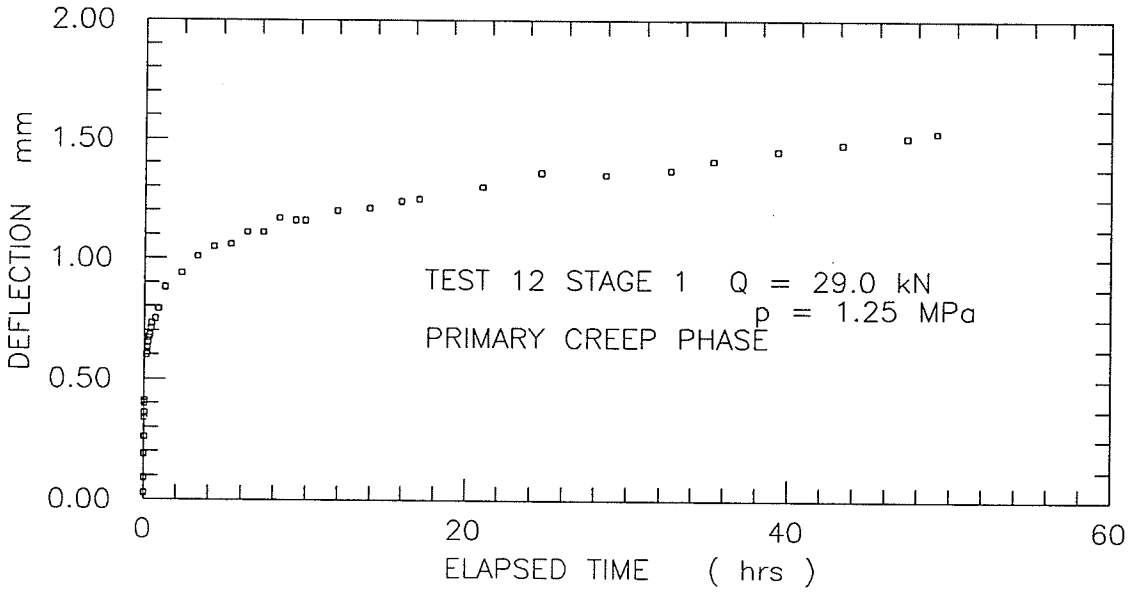


Figure C.25 Multi-stage Test 12, Stage 1: displacement versus time.

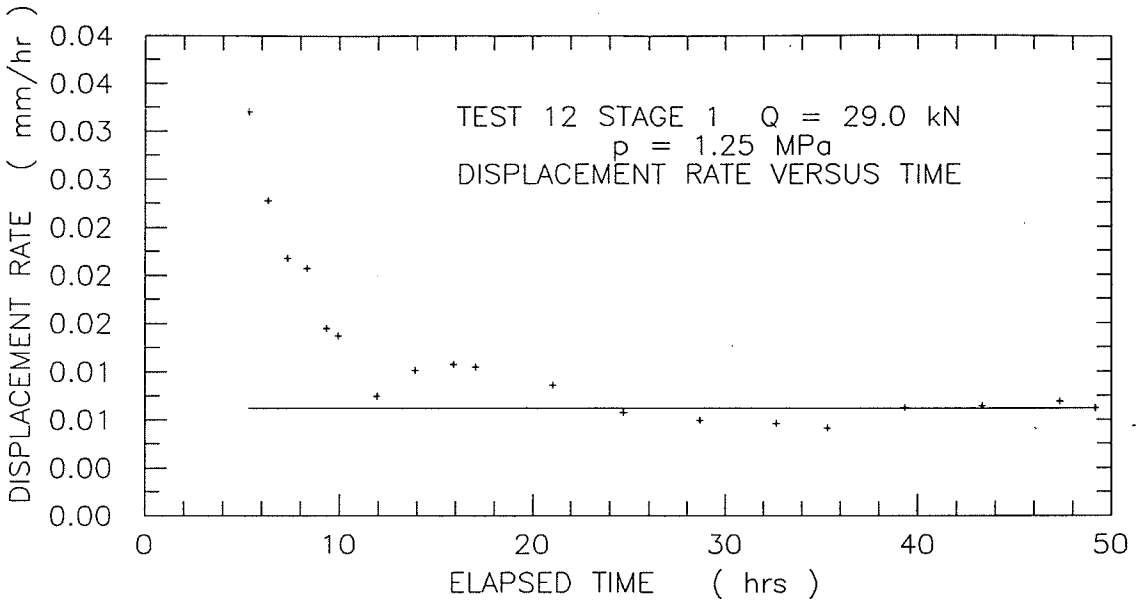


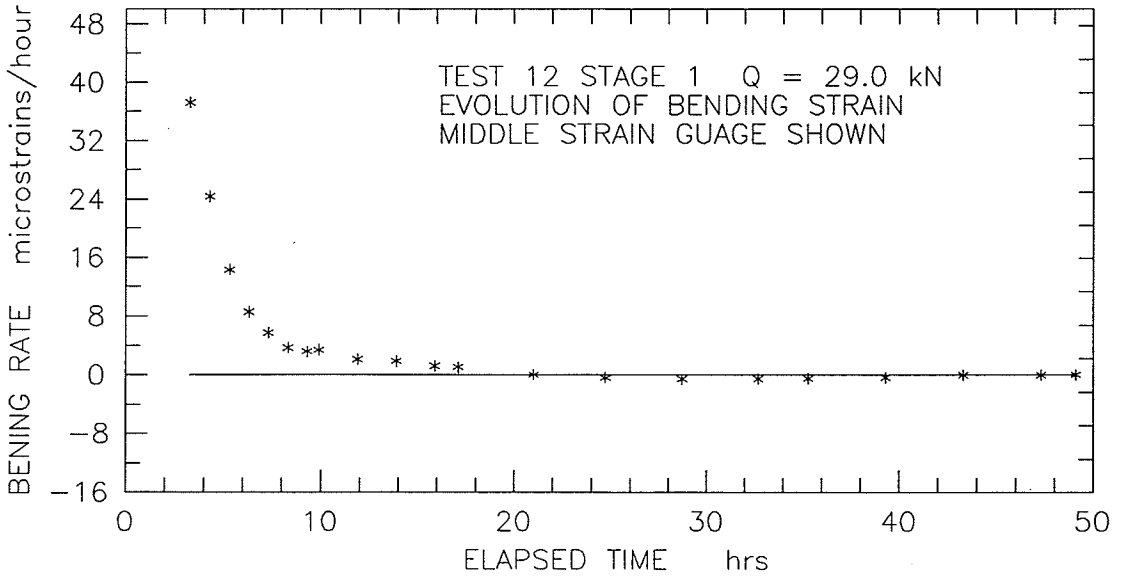


Figure C.26 Multi-stage Test 12, Stage 1: displacement rate and evolution of bending strain (middle strain gauge) versus time.

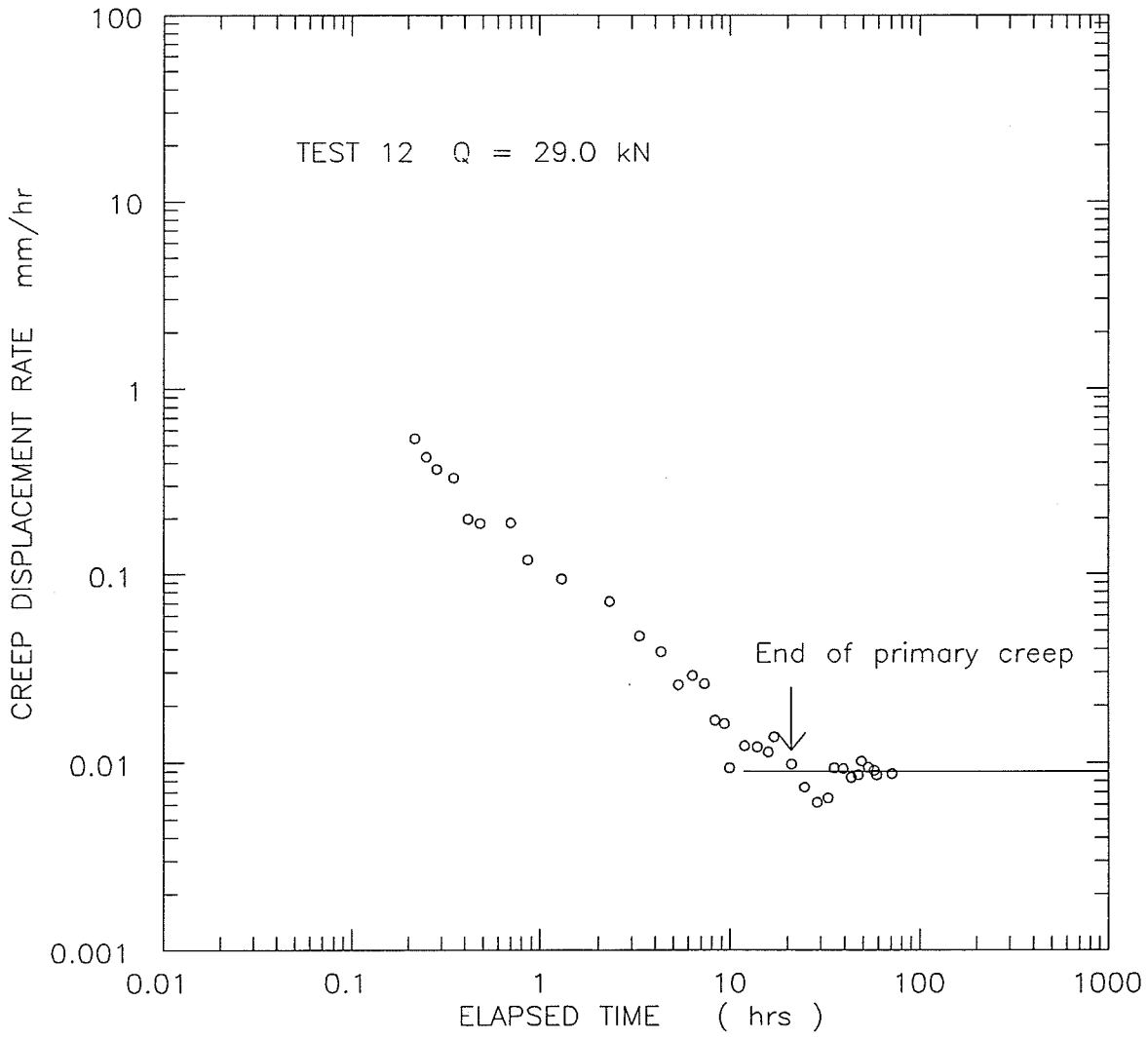


Figure C.27 Multi-stage Test 12, Stage 1: creep displacement rate versus time (log-log).

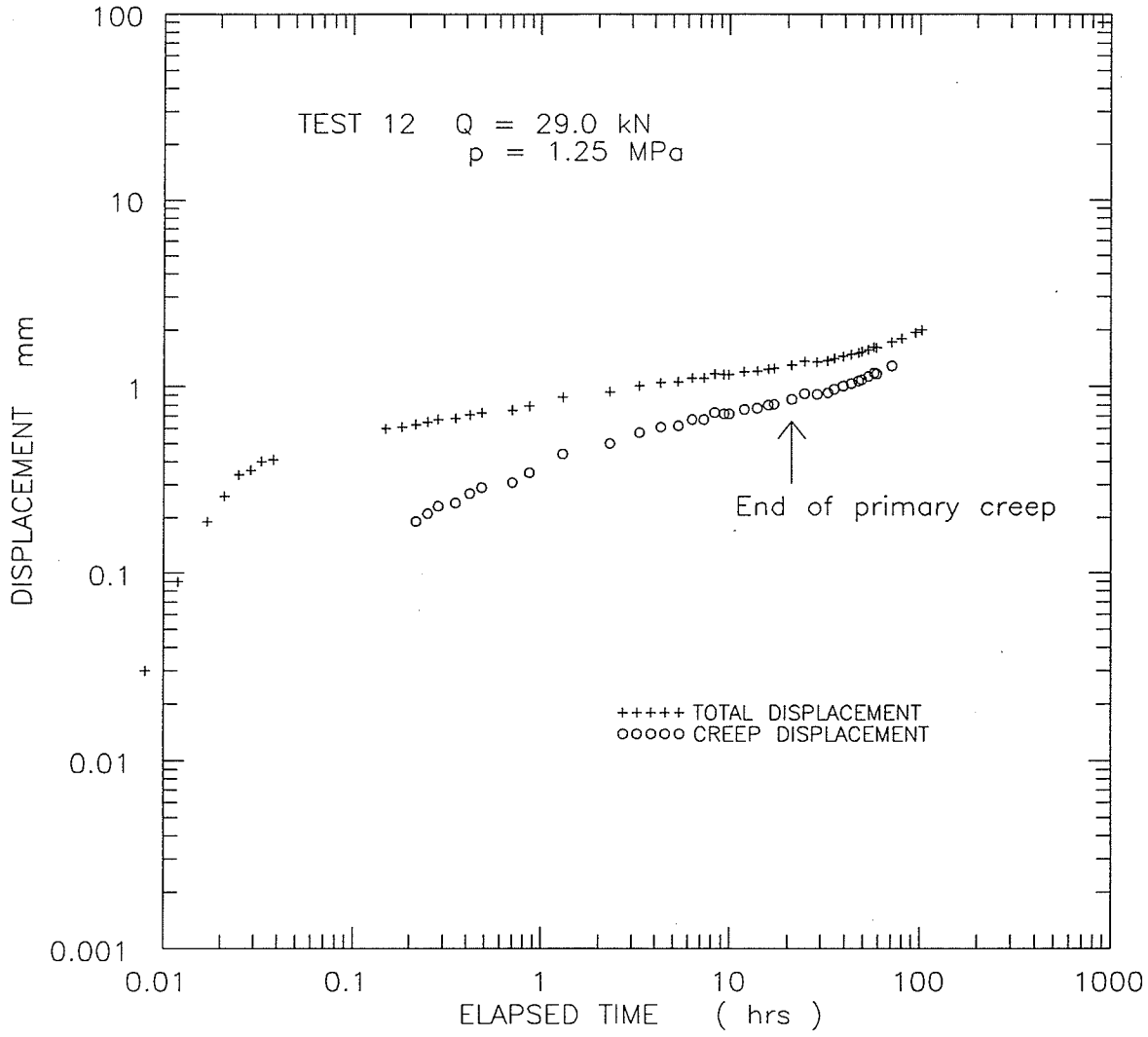


Figure C.28 Multi-stage Test 12, Stage 1: total and creep displacement versus time (log-log).

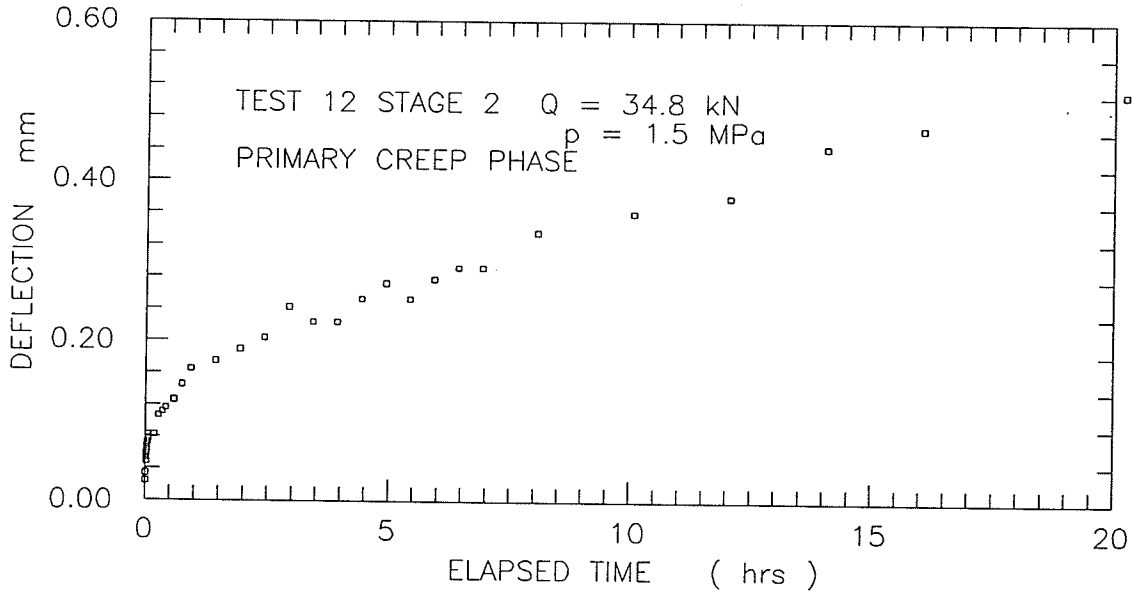


Figure C.29 Multi-stage Test 12, Stage 2: displacement versus time.

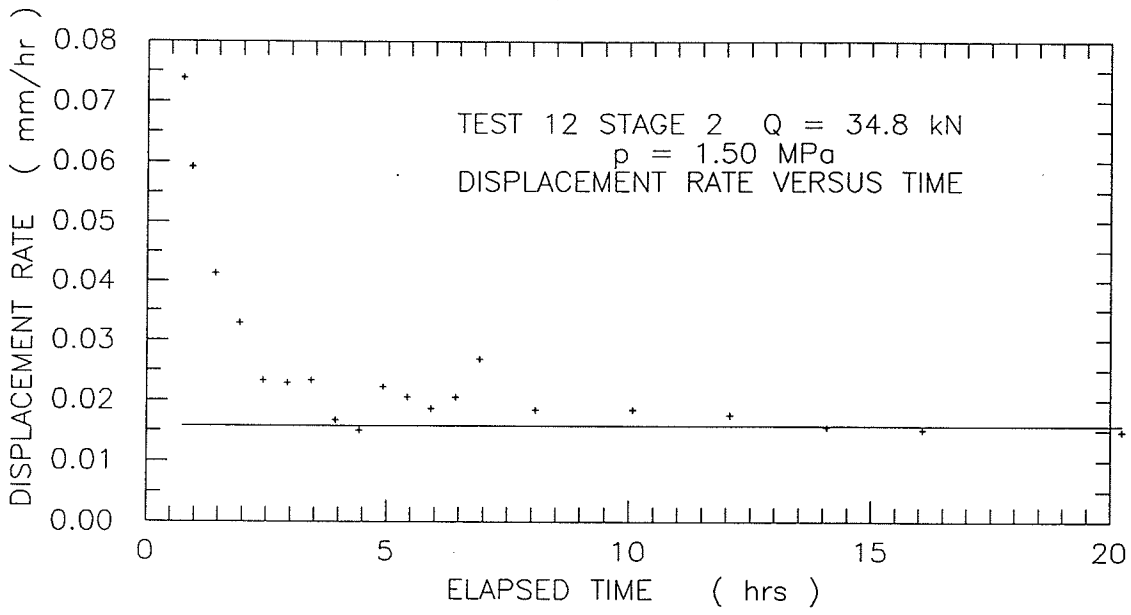


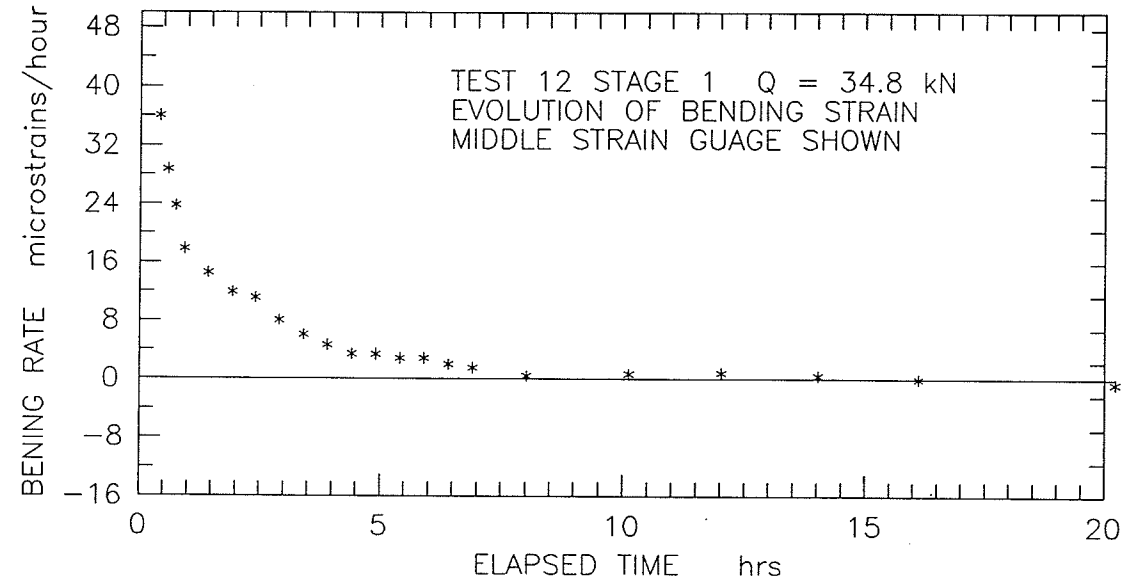


Figure C.30 Multi-stage Test 12, Stage 2: displacement rate and evolution of bending strain (middle strain gauge) versus time.

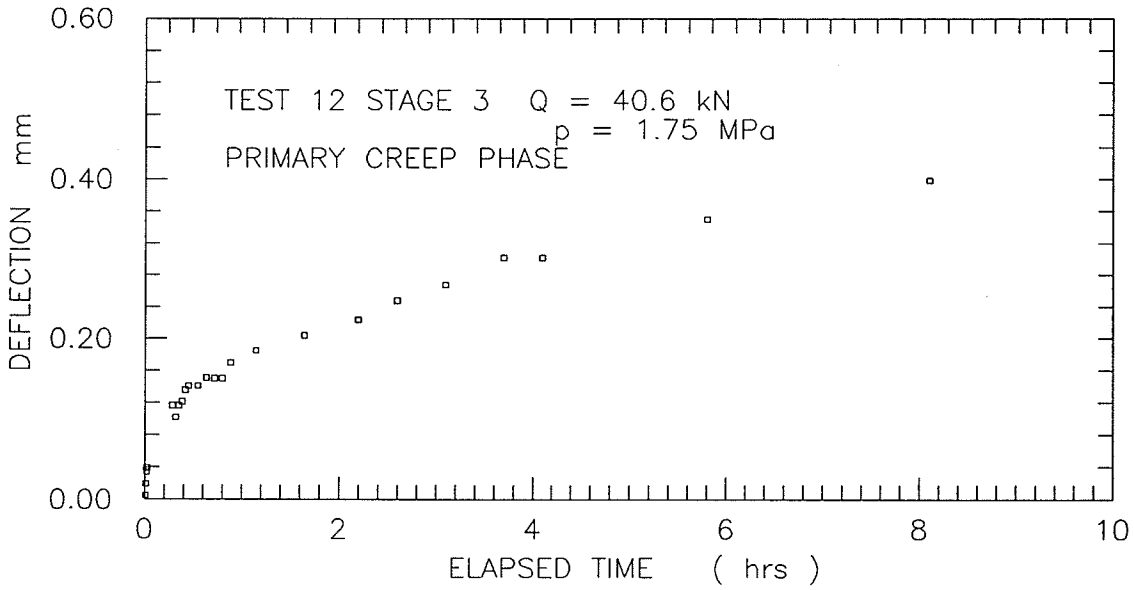


Figure C.31 Multi-stage Test 12, Stage 3: displacement versus time.

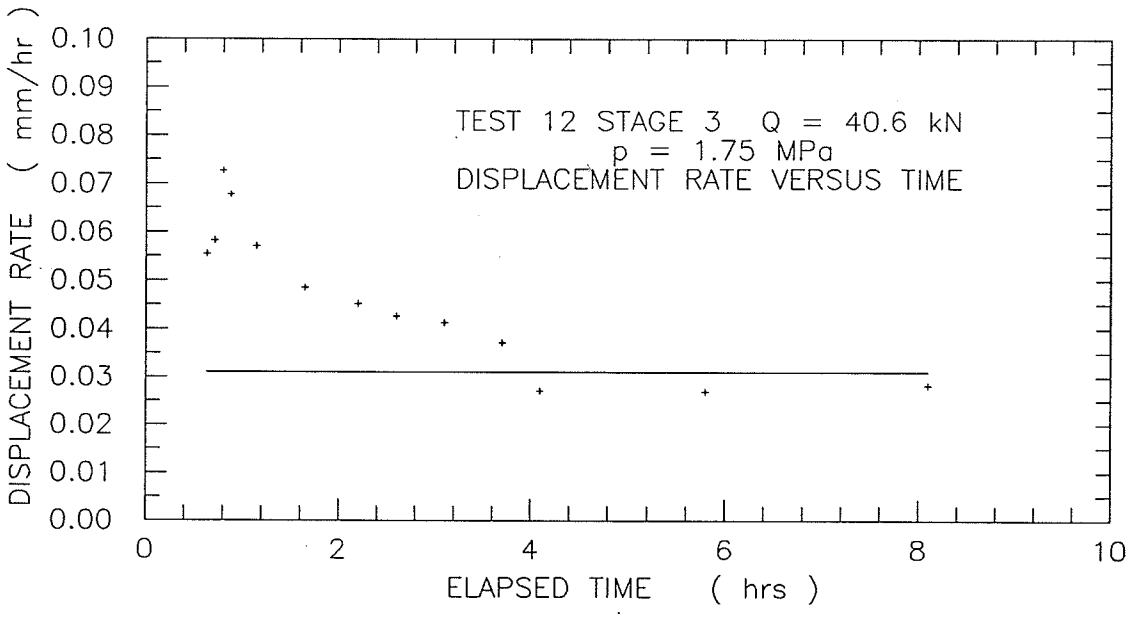


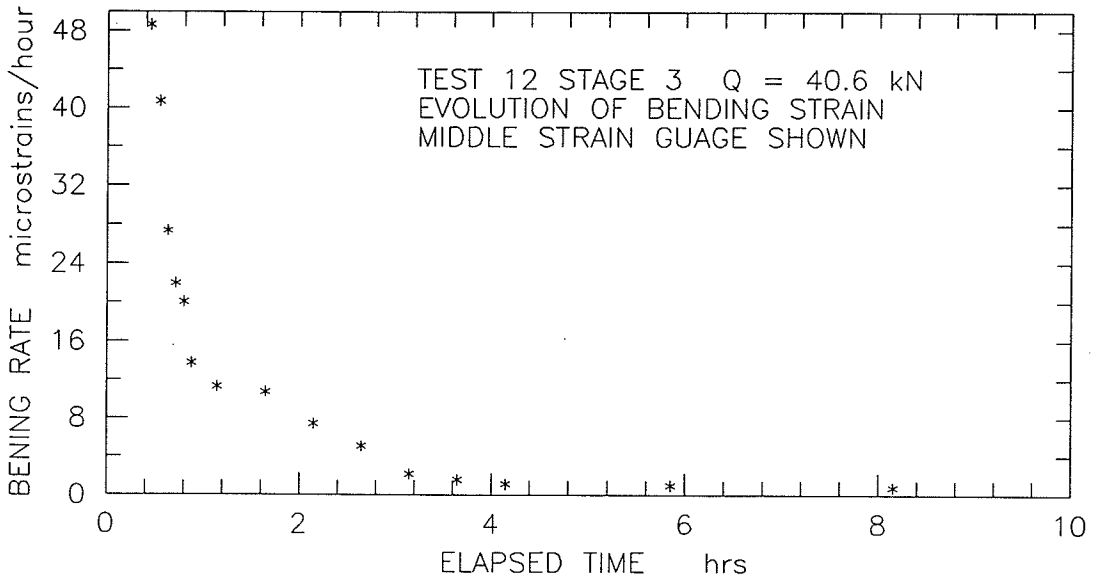


Figure C.32 Multi-stage Test 12, Stage 3: displacement rate and evolution of bending strain (middle strain gauge) versus time.

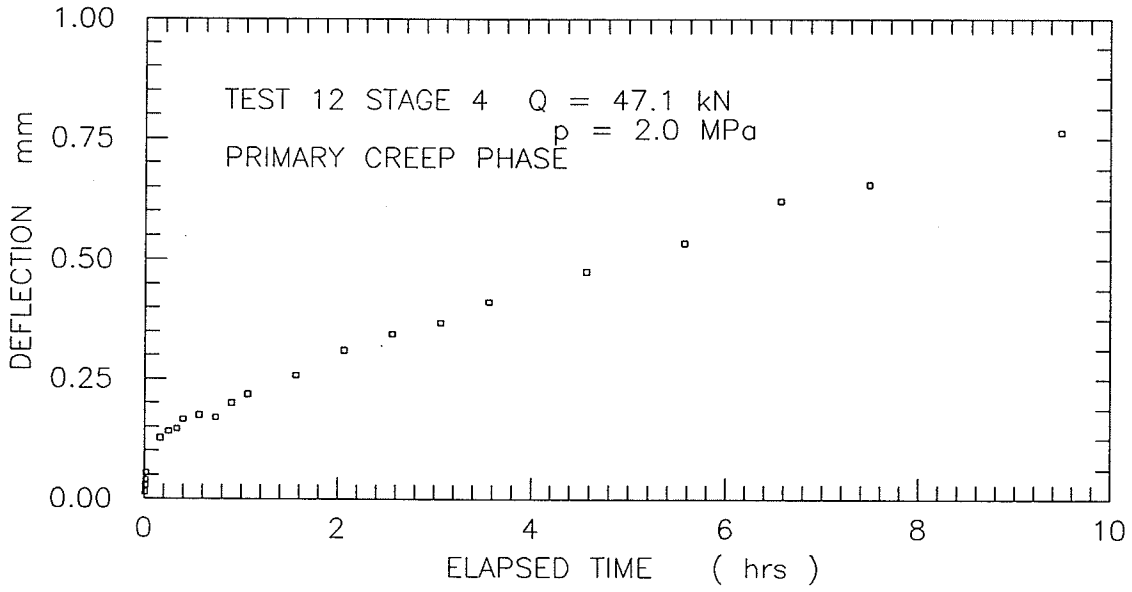


Figure C.33 Multi-stage Test 12, Stage 4: displacement versus time.

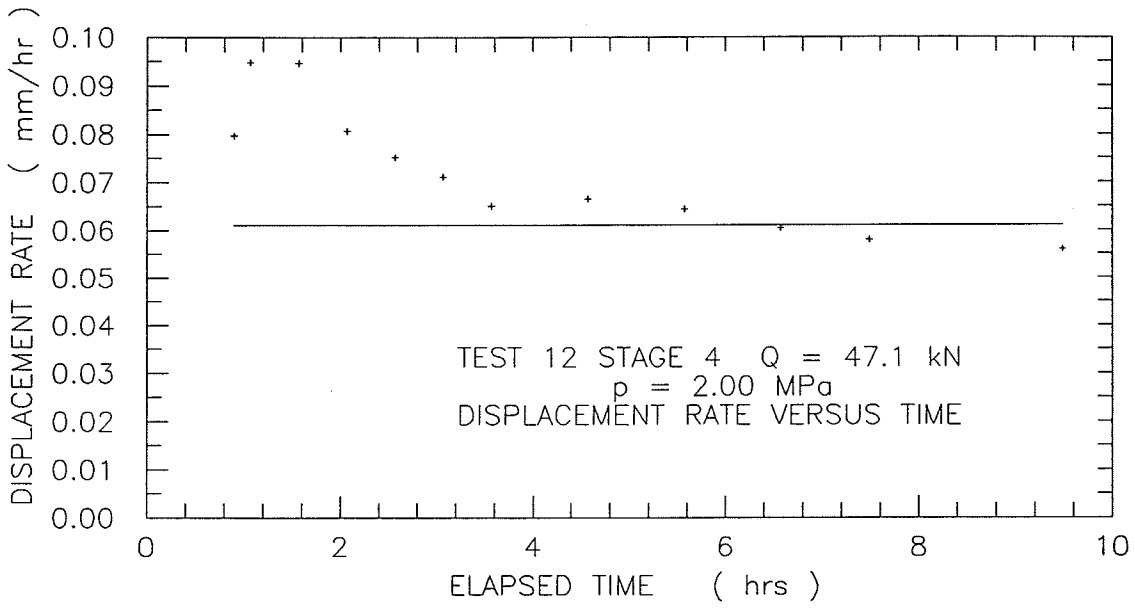


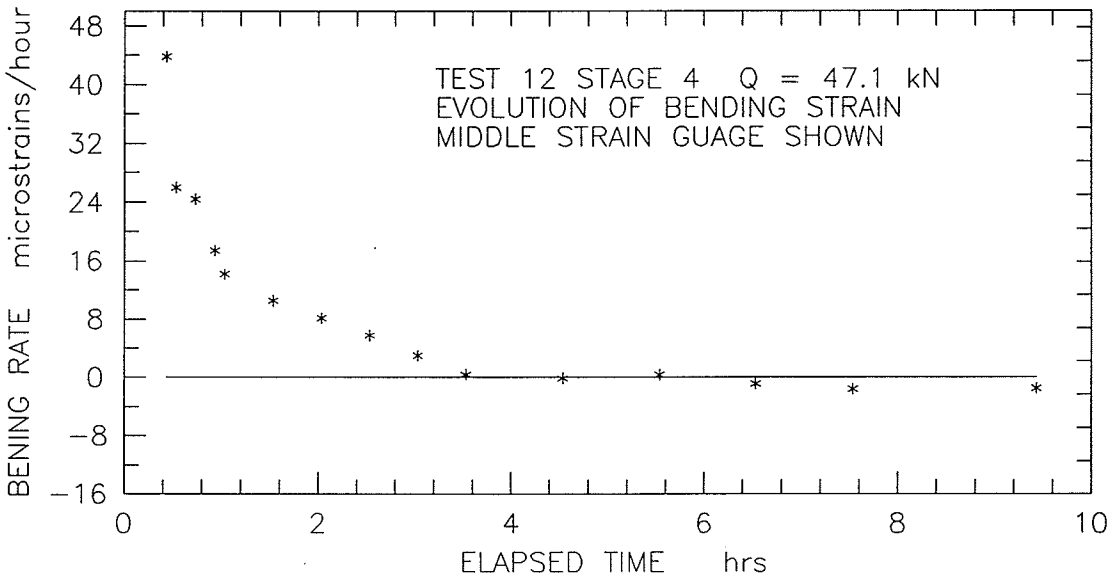


Figure C.34 Multi-stage Test 12, Stage 4: displacement rate and evolution of bending strain (middle strain gauge) versus time.

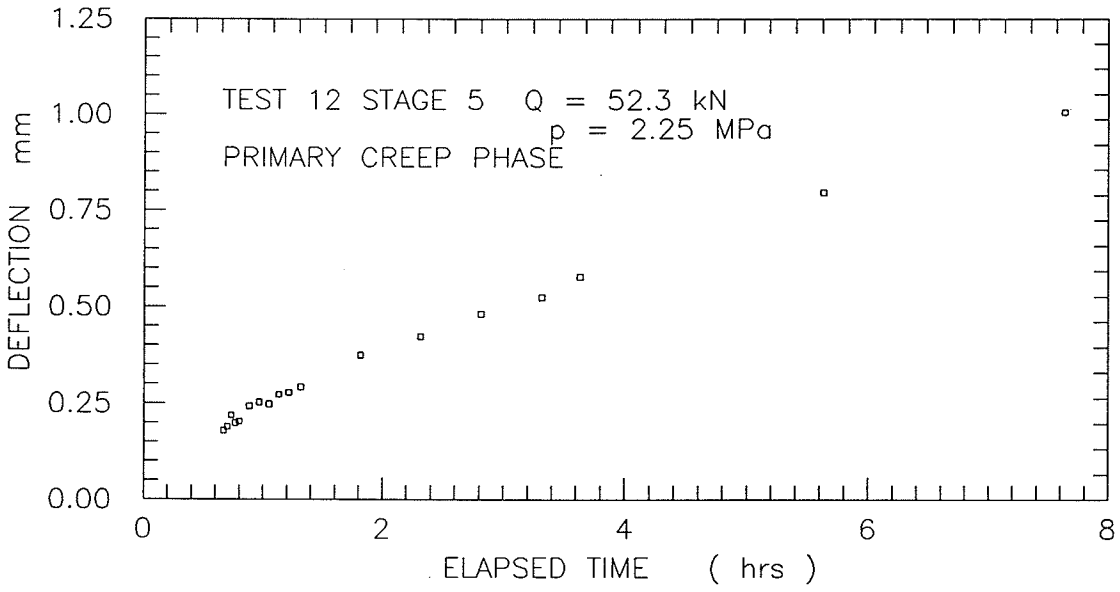


Figure C.35 Multi-stage Test 12, Stage 5: displacement versus time.

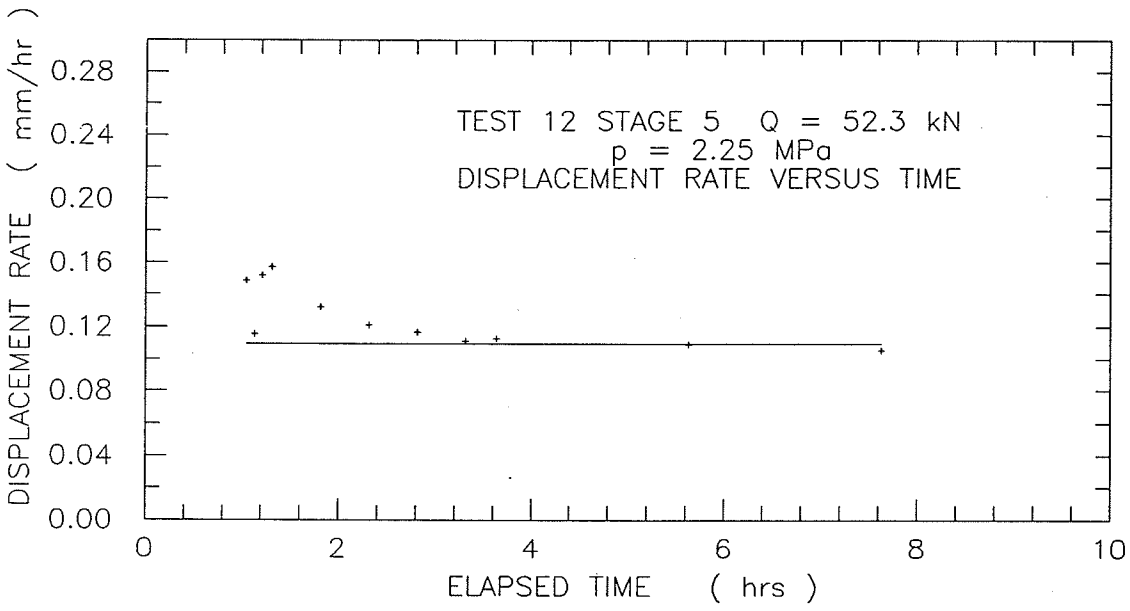


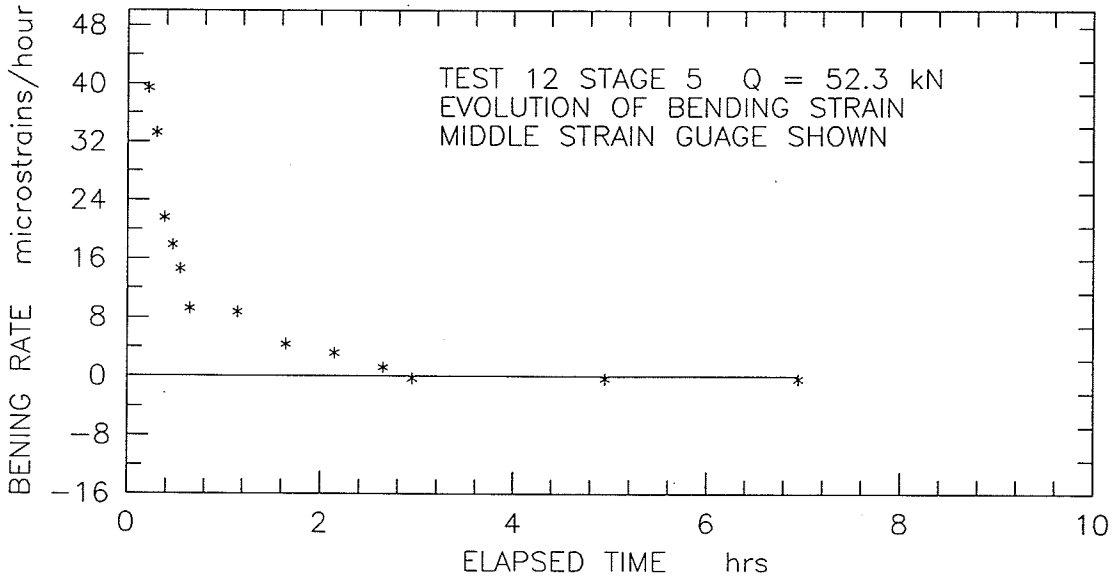


Figure C.36 Multi-stage Test 12, Stage 5: displacement rate and evolution of bending strain (middle strain gauge) versus time.

# APPENDIX D

## PLOTS OF LOG CREEP DISPLACEMENT VERSUS LOG TIME, USED TO CALCULATE PRIMARY CREEP EXPONENT b

## SINGLE STAGE TESTS

## TRIAL # 1

**(Best fit through all primary creep data)**

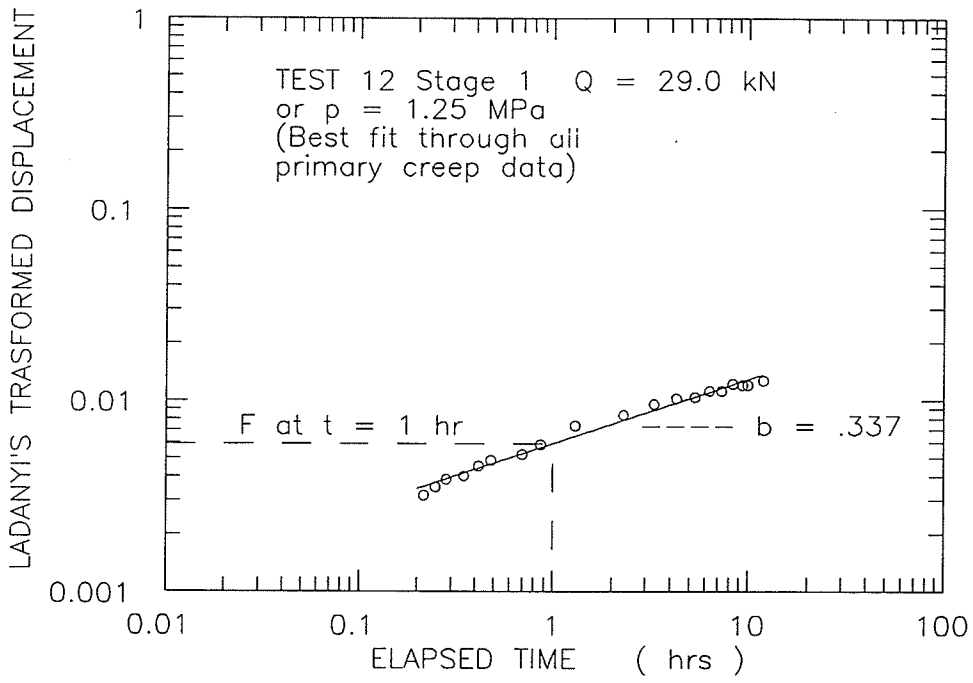


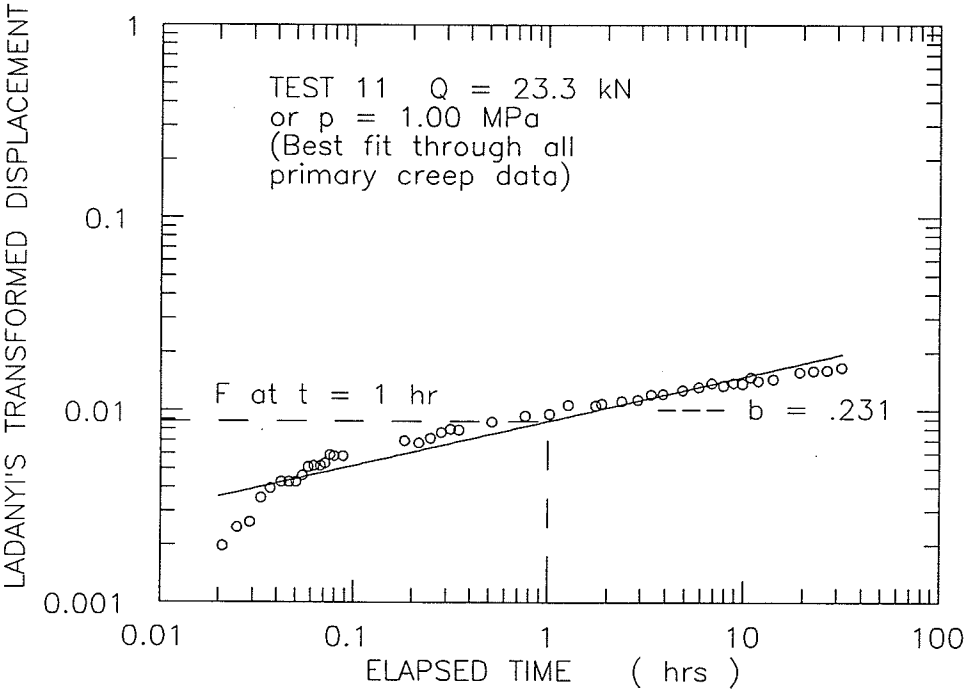


Figure D.1 Single stage tests. Determination of primary creep parameter "b". Best fit through all primary creep data for p = 1.00 MPa and p = 1.25 MPa.

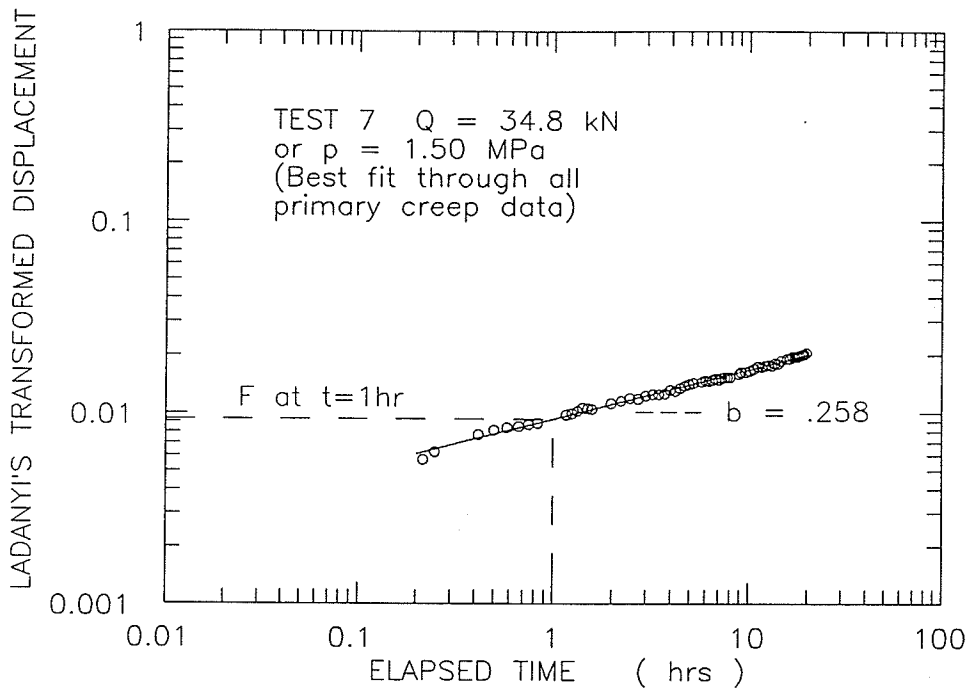


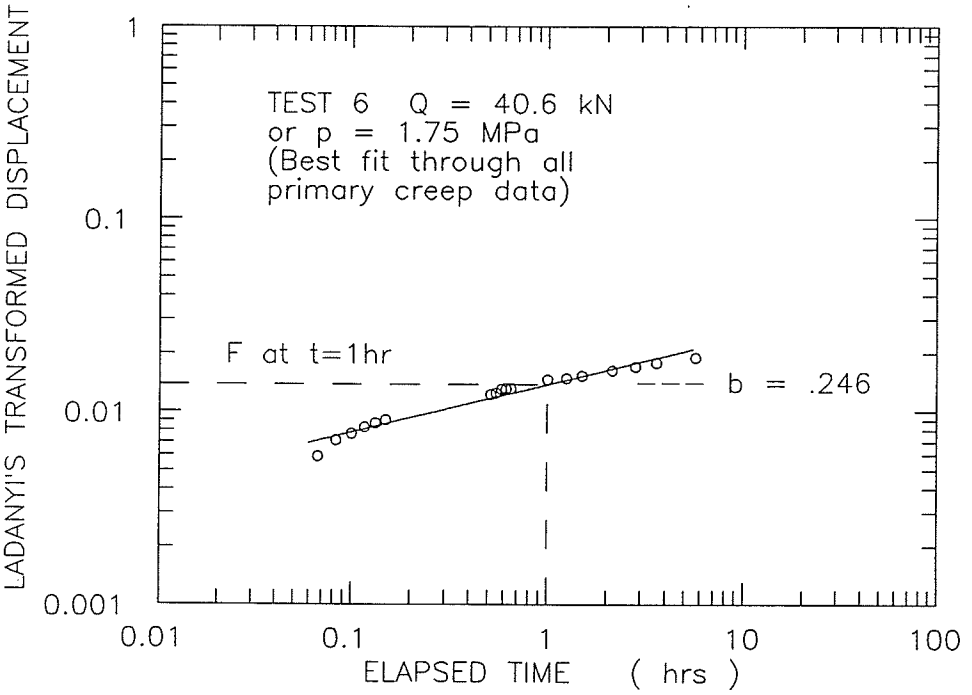


Figure D.2 Single stage tests. Determination of primary creep parameter "b". Best fit through all primary creep data for p = 1.50 MPa and p = 1.75 MPa.

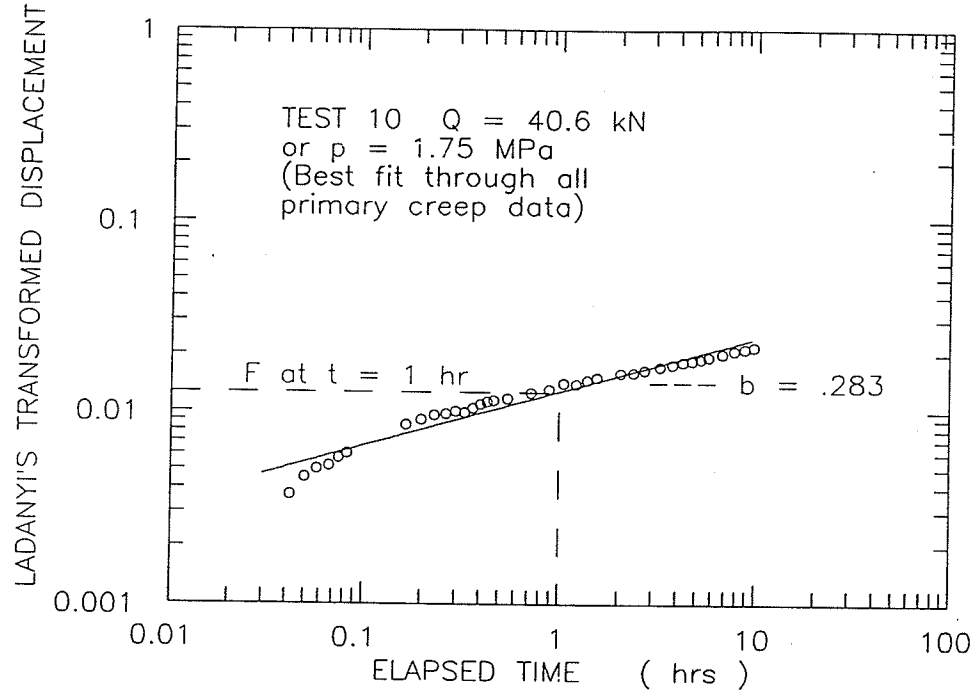


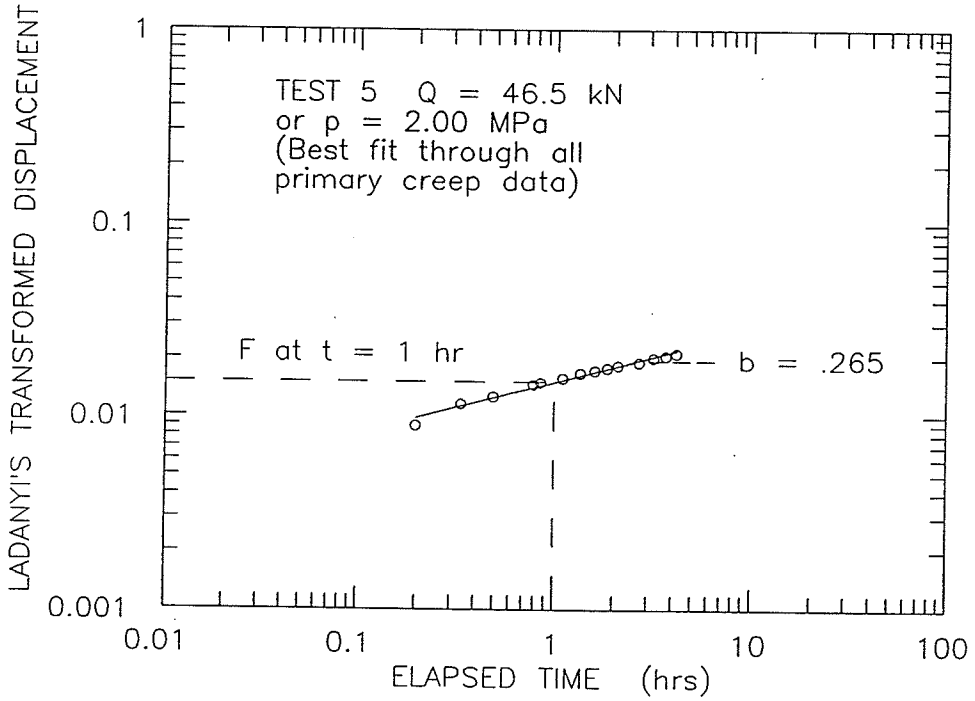


Figure D.3 Single stage tests. Determination of primary creep parameter "b". Best fit through all primary creep data for p = 1.75 MPa and p = 2.00 MPa.

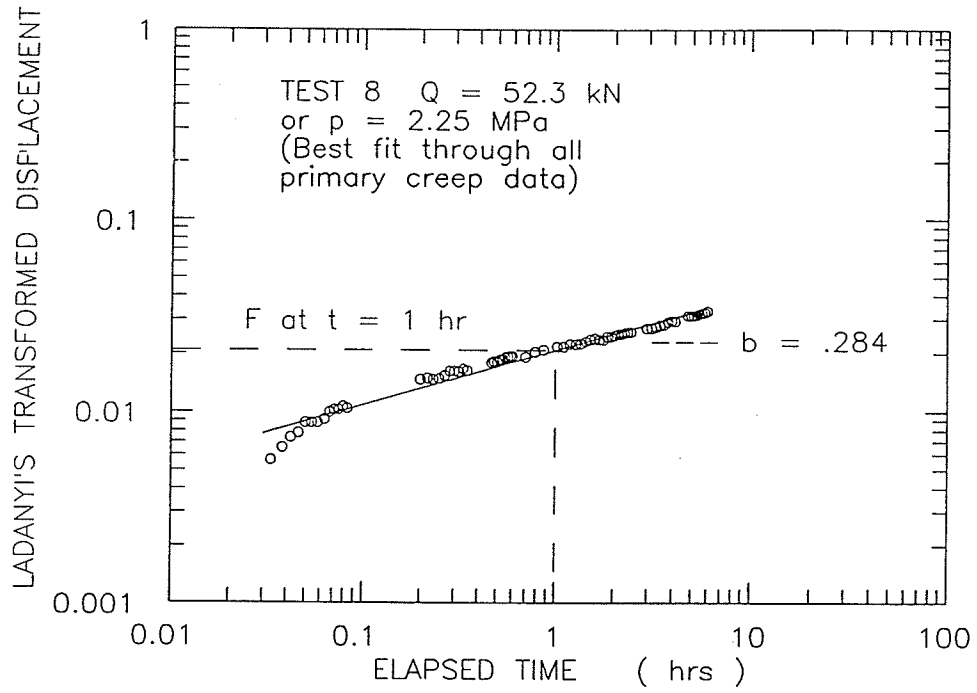


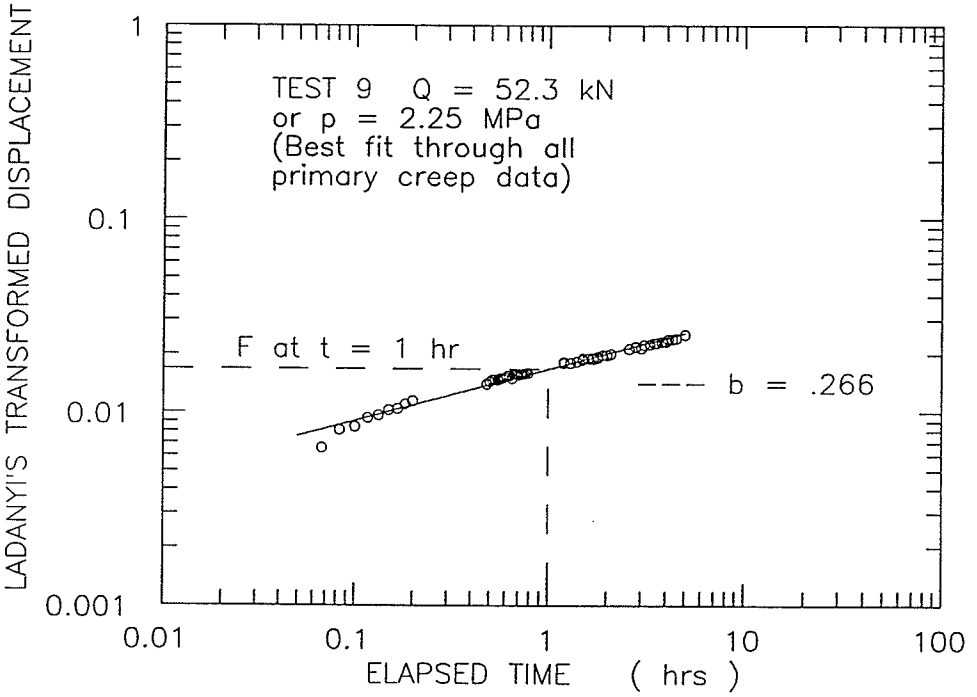


Figure D.4 Single stage tests. Determination of primary creep parameter "b". Best fit through all primary creep data for p = 2.25 MPa.

SINGLE STAGE TESTS

TRIAL # 2

(Best fit through straight line portions of primary creep data)

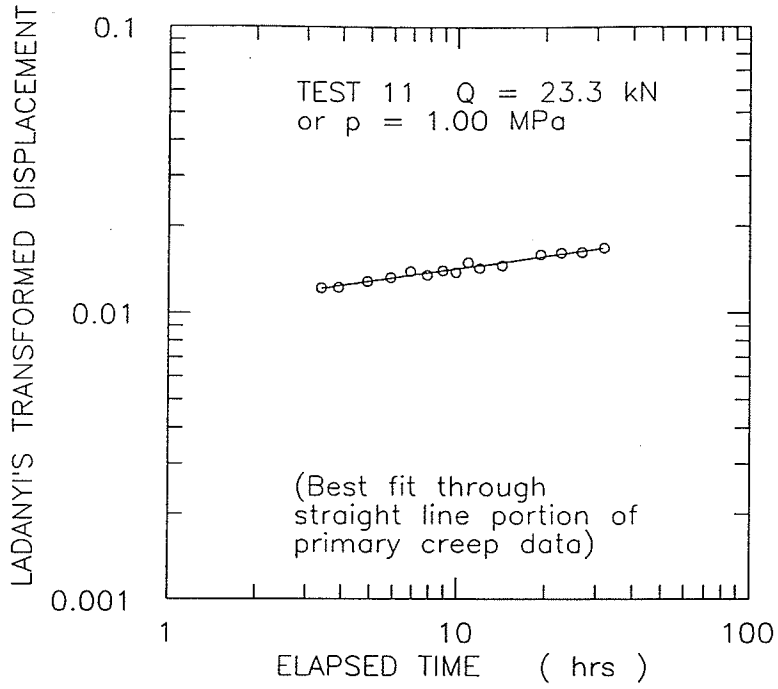


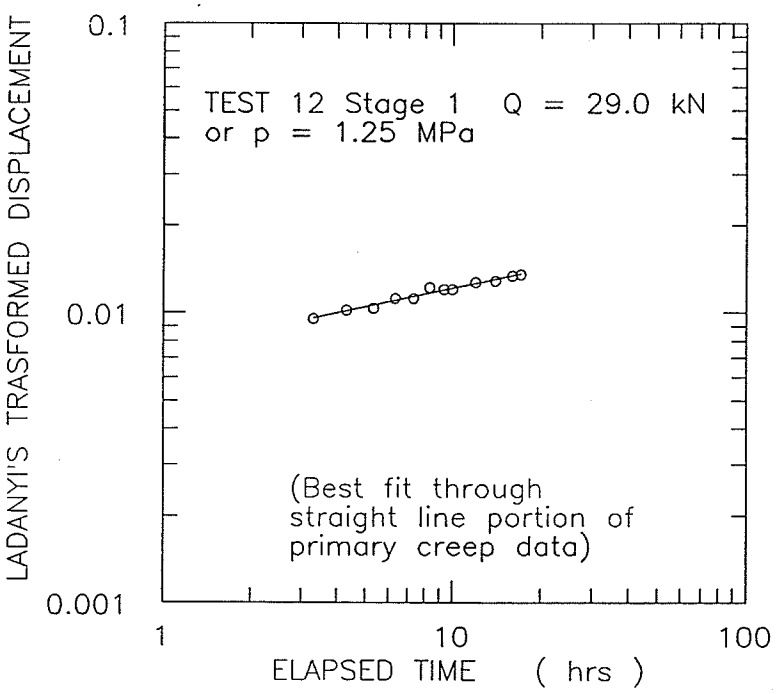


Figure D.5 Single stage tests. Determination of primary creep parameter "b". Best fit through straight line portion of primary creep data for p = 1.00 MPa and p = 1.25 MPa.

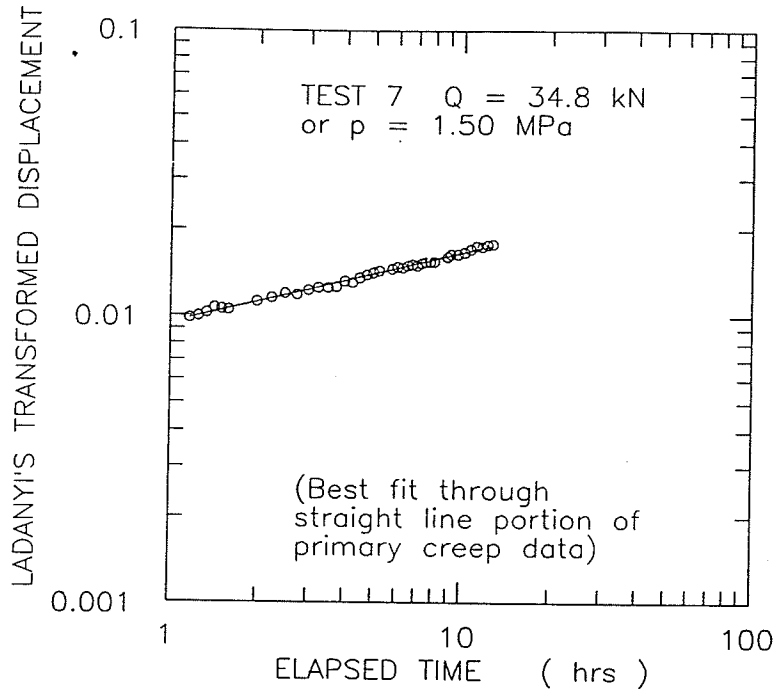


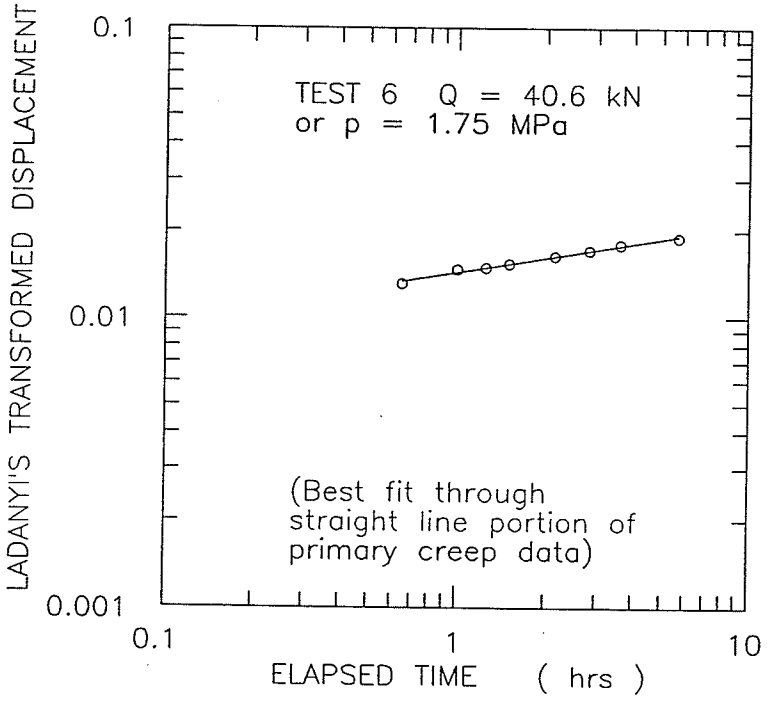


Figure D.6 Single stage tests. Determination of primary creep parameter "b". Best fit through straight line portion of primary creep data for p = 1.50 MPa and p = 1.75 MPa.

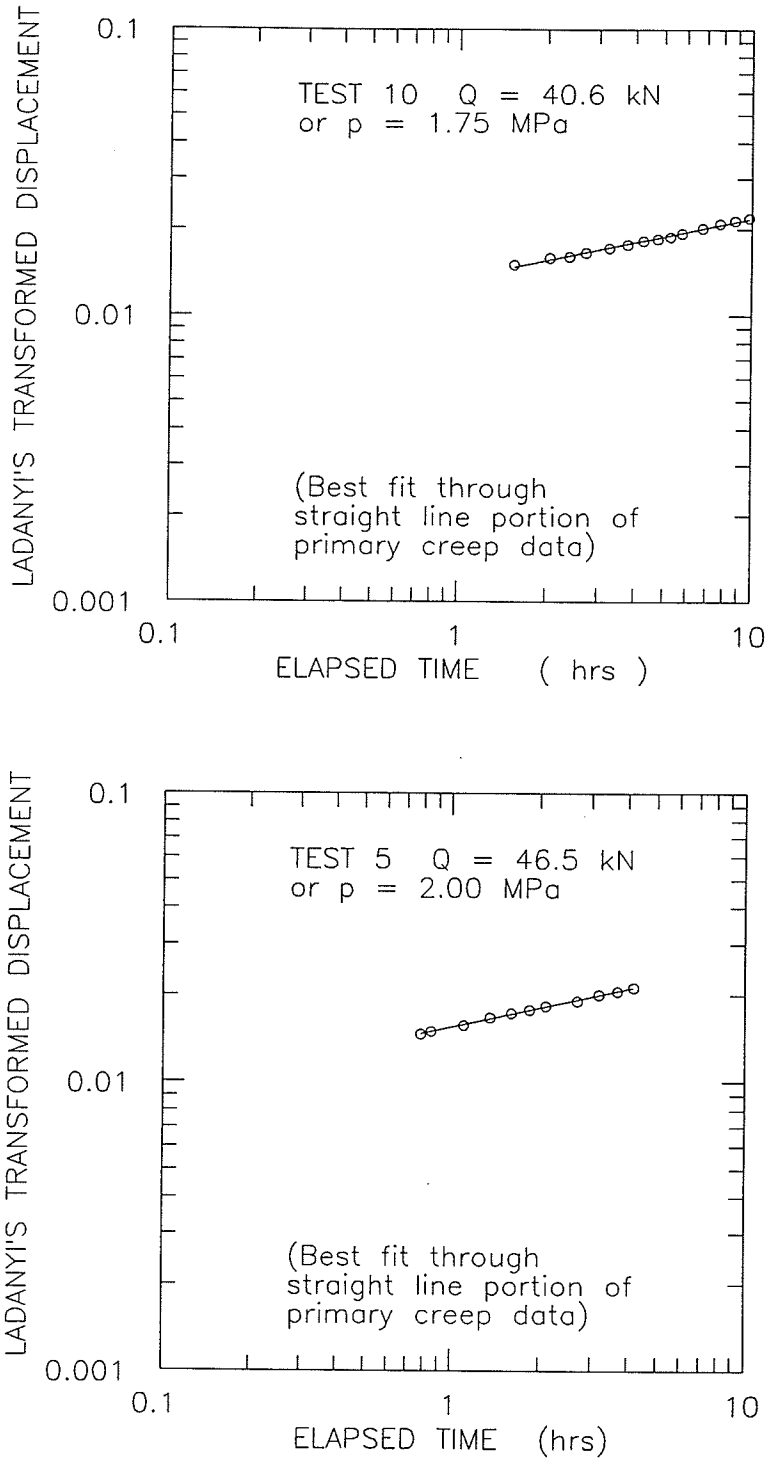


Figure D.7 Single stage tests. Determination of primary creep parameter "b". Best fit through straight line portion of primary creep data for p = 1.75 MPa and p = 2.00 MPa.

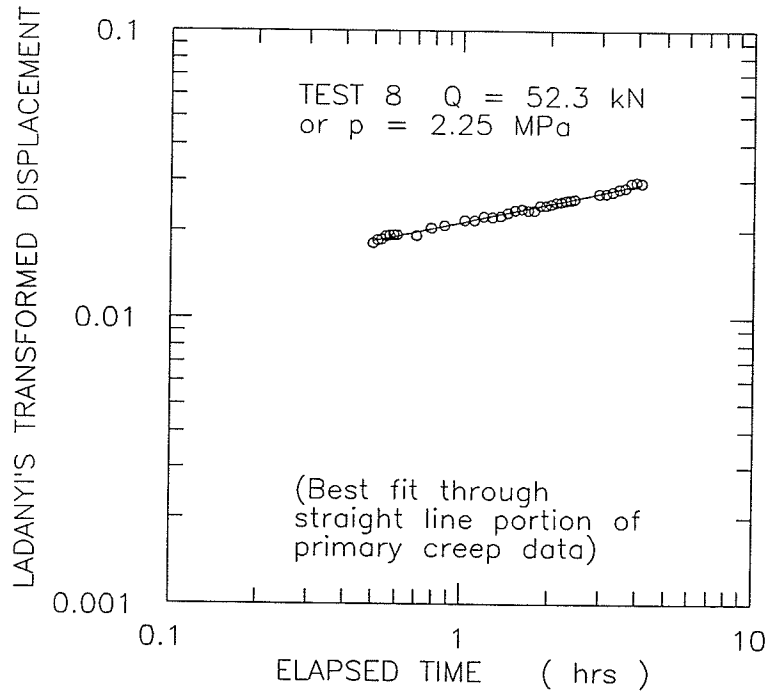


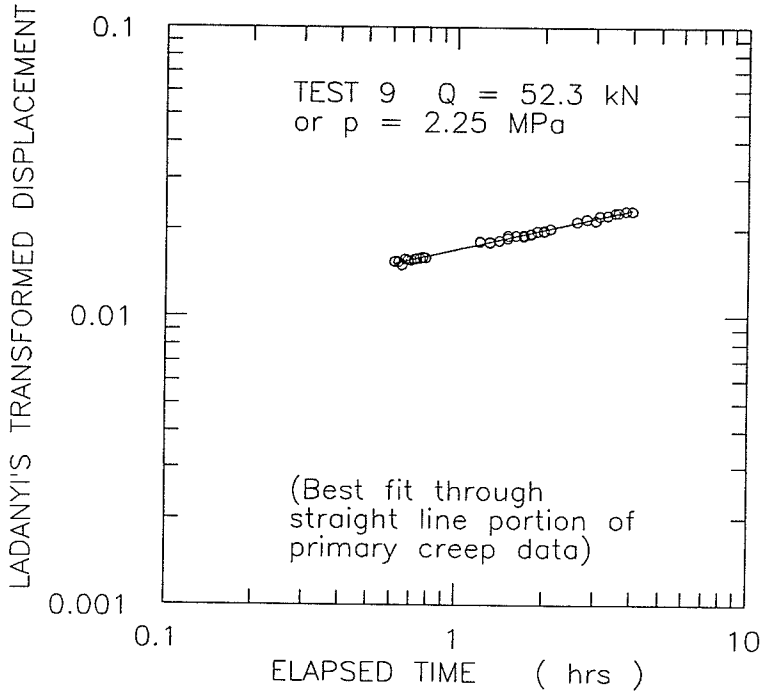


Figure D.8 Single stage tests. Determination of primary creep parameter "b". Best fit through straight line portion of primary creep data for p = 2.25 MPa.

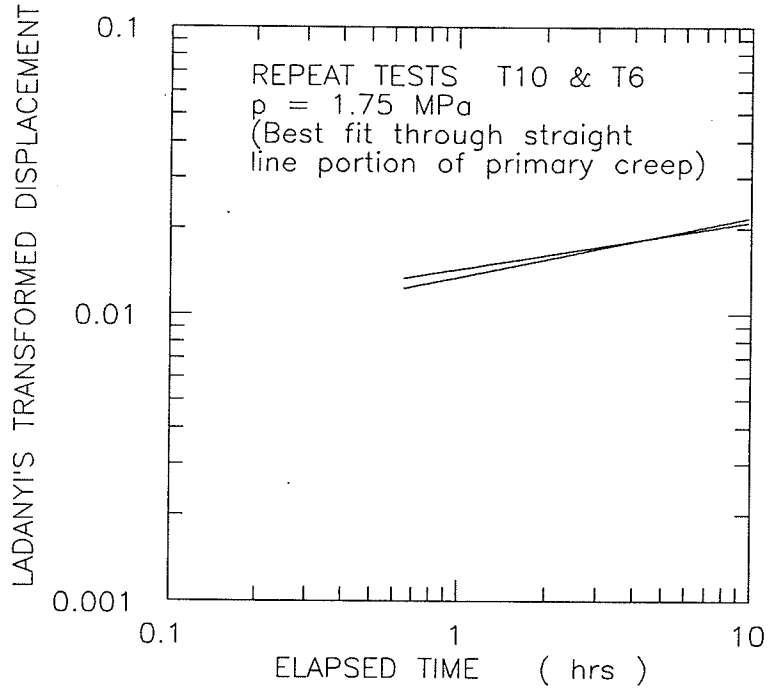


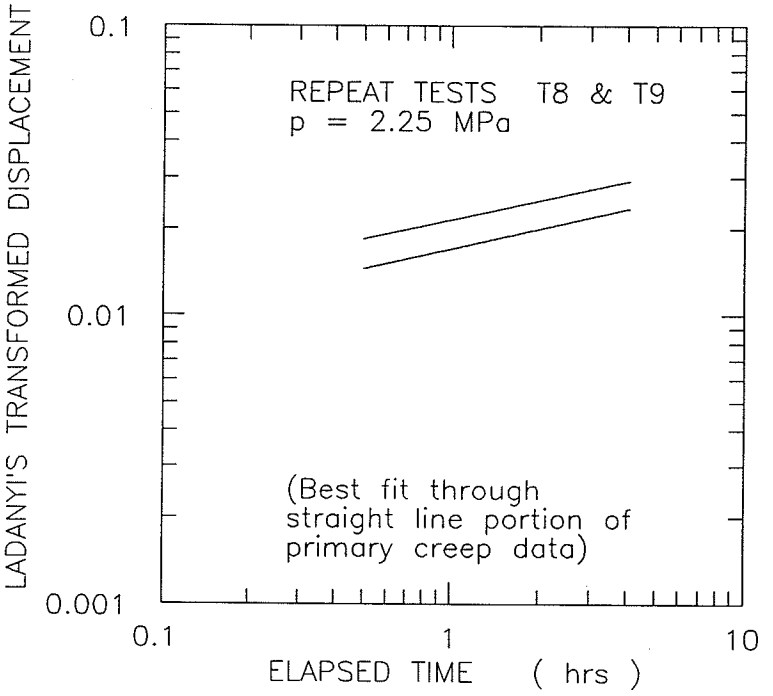


Figure D.9 Single stage tests. Determination of primary creep paramater "b". Best fit through straight line portion of primary creep data for repeat tests.

## SINGLE STAGE TESTS

## TRIAL # 3

**(Using creep displacements of the mid-point of the bar)**

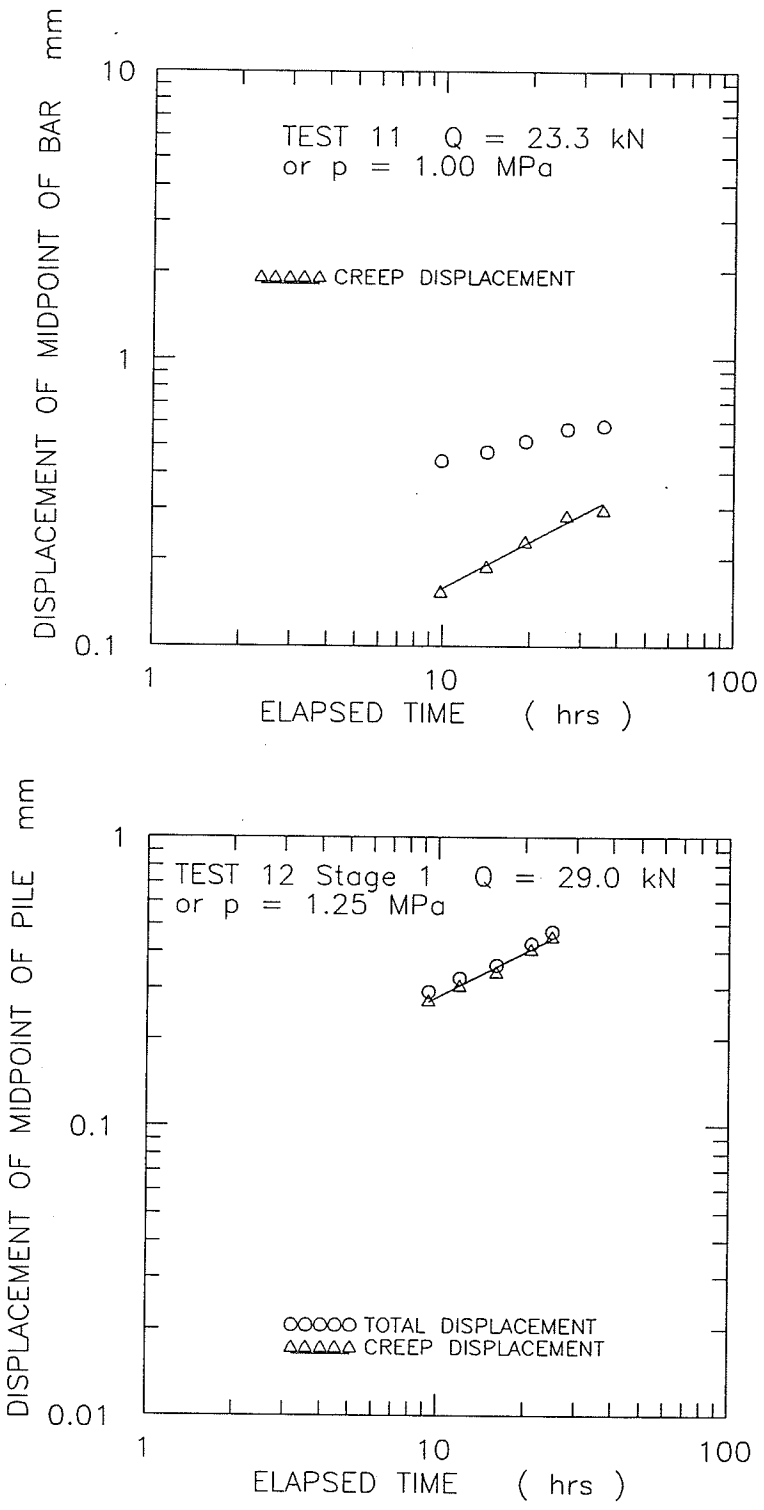


Figure D.10 Single stage tests. Determination of primary creep parameter "b". Best fit through straight line portion of primary creep data and using creep displacements calculated at midpoint of embedded length of bar for p = 1.00 MPa and p = 1.25 MPa.

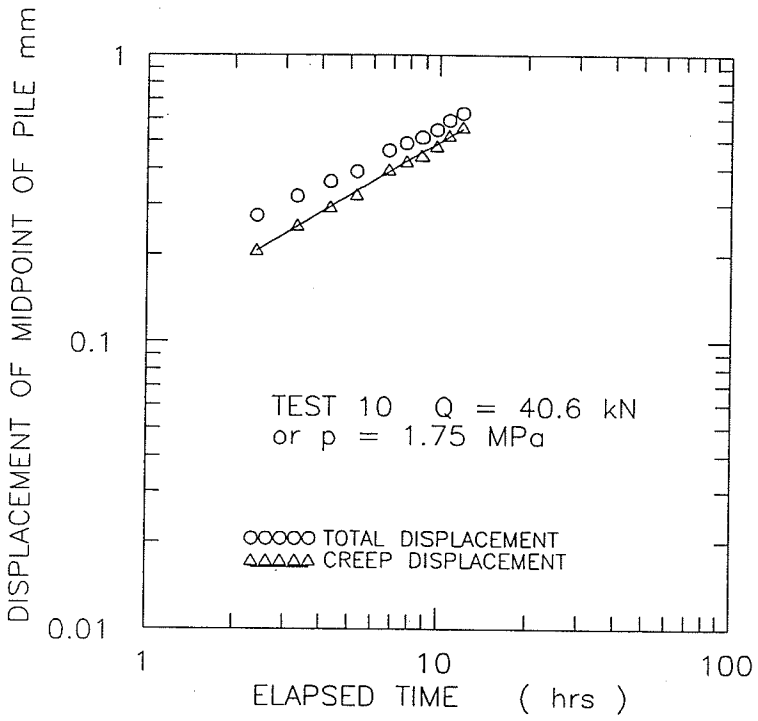


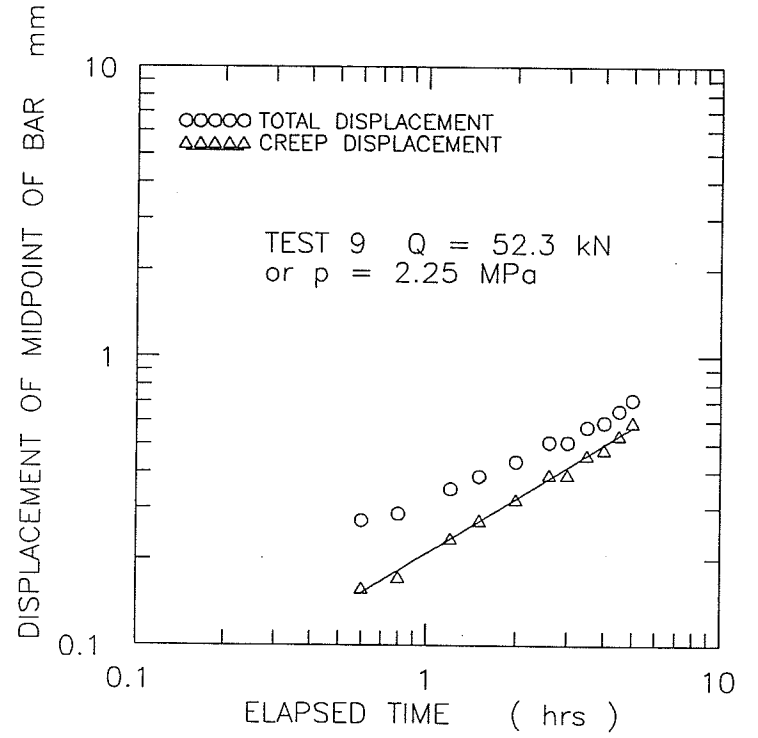


Figure D.11 Single stage tests. Determination of primary creep parameter "b". Best fit through straight line portion of primary creep data and using creep displacements calculated at midpoint of embedded length of bar for p = 1.75 MPa and p = 2.25 MPa.